The copyright of this thesis vests in the author. No quotation from it or information derived from it is to be published without full acknowledgement of the source. The thesis is to be used for private study or non-commercial research purposes only.

Published by the University of Cape Town (UCT) in terms of the non-exclusive license granted to UCT by the author.

University of Cape Town

DECLARATION

I know the meaning of plagiarism and declare that all of the work in this thesis, save for that which is properly acknowledge, is my own.

.....
Francois Wewers
February 2012

Transition metal complexes of bis(diphenylphosphino)methane, dithizone and dithiolenes: structural, spectroscopic, electrochemical and computational studies

A thesis submitted in fulfilment of the requirements for the degree

DOCTOR OF PHILOSOPHY

Department of Chemistry

University of Cape Town

by

Francois Wewers

BSc(Hons) Cape Town

February 2012

ACKNOWLEDGEMENTS

I want to thank Prof. Alan. T. Hutton, my supervisor, for all his help, understanding, patience and guidance during these studies. For introducing me to so many different aspects of chemistry.

Dr. Gerhard Venter who has introduced me to computational chemistry. There is still so much to learn.

All colleagues past and present who in some way made a contribution.

I thank Dr. Hong Sue for help with the solution of the X-ray crystal structures, Mr. Noel Hendricks for the many NMR's he produced, Mr. P. Benincasa for the micro-analytical work

Most of all I want to thank my parents who made all this possible, for their sacrifices and encouragement.

Not forgetting my family, for always being there, spurring me on. Thank you Charmaine, Lisa and Laura.

CONTENTS

			Page
Abstract			(ix)
List of abbreviations			(xi)
CHAPTER 1: Introduction			
1.1	The chemistry of bis(diphenylphosphino)methane		1
	1.1.1	Synthetic routes	3
	1.1.2	Deprotonation of dppm	3
	1.1.3	Alkylation of dppm	5
	1.1.4	*C*-metallation of dppm	8
		1.1.4.1 Bonding modes (I),(II) and (III)	9
		1.1.4.2 Bonding mode (IV)	9
		1.1.4.3 Bonding mode (V)	10
		1.1.4.4 Bonding modes (VI) and (VII)	11
		1.1.4.5 Bonding modes (VIII), (IX) and (X)	11
		1.1.4.6 Bonding modes (XI) and (XII)	13
1.2	The chemistry of dithizone		16
	1.2.1	Early work	16
	1.2.2	Photochromism	17
	1.2.3	Metal dithizonate complexes	19
1.3	The chemistry of dithiolenes		22
	1.3.1	Early work	22
	1.3.2	Complexes of dithiolenes	23
	1.3.3	Electrochemistry	25

1.3.4 Applications 25
1.3.4.1 Conduction and magnetism 26
1.3.4.2 Non-linear optics 27
1.4 Aims of the study 28
References 30

CHAPTER 2: Structural and electrochemical study of mercurated Group 6-dppm complexes

2.1 Introduction 38
2.2 Long chain complexes 42
2.2.1 Synthesis of 4-(4'-n-alkoxybenzylidine-*N*-methylanilino)mercury(II) chlorides 42
2.3 Preparation of mercurated Group 6 dppm complexes 44
2.4 Spectroscopic studies 46
2.4.1 Infrared spectra 46
2.4.2 H-NMR 47
2.4.3 ^{31}P NMR 49
2.5 Bimetallic gold(I) complexes 53
2.6 Crystallographic study of mercurated complexes 55
2.7 Electrochemical study of Group 6 metal complexes 63
2.7.1 Electrochemistry of unsubstituted complexes 63
2.7.2 Electrochemistry of metallated complexes 64
2.7.3 Correlation studies 68
2.7.3.1 Correlation of oxidation potentials with NMR parameters 68
2.7.3.2 Correlation of oxidation potentials with IR parameters 70
References 72

CHAPTER 3: Structural and electrochemical study of mercurated Pd-, Pt- and Ru-dppm complexes

3.1 Introduction 76
3.2 Preparation of Pd- and Pt dithiolene-dppm complexes 76
3.3 Mercuration of X_2Pd- and X_2Pt-dppm complexes 79
3.4 Auration of Pd- and Pt-dppm complexes 80
3.4.1 Spectroscopic studies 80
3.5 Mercuration of (dithiolene)Pd- and (dithiolene)Pt-dppm complexes 81
3.5.1 Spectroscopic studies 81
3.6 Electrochemical studies 84
3.6.1 Electrochemistry of unsubstituted Pd and Pt dithiolene-dppm complexes 84
3.6.2 Electrochemistry of metallated Pd and Pt dithiolene-dppm complexes 86
3.7 Ruthenium complexes 89
3.8 Crystal and molecular structure of complex [3.22] 92
3.9 Electrochemistry of ruthenium complexes 96
References 99

CHAPTER 4: Structural and computational studies of dithizone and its anion

4.1 General introduction 100
4.2 Preparation of 1,5-diphenylthiocarbazonate salt 101
4.3 Crystal and molecular structure of Bu_4N[Hdptc] 103
4.4 Crystal and molecular structure of dithizone 107
4.5 DFT calculations 111
4.5.1 Calculations based on the parent dithizone molecule 112
4.5.2 Calculations based on the dithizone anion 113
4.6 NMR Spectra 115
References 118

CHAPTER 5: Structural, spectrochemical and electrochemical studies of dithizone complexes of Pd and Pt

5.1 General introduction 119
5.2 Reaction of [X_2Pt(COD)] with dithizone 119
5.3 Platinum and palladium phosphine-dithizone complexes 121
5.3.1 Reaction of dithizone with platinum and palladium phosphine precursors 121
5.4 Crystal and molecular structure of complex [4.3] 124
5.5 UV/vis spectrophotometry 128
5.6 Crystal and molecular structure of complex [5.18] 130
5.7 Electrochemistry of complexes 133
References 135

CHAPTER 6: Synthetic, structural and electrochemical studies of mixed dithizone-dithiolene complexes of Hg and Pt

6.1 Introduction 137
6.2 Mixed dithiolene-dithizone complexes of mercury 137
6.3 Spectroscopic studies 138
6.3.1 Infrared spectroscopy 138
6.3.2 Electronic spectroscopy 141
6.4 Crystal and molecular structure of [6.4] 143
6.5 Electrochemistry 147
6.6 Mixed dithiolene-dithizone complexes of platinum 149
6.6.1 Reaction of metal halides with dithizone 150
6.6.2 Reaction of cyclooctadiene platinum salt with dithizone 151
6.6.3 Reaction of [(dithiolene)Pt(COD)] with dithizonate salt 151
6.7 Crystal and molecular structure of [6.7] 153
6.8 Cyclic voltammetry 157
References 159

CHAPTER 7: Concluding remarks 161

CHAPTER 8: Experimental

8.1 General procedures 164
8.2 Instrumentation 165
8.2.1 Molecular spectroscopy 165
8.2.2 Cyclic voltammetry 165
8.2.3 X-ray crystallography 165
8.2.4 Computational studies 167
8.3 Preparations pertaining to Chapter 2 168
8.4 Preparations pertaining to Chapter 3 188
8.5 Preparations pertaining to Chapter 4 198
8.6 Preparations pertaining to Chapter 5 199
8.7 Preparations pertaining to Chapter 6 208
References 212

Appendices

ABSTRACT

A series of heterobi- and tri-metallic complexes were prepared by the metallation of the carbanion derived from $[M(CO)_4(dppm)]$ (M = Cr, Mo or W), [ML(dppm)] (L= dithiolene; M = Pd or Pt), or the cationic precursor, $[Ru(Cp)(PPh_3)(dppm)]PF_6$. The complexes were characterized by ^1H and ^{31}P NMR, IR and UV/Vis spectroscopies and X-ray crystallography.

The presence of electrochemical communication in these complexes was investigated by means of cyclic voltammetry. Correlation studies of electrochemical potentials and ^{31}P NMR data or carbonyl stretching frequencies of the Group 6 mercurated complexes show that the mercury atom does facilitate the flow of electrons through the four-membered chelate ring. However, this effect has been established to be weak. Similar weak electronic effects were found to exist in the case of the Ru, Pd and Pt complexes. Evidence of "through-space" communication was established to be present in the ferrocenyl derivatives.

X-ray crystallographic studies show that mercuration of the carbanion neutralizes the residual electron density in the chelate ring for the chromium bi- and tri-metallic complexes. This was also demonstrated for the cationic ruthenium complex.

X-ray crystallographic studies were performed on dithizone and its corresponding salt in an attempt to resolve or explain the often debated tautomerism of this molecule in the solid state and in solution. The structure of the parent molecule showed the co-existence of the two tautomeric forms in a single structure, with a 2:1 preference for the symmetrical keto form, compared to the enol form. DFT calculations have been performed and have been shown to be mutually consistent with structural data, showing a negligible energy difference of 3.1 kcal mol^{-1} between the two forms. Computational calculations were also performed to investigate the solution characteristics of the dithizonate salt. An analysis of the HOMO and Fukui functions show the sulfur atom to be the most nucleophilic and therefore the preferred site for deprotonation with an energy barrier of 17 kJ mol^{-1} compared to the nitrogen atom. While the ^1H NMR spectrum shows evidence of the

existence of proton exchange in solution, we were unable to model this. However, DFT solution studies show that the keto form is most stabilized.

A series of palladium and platinum dithizonate complexes, with the general formula, [M(PP)(Hdptc)]X or [M(PP)(dptc)] (PP = mono- or bidentate phosphine ligand; M = Pd or Pt; X = PF_6 or BPh_4), was prepared and investigated for their photochromic behaviour. None of these complexes exhibited any photochromism. X-ray crystal structures of [Pt(COD)(dptc)] and [Pt(dppf)(dptc)] were determined. Both complexes contain the dithizone ligand in a doubly deprotonated, or secondary, form.

Synthetic routes to the preparation of mixed dithiolene-dithizone complexes of mercury and platinum were developed. The complexes were characterized by ^{1}H and ^{13}C NMR, IR and UV/Vis spectroscopies and X-ray crystallography. Spectroscopic studies show that the mercury complexes are all photochromic, while the platinum complex showed no photochromism in solution. Electrochemical studies show the absence of rich electrochemical activity for the Hg complexes. The $[Pt(mnt)(Hdptc)]^{+}$ complexes, in contrast, showed greater redox activity.
X-ray studies on the analogous complexes, $Ph_4As[Hg(mnt)(Hdptc)]$ and $Bu_4N[Pt(mnt)(Hdptc)]$ revealed an absence of any *S*···*S* or Metal···*S* interactions, often associated with planar sulfur rich ligands.

LIST OF ABBREVIATIONS AND SYMBOLS

Å	Angstrom
B3LYP	Becke 3-parameter Lee, Yang, Parr
COD	1,5-cyclooctadiene
Cp	cyclopentadienyl ring
CV	cyclic voltammetry
dec	decompose
Dec	decyl
dddt	5,6-dihydro-1,4-dithiine-2,3-dithiolate
dmid	4,5-dimercapto-1,3-dithia-2-one
dmit	4,5-dimercapto-1,3-dithia-2-thione
dppe	bis(diphenylphosphino)ethane
dppf	bis(diphenylphosphino)ferrocene
dppm	bis(diphenylphosphino)methane
dppm-H	deprotonated dppm
dppp	bis(diphenylphosphino)propane
dptc	secondary dithizone (doubly deprotonated)
DFT	density functional theory
ΔG	Gibbs free energy
ΔH	Enthalpy
ECP	effective core potential
E_{pa}	anodic peak potential
E_{pc}	cathodic peak potential
Et	ethyl
Et_3N	triethylamine
Fc	ferrocene or ferrocenyl
Fc^+	ferrocenium
GIAO	gaussian independent atomic orbitals
H_2dptc	dithizone or 1,5-diphenylthiocarbazone
Hdptc	primary dithizone (singly deprotonated)
HF	Hartree-Fock approximation

HOMO	highest occupied molecular orbital
IR	infrared
J	coupling constant
K	equilibrium constant
LANL2DZ	Los Alamos National Laboratory second double-zeta basis set
Me	methyl
mnt	maleonitriledithiolene
m.p.	melting point
NMR	nuclear magnetic resonance
^{1}H NMR	proton nuclear magnetic resonance
^{13}C NMR	carbon nuclear magnetic resonance
^{31}P NMR	phosphorus nuclear magnetic resonance
NLO	non-linear optics
Oct	octyl
PCM	polarized continuum model
Ph	phenyl
PPh_3	triphenylphosphine
Pr	propyl
ppm	parts per million
R	Gas constant
SCRF	self-consistent reaction field
T	temperature
TBAP	tetrabutylammonium perchlorate
$TBAPF_6$	tetrabutylammonium hexafluorophosphate
THF	tertahydrofuran
tht	tetrahydrothiophene
TMS	tetramethylsilane
UV/vis	ultraviolet/visible spectroscopy
°	degree
δ	chemical shift
λ_{max}	maximum absorption wavelength
ε	molar extinction coefficient

CHAPTER 1

Introduction

There has been an exponential growth in the area of new materials chemistry over the past few decades. Of interest here, are complexes which find application in the area of non-linear optics, molecular switches, liquid crystals, conduction, magnetism, photochromism, etc. Central to most of these properties are the electrochemical and structural characteristics of the molecules. Here, substantial efforts have been devoted to the preparation of molecules exhibiting electrochemical communication by having metals in close proximity, introduction of electro-active centres and fine-tuning these by introducing functionality or substitution with varying electron-donating or withdrawing ability. Often appropriate spacers are introduced to facilitate the interaction between remote groups.

In our work we have concentrated on the preparation of dppm, dithizone and dithiolene complexes. In this chapter we will therefore focus on the relevant literature pertaining to these ligand systems.

1.1 The chemistry of bis(diphenylphosphino)methane

Bis(diphenylphosphino)methane, dppm, has now been established to be a very versatile ligand in coordination and organometallic chemistry. The versatility of this ligand arises from its ability to coordinate to metal centres through the lone pair of electrons on one or both of the phosphorus atoms. As a result we encounter complexes where dppm bridges metal centres, stabilizes cluster complexes, forms chelate complexes and those where dppm acts as a monodentate ligand.

It was the ability to act as an inert linkage, keeping two metal centres in close proximity, that was the key interest in the 70's and 80's.[1,2] Since then new objectives have appeared

which revealed new chemistry and reactivity for this ligand. Thus, for example, deprotonation of this ligand to form a tridentate ligand has shown that it was not as inert as previously perceived. Dppm complexes also exhibit fluxional behaviour and in some instances undergo ring opening and ring expansion reactions.

Complexes of dppm have found application as homogeneous catalysts,[1,3] as biological reagents, NLO and photochromic materials. [4] Cluster compounds such as **[1.1]**, shown in **Figure 1.1**, have been shown to display NLO properties,[5] while complex **[1.3]** has been shown to exhibit photochromism.[4] The ability of dppm to keep metal centres in close proximity makes it suitable for studying electronic communication between redox centres,[6,7,8] with a possible application as NLO material as shown by complexes **[1.2]** and **[1.4]**.

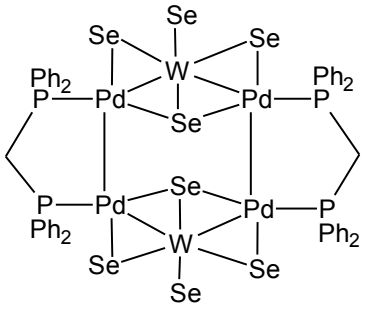

[1.1]

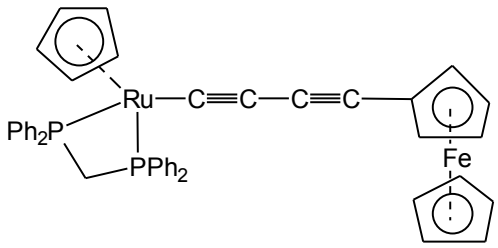

[1.2]

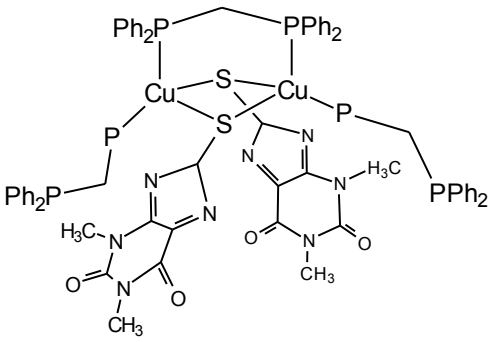

[1.3]

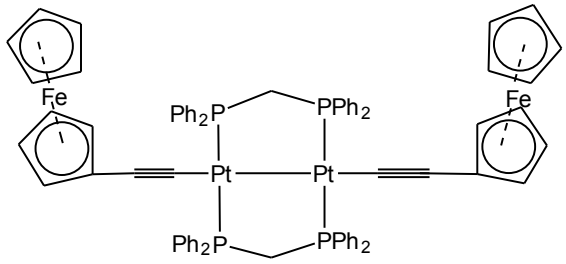

[1.4]

Figure 1.1 Example of complexes of dppm, with various bonding modes, exhibiting special properties.

In this section we will predominantly focus on the chemistry of deprotonated dppm and its resultant chemistry, giving special attention to *C*-metallation of the deprotonated ligand.

1.1.1 Synthetic routes

The first report on the preparation of dppm appeared in 1959 by Issleib.[9] In this synthesis, $NaPPh_2$ reacted with methylene chloride in a dioxane-THF mixture to yield dppm in good (78%) yield.
Dppm and other diphosphines are generally prepared according to the following reaction:

$$2\ R_2PM + X(CH_2)_nX \rightarrow R_2P(CH_2)_nPR_2 + 2\ MX$$

R = alkyl or aryl, X = halogen
M = alkali metal, n = integer

The metal organophosphides (R_2PM) used are prepared by either cleavage of triphenylphosphine, metallation of a secondary phosphane or reaction of chlorodiphenylphosphine with a metal.

1.1.2 Deprotonation of dppm

Of relevance to this work is the deprotonation and resultant chemistry of this diphosphine. It has long been known that dppm can be deprotonated by a strong base such as BuLi and MeLi to give the anion $[Ph_2PCHPPh_2]^-$.[10] The activation of the methylene protons led to a new trifunctional ligand which exhibits rich reactivity as witnessed over the past two decades.

The first preparative method for the deprotonation of dppm was reported in 1970 by Issleib.[10] One method involved the addition of BuLi to a solution of dppm in ether. After stirring a strong yellow solution was obtained which was immediately used for further reactions. In another method, he isolated the moisture sensitive lithiated ligand as a light yellow powder after refluxing a solution of dppm and BuLi in benzene. As demonstrated in some of his reactions, the lithiated dppm is an ambidentate nucleophile and gave mixtures of products due to attack on the carbon and phosphorus atoms when alkylated. Two years

later he showed that the anion is a strong ligand to transition metals when he used $Li[Ph_2PCHPPh_2]$ to synthesize $[Pd_2Cl_2\{CH(PPh_2)_2\}_2]$ and $[Pd_2(\eta^3\text{-}C_3H_5)_2\{CH(PPh_2)_2\}_2]$.[11] It was initially thought that the compounds were polymeric due to their insolubility in common organic solvents. Characterization was thus very difficult, almost impossible. The first of such compounds to be fully characterized was the trimeric Cu(I) derivative, $[Cu_3(\mu\text{-}Ph_2PCHPPh_2)_3]$**[1.5]**.

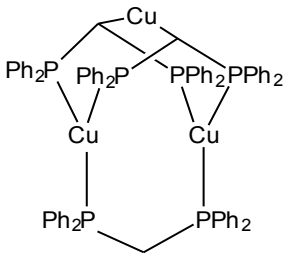

[1.5]

Figure 1.2 Trimeric Cu-dppm complex.

From X-ray crystallography the dppm ligands in complex **[1.5]** were found to be bridging two and three coordinate copper atoms such that both phosphorus atoms together with the carbanion participate in the coordinative bonding. Two phosphine ligands have an average P-C bond length of 1.84 Å , while the third has an equivalent bond length of 1.74 Å, suggesting the presence of double bond character within the dppm chelate.[12]

Since then more tractable derivatives have been reported in 1977[13] and 1980[14] by Schmidbaur. In these preparations bis(trimethylphosphane)-metal chlorides, $[MCl_2(PMe_3)]$ (M = Ni, Pd or Pt) were converted into the bis(dimethylphosphino)-methanides using lithiated dppm. These were again insoluble in common organic solvents but further reactions with trialkylphosphonium methylides, $(CH_3)_3PCH_2$, yielded the more soluble mixed bis(phosphine)-methanide/phosphonium bis(methylide) complexes, $[M\{CH(PPh_2)_2\}\{(CH_3)_2P(CH_2)_2\}]$ in high yields.

Browning[15] was the first to demonstrate that chelated dppm could be deprotonated. This was achieved by deprotonating $[PtCl(PEt_3)(Ph_2PCH_2PPh_2)]BF_4$ with NaH in THF. Air-stable yellow crystals were obtained which were analyzed to be the neutral deprotonated complex, $[PtCl(PEt_3)(Ph_2PCHPPh_2)]$.

Structural evidence obtained from an X-ray crystallographic analysis supported the formulation of the ligand as the anion. The two P-C(methylene) bonds are equal at 1.72 Å. The shortening of these bonds from an average of 1.83 Å (in other chelating dppm structures) is clear evidence of double bond character. Another structural feature typical of chelating dppm complexes is the strained chelate ring, as was seen by the small PMP and PCP angles of 98.6(5) and 69.65(8)°, respectively.

Deprotonation of dppm could also occur by hydrogen transfer to coordinated amine ligands, [16] or addition of an excess of a coordinating ligand,[17] and by hydrogen abstraction by a free radical (**Scheme 1.1**).[18] More recently examples of C-H activation by formation of a metal hydride were also reported.[19,20]

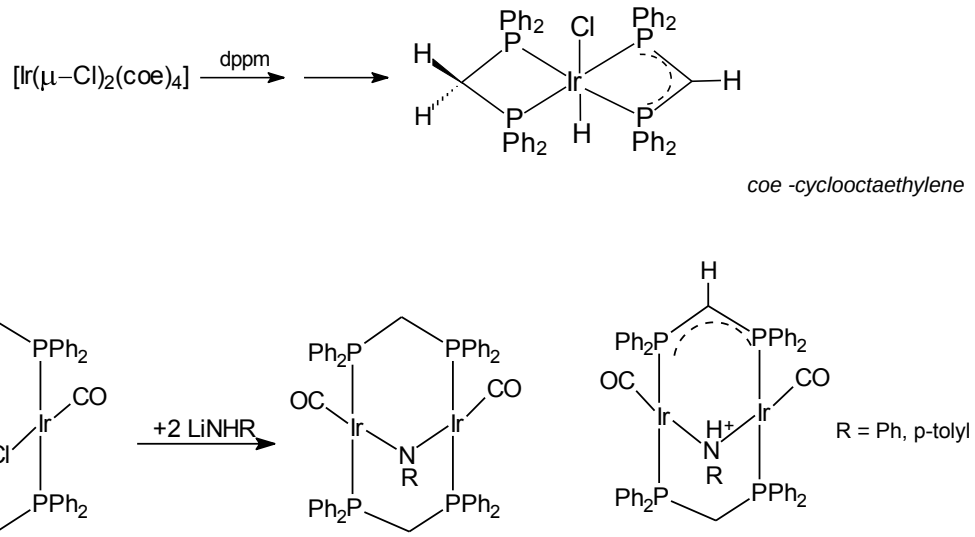

Scheme 1.1 Alternative methods for deprotonation of dppm.

1.1.3 Alkylation of dppm

Alkylating agents would generally give mixtures of products corresponding to attack on carbon and phosphorus. By coordination through both phosphorus atoms and subsequent deprotonation a carbanion which is not ambidentate would be formed as demonstrated by Browning[15] and Issleib[7]. Alkylation would then selectively occur at the carbon centre.

This was the methodology used by Al-Jibori and Shaw in their study on the alkylation of dppm coordinated to Group 6 metal carbonyls (**Scheme 1.2**).[21,22,23] The methylene proton was abstracted by using either BuLi or MeLi as the base. The resulting carbanions or lithio derivatives obtained were subsequently alkylated or acylated by electrophiles such as RX (X = halogen, R = Me, Et, MeSi or $PhCH_2$) and PhCOX, respectively, to give $[M(CO)_4(Ph_2CHRPPh_2)]$ or $[M(CO)_4(Ph_2CH(COPh)PPh_2)]$ when acylated. Double alkylation/methylation was achieved by using a large excess of the base and excess of the alkyl halide.[22]

These workers obtained similar chemistry with $[M(PPh_2CH_2PPh_2)]$ (M = Pt or Pd, X = Cl, Br or I). To prevent alkylation of the metal centre they used the bulky, non-nucleophilic base $LiN(SiMe_3)_2$ for deprotonations.[24]

The only reported example of alkylation of a bridged dppm dimer was achieved by treating the Rh-Os-dppm methanide with methyl triflate, $CH_3SO_3CF_3$.[25]

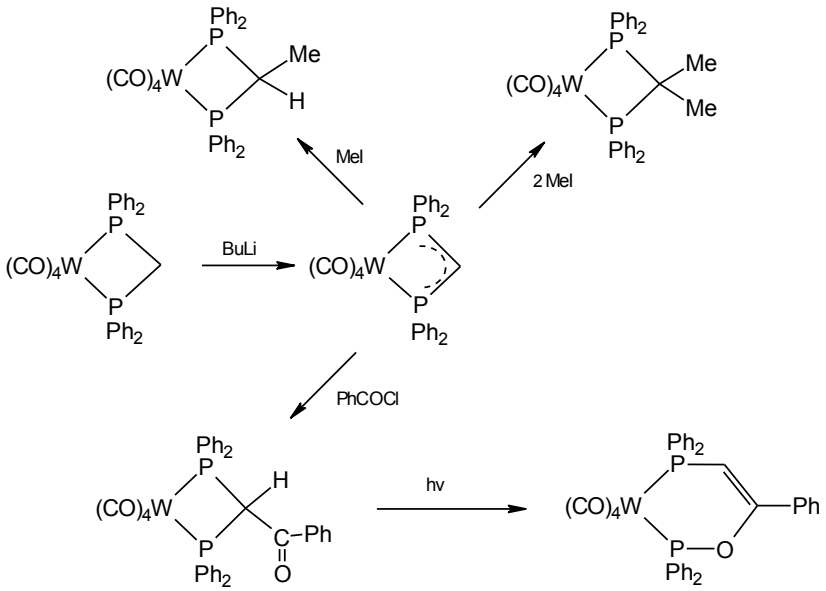

Scheme 1.2 Methodology for alkylation of coordinated dppm.

An interesting recent example involves the $TpIr(C_2H_4)_2$ complex, which on addition of dppm forms the methanide TpIr(dppm-H), due to the transfer of hydrogen to the metal

centre. Addition of MeI leads to the methylated cation and the neutral methylated complex (**Scheme 1.3**).[26]

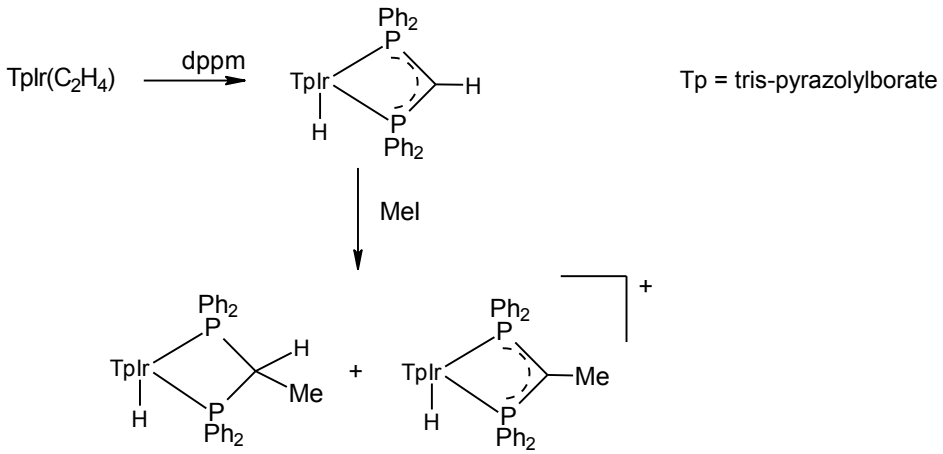

Scheme 1.3 Alkylation of Ir-dppm complex.

Fornies *et al*. showed that complexes of the type $[(C_6F_5)M(PPh_2CHPPh_2)]^-$(M = Pd or Pt) react with an excess of MeI to afford the corresponding *C*-mono- and di-alkylated derivatives.[27] Deprotonation of the neutral $[(C_6F_5)M(PPh_2CH_2PPh_2)]$ complexes was achieved by employing strong bases such as LDA or ^{t}BuLi as the more common ^{n}BuLi failed to yield the methanide derivative.

In contrast with the straightforward *C*-ethylation described by Shaw, ethylation of these methanides proved to be problematic. Reactions with benzylbromide gave poor yields and ^{n}PrI or ^{t}PrI failed to react. This behaviour was attributed to the electron-withdrawing nature of the C_6F_5 ligand, resulting in a decrease in electron density at the metal centre and a subsequently less nucleophilic carbanion. Another contributing factor is the decreasing alkylating power of the aliphatic series.

Many attempts at alkylating deprotonated dppm have been unsuccessful. For example, the cationic iron complex, $[FeL(dppm)(CNPh)_3]^{n+}$ (L = I or CNPh, n = 1 or 2) gives $[FeL(PPh_2CHPPh_2)(CNPh)_3]^{n-1}$ on deprotonation with KOH, which failed to react with MeI or stronger alkylating agents such as $Me_3O^+SbCl_6^-$.[28] Another example involves the dppm bridged Re dimer, $[Re_2(CO)_8(dppm)]$, which was deprotonated by $LiAlH_4$ in THF to

yield the corresponding methanide. This complex also showed surprising resistance towards electrophilic attack by organic halides such as MeI, Me_3SiCl and Ph_2PCl.[29]

Recently, Hogarth[30] and Dulai *et al*.[31] used the methodology reported by Shaw in the preparation of catalysts via *C*-alkylation of $[M(CO)_4(dppm)]$ (M = Cr, Mo or W). Diphosphine complexes with small bite-angles have been shown to be excellent catalysts for a number of catalytic processes.[32]

1.1.4 *C*-metallation of dppm

In 1990 Laguna published a review on bis(diphenylphosphino)methanide and its derivatives as ligands in gold chemistry.[33] What is evident from this report is the considerable coordination potential of the deprotonated ligand compared to free dppm. This would be expected in view of the ligand becoming a six electron donor on deprotonation and therefore having an additional donor site. In some instances even an eight electron donor ligand was reported due to double deprotonation. The Cu(I) derivative **[1.5]** mentioned earlier was the first example of the metallation of bis(diphenylphosphino)-methanide.[12] It is also a typical example of bonding occurring through all three donor atoms.

A literature search has revealed that there are nine transition metals which have been reported to have acted as electrophiles towards *C*-metallation, i.e. Au,[34,35-43] Ag,[344-35] Fe, [44,45] Rh,[46,47] Pd,[48] Pt,[49] Cu,[12] Os[45] and Hg[50]. Of these, Ag and Au received the most attention. Of the *p*-block metals only Al, Ga, Sn[51] and Pb[52] have been involved in *C*-metallation.

The possible coordination modes for the deprotonated ligand are given in **Figure 1.3**. Coordination modes **X** and **XII** are examples where double deprotonation was achieved, resulting in dppm acting as an eight-electron donor.

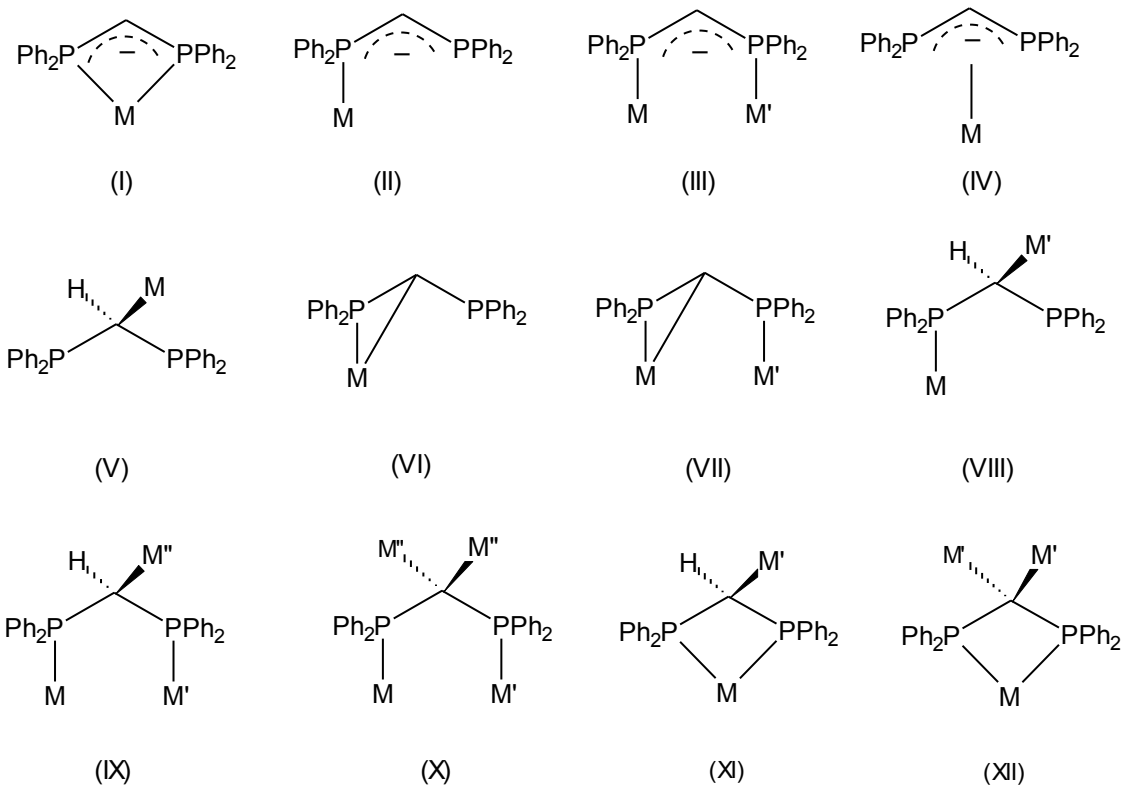

Figure 1.3 Bonding modes of deprotonated dppm.

1.1.4.1 Bonding modes (I), (II) and (III)

There are no examples in the literature of complexes displaying bonding mode (II). Examples of bonding modes (I) and (III) have been discussed earlier.

1.1.4.2 Bonding mode (IV)

Previous examples indicate that bis(diphenylphosphino)methanides have a strong tendency to form M-P σ bonds. We also encounter monodentate *C*-coordination. In 1986 Karsch and Muller reported a novel π-allyl type bonding mode for this ligand.[53] The reaction of $LaCl_3$ with the potassium salt of bis(diphenylphosphino)methanide yielded the first complex displaying π-allyl-like η^3-coordination for bis(diphenylphosphino)-methanide ligands.

An X-ray crystallographic analysis of this compound revealed that the lanthanide atom is surrounded by three bis(diphenylphosphino)methanide ligands in a trigonal planar arrangement. The distance from the central metal centre to the bis(diphenylphosphino)-methanide atoms vary between 2.790(4) and 3.035(1) Å. The La-C bonds were found to be slightly shorter than the La-P bonds. The P-C-P angles vary from 111.2(3) to 115.9(3)°. This complex has been shown to exhibit fluxional behaviour which is not uncommon for main group and transition metal bis(diphenylphosphino)methanide complexes.[54]

1.1.4.3 Bonding mode (V)

This type of bonding is very rare. This is ascribed to the ambidentate nature of deprotonated dppm as demonstrated by Issleib.[9] The only examples all appeared in 1986, when Lusser and Perringer prepared the mercurated derivative $[(Ph_2P)_2CH]_2Hg$ by the reaction of lithiated dppm with $HgCl_2$ in THF at 0°C.[55] The occurrence of *C*-metallation is interesting in view of the known ambidentate nature of deprotonated dppm. It was concluded that the bonding mode was not due to the preference of mercury for carbon but rather due to steric factors posed by the crowding aromatic rings. The compound was not isolated due to it being moisture sensitive. The bonding mode was established by ^{199}Hg and ^{31}P NMR. We have obtained stable derivatives of this compound where the phosphorus atoms are chelated to the $Cr(CO)_4$ fragment (see **Chapter 2**).

Two further examples involving *p*-block elements were independently reported by Balch[56] and Karsch[57]. Balch has shown that the treatment of $SnCl_2$ or $PbCl_2$ with lithiated dppm in THF produced $Sn[CH(PPh_2)_2]_2$ and $Pb[CH(PPh_2)_2]_2$, respectively.
X-ray crystallographic analysis showed that the two complexes are structurally similar. Of interest here is the unusual combination of one mondentate and one bidentate $(Ph_2P)_2CH^-$ ligand in the same molecule which results in tin and lead having very rare monomeric three-coordinate geometry. Stability in these complexes is ascribed to chelation to the phosphorus donors and the bulkiness of the monodentate ligand.

1.1.4.4 Bonding modes (VI) and (VII)

There appear to be no examples in the literature of dppm complexes exhibiting bonding mode VI, although Karsch[54,58] has reported the formation of lithio-, Co- and Fe-dimethylphosphino complexes with a strained MCP three-membered ring (see complex **[1.6]**, **Figure 1.4**).

The first example involving the deprotonation of bridging dppm and subsequent formation of a strained three-membered CH-P-M ring, bonding mode VII, appeared in 1980.[44,45] The complex $[Fe_2(\mu\text{-CO})(dppm)(CO)_6]$ was deprotonated by LiMe in refluxing THF. Subsequent treatment with CF_3COOH yielded $[(CO)_3Fe(\mu\text{-}PPh_2CHPPh_2)Fe(CO)_3]$ **[1.7]**.

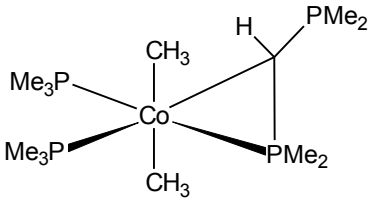

[1.6]

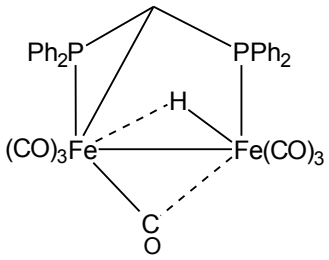

[1.7]

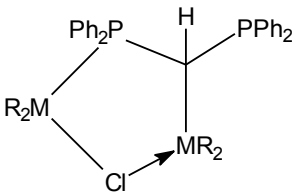

M = Al or Ga, R = Me or Et

[1.8]

Figure 1.4 Selected **c**omplexes displaying bonding modes (VI), (VII) and (VIII).

1.1.4.5 Bonding modes (VIII), (IX) and (X)

Metallation involving *p*-block elements is very rare. Examples of *C*-metallation involving Al and Ge were reported by Schmidbaur.[59] He has shown that lithiated dppm reacts with two equivalents of the dialkylchloro-alane or -gallane, R_2MCl (R = Me or

Et), to give coordination compounds with an unusual structure and fluxionality. Reactions with one molar equivalent of the allane or gallane gave a mixture of intractable material. A crystal study of the Al derivative, $[(Ph_2P)_2CH(EtAl)_2Cl]$, showed the molecule to exist as a five-membered P-C-Al-Cl-Al ring with a chiral centre at the carbon atom of the diphosphine (see complex **[1.8]**, **Figure 1.4**). Variable temperature NMR studies showed the phosphorus atoms to be equivalent due to the rotation of R_2MClMR_2 around the central P_2C-M bond, through alternating breaking and reformation of the M-P bond.

Lusser and Perringer[60,61] showed that *C*-mercuration occurs readily when $Hg(OAc)_2$ and $[Hg(Me_2SO)_6](O_3SCF_3)_2$ react with dppm to give the trimetallic mercury compound **[1.9]** (**Scheme 1.5**). Furthermore, reaction with another equivalent of $Hg(OAc)_2$ leads to the dimercurated product **[1.10]**. As opposed to compound **[1.9]**, **[1.10]** could not be isolated. The structures of these compounds were confirmed by ^{199}Hg and ^{31}P NMR. The occurrence of these reactions is quite significant, since dppm itself is not very acidic (pK_a = 29.9) and therefore requires a strong base for proton abstraction. It was proposed that the methylene hydrogens are activated by the highly electron withdrawing $(PPh_2HgOAc)^+$ groups.

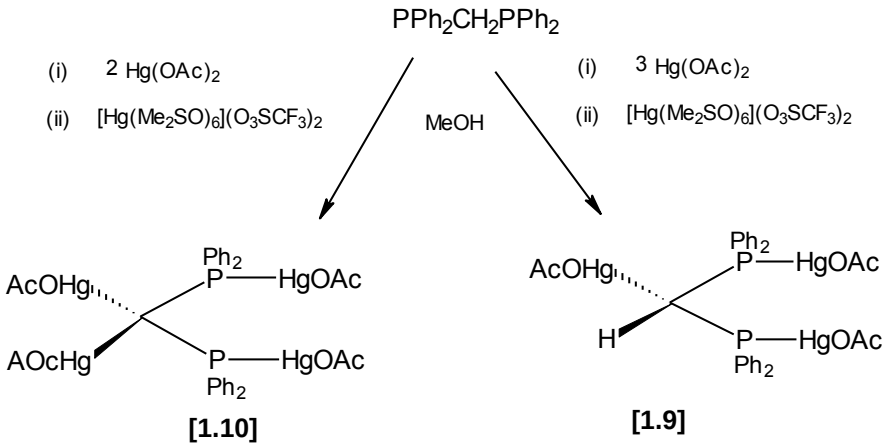

Scheme 1.5 Mercuration of uncoordinated dppm.

1.1.4.6 Bonding modes (XI) and (XII)

Uson and Laguna[31] were the first to report on the use of chelated dppm as a *C*-donor ligand to another metal centre. The cationic gold complex $[(C_6H_5)_2Au(dppm)]ClO_4$ was deprotonated using NaH or Na_2CO_3 in diethyl ether to yield the neutral gold bis(diphenylphosphino)methanide complex. Reacting this with either Au(I)- or Ag(I)-triphenylphosphine salts gave the bi- or tri-metallic complexes $[(C_6H_5)_2Au(Ph_2PCH(MPPh_3)PPh_2]ClO_4$ (M = Ag or Au) or $[(C_6H_5)_2Au(Ph_2PCH(MM´(PPh_3)_2)\ PPh_2]ClO_4$ (M = Ag, M´ = Au) **[1.11]**. A ring opening reaction was also encountered when this neutral goldbis(diphenylphosphino)-methanide derivative reacted with two equivalents of [AuXL] (X = halogen, L = tht or PPh_3). The P-C-P ring opens to yield the trinuclear derivative $[AuX(C_6F_5)_2\{PPh_2CH(AuL)PPh_2\}AuX]$. The structures of these compounds have been determined by X-ray crystallography. A distinguishing feature of the bimetallic gold complex compared to the unsubstituted derivative is the shorter P-C bond lengths for the bimetallic complex [1.815(6) Å, *cf.* 1.845(9) Å]. This shortening of the P-C bonds suggests significant double-bond character and is present in all related cationic bimetallic complexes and was attributed to the metal centre not being able to neutralize the excess electron density as effectively as the methylene hydrogen.

In 1986 Ruiz[37] showed that treatment of the ionic complex $[Fe(L)(CNPh_3)_3dppm]^{n+}$ with KOH in dichloromethane gave the bis(diphenylphosphino)methanide complex $[Fe(L)(CNPh_3)_3(dppm\text{-}H)]^{(n-1)+}$. Reacting this with Au^I or Ag^I triphenylphosphino complexes yielded bimetallic Fe cationic complexes. Reaction with two equivalents of $ClAuPPh_3$ yielded the trimetallic derivative $[Fe(L)(CNPh_3)_3\{PPh_2C(AuPPh_3)_2PPh_2\}]^{n+}$ **[1.12]**. The structure of the trimetallic complex where L = Cl has been determined and shows an interaction between the two gold atoms with a distance of 2.891(4) Å. This was also the first example of dppm acting as an eight-electron *C*-donor ligand.

Another noteworthy preparation is that reported by Nixon in 1986.[48] The synthesis of a novel bimetallic carbene complex derived from the reaction of $[PdCl_2(PhCN)_2]$ and $[Pt(PPh_2CHPPh_2)_2]$ is described. An X-ray crystallographic analysis showed the formation of an infinite chain carbene complex of alternating Pt and Pd units. The metal

centres in the chain are regarded as being three-coordinate Pd^0 and four-coordinate Pt^{II}. The Pd-C(carbene) bond length was also found to be shorter than that of other Pd carbene complexes.

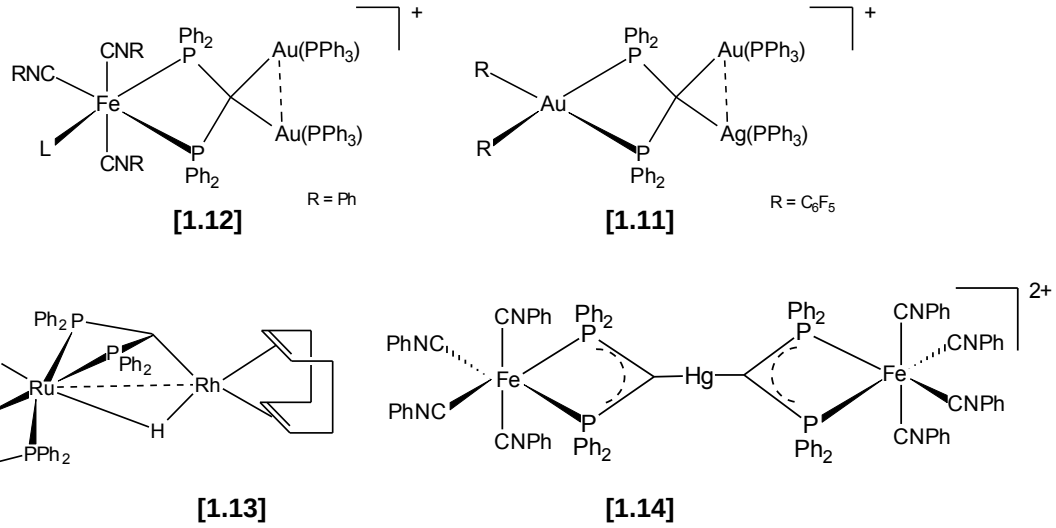

Figure 1.5 *C*-metallated complexes of coordinated dppm.

An important reaction is that of Chaudret *et al*. in their study on the preparation of heterobimetallic hydrido complexes.[46] The bimetallic complex $[RuRhH_2Cl(COD)(dppm)_2]$ exhibited remarkable reactivity, of which the most significant was its reactions with $KBH(sec\text{-}Bu)_3$ in THF. Under these conditions the bridging dppm undergoes deprotonation to form the methanide, which subsequently attacks the rhodium metal centre to form the complex $[RuRhH_2(PPh_2CHPPh_2)(dppm)]$ **[1.13]**. This is probably the only example where dppm bridges two metal centres through this type of coordination. It is also worth mentioning the effect that reagent basicity has in view of the fact that proton abstraction was not encountered for bases such as MeLi and $LiAlH_4$.

Coordinated dppm has also been shown to undergo mercuration by addition of HgI_2 to, for example, the methanide derivative $[Fe(CNPh)_4(PPh_2CHPPh_2)]^-$, deprotonated by KOH in dichloromethane, to yield $[Fe(CNPh)_4(PPh_2CHPPh_2)]_2Hg$ **[1.14]**.[50] The complex is air sensitive and readily reverts to the methanide precursor. Of interest is the fact that the P-C bond lengths indicate double bond character, as found for related metallated

complexes, implying that mercury does not neutralize the excess electron density as effectively as the methylene hydrogen.

Complexes exhibiting bonding mode XII are readily obtained by metallation of the doubly deprotonated, 8-electron donor ligand. Workers such as Ruiz and Laguna have shown that cationic metal-dppm precursors could readily undergo double deprotonation with an excess of KOH in dichloromethane. Addition of electrophiles such as Ag or Au, yield the desired heteronuclear complexes.

Crystallographic studies show the presence of geminal metal-metal interactions. The Fe-dppm complex **[1.12]** above shows Au-Au distances of 2.891 Å, which is close to the interatomic separation in metallic gold of 2.884 Å. Uson *et al*. reported a distance of 2.826 Å for the trimetallic gold complex $[Au(C_6F_5)_2\{(Ph_2P)_2C(AuPPh_3)_2\}]ClO_4$. These workers also prepared the heterotrimetallic complex $[Au(C_6F_5)_2\{(Ph_2P)_2C(AuPPh_3)(AgPPh_3)\}]ClO_4$. No crystal structure was reported for this complex.[33]

All examples of *C*-metallation discussed involve complexes where the chelating metal is in a non-zero oxidation state. The derivatives are also mostly ionic except in a few cases. Uson *et al.*[43] reported on the reaction of deprotonated $[M^0(CO)_4(dppm)]$ where M = Cr, Mo or W with gold(I) salts.

The above survey of dppm complex chemistry is not meant to be comprehensive or complete, but rather to impart a flavour for the wide-ranging adaptability of the ligand, especially focusing on aspects related to this thesis.

1.2 The chemistry of dithizone

1.2.1 Early work

Dithizone or 1,5-diphenylthiocarbazone (3-mercapto-1,5-diphenylformazan) is a violet-black solid, which is sparingly soluble in water and exhibits low solubility in most organic solvents to give strongly coloured solutions. It was first synthesized by Fischer in 1878, while investigating reactions of phenylhydrazine with carbon disulfide.[62] In later work he noticed that dithizone forms brilliantly coloured complexes with heavy metals.[63] About 40 years later, Bamberger reported an alternative route to the preparation of dithizone and some dithizonate complexes.[64]

In 1977, Irving published a review of dithizone and its application in the area of analytical chemistry, where it has been shown to be a very useful ligand in trace metal analysis, as well as extraction of heavy metals.[65,66] Since then, dithizone has received significant attention in the area of biological sciences[67,68] and analytical chemistry,[69,70,71] e.g. as optical sensors for environmental monitoring,[72] and by doping electrodes for selective metal analysis. [73,74] It has also been investigated for use as optical recording and display devices, photochromic dyes, photochromic films, glasses, or lenses.[75,76] The parent bis-dithizonate complex [Hg(Hdptc)$_2$] has already been established as a reusable optical recording medium for use in data processing, while the analogous zinc dithizonate has been shown to have semiconducting properties.[77] More recent work has shown the use of dithizone in the preparation of nanostructures.[78,79]

In organic solvents dithizone exists as a tautomeric equilibrium mixture of the thione and the thiol forms, giving rise to two intense absorption bands in the visible spectrum at ca. 450 and 620 nm (**Figure 1.6**).

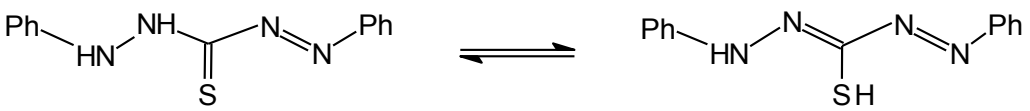

thione thiol

Figure 1.6 Thione and thiol forms of dithizone.

Dithizone behaves as a weak monobasic acid of *p*K ~ 4.5 towards certain metallic ions.[80] The resulting strongly coloured solutions of metal dithizonates are characterized by a single intense absorption band in the visible spectrum between 430 and 550 nm (**Figure 1.7**).

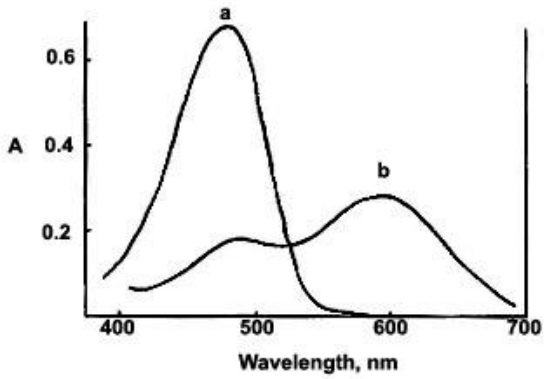

Figure 1.7 UV/Vis spectrum of the thiol, **a**, and thione, **b**, forms of dithizone.[81]

Irving, while investigating the use of dithizone in mercury determination, observed the colour change of a solution of mercury(II) bis(dithizonate), [Hg(Hdptc)$_2$], from orange-yellow to royal blue upon exposure to sunlight.[82] This photochromic effect was later reported on by Webb *et al.*[83], but it was Meriwether *et al.*[84] who found this phenomenon to be a general reaction of all metal dithizonates. However, besides mercury, the reverse reaction is too rapid to be observed visually.

1.2.2 Photochromism

Metal dithizonates exhibit photochromism, i.e. a reversible colour change, on irradiation (see **Figure 1.8**). However, it is only in the case of the mercury analogue where the half-life of the irradiated form is long enough to be investigated. The rates of the thermal return reaction for the other metals are too fast for conventional measurement. Meriwether[84] in his study of 24 metal dithizonate complexes has shown an approximate lifetime from 30 to 90 sec for the [Hg(Hdptc)$_2$] complex to less than 1 sec for the cadmium analogue. Flash studies revealed half lives of less than 50 µsec and 30 µsec for

$[Ni(Hdptc)_2]$ and [Tl(Hdptc)], respectively. Of all the complexes studied, only $[Hg(Hdptc)_2]$ is photochromic in the solid state, with a half life of return of several hours. On the basis of spectroscopic and kinetic studies, Meriwether *et al.*[85] proposed the equilibrium for the reversible colour change to involve a *trans-cis* isomerization about the C=N bond and the N-to-N hydrogen transfer of the ground state form **A** to give the excited form **B**. An alternative structure of the excited blue form was recently proposed on the basis of computational studies (isomer **D**).[86]

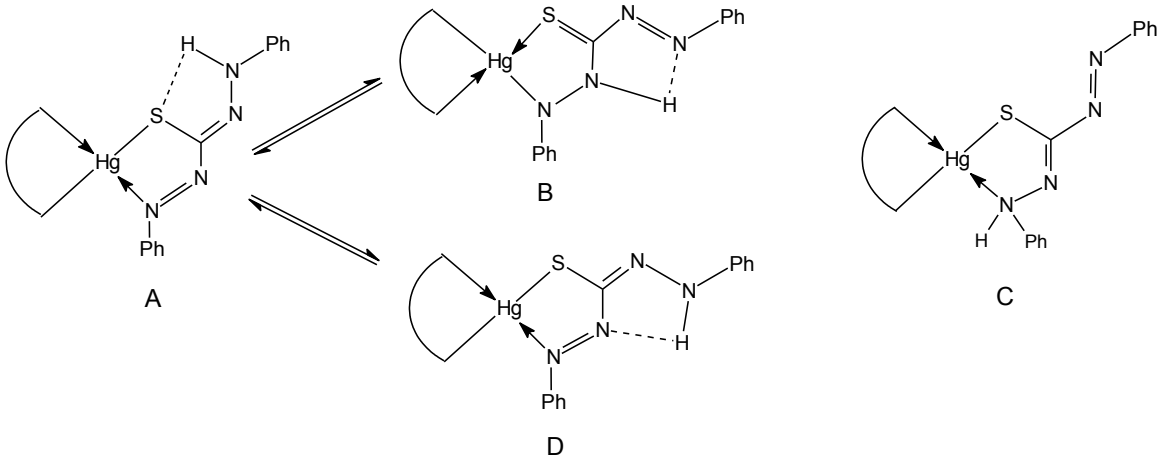

Scheme 1.6 Isomerism of dithizone in solution for the complex $[Hg(Hdptc)_2]$.

The reason for the red shift in **B** is proposed to be the rotation about the C=N double bond. [87]

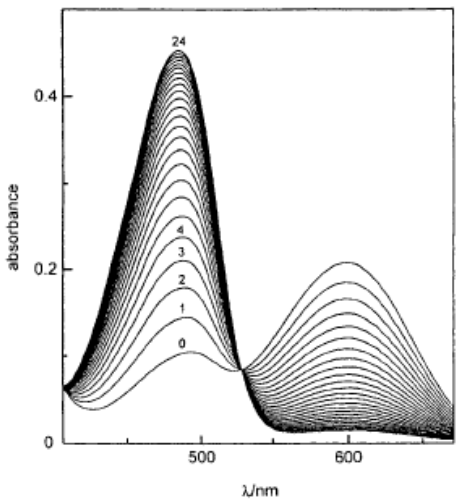

Figure 1.8 Typical visible absorption spectra of return reaction after irradiation of a mercury-dithizonate complex.[88]

More recently photochemical studies on [Hg(Hdptc)$_2$] showed that the excited form **B** could transform into another isomeric form, **C** (**Scheme 1.6**).[87] This assignment explained the shoulders observed in the longer wavelength bands at 580 and 590 nm. This confirmed a proposal made earlier by Meriwether[85] and Goesling[89] independently.

1.2.3 Metal dithizonate complexes

Since its introduction in 1925 there has been extensive debate on the structure of metal complexes with dithizone. Two forms were proposed, viz. keto and enol forms, with both adopting *N,N* coordination with a metal ion, giving rise to the so called "primary" and "secondary" dithizonates, respectively. The *N,N* coordination of the keto form was ultimately rejected in 1954 when Irving proved that *S,N* coordination occurs in metal complexes.[90] The structure of the enol form was still heavily debated twenty years later.[91,92] The first structural confirmation only appeared in 1989.[93]

In 1958 Harding established by means of X-ray diffraction the structure of [Hg(Hdptc)$_2$], confirming *N,S* chelation.[94] Subsequent X-ray crystallographic studies were reported by Bryan and Knoff in 1961,[95] Laing and Sommerfield in 1971[96] and Irving and Mawby 1971[97] on Cu-, Ni- and Zn-dithizonate complexes, respectively. More recently Ma *et al*. reported on the structure of the organometallic tin bis(Hdptc)(di-n-butyl) complex, which shows a distorted octahedron around the metal centre.[98]

While the bonding and structure of dithizonate complexes have been established, it is only fairly recently that alternative bonding modes were observed. Examples of these bonding modes are given in **Figure 1.9**.

In 1987 Singh *et al*.[99] reported the preparation of a series of dithizonate complexes of titanium in which dichlorobis(methylcyclopentadienyl)titanium(IV) reacts with 1,5-diarylthiocarbazones in the presence of triethylamine to give mono- and di-substituted complexes. An excess of triethylamine yields the secondary dithizonates. However, no structures were reported. The bonding mode of the secondary complex **[1.15]** was given tentatively as shown in **Figure 1.10**.

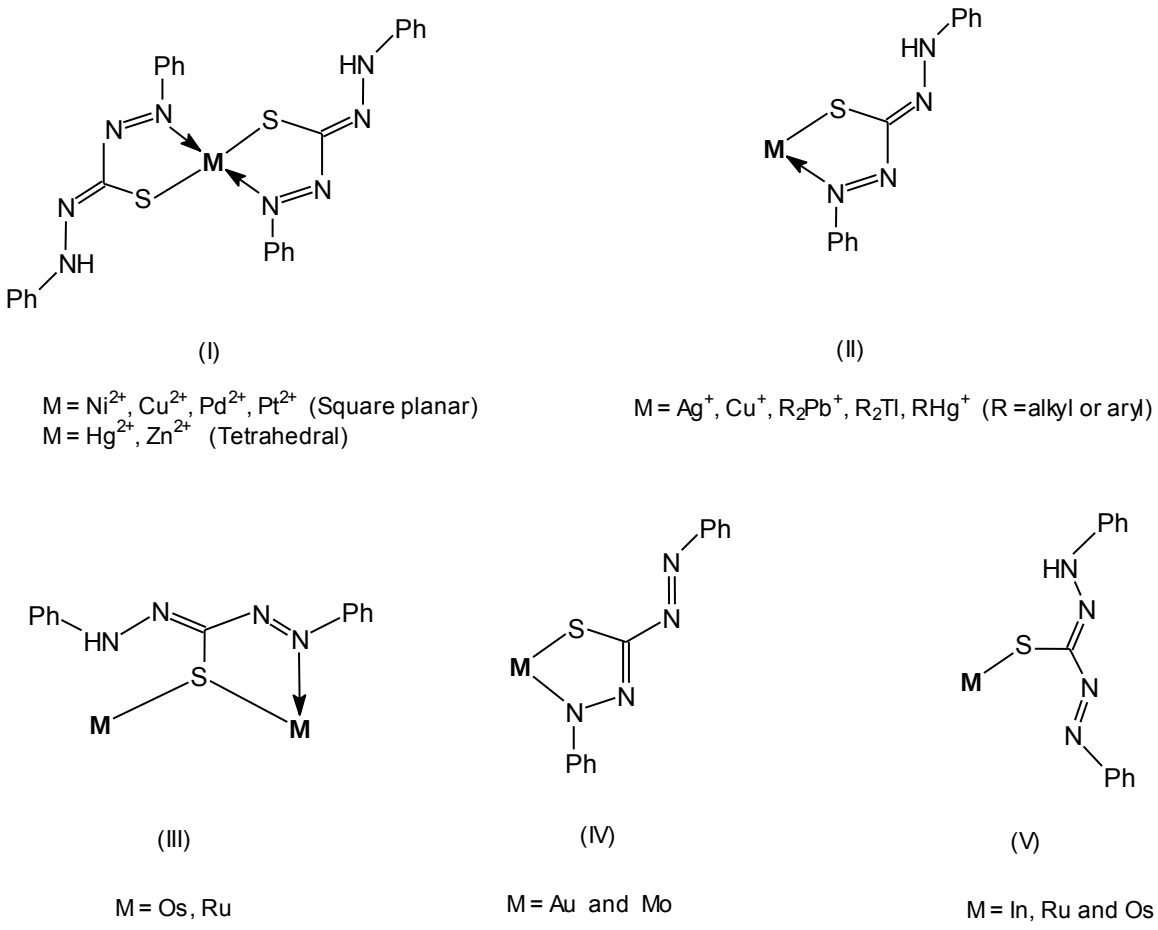

Figure 1.9 Coordination modes of dithizone.

In 1983 Harrowfield reported the first example of a metal dithizonate complex with dithizonate acting as a monodentate chelate ligand.[100] In the [In(Hdptc)$_3$] complex, two dithizone ligands participate in *N,S* coordination, while the third shows unidentate *S*-coordination. In their preparation of Ru and Os carbonyl cluster complexes, Kong and Wong characterized a similar unidentate *S*-coordination of dithizone **[1.16]**.[101,102] What makes the structure more significant is that the dithizone ligand also serves to bridge two Os centres. An X-ray crystallographic structure of the bis-dithizonate complex, [Ru(bipy)$_2$(Hdptc)] **[1.17]**, prepared by Walsh, also shows the ligand in monodentate *S*-coordination.[103] The three aforementioned structures show *trans-trans* geometry about the *N*-atoms, similar to that found in bidentate Hdptc$^-$ coordination.

In 1989, Liu and Zubieta reported the first example of dithizone existing in its enol or secondary form. In their work, dithizone was reacted with α-$(BuN_4)_4[Mo_8O_{26}]$ to yield $[MoO_2$[PhNHNC(S)NNPh}{PhNNC(S)NNPh}]**[1.18]**.[93] Of significance is the fact that it is also the first dithizonate complex in which dithizone exists in both keto and enol forms.

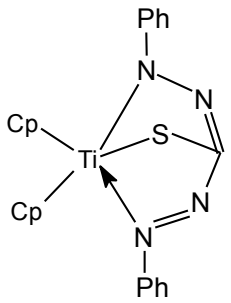

[1.15]

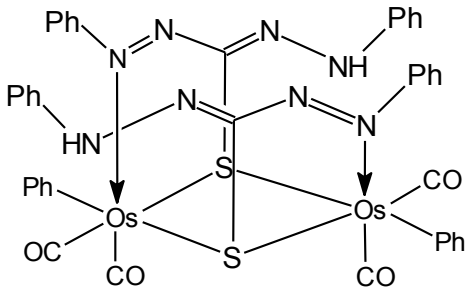

[1.16]

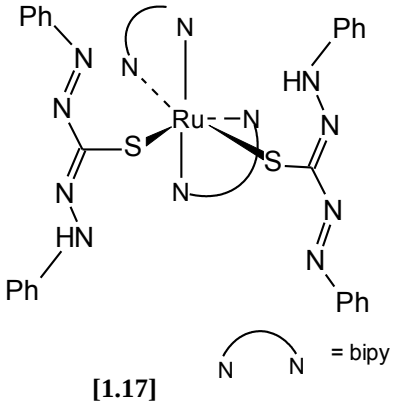

[1.17]

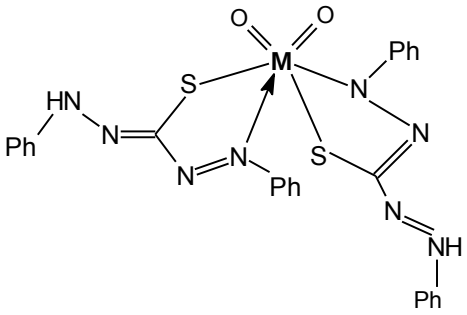

[1.18]

Figure 1.10 Dithizonate complexes.

More recently, Abram reported the structure of the gold-dithizonate complex [Au(H-damp-C^1){PhNNC(S)NNPh}(Smetetraz)] (Smetetraz = 2-methylmercaptotertrazole), only the second example in the literature of a complex of dithizone in its enol form.[104] In this paper it was also shown that the keto gold-dithizonate complex [Au(H-damp-C){PhNHNC(S)NNPh}Cl]Cl [(H-damp-C) = 2-(dimethylammonium-methyl)phenyl], undergoes deprotonation of dithizone by the reaction of sodium-2-methylmercaptotetrazolate to form the target zwitterionic complex.

1.3 The chemistry of dithiolenes

1.3.1 Early work

Dithiolenes are essentially 1,2-dithio ligands in which the sulfur donor atoms are connected by an ethylene bridge, with the general formula, $[S_2C_2R_2]$. Depending on the choice of *R*, various dithiolene salts can be obtained of which the ones receiving most attention are $dmit^{2-}$, $dmid^{2-}$and mnt^{2-}. There are various synthetic routes to the preparation of dithiolenes (**Scheme 1.8**). For example, the sodium salt of maleonitriledithiolene, Na_2mnt, which is the only dithiolene stable for an extended period, is conveniently prepared by the reaction of sodium cyanide and DMF.[105,106]

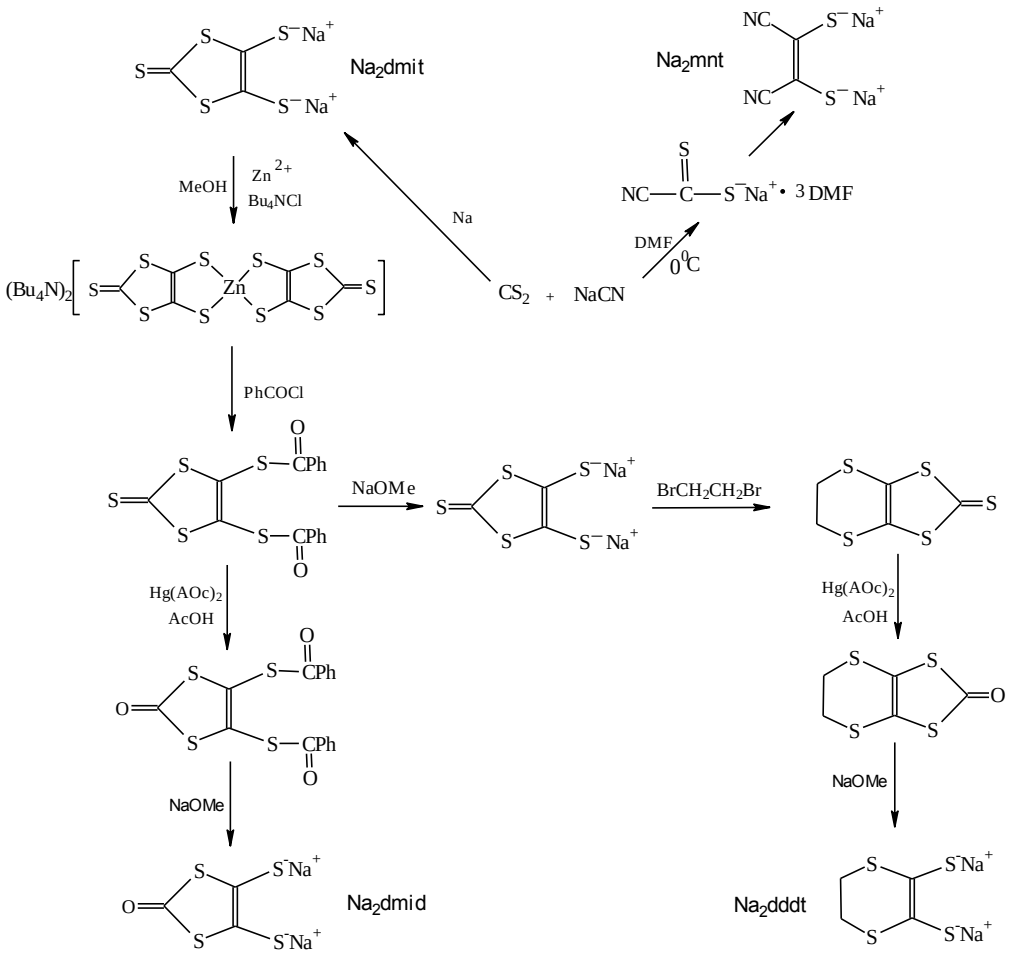

Scheme 1.8 Synthetic routes for the preparation of the most widely used dithiolenes.

The most widely studied dithiolene, $dmit^{2-}$, is conveniently synthesized by the reduction of CS_2 with sodium metal in DMF, to yield 1,3-dithiol-2-thione-4,5-dithiolate, which is stabilized by precipitation as the $[Zn(dmit)_2]^{2-}$ salt. Further stability is obtained by reaction of the salt with benzoyl chloride, giving a derivative which is readily converted into a salt by the addition of a base.[107] The benzoyl derivative can be easily converted into other useful dithiolenes by cleavage with a base, followed by the addition of an appropriate alkylhalide (see **Scheme 1.8**).

1.3.2 Complexes of dithiolenes

The first preparation of metal-dithiolene complexes was reported by Clark and co-workers in 1936, who used the ligand as an analytical reagent for the determination of zinc, mercury and cadmium.[108,109] In 1956, Bahr and Schleitzer reported the preparation of metal chelates of maleonitriledithiolene (mnt^{2-}).[105,110] This was followed by the preparation of metal-dithiolene complexes other than mnt^{2-}, by authors such as Schrauzer[111], Gray[112] and Davison.[113]

These complexes were found to possess a high degree of electronic delocalization which resulted in high thermal and photochemical stability and intense electronic transitions at unusually low energies. These properties, coupled with its highly reversible redox chemistry, led to the rapid expansion in the field of dithiolene chemistry, evidenced by the numerous reviews that followed.[114-123]

While dithiolene chemistry has predominantly focused on the preparation of complexes with transition metals, dithiolenes have been shown to form complexes with main-group[124,125,126,127,128] and *f*-block[129,130,131] elements just as readily. For example, Group 13 metal trihalides react with mnt^{2-} to give complexes such as $[Ga(mnt)_2]^{2-}$ and $[Tl(mnt)_3]^{3-}$. Urliguie and co-workers have prepared mononuclear, infinite chain or honeycomb complexes of Ce(III), Ne(III) and U(IV) with $dddt^{2-}$.[130,132] Other authors such as Tang *et al*. found that the reaction of lanthanum trichlorides with K_2dmit and 1,10-phenanthroline resulted in the formation of mono-dithiolene complexes of the type $K_2[LnCl_3(dmit)(phen)]$ (Ln = La, Er, Gd, Nd, Sm or Y). These complexes were shown to

behave as insulators but could readily be transformed into semiconductors by doping with iodine.[133]

While the majority of dithiolene complexes are symmetrical and exist as *S,S*-chelates, unsymmetrically substituted **[1.22]**[134] and bridging dithiolene complexes,[135,136,137] e.g. **[1.19]** and **[1.21]**, are also encountered. Dithiolenes have also been shown to exist in unusual monodentate coordination modes, e.g. **[1.23]** (**Figure 1.11**).[138]

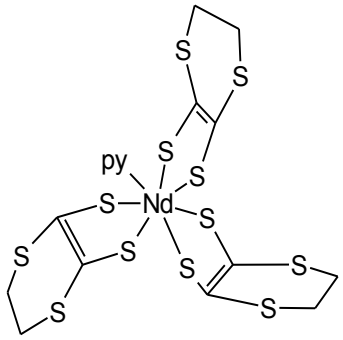

[1.20]

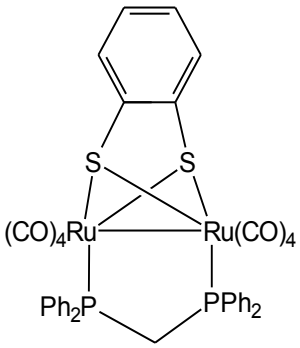

[1.19]

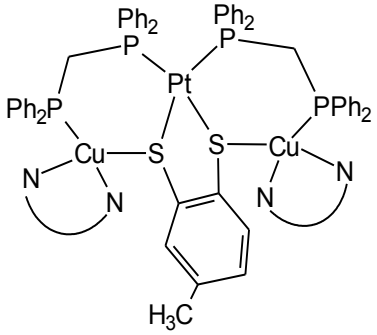

[1.21]

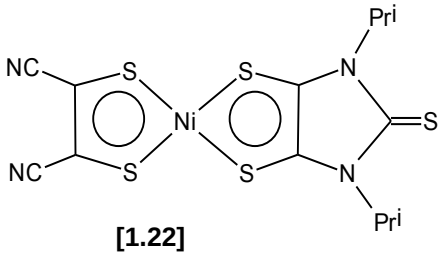

[1.22]

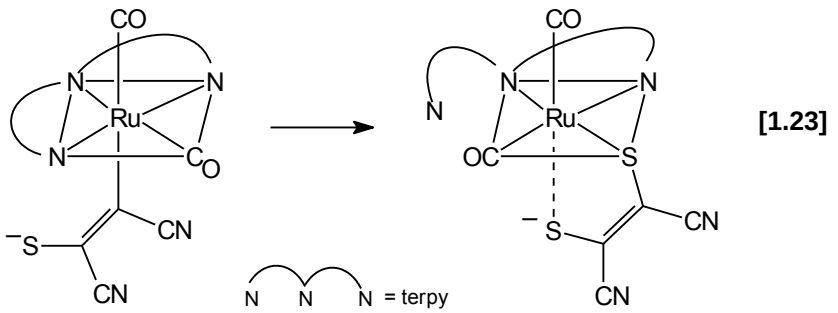

[1.23]

Figure 1.11 Complexes showing various bonding modes of dithiolenes

1.3.3 Electrochemistry

Davison *et al.*[139,140] was the first to observe the electrochemistry of dithiolenes while investigating some of the first dithiolene complexes prepared, viz. the neutral $Ni(S_2C_2Ph_2)_2$ and the ionic $[Ni(mnt)_2]^-$. Both complexes were shown to undergo reversible, two-step, one-electron redox processes, thereby revealing the rich electrochemistry of these complexes.

Kajitani and Nomura[141] described the coordination mode of dithiolene ligands as having three types of resonance structures, i.e. the dithioketone (A), the dithiosemiquinone (B) and the dithiolate (C) forms. Interconversion between these structures takes place via a multistep redox process.

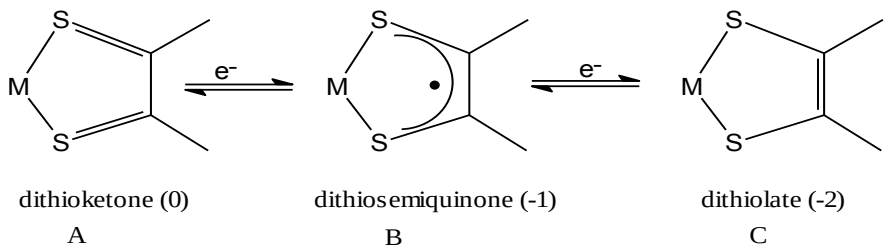

Scheme 1.9 Resonance forms of dithiolene.

1.3.4 Applications

The interest in dithiolenes was re-ignited by the discovery of superconduction in organic charge transfer salts containing the tetrathiofulvalene (TTF) moiety, which is essentially composed of two bridging 1,2-dithiolene ligands.[142,143] Since then dithiolenes have found potential application in other areas of advanced materials chemistry such as magnets,[144,145] infrared dyes,[146] non-linear optical material (NLO),[147] liquid crystals[148] and catalysis.[149] More recently, these ligands attracted interest in the area of biology, e.g. as models of metalloenzymes, since most known Mo- and W-containing enzymes feature the molybdopterin cofactor, i.e. a dithiolene linked to a nucleotide.[150,151,152]

1.3.4.1 Conduction and magnetism

Bis-dithiolene metal complexes share an isolobal similarity with TTF as the bonding orbitals of the metal mimic the ethylene bridge of TTF.

Conductors

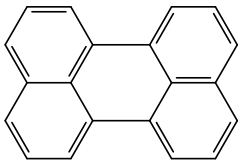

Perylene

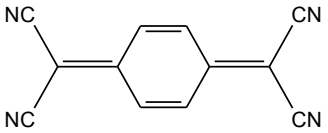

TCNQ

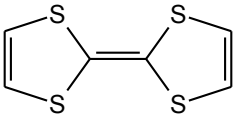

TTF

Superconductors

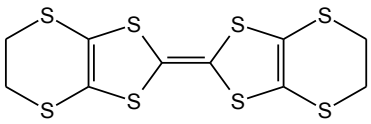

BEDT-TTF

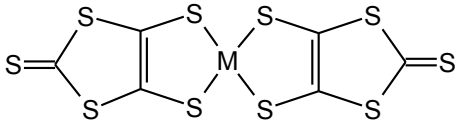

$M(dmit)_2$

Figure 1.12 Examples of early organic and inorganic conductors and superconductors.

TTF was one of the first organic conducting materials identified, the other being pyrelene, with potassium tetracyanoplatinate (KCP) being representative of a range of inorganic conducting materials. The common structural feature of these molecules is their one-dimensionality, i.e. the stacking of the molecules along one direction in the crystal, where intermolecular interaction exists along the stack only.

The first metal dithiolene complex to exhibit superconductivity at low temperatures was reported in 1981 by Ribsa and Cassoux.[153] To date there are nine complexes showing superconducting behaviour, all sharing one common feature in that they all contain the $dmit^{2-}$ ligand. These complexes all contain a d^8 metal ion and adopt two common structures, viz. $[cation]_{0.5}[M(dmit)_2]$, [154-157] where the cation is tetra-alkyl-N, -P or -Sb, and $D[M(dmit)_2]$,[158-161] where D is a donor group such as TTF.

The ligand $dmit^{2-}$, being sulfur rich, forms complexes which exhibit different behaviour due to the chalcogen-chalcogen interactions between the molecules of adjacent stacks, resulting in 2-dimensional-systems.

Maleonitrile and its metal complexes, likewise, have received considerable attention in the area of conduction and magnetism, due to the presence of a highly delocalised system which extends into the nitrile groups. Complexes such as $[NH_4][Ni(mnt)_2]$, for example, exhibit ferromagnetism.[162] Charge transfer salts of $[M(mnt)_2]$ with 4,9-bis(1,3-benzodithiol-2-ylidene-4,9-dihydronaphthol[2,3-c]-1,2,5-thiadiazole (BDNT), e.g. $[BDNT]_2[M(mnt)_2]$ (M = Ni, Pd, Au or Pt) has been shown to manifest significant conductivity.[163]

1.3.4.2 Non-linear optics

Dithiolene complexes have over the past decade also been studied as materials for optical devices, mainly due to their delocalized structure, their various oxidation states and their high thermal stability. Electron transfer between the metal and ligand has been shown to give rise to intense near-IR absorption transitions. It is especially unsymmetrical dithiolene complexes that display appreciable nonlinear optical properties.[164,165]

There is a vast literature devoted to dithiolene ligands and their metal complexes; this section has merely touched on their particularly useful properties and applications with a view to providing some background for the work described in the present thesis.

1.4 Aims of the study

We have shown that there is a great interest in the preparation of complexes with metal centres in close proximity. Having metals in close proximity could impact on the reactivity of the resulting complex, or result in electronic communication between redox centres, which could be exploited in the area of catalysis or the formation of new materials. The ligand dppm has been shown to be a very versatile ligand and has been extensively used for its ability to coordinate metals in close proximity. Moreover, we have shown that the versatility of deprotonated dppm allows for the preparation of bi- and tri-metallic systems through *C*-metallation.

All such systems, but one, exhibited the chelating metal centre in a high oxidation state. In **Chapter 2** and **Chapter 3** we set out to investigate the reactivity of Group 6 metal tetracarbonyls $[(CO)_4M(dppm)]$ (M = Cr Mo or W), and Group 10 dithiolenes, $[(R_2C_2S_2)M(dppm)]$ (M = Pd or Pt), toward *C*-metallation. Mercury salts were employed as the electrophile for their versatility, since the electronic nature of mercury could be altered or 'tuned' by using different substituent groups, allowing investigation of effects. Moreover, it is of interest to assess whether the chelate ring facilitates any electronic communication between the metal/redox centres. Metal carbonyls and metal dithiolenes are ideal precursors as the presence of the carbonyl group or the dithiolene moiety serve as probes providing an additional tool, via spectroscopic and electrochemical methods, to assess changes in electron density within the molecule.

The ligand dithizone itself still warrants further investigation into its structural properties, and we sought to use X-ray crystal structure analysis and DFT calculations to provide new information on dithizone and its anion. This will allow for a better understanding of the reactivity of these molecules. This will be covered in **Chapter 4**.

Photochromism in dithizonate complexes is currently limited to mercury complexes. We will seek to prepare mixed dithizonate complexes and investigate the possibility of obtaining photochromic complexes with Pd and Pt as metal centres. This is covered in **Chapter 5**.

In the latter part of this Introduction, we have briefly dealt with the growing interest in hybrid systems, i.e. combining ligand systems with different physical properties to prepare molecules where there is a co-existence of two or more physical properties. To this end we set out to prepare, as a preliminary investigation, long-chain benzylidine complexes as potential mesogenic material. If successful, the liquid crystalline material will be combined with, for example, the photochromic dithizone or electron-rich dithiolene ligands. We will also investigate the preparation of mixed dithiolene-dithizone Hg and Pt complexes, therefore combining the redox activity of dithiolenes with the photochromism of dithizone. The resultant complexes will be investigated by spectrophotometric and electrochemical techniques to assess their redox and photochromic behaviour (**Chapter 6**).

All complexes will be characterized using a wide range of spectroscopic techniques. Electrochemical investigations will be conducted to assess the presence of electronic communication within complexes or where complexes have redox centres. X-ray crystallographic studies will be done to assess any special structural features molecules may have. Computational techniques will be employed as a tool in cases where support and/or clarification of spectroscopic and crystallographic findings are required.

REFERENCES

1 R. J. Puddephatt, *Chem. Soc. Rev.*, 1983, **12**, 99.

2 B. Chaudret, B. Delavaux and R. Poilblanc, *Coord. Chem. Rev.*, 1988, **86**, 191.

3 C. Tai, J. Pitts, J. C. Linehan, A. D. Main, P. Munshi and P. G. Jessop, *Inorg. Chem.*, 2002, **41**, 1606.

4 E. Colacio, R. Cuesta and J. M. Moreno, *Inorg. Chem*., 1997, **36**, 1084.

5 W. L. Tan, H. G. Zheng, Q. H. Jin, G. C. Jin, W. Ji, D. L. Long and X. Q. Xin, *Polyhedron*, 2000, **19**, 1545.

6 L. Hore, C. J. McAdam, J. L. Kerr, N. W. Duffy, B. H. Robinson and J. Simpson, *Organometallics*, 2000, **19**, 5039.

7 J. H. K. Yip, J. Wu, K. Wong, K. P. Ho, C. S. Pun and J. J. Vittal, *Organometallics*, 2002, **21**, 5292.

8 M. I. Bruce, F. de Montigny, M. Jevric, C. Lapinte, B. W. Skelton, M. E. Smith and A. H. White, *J. Organomet. Chem.*, 2004, **689**, 2860.

9 K. Issleib and D. W. Muller, *Chem. Ber*, 1959, **92**, 3175.

10 K. Issleib and H. P. Abicht, *J. Prakt. Chem.*, 1970, **312**, 456.

11 K. Issleib, H. P. Abicht and H. Winkelmann, *Z. Anorg. Allg. Chem.*, 1972, **388**, 89.

12 A. Camus, N. Marsich, G. Nardin and L. Randaccio, *J. Organomet. Chem.*, 1973, **60**, C39.

13 J. Basset, J. R. Mandl and H. Schmidbaur, *Chem. Ber.*, 1980, **113**, 1145.

14 H. Schmidbaur and J. R. Mandl, *Angew. Chem.*, 1977, **16**, 640.

15 J. Browning, G. W. Bushnell and K. R. Dixon, *J. Organomet. Chem*., 1980, **198**, C11.

16 C. Ye and P. R. Sharp, *Inorg. Chem.*, 1995, **34**, 55.

17 K. D. Wells, R. McDonald, M. J. Ferguson and M. Cowie, *Organometallics*, 2011, **30**, 2654.

18 J. R. Torkelson, O. Oke, J. Mutitu, R. McDonald, M. Cowie, *Organometallics*, 2000, **19**. 854.

19 J. S. Wiley and D. M. Heinekey, *Inorg. Chem*., 2002, **41**, 4961.

20 C. Tejel, M. A. Ciriano, S. Jimenez, L. A. Oro, C. Graiff and A. Tiripicchio, *Organometallics*, 2005, **24**, 1105.

21 S. Al-Jibori and B. L. Shaw, *J. Chem. Soc., Chem. Commun.*, 1982, 286.

22 S. Al-Jibori and B. L. Shaw, *Inorg. Chim. Acta.*, 1983, **74**, 235.

23 S. Al-Jibori, M. Hall, A. T. Hutton and B. L. Shaw, *J. Chem. Soc., Dalton Trans.*, 1984, 863.

24 S. Al-Jibori and B. L. Shaw, *Inorg. Chim. Acta.*, 1982, **65**, L123.

25 B. T. Steenberg, R. W. Hilts, G. Moro, R. McDonald and M. Cowie, *J. Am. Chem. Soc.*, 1995, **117**, 245.

26 S. Jackson and D. M. Heinekey, *Inorg. Chem*., 2002, **41**, 4961.

27 L. R. Falvello, J. Fornies, R. Navarro, A. Rueda and E. P. Urriolabeitia, *Organometallics*, 1996, **15**, 309.

28 V. Riera and J. Ruiz, *J. Chem. Soc., Dalton Trans.*, 1990, 1607.

29 R. Dominguez, T. J. Lynch and F. Wang, *J. Organomet. Chem.*, 1988, **338**, C7.

30 G. Hogarth and J. Kilmartin, *J. Organomet. Chem*, 2007, **692**, 5655.

31 A. Dulai, H. de Bod, M. J. Hanton, D. M. Smith, S. Downing, S. M. Mansell and D. F. Wass, *Organometallics*, 2009, **28**, 4613.

32 A. S. Singh, B. M. Bhanage and J. M. Nagarkar, *Tet. Lett.*, 2011, **52**, 2383.

33 A. Laguna and M. Laguna, *J. Organomet. Chem.*, 1990, **394**, 743.

34 R. Uson, A. Laguna, M. Laguna, B. R. Manzano, P. G. Jones and G. M. Sheldrick, *J. Chem. Soc., Dalton Trans.*, 1984, 839.

35 R. Uson, A. Laguna, M. Laguna, M. Concepcion Gimeno, P. G. Jones, C. Fittschen and G. M. Sheldrick, *J. Chem. Soc., Chem, Commun.*, 1986, 509.

36 E. J. Fernandez, M. Concepcion-Gimeno, P. G. Jones, A. Laguna, M. Laguna and J. M. Lopez-de-Luzuriaga, *J. Chem. Soc., Dalton Trans.*, 1992, 3365.

37 M. Concepcion-Gimeno, P. G. Jones, A. Laguna, M. Laguna, *J. Chem. Soc., Dalton Trans*, 1993, 2223.

38 R. Uson, A. Laguna, M. Laguna, B. R. Manzano, P. G. Jones and G. M. Sheldrick, *J. Chem. Soc., Dalton Trans.*, 1985, 2417.

39 E. J. Fernandez, M. Concepcion-Gimeno, P. G. Jones, A. Laguna, M. Laguna and J. M. Lopez-de-Luzuriaga, *Angew. Chem. Int. Ed. Engl.*, 1994, **33**, 87.

40 V. Riera and J. Ruiz, *J. Organomet. Chem.*, 1986, **310**, C36.

41 M. Concepcion-Gimeno, J. Jimenez, P. G. Jones, A. Laguna, M. Laguna, *Organometallics*, 1994, **13**, 2508.

42 V. Riera and J. Ruiz, *J. Chem. Soc., Dalton Trans.*, 1990, 1607.

43 E. J. Fernandez, M. Concepcion Gimeno, P. G. Jones, A. Laguna, M. Laguna and E. Olmos, *Inorg. Chim. Acta*, 1995, **238**, 173.

44 G. M. Dawkins, M. Green, J. C. Jeffery and F. G. A. Stone, *J. Chem. Soc., Chem. Commun.*, 1980, 1120.

45 G. M. Dawkins, M. Green, J. C. Jeffery and F. G. A. Stone, *J. Chem. Soc., Dalton Trans.*, 1983, 499.

46 H. Benlaarab, B. Chaudret, F. Dahan and R. Poilblanc, *J. Organomet. Chem.*, 1987, **320**, C51.

47 K. D. Wells, R. McDonald, M. J. Ferguson and M. Cowie, *Inorg. Chem*, 2011, **50**, 3523.

48 S. Al-Resayes, P. B. Hitchcock and J. F. Nixon, *J. Chem. Soc., Chem. Commun.*, 1986, 1710.

49 M. P. Brown and A. Yavari, *J. Organomet. Chem*., 1983, **256**, C19.

50 J. Ruiz, R. Aruaz, V. Riera, M. Vivanco, S. Garcia-Granda and E. Perez-Carreno, *J. Chem. Soc., Chem. Commun.*, 1993, 740.

51 H. H. Karsch, A. Appelt and G. Hanika, *J. Organomet. Chem.*, 1986, **312**, C1.

52 A. L. Balch and D. E. Oram, *Inorg. Chem*., 1987, **26**, 1906.

53 H. H. Karsch, A. Appelt and G. Muller, *Angew. Chem. Int. Ed. Engl.*, 1986, **25**, 823.

54 H. H. Karsch, *Chem. Ber.*, 1984, **117**, 783.

55 M. Lusser and P. Peringer, *J. Organomet. Chem.*, 1986, **312**, C61.

56 A. L. Balch and D. E. Oram, *Organometallics*, 1986, **5**, 2159.

57 H. Karsch, A. Appelt and G. Muller, *Organometallics*, 1986, **5**, 1664.

58 H. H. Karsch, B. Deubelly and G. Muller, *J. Organomet. Chem*., 1988, **352**, 47.

59 H. Schmidbaur, S. Lauteschlager and G. Muller, *J. Organomet. Chem.*, 1985, **281**, 33.

60 M. Lusser and P. Perringer, *Organometallics*, 1984, **3**, 1916.

61 M. Lusser and P. Perringer, *J. Organomet. Chem.*, 1986, **301**, 269.

62 E. Fischer, *Annalen*, 1878, **190**, 67.

63 E. Fisher and E. Besthorn, *Annalen*, 1882, **212**, 316.

64 E. Bamberger, R. Padova and E. Oremerod, *Annalen*, 1926, **446**, 260.

65 H. M. N. H. Irving, *Dithizone, Analytical Sciences Monograph No.5, The Chemical Society, London*, 1977.

66 H. M. N. H. Irving, *CRC Crit. Rev. Analyst. Chem.*, 1980, **8**, 321.

67 G. Basta, L. Racancchi, F. Mancuso, L. Guido, G. Macchiaulo, G. Luca, G. Calabrese , P. Brunetti and R. Calafiore, *Transpl. Proc.*, 2004, **36**, 609.

68 L. Cortes, C. K. Y. A. Okio and P. F. B. Brandao, *Phoshorus, Sulphur and Silicon*, 2011, **186**, 1356.

69 H. Yu, H. Song and M. Chen, *Talanta*, 2011, **85**, 625.

70 F. Abbasitabar, V. Zare-Shahabadi, M. Shamsipur and M. Akhond, *Sensors and Actuators B: Chemical*, 2011, **156**, 181.

71 F. Pena-Pereira, I. Lavilla and C. Bendicho, *Anal. Chim. Acta.*, 2010, **669**, 1.

72 O. S. Wolfbeis, *Anal. Chem.*, 2000, **72**, 81.

73 T. Molina-Holgado, J. M. Pinilla-Macias and L. Hernández-Hernández, *Anal. Chim. Acta.*, 1995, **309**, 117.

74 Q. Wan, F. Yu, L. Zhu, X. Wang and N. Yang, *Talanta*, 2010, **82**, 1820.

75 J. P. Raval and K. R. Desai *Chemistry*, 2004, **1**, 569.

76 Y. Sumitomo, K. Tsuboshima and A. Hayakawa, *Chem. Abs.*, 1972, **76**, 15 494g.

77 S. C. Dahlberg and C. B. Reinganum, *J. Chem. Phys.*, 1982, **76**, 5515.

78 J. Zhou, G. Zhao, J. Yang and G. Han, *J. Alloys and Compounds*, 2011, **509**, 6731.

79 H. Zhou, S. Xiong, L. Wei, B. Xi, Y. Zhu and Y. Qian, *Cryst. Growth and Design.*, 2009, 9, 3862

80 R. W. Geiger and E. B. Sandell, *Analyt. Chim. Acta.*, 1953, **8**, 197.

81 A. T. Hutton, *Ph.D. Thesis*, University of Cape Town, 1980.

82 H. M. N. H. Irving, G. Andrew and E. J. Risdon, *J. Chem. Soc.*, 1949, 541.

83 J. L. A. Webb, I. S. Bhatia, A. H. Corwin and A.G. Sharp, *J. Am. Chem. Soc.*, 1950, **72**, 91.

84 L. S. Meriwether, E. C. Breitner and C. L. Sloan, *J. Am. Chem. Soc.*, 1965, **87**, 4441.

85 L. S. Meriwether, E. C. Brietner and N. B. Colthup, *J. Am. Chem. Soc.*, 1965, **87**, 4448.

86 K. G. von Eschwege, J. Conradie and J. C. Swarts, *J. Phys. Chem. A*, 2008, **112**, 2211.

87 N. Sertova, I. Petkov and J. M. Nunzi, *J. Photochem. Photobio. A Chem.*, 2000, **134**, 163.

88 N. L. Cromhout and A. T. Hutton, *Appl. Organomet. Chem*., 2000, **14**, 66.

89 C. Goesling, A. W. Adamson, A. R. Gutierrez, *Inorg. Chim. Acta.*, 1978, **29**, 279.

90 H. M. N. H. Irving and C. F. Bell, *J. Chem. Soc.*, 1954, 4253.

91 B. S. Freiser and H. Freiser, *Anal. Chem*., 1970, **42**, 305.

92 H. Freiser and P. Brand, *Anal. Chem*., 1974, **46**, 1147.

93 S. Liu and J. Zubieta, *Polyhedron*, 1989, **8**, 677.

94 M. M. Harding, *J. Chem. Soc.*, 1958, 4136.

95 R. F. Bryan and P. M. Knoff, *Proc. Chem. Soc.*, 1961, 203.

96 M. Laing and P. Sommerfield, *J. Chem. Soc. (A)*, 1971, 1247.

97 A. Mawby and H. M. N. H. Irving, *Anal. Chim. Acta.*, 1971, **55**, 269.

98 C. Ma, F. Li, R. Zhang and H. Yin, *Ch. J. Org. Chem.*, 2003, **23**, 595.

99 Y. Singh, R. Sharan and R. N. Kapoor, *Transition Metal Chem.*, 1987, **12**, 335.

100 J. M. Harrowfield, C. Pakawatchai and A. H. White, *J. Chem. Soc., Dalton Trans.*, 1983, 1109.

101 F. S. Kong and W. T. Wong, *J. Chem. Soc., Dalton Trans.*, 1999, 2497.

102 F. S. Kong and W. T. Wong, *J. Organomet. Chem.*, 1999, **589**, 191.

103 G. L. Seamans, J. L. Walsh, M. Krawiec and W. T. Pennington, *Acta. Cryst.*, 2003, C59.

104 K. Ortner and U. Abram, *Polyhedron*, 1999, **18**, 749.

105 G. Bahr and G. Schleitzer, *Chem. Ber.*, 1957, **90**, 438.

106 J. Bray, J. Locke, J. A. McCleverty and D. Coucouvanis, *Inorg. Synth. XIII*, 1972, 187.

107 G. Steimecke, H. Sieler, R. Kirmse and E. Hoyer, *Phos. Sulfur*, 1979, **7**, 49.

108 R. E. D. Clark, *Analyst*, 1936, **60**, 242.

109 W. H. Mills and R. E. D. Clark, *J. Chem. Soc.*, 1936, 175.

110 G. Bahr and G. Schleitzer, *Angew. Chem.*, 1956, **68**, 525.

111 G. N. Schrauzer and V. P. Mayweg, *J. Am. Chem. Soc.*, 1962, **84**, 3221.

112 H. B. Gray and E. Billig, *J. Am. Chem. Soc.*, 1963, **85**, 2019.

113 A. Davison, N. Edelstein, R. H. Holm and A. H. Maki, *J. Am. Chem. Soc.*, 1963, **85**, 2029.

114 J. A. McCleverty, *Prog. Inorg. Chem.*, 1968, **10**. 49.

115 G.N. Schrauzer, *Transition Met. Chem.(N.Y.)*, 1968, **4**, 299.

116 G.N. Schrauzer, *Acc. Chem. Res.*, 1969, **2**, 72.

117 R. E. Eisenberg, *Prog. Inorg. Chem.*, 1970, **12**, 295.

118 R. H. Holm and M. J. O'Connor, *Prog. Inorg. Chem.*, 1971, **14**, 241.

119 K. W. Browall, L. V. Interrante and J. S. Kasper, *J. Am. Chem. Soc.*, 1971, **93**, 6289.

120 K. W. Browall, T. Bursh, L. V. Interrante and J. S. Kasper, *Inorg. Chem.*, 1972, **11**, 1800.

121 K. W. Browall and L. V. Interrante, *J. Coord. Chem.*, 1973, **3**, 27.

122 A. E. Smith, G. N. Schrauzer, V. Mayweg and W. Heinrich, *J. Am. Chem. Soc.*, 1965, **87**, 5798.

123 N. Robertsen and L. Cronin, *Coord. Chem. Rev.*, 2002, **227**, 93.

124 F. W. B. Einstein, G. Hunter, D. G. Tuck and M. K. Yang, *Chem. Commun.*, 1968, 423.

125 E. S. Bretschneider, C. W. Allen and J. H. Waters, *J. Chem. Soc. (A)*, 1971, 500.

126 A. F. Berniaz, G. Hunter and D. G. Tuck, *J. Chem. Soc. (A)*, 1971, 3254.

127 G. Hunter and T.J.R. Weakley, *J. Chem. Soc., Dalton. Trans.*, 1983, 1067.

128 J. M. Kisenyi, G. R. Willey, M. G. B. Drew and S. O. Wandiga, *J. Chem. Soc., Dalton Trans.*, 1985, 69.

129 J. C. Berthet, M. Nierlich and M. Ephritikhine, *Polyhedron*, 2003, **22**, 3475.

130 T. Arliguie, M. Fourmique and m. Ephritikhine, *Organometallics*, 2000, **19**, 109.

131 L. Belkhiri, T. Arliquie, P. Thuery, and M. Ephritikhine, *Organometallics*, 2000, **19**, 109.

132 M. Roger, T. Arliquie, P. Thuery, M. Fourmique and M. Ephritikhine, *Inorg. Chem.*, 2005, **44**, 584.

133 Y. Tang, X. Gan, M. Tan and X. Zheng, *Polyhedron*, 1998, **17**, 429.

134 F. Bigoli, P. Casoux, P. Deplano, M. L. Mercuri, M. A. Pellinghelli, G. Pintus, A. Serpe and E. F. Trogu, *J. Chem. Soc., Dalton Trans.*, 2000, 4639.

135 G. M. G. Hossain, M. I. Hyder, S. E. Kabir, K. M. Malik, M. A. Miah and T. A. Siddiquee, *Polyhedron*, 2003, **22**, 633.

136 Y. Chen, Y. Qin, L. Zhang and Z. Chen, *Inorg. Chem.*, 2004, **43**, 1197.

137 M. Don, K. Yang, S. G. Bott and M. G. Richmond, *J. Organomet. Chem.*, 1997, **544**, 15.

138 H. Sugimoto, K. Tsuge and K. Tanaka, *J. Chem. Soc., Dalton Trans.*, 2001, 57.

139 A. Davison, N. Edelstein, R. H. Holm and A. H. Maki, *Inorg. Chem.*, 1963, **2**, 1227.

140 A. Davison, N. Edelstein, R. H. Holm and A. H. Maki, *Inorg. Chem.*, 1964, **3**, 814.

141 M. Nomura, C. Takayama and M. Kajitani, *Inorg. Chem. Acta.*, 2004, **357**, 2294.

142 F. Wudl, E. J. Wobschall and E. J. Hufnagel, *J. Am. Chem. Soc.*, 1972, **94**, 671.

143 J. P. Ferraris, D. O. Cowan, V. Valatka and J. H. Perlstein, *J. Am. Chem. Soc.*, 1973, **95**, 948.

144 T. Mochida, E. Nagabuchi and M. Ueda, *Inorg. Chim. Acta.*, 2010, **363**, 4108.

145 N. Roberts and S. Tiwary, *Polyhedron*, 2003, **22**, 2339.

146 L. Hu, J. Qin, N. Zhou, Y-F. Meng, Y. Xu, J-L. Zuo and X-Z. You, *Dyes and Pigments*, 2011, 23, 120.

147 G. Chatzikyriakos, I Papagiannouli, S. Couris, G. C. Anyfantis and G. C. Papavassiliou, *Chem. Phys. Lett.*, 2011, **513**, 229.

148 K. Ohta, Y. Inagaki-Oka, H. Hasebe and I. Yamamoto, *Polyhedron*, 2000, **19**, 267.

149 K. Wang, A. O. Patil, S. Zushma and J. M. McConnachie, *J. Inorg. Biochem.*, 2007, **101**, 1883.

150 K. Sung and R. H. Holm, *J. Am. Chem Soc.*, 2001, **123**, 1931.

151 B. S. Lim, J. P. Donahue and R. H. Holm, *Inorg. Chem.*, 2000, **39**, 263.

152 B. Domercq, C. Coulon and M. Fourmigue, *Inorg. Chem.*, 2001, **40**, 378.

153 J. Ribsa and P. Cassoux, *C. R. Acad. Sci. Ser. 2*, 1981, **293**, 287.

154 A. Kobayashi, H. Kim, Y. Sasaki, R. Kato, H. Kobayashi, S. Moriyama, Y. Nishio, K. Kajita and W. Sasaki, *Chem. Lett.*, 1987, 1819.

155 H. Kobayashi, K. Bun, T. Naito, R. Kato and A. Kobayashi, *Chem. Lett.*, 1992, 1909.

156 A. Kobayashi, H. Kobayashi, A. Mayimoto, R. Kato, R. A. Clark and A. E. Underhill, *Chem. Lett.*, 1991, 1235.

157 P. Cassoux, *Coord. Chem. Rev.*, 1999, **185-186**, 213.

158 H. Tajima, M. Inokuchi, A. Kobayashi, T. Ohta, R. Kato, H. Kobayashi and H. Kuroda, *Chem. Lett.*, 1993, 1235.

159 L. Brossard, H. Hurdequint, M. Ribault, L. Valade, J. P. Legros and P. Cassoux, *Synth. Met.*, 1988, **27**, B158.

160 L. Brossard, M. Ribault, L. Valade and P. Cassoux, *J. Phys.*, 1989, **50**, 1521.

161 G. C. Anyfantis, G. C. Papavassiliou, P. Aloukos, S. Couris, Y. F. Weng, H. Yoshino and K .Murata, *Zeitschrift fuer Naturforschung, B*: Chem. Sciences, 2007, **62**, 200.

162 M. Uruichi, K. Yakushi, Y. Yamashita and J. Qin, *J. Mater. Chem*., 1998, **8**, 141.

163 P. Aloukos, S. Couris, J. B. Koutselas, G. C. Anyfantis, G. C. Papavassiliou, *Chem. Phys. Lett.*, 2006, **428**, 109.

164 G. C. Anyfantis, G. C. Papavassiliou, N. Assimomytis, A. Teris, V. Psycharis, C. P. Raptopoulou, P. Kyritsis, V. Thoma and I. B. Koutselas, *Solid State Science*, 2008, **10**, 1729.

CHAPTER 2

Structural and electrochemical studies of mercurated Group 6-dppm complexes

2.1 Introduction

There has been a great interest over the past few decades in molecules with metal centres in close proximity as this can profoundly affect both the reactivity and physical properties of the molecules. Properties such as non-linear optical activity, redox behaviour, luminescence can vary significantly due to the presence of the second metal. The electrochemical communication between metal centres is probably the phenomenon which has received the most significant attention as it is central to many of the physical properties of interest to chemists.

Considerable attention has been given to the study of homobimetallic and heterobimetallic complexes where the metal centres are linked by, for example, hydrocarbon bridges,[1] fulvalene or fulvalene-like bridges,[2] fluorenyl,[3] dipridylamine[4] or carborane cages.[5] Hong,[6] for example, has prepared complexes with an unsaturated hydrocarbon chain containing a terminal phosphine acting as a bridge between ruthenium and/or osmium metal centres (**Figure 2.1**). Cyclic voltammetry was employed to investigate the degree of electronic communication in these ethynyl/butadiynyl phosphine complexes. The electronic interaction was found to be very weak, resulting in overlapping metal-centred oxidations. The electronic interaction was also found to decrease on increasing the number of carbons in the bridge from 2 to 4. Hong has also shown that the ability of dppm chelates, linked by an unsaturated hydrocarbon chain, to be more effective in facilitating electron transfer between terminal metal centres. The homo- and heterobimetallic complexes prepared were linked by a polyphosphine/cumulene spacer, i.e. 1,1',4,4'-tetrakis(diphenylphosphinomethane)cumulene (C_4P_4)[7] or 1,1',3,3'-tetrakis(diphenylphosphinomethane)cumulene (C_3P_4),[8] as shown in **Figure 2.1**. While the

C_3P_4 complexes gave comparable electrochemical results (**Figure 2.2a**) to the ethynyl/butadiynyl phosphine complexes, the C_4P_4 complexes showed relatively large peak separations between the redox potentials of the two metal centres, indicative of a strong electronic interaction between the terminal metal centres (**Figure 2.2b**).

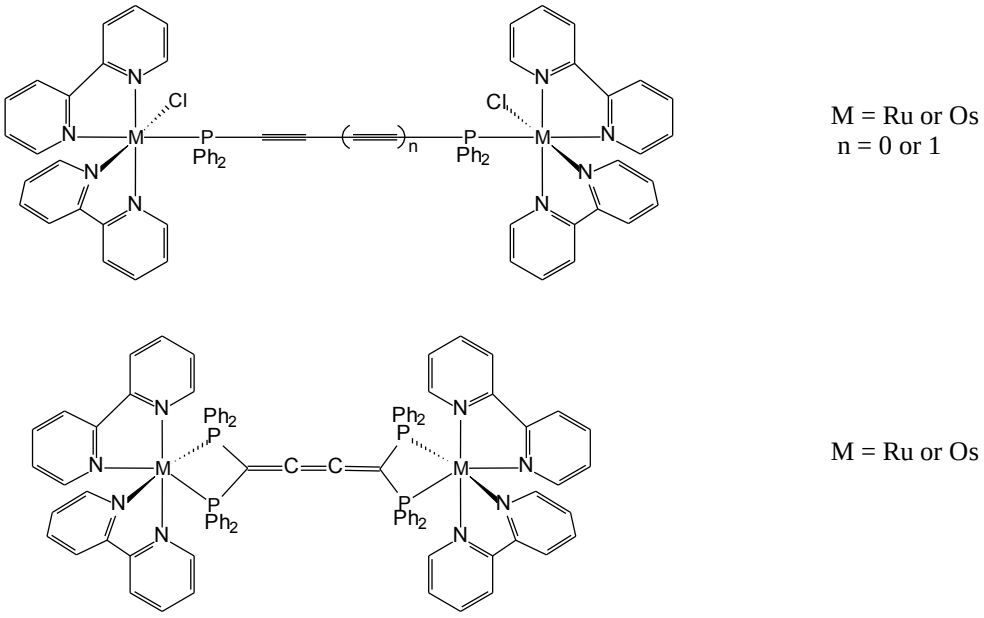

Figure 2.1 Bimetallic complexes with phosphine-hydrocarbon spacers.

Robin and Day[9] have attempted to classify the degree of electronic interaction between the metal centres by considering: (i) the difference in their redox potentials, ΔE (homobimetallic complexes), or (ii) the difference in the redox potential compared to the monometallic moiety (heterobimetallic complexes). The resultant electronic interactions could then be categorised as being either Class I (non-existent), Class II (moderate) or Class III (strong).

A class III interaction is clearly illustrated in the cyclic voltammograms depicted in **Figures 2.2b** and **2.2c**. The oxidation potentials for the homobimetallic Ru-complex appear well separated, while the oxidation potentials in the heterobimetallic Re-Fe complex differ significantly from the potentials of the respective monometallic precursors.

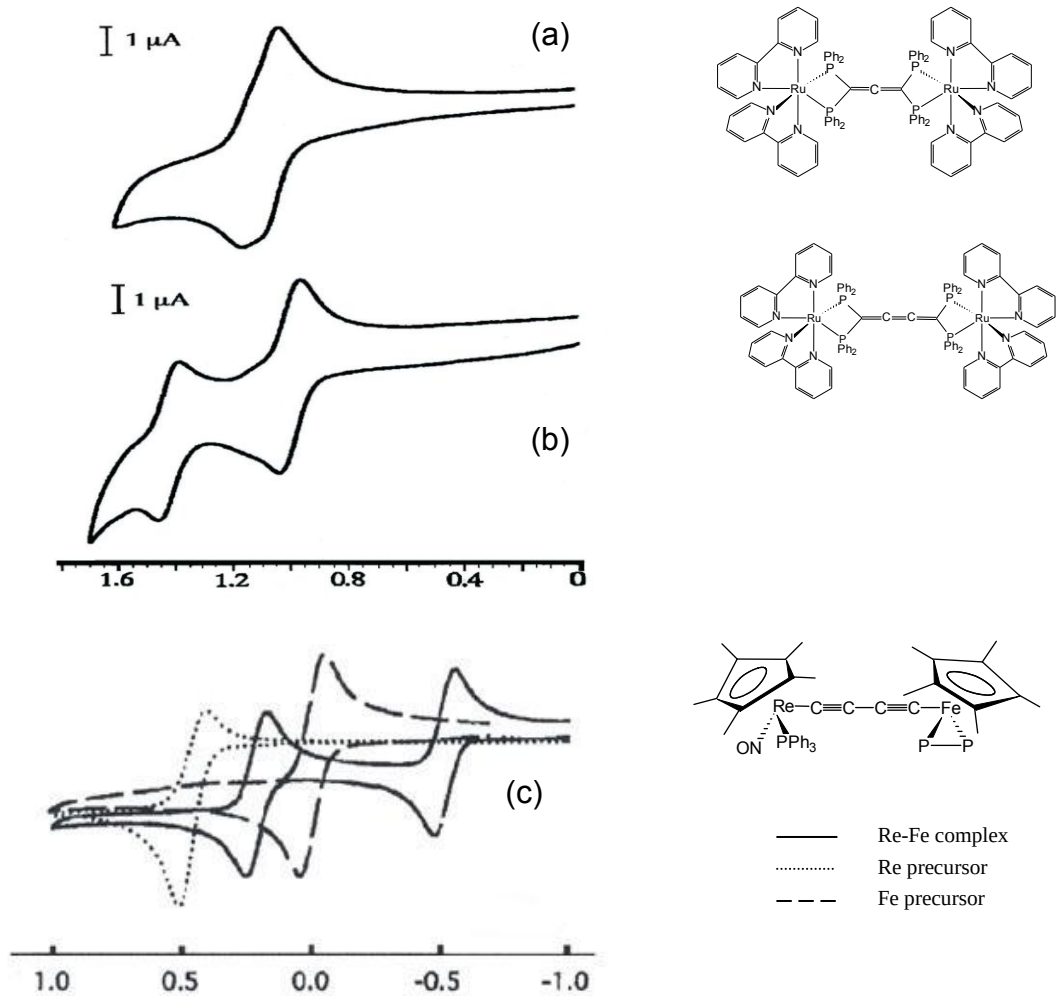

Figure 2.2 Cyclic voltammograms showing the degree of electronic communication between metal centres of (a) homobimetallic Ru-C_3P_4 complex, (b) homobimetallic Ru-C_4P_4 complex and (c) hetero-bimetallic Re-Fe complex.

In **Chapter 1** we have discussed the synthetic methodology used by Shaw in the functionalization of coordinated dppm complexes of zerovalent Group 6 metal carbonyls. Metallations were predominantly performed using $[Ph_3PAg]^+$ or $[Ph_3Pau]^+$ as electrophiles. One example occurs where mercury was used in the metallation of dppm.[10] Spectroscopic and structural studies revealed that the metal electrophiles did not completely neutralize the negative charge on the methylene carbon. In the mercurated complex, for example, crystallographic studies showed the mercury to be bonded to the methylene carbon as a carbene.

Bildstein[11] has synthesized a series of ferrocenyl containing complexes where W-, Pd- and Hg-carbenes were used as spacers and compared to the analogous methylene spaced derivatives (**Figure 2.3**). While significant electronic communication was found to exist for the W derivatives, no data was obtained for the Hg derivatives due to poor solubility. More recently, Hawthorne used Hg as a spacer to assess metal-metal communication between carborane cages.[5]

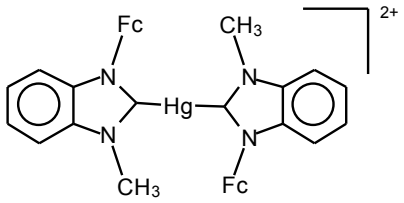

Figure 2.3 Ferrocenyl benzimidazolium complex with mercury(II) spacer.

Organomercury compounds are among the most studied classes of organometallic compounds. The interest in these compounds stems from their potential application as molecular recognition, chemo-sensing, optical and NLO materials.[12] Furthermore, organomercury compounds are receiving considerable attention in the area of environmental[13,14] and biological[15,16] chemistry.

In this chapter we will outline the deprotonation and subsequent metallation of dppm using Group 6 metal dppm-carbonyls. We will discuss some structural features of selected mercurated derivatives as determined by X-ray crystallography and also investigate the electrochemical behaviour of the resultant dppm compounds.

In a preliminary study, several long-chain mercury(II) chloride complexes were synthesized with a view to examining their potential as metallomesogens. The new compounds did not show mesogenic properties; however, some were used as ligands in subsequent work in this Chapter. These long-chain complexes are described in the next section.

2.2 Long chain complexes

2.2.1 Synthesis of 4-(4'-n-alkoxybenzylidine-*N*-methylanilino)mercury(II) chlorides

In search for organometallic mesogens, we have synthesized compounds of the type $CH_3[CH_2]_nO\text{-}C_6H_4\text{-}N(CH_3)C(O)\text{-}C_6H_4HgCl$, where n = 1, 4, 6, 8 and 11. Mesomorphism has been reported by Vorlander for the complex, 4-(4'-methoxybenzylideneanilino)mercury(II)acetate.[17] We anticipated that a new range of mesogens could be prepared by changing the linkage between the two aromatic rings from an azomethine to an amide.

The ligands were synthesized by standard methods according to **Scheme 2.1**, i.e. by the reaction of the secondary amine, 4-*N*-aminophenylmercury(II)chloride, $ClHg\text{-}C_6H_4\text{-}N(Me)H$, the appropriate 4-alkoxybenzoylchloride, $RO\text{-}C_6H_4\text{-}COCl$ and triethylamine in THF. The reaction is spontaneous with the formation of the hydrochloride salt, $Et_3NH^+Cl^-$, on addition of the acid chloride. The products were all colourless and were obtained in good yield, 93-98%. $SOCl_2$ was used to obtain the acid chloride in cases where the alkoxy precursor exists as an acid.

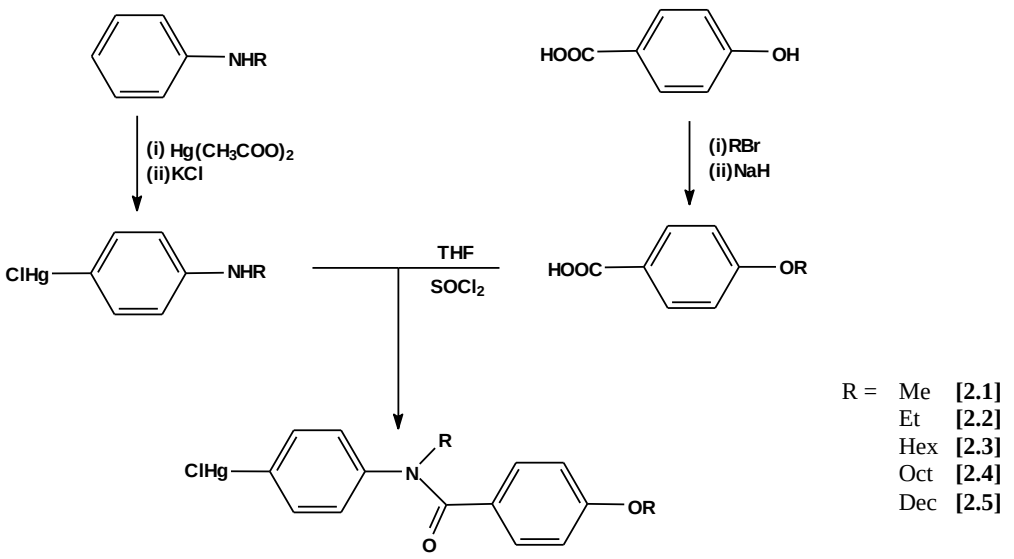

Scheme 2.1 Preparation of long-chain amide complexes.

The ^{1}H NMR spectra of the compounds **[2.1]-[2.5]** show the expected resonances for the two *para* substituted benzene rings, viz., two sets of doublets. The assignment for the aromatic protons was based on the values for the coupling constants and the appearance of the spectrum, i.e. symmetry (mutually coupled doublets point to one another).
The H_a and H_b protons are coupled together in a pattern which appears superficially like an AB system δ_{ab} = 7.08 ppm, J_{ab} = 8.62 Hz, but exhibit a fine structure (see complex **[2.1]**). This is normally due to the fact that the pair and all the other pairs are not magnetically equivalent and should ideally be named a AA'BB' system. The H_c and H_d protons likewise give rise to a set of two doublets, δ_{cd} = 7.20 ppm, J_{cd} = 8.91 Hz.

None of the long chain complexes synthesized showed any mesogenic behaviour. Only the expected trend of decreasing melting point with increase in chain length was observed. These complexes closely resemble the metallomesogens synthesized by Vorlander, the difference being the amide linkage compared to the imine linkage in the metallomesogens. In an X-ray crystallographic study, Itai *et al*. has shown that opposed to 2° amides, the 3° methyl amide prefers the *cis* geometry.[18] This could partly explain the difference in mesogenic behaviour between the two systems.

The structural preference was ascertained by computational calculations, using a 4-para-methoxy derivative as a basis for the calculation. Both geometries were optimized in Gaussion 09,[19] using the B3LYP[20] functional with the 6-31+G(d,p) basis functions. The optimized geometries are depicted in **Figure 2.4** below and support the preference for the *cis* conformer. A comparison of the ground-state energies shows the *cis* geometry to be more stabilized, with an energy of 10 kJ mol^{-1} (2.7 kcal mol^{-1}) lower than the *trans* geometry.

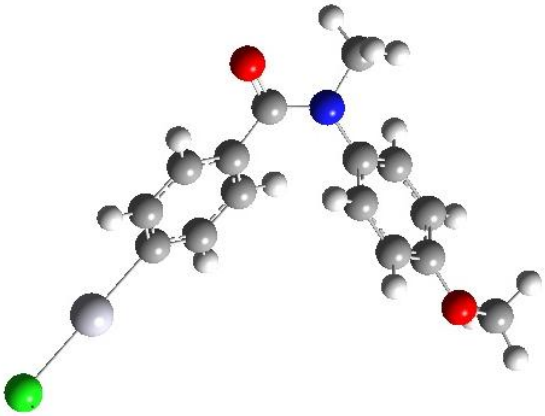

-1287.96007 amu

(a)

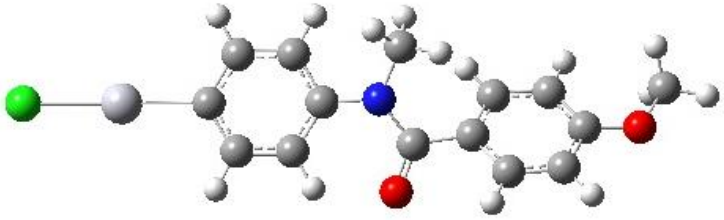

-1287.956133 amu

(b)

Figure 2.4 DFT optimized structures for cis- and trans amide compounds, with corresponding energies in hartrees.

2.3 Preparation of mercurated Group 6 dppm complexes

The heterobi- and tri-metallic mercurated complexes were prepared according to the general mechanism outlined, for chromium complexes, in **Scheme 2.2** below. The dppm metal-carbonyls were prepared according to literature methods. The treatment of a THF solution of $[M(CO)_4(Ph_2PCH_2PPh_2)]$ (M = Cr, Mo or W) at 0°C with BuLi yields the anion $[M(CO)_4(PPh_2CHPPh_2)]^-$ as shown by Shaw.[21,22] The appropriate metal salt was added after 1.5 h. The reaction mixture was allowed to warm to room temperature and stirred for an additional 1.5 h. A list of complexes synthesized is given in **Table 2.1**.

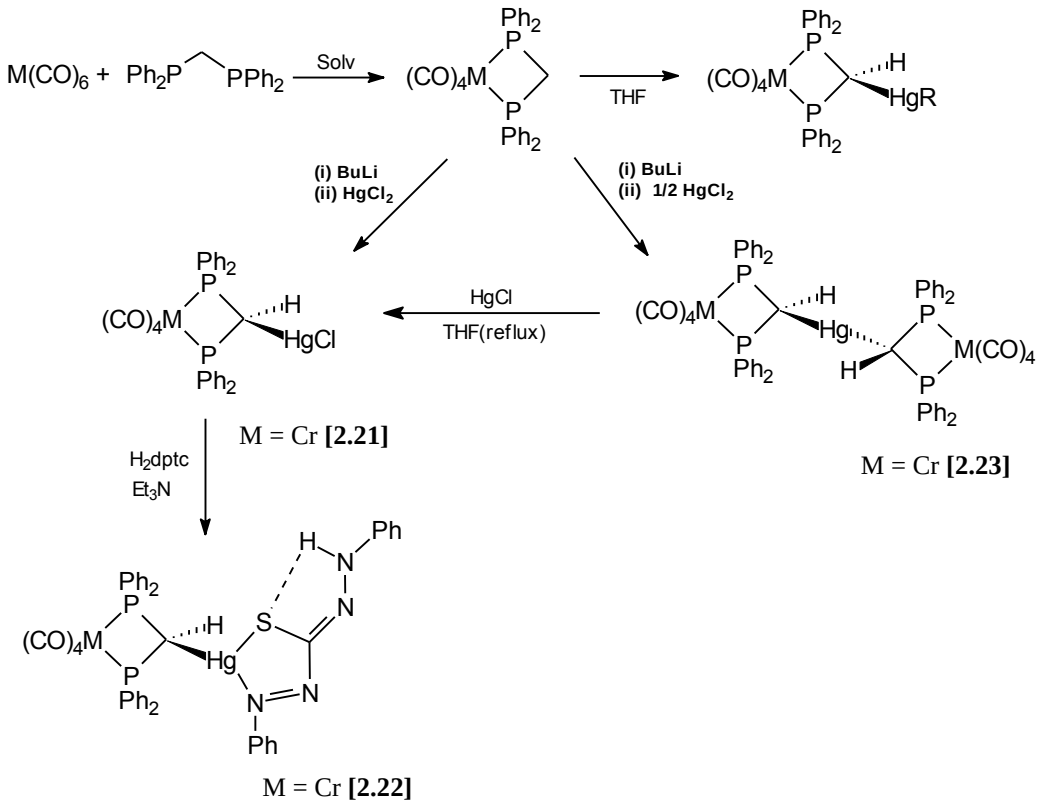

Scheme 2.2 Preparative route to homo- and heterobi- and trimetallic complexes.

An attempt to synthesize the mercury chloride derivative lead to a mixture of the desired product **[2.21]** (see **Table 2.1**) and the disubstituted mercury derivative, $[Cr(CO)_4(Ph_2PCHPPh_2)]_2Hg$ **[2.23]**. Only the chromium-HgCl derivative was obtained. The molybdenum and tungsten derivatives underwent decomposition in solution. We followed a cleaner route to the preparation of **[2.21]**. This involved the preparation of the trimetallic derivative **[2.23]** by the reaction of two molar equivalents of $[Cr(CO)_4\{PPh_2CHPPh_2\}]^-$ with $HgCl_2$. The tungsten derivative could not be isolated as it decomposed in solution. The chromium derivative was subjected to desymmetrization by the reaction of **[2.23]** with a stoichiometric amount of $HgCl_2$ in refluxing THF to yield the $[Cr(CO)_4\{(PPh_2)_2CH(HgCl)\}]$ derivative **[2.21]**. We found that **[2.21]** readily reacts with dithizone in the presence of Et_3N to give **[2.22]**.

2.4 Spectroscopic studies

2.4.1 Infrared spectra

The infrared spectra of the metallated derivatives generally showed four bands for the terminal carbonyl groups, which is typical for *cis*-$[M(CO)_4L_2]$ systems.[23] In some instances three bands were observed, which is also in agreement with observations for other Group 6 tetracarbonyls.[24] However, this was only observed for a few molybdenum complexes. The infrared spectra of all derivatives show a change towards lower frequencies compared to the respective unsubstituted precursors. This would indicate increased π-backbonding between the Group 6 metal and the p_{π^*} orbitals of the carbonyl group, resulting in weakening of the C=O bond. It is interesting to note that the *C*-alkylated derivatives reported by Shaw show an increase in ν(CO).[25] This would imply an electron withdrawal from the phosphorus atoms which would lead to a weakening in M-CO bonding and a resultant favouring of the M-C≡O resonance component. A similar deshielding of the phosphorus atoms with a corresponding increase in ν(CO) is reported for the mono-and di-halogenated dppm derivatives reported by Riera *et al*. for the complex $[Mn(CO)_4(dppm)]ClO_4$.[26] The stretching frequencies for all metallated derivatives increase in the order Cr<W<Mo. This trend is well documented and similar to that observed by Shaw.[22]

2.4.2 ^{1}H NMR

The most characteristic resonance in the ^{1}H NMR spectra of the mercurated complexes is that of the methylene proton. It was observed that on replacement of a methylene proton for the $[HgR]^+$ fragment that the triplet moves downfield indicating deshielding of the remaining methylene hydrogen. Shielding was however observed for complex **[2.23]** (discussed later). There appears to be no significant difference in the two bond coupling constant ^2J(PH), which falls in the narrow range of 12.0-18.0 Hz.

Most interesting in the methylmercury complexes is the significant upfield shift of the methyl resonance. We observed that δ_H for the methyl group shifts from 1.11 ppm in

MeHgCl to -0.12, -0.13 and -0.13 ppm for the Cr-, Mo- and W-methylmercury complexes, respectively.

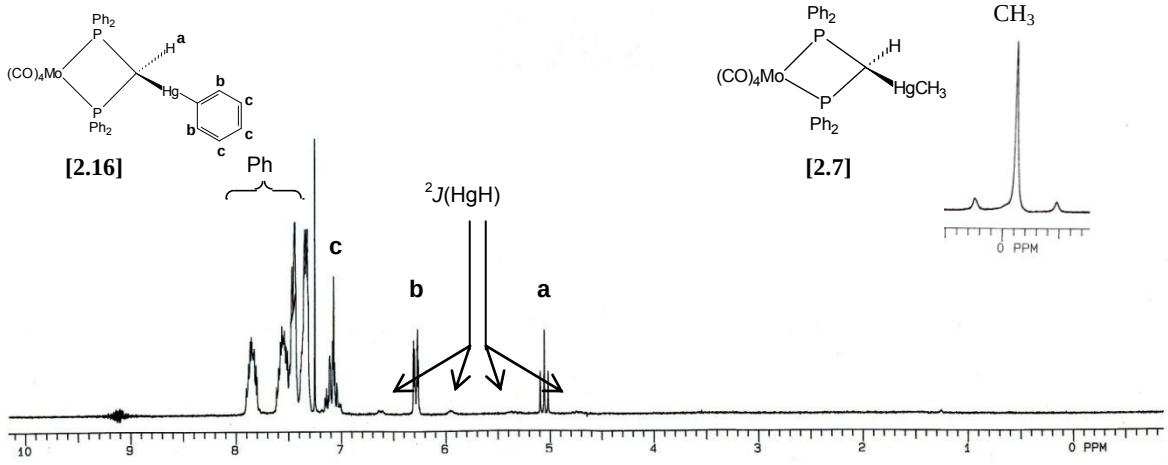

Figure 2.4 ^{1}H NMR spectrum of the phenyl complex **[2.16]** showing the mercury-hydrogen coupling. Inset showing the upfield methyl resonance for derivative **[2.7]**, with corresponding satellites for ^{2}J(HgH) coupling.

Hatton has shown for a series of MeHgX complexes that a rough correlation exists between $\delta(^{1}H)$ and the electronegativity of the group 'X' attached to mercury. For example, going from MeHgCl to the more ionic $MeHgClO_4$ results in an upfield shift of ca. 0.3 ppm.[27] In another study Bach reported a similar upfield shift for a phenylthiomercury complex, which he attributed to the anisotropy of the aromatic ring of the benzyl group. He estimated the methyl group to be approximately 4.6 Å above the centre of the ring. This, according to published values for aromatic ring current anisotropy, typically gives rise to an upfield shift in the order of 0.32-0.47 ppm for the methyl protons, in agreement with his findings of an upfield shift of 0.4 ppm.[28] Following from the findings by Bach and Hatton it would appear that the significant upfield shift observed for these complexes is a result of the shielding effect of the dppm phenyl rings on the methyl protons. In the solid state structure of **[2.6]** (see **Section 2.7**) the phenyl rings of the dppm flank the methyl groups on either side. The distance from the methyl group to the two flanking phenyl rings was calculated to be 4.85 Å (avg.). It would then appear as if a

cumulative shielding is experienced by the methyl protons resulting in the observed upfield shift of approximately 1.0 ppm.

The difference in the coupling constants $^{2}J(^{199}HgH)$ from 205 Hz for the MeHgCl complex to an average 144 Hz for the methylmercury derivatives is as expected when the largely ionic chloride is replaced with the more covalent carbon of an electron-rich four-membered M-P-C-P ring. **Figure 2.4** shows the ^{1}H NMR spectrum for the phenylmercury derivative **[2.16]**, the mercury satellites clearly visible for the phenyl protons, H_b and the alkyl substituent of the methyl derivative **[2.7]**(inset). Whereas the mercury satellites for the alkyl substituents are always present, except in cases where they are obscured by neigbouring resonances, satellites for the methylene resonance are less pronounced and often not discernable from the baseline.

In the chloromercury-derivative **[2.21]** the methylene proton is observed at 6.03 ppm, which would be expected due the electronegativity of chlorine. The trimetallic derivative **[2.23]** showed a triplet at 4.1 ppm indicating extreme shielding of the methylene proton. This is contrary to what would be expected for the electron rich 4-membered chelate ring. A crystallographic study of this compound (see **Section 2.7**) shows it to exist in an antiparallel conformation with the methylene hydrogen surrounded by crowding phenyls. The upfield shift could be ascribed to the shielding of the methylene proton as was found for the methylmercury derivatives.

The ^{1}H NMR spectra showed the expected resonances for the phenyl- and substituted phenylmercury derivatives. The *para*-alkyl and *N*-methyl protons appear to be unaffected by the coordination to the dppm chelate as manifested by their respective chemical shifts. The aromatic hydrogens do show a general upfield shift with the H_a hydrogens being mostly affected (shielding due to chelate ring phenyls) as seen in the large shift of about 1.0 ppm. Assignment of the aromatic hydrogens was made by considering coupling constants and symmetry and was simplified by the presence of Hg satellites for the equivalent H_a protons.

2.4.3 ^{31}P NMR

All spectra are characterized by a single resonance with satellites due to spin-spin coupling of the two equivalent phosphorus atoms with ^{199}Hg (relative abundance 16.8%, spin = ½). In the case of the tungsten complexes a second set of satellites is present due to spin-spin coupling with ^{183}W (relative abundance 14%, spin = ½).

The chemical shifts and coupling constants for the bimetallic and trimetallic derivatives are given in **Table 2.1**. A typical ^{31}P NMR spectrum for the tungsten complex **[2.17]** is given in **Figure 2.5**.

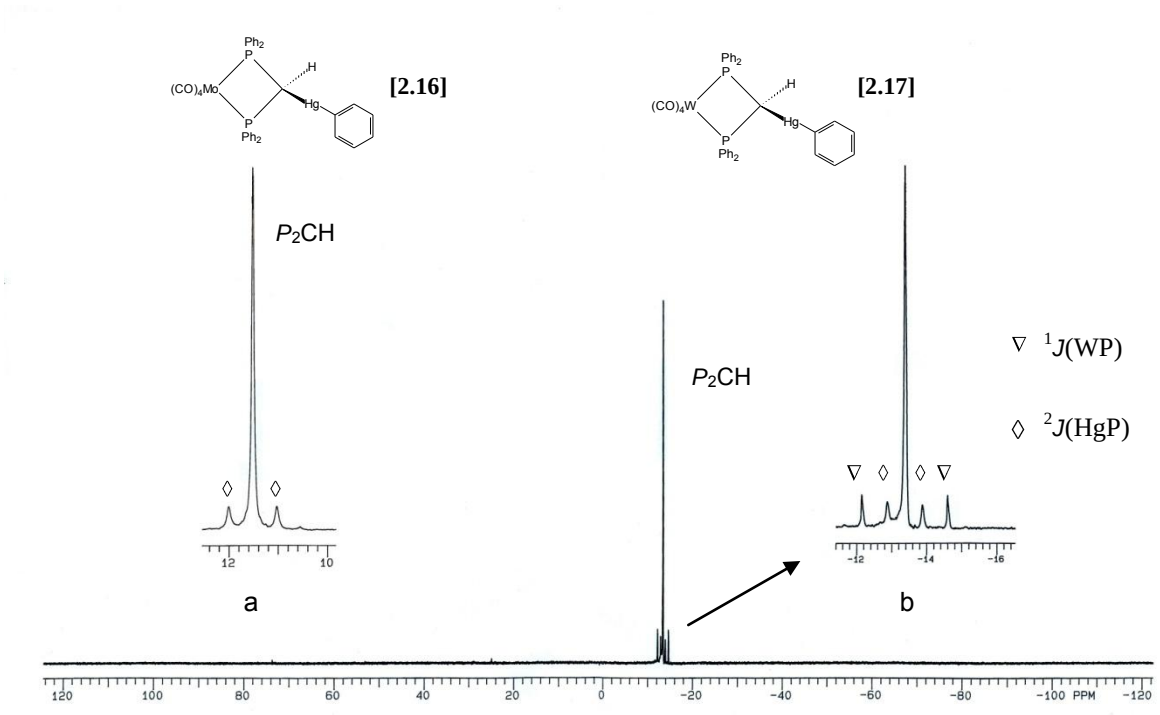

Figure 2.5 ^{31}P NMR spectrum of **[2.17]** and **[2.16]** (inset **a**). Inset **b** also shows the ^{1}J(WP) satellites.

Table 2.1 ^{31}P NMR data for bi- and trimetallic complexes

Complex		^{31} P NMR	
		δ(P), ppm	^{2}J(HgP), Hz
$[Cr(CO)_4(PPh_2CH(HgMe)PPh_2)]$	**[2.6]**	33.1	76.8
$[Mo(CO)_4(PPh_2CH(HgMe)PPh_2)]$	**[2.7]**	11.3	70.0
$[W(CO)_4(PPh_2CH(HgMe)PPh_2)]$	**[2.8]**	-13.47	70.5, ^{1}J(WP)=197.4
$[Cr(CO)_4(PPh_2CH(HgEt)PPh_2)]$	**[2.9]**	32.7	58.9
$[Mo(CO)_4(PPh_2CH(HgEt)PPh_2)]$	**[2.10]**	8.8	50.3
$[W(CO)_4(PPh_2CH(HgEt)PPh_2)]$	**[2.11]**	-15.9	51.8, ^{1}J(WP)=196.8
$[Cr(CO)_4(PPh_2CH(HgPr)PPh_2)]$	**[2.12]**	34.5	60.3
$[Cr(CO)_4(PPh_2CH(HgOct)PPh_2)]$	**[2.13]**	34.6	59.7
$[Cr(CO)_4(PPh_2CH(HgDec)PPh_2)]$	**[2.14]**	34.6	59.5
$[Cr(CO)_4(PPh_2CH(HgPh)PPh_2)]$	**[2.15]**	33.84	87.4
$[Mo(CO)_4(PPh_2CH(HgPh)PPh_2)]$	**[2.16]**	11.5	79.3
$[W(CO)_4(PPh_2CH(HgPh)PPh_2)]$	**[2.17]**	-13.36	81.3, ^{1}J(WP)=198.7
$[Cr(CO)_4(PPh_2CH(HgFc)PPh_2)]$	**[2.18]**	35.5	95.6
$[Mo(CO)_4(PPh_2CH(HgFc)PPh_2)]$	**[2.19]**	11.4	88.0
$[W(CO)_4(PPh_2CH(HgFc)PPh_2)]$	**[2.20]**	-14.1	89.9, ^{1}J(WP)=198.4
$[Cr(CO)_4(PPh_2CH(HgCl)PPh_2)]$	**[2.21]**	41.7	212.4
$[Cr(CO)_4(PPh_2CH(HgHdptc)PPh_2)]$	**[2.22]**	40.2	194.2
$[\{Cr(CO)_4(PPh_2CHPPh_2)\}_2Hg]$	**[2.23]**	40.5	135.1
$[\{Mo(CO)_4(PPh_2CHPPh_2)\}_2Hg]$	**[2.24]**	16.9	123.8
$[Cr(CO)_4(PPh_2CH(Hg\ p\text{-}C_6H_4\text{-}OCH_3)PPh_2)]$	**[2.25]**	35.6	88.4
$[W(CO)_4(PPh_2CH(Hg\ p\text{-}C_6H_4\text{-}OCH_3)PPh_2)]$	**[2.26]**	-13.24	81.9, ^{1}J(WP)=198.5
$[Cr(CO)_4(PPh_2CH(p\text{-}C_6H_4\text{-}N(CH_3)_2)PPh_2)]$	**[2.27]**	37.2	62.5
$[W(CO)_4(PPh_2CH(p\text{-}C_6H_4\text{-}N(CH_3)_2)PPh_2)]$	**[2.28]**	-10.46	80.0, ^{1}J(WP)=192.8
$[Cr(CO)_4(PPh_2CH(HgL)PPh_2)]$ [a]	**[2.29]**	35.9	90.3
$[Cr(CO)_4(PPh_2CH(HgL)PPh_2)]$ [a]	**[2.30]**	35.6	91.6
$[Cr(CO)_4(PPh_2CH(HgL)PPh_2)]$ [a]	**[2.31]**	36.0	90.8
$[Cr(CO)_4(PPh_2CH(HgL)PPh_2)]$ [a]	**[2.32]**	35.9	90.8
$[Cr(CO)_4(PPh_2CH(HgL)PPh_2)]$ [a]	**[2.33]**	35.9	90.8

[a] L for complexes **[2.29], [2.30], [2.31], [2.32]** and **[2.33]** derived from **[2.1] - [2.5],** respectively

The substitution of a proton for the fragment, $[HgR]^+$ in $[M(CO)_4(Ph_2PCH_2PPh_2)]$ results in a downfield shift of the equivalent phosphorus atoms. The chemical shifts increase in

the order W < Mo < Cr. The Cr, Mo and W complexes have δ(P) values in the range 33 to 42 ppm, 9 to 17 ppm and -16 to -10 ppm, respectively. This translates to a range in phosphorus chemical shift values of 9, 8 and 6 ppm, respectively; indicating that the phosphorus chemical shift is independent of the metal centre. The slightly lower variation in phosphorus chemical shifts for the W complexes is to be expected, the narrower range being due to the absence of the derivatives with the more electron-rich Cl^- and $[W(CO)_4(Ph_2PCHPPh_2)]^-$ groups.

It is evident from **Table 2.1** that δ(P) is dependent upon the substitution on the mercury atom. The ethyl substituent results in greater shielding of the phosphorus atoms, translating in a lower δ(P) compared to the greater deshielding chlorine substituent which results in a significantly higher δ(P). For example, in the chromium complexes the ethyl derivative **[2.9]** has δ(P) at 33.0 ppm while the corresponding chlorine derivative **[2.21]** has δ(P) at 41.7 ppm. It is interesting to note that the inductive effect of the alkyl groups increases as expected in the order Me < Et, with higher homologs such as propyl showing a decreased inductive effect. Octyl and decyl groups exhibit approximately the same degree of shielding as the propyl group. From this it is clear that the inductive effect is maximum when the substituent is ethyl.

It was of interest to note that the substituent effect is further manifested in the two bond coupling constant, ^2J(HgP). For the chromium complexes, ^2J(HgP) ranges from 58.9 to 212.4 Hz for the ethyl and Cl substituent, respectively. This is in line with what would be expected when the two equivalent phosphorus atoms couple with mercury whose nuclear charge is either decreased or increased by the presence of an electron-donating or electron-withdrawing group such as ethyl or chlorine, respectively. A similar observation was made for the molybdenum compounds. This trend could unfortunately not be assessed for the W complexes due to the decomposition of the chlorine and $[W(CO)_4$(dppm-H)] derivatives.

It was not surprising to find a significant correlation (r^2 = 0.96), as shown in **Figure 2.7**, between δ(P) and ^2J(HgP) for the chromium compounds, confirming the presence of electronic effects in these complexes and the ability of the mercury atom to facilitate such effects.

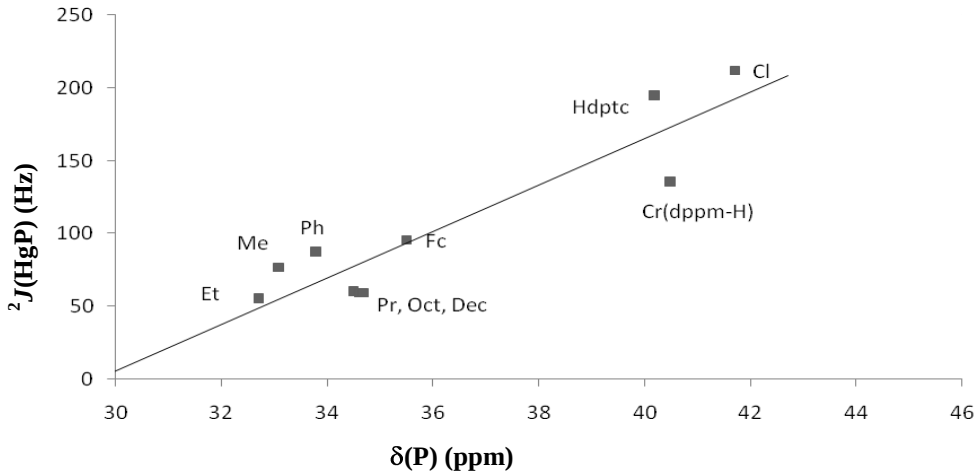

Figure 2.7 Correlation between δ(P) and ^2J(HgP) for [$Cr(CO)_4(PPh_2CH(HgR)PPh_2\}$] complexes.

In view of the fact that δ (P), ^2J(HgP) and ν(CO) respond to the substituent on the mercury atom, it was not surprising that the phosphorus NMR parameters correlate quite well with the carbonyl stretching frequency as shown in **Figure 2.8** and **Figure 2.9**. Correlation of coefficients, r^2, of 0.85 and 0.90 were found for δ (P) and ^2J(HgP) with $\nu(CO)_{total}$, respectively. It should be noted that $\nu(CO)_{total}$ for the chromium complexes constitute the sum of the four individual carbonyl stretching vibrations.

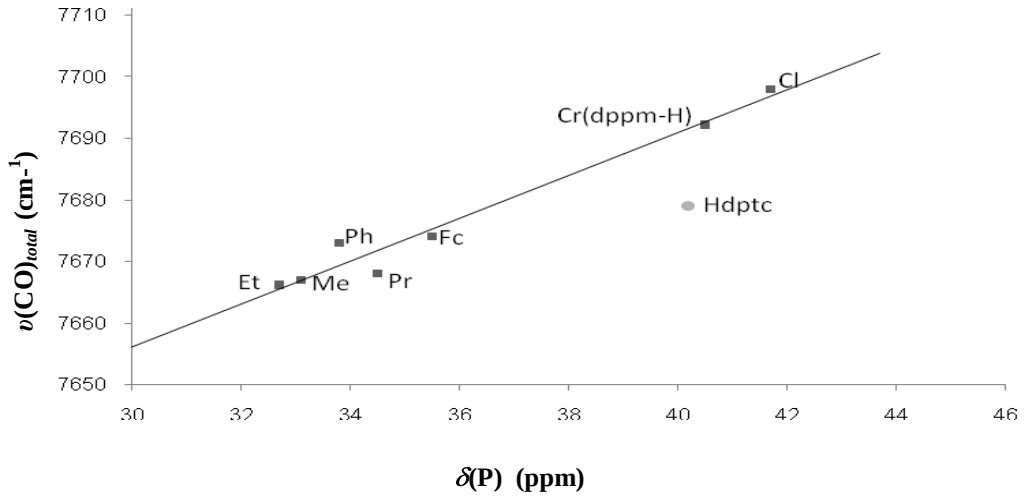

Figure 2.8 Correlation between δ(P) and $\upsilon(CO)_{total}$ for [$Cr(CO)_4(PPh_2CH(HgR)PPh_2\}$].

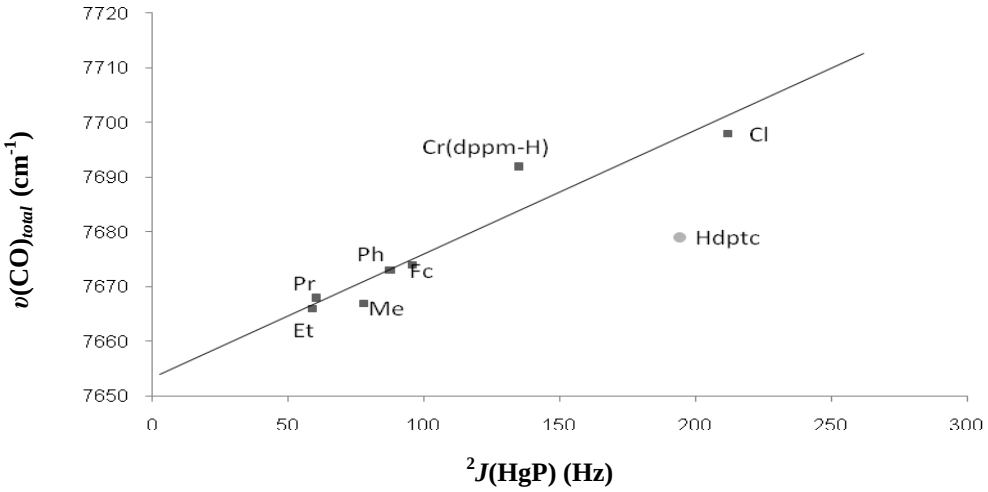

Figure 2.9 Correlation between $^{2}J(HgP)$ and $\upsilon(CO)_{total}$ for $[Cr(CO)_4(PPh_2CH(HgR)PPh_2\}]$.

The dithizonate complex with ligand Hdptc was excluded from the determination of the correlation coefficient as it is evident from the plots that the dithizonate derivative does not fit the correlation. This could be attributed to the difference in the bonding mode of mercury with dithizone.

2.5 Bimetallic gold(I) complexes

In view of the fact that the $R_3PAu(I)^+$ unit is isolobal and isoelectronic with the organomercury RHg^+ fragment, we thought that it would be of interest to compare the two classes of compounds. Gold-phosphine complexes have been widely explored by Laguna and co-workers. [29]

The bimetallic gold complexes were prepared following the same methodology as for the mercury analogues. The $Ph_3PAu(I)$ derivatives of $[M(CO)_4dppm)]$ (M= Cr, Mo or W) **[2.34]-[2.36]** have been prepared previously.[29] **Table 2.2** shows the spectroscopic data, ^{1}H and ^{31}P NMR, for complexes **[2.34]-[2.41]**.

Table 2.2 ^{1}H and ^{31}P NMR data for bimetallic gold complexes

Complex		^{1}H NMR	^{31}P NMR	
		δ, ppm	**δ(^{31}P, ppm) (*J*, Hz)**	**^{2}J (PP), ^{2}J (PP) ($^{1}J_{WP}$, Hz)**
$[Cr(CO)_4(PPh_2CH(AuPPh_3)PPh_2)]$	**[2.34]**	5.2,(t, P_2CH)	35.8(d, P_2Cr) 40.1(t, PPh_3)	9.9, 21.9
$[Mo(CO)_4(PPh_2CH(AuPPh_3)PPh_2)]$	**[2.35]**	5.24 (t, P_2CH)	12.5(d, P_2Cr) 40.1(t, PPh_3)	10.4, 21.9
$[W(CO)_4(PPh_2CH(AuPPh_3)PPh_2)]$	**[2.36]**	6.10 (t, P_2CH)	-11.93(d, P_2Cr) 40.26(t, PPh_3)	^{3}11.1, 22.0 ^{1}J(WP)= 192.9
$[Cr(CO)_4(PPh_2CH(AuPEtPh_2)PPh_2)]$	**[2.37]**	0.6(dt, Ha) 1.9(oct, Hb) 5.09 (t, P_2CH)	36.1(d, P_2Cr) 35.4(t, PEt_2Ph)	10.9, 21.99
$[Mo(CO)_4(PPh_2CH(AuPEtPh_2)PPh_2)]$	**[2.38]**	0.6 (dt, Ha) 1.9 (oct, Hb) 5.19 (t, P_2CH)	15.2(d, P_2Cr) 39.4(t, PEt_2Ph)	10.9, 21.97
$[W(CO)_4(PPh_2CH(AuPEtPh_2)PPh_2)]$	**[2.39]**	0.6(dt, Ha) 1.9(oct, Hb) 6.0 (t, P_2CH)	-12.25(d, P_2Cr) 39.07(t, PEt_2Ph)	9.9, 21.84 ^{1}J(WP)= 192.3
$[Cr(CO)_4(PPh_2CH(AuAsPh_3)PPh_2)]$[a]	**[2.40]**	5.29 (t, P_2CH)	35.9 (s, P_2Cr)	9.9
$[W(CO)_4(PPh_2CH(AuAsPh_3)PPh_2)]$[a]	**[2.41]**	5.89 (t, P_2CH)	-11.6(s, P_2Cr)	10.1 ^{1}J(WP)= 193.0

[a]The arsine complexes **[2.40]** and **[2.41]** show only the characteristic triplet attributed to the methylene proton.

The infrared spectra showed a similar trend as was observed for the mercurated derivatives, with the carbonyl stretching frequencies decreasing in the order Mo > W > Cr. As expected, the ν(CO) frequency showed a shift towards lower frequency when compared to the unsubstituted precursors. It is also interesting to note that the aurated derivatives have ν(CO) values that are on average only 4, 7 and 5 cm^{-1} lower than the mercurated derivatives for the Cr, Mo and W complexes, respectively. This indicates that the bonding is similar between the two isoelectronic fragments, resulting in a comparable Group 6 M-CO bonding interaction.

The ^{1}H NMR spectra for the gold-phosphine complexes show the P_2CH proton as a pseudoquartet, probably due to ^{2}J(PH) and ^{3}J(PH) being similar. This has been observed

by Laguna *et al*.[29] The ethyldiphenylphosphine complexes show a doublet of triplets at ca. 0.6 ppm for the methyl protons due to coupling to the *P*-methylene protons which is further split by the gold-phosphorus atom. A pseudo-octet is observed at ca. 1.9 ppm for the *P*-methylene protons, indicating a typical ABX pattern, where the quartet is further split by the gold-phosphorus atom.

The ^{31}P NMR spectra show the expected two resonances for the gold-phosphine complexes. The two equivalent phosphorus atoms of the 4-membered chelate show a doublet due to coupling to the gold-phosphine atom. Slightly downfield from this we observe a triplet for the PR_3 phosphorus due to coupling to the two diphosphine phosphorus atoms. The arsine complexes are characterized by a singlet for the phosphorus atoms of the diphosphine.

The tungsten complexes show the expected satellites due to ^1J(PW). There are no significant differences in the coupling constants for the three W-Au complexes, as seen by the narrow range of 192.3-193.0 Hz. ^1J(WP) values do appear to be ca. 6 Hz lower than those of the mercurated complexes, again showing the similarity between the two classes of compounds.

2.6 Crystallographic study of mercurated complexes

Yellow crystals of the –HgMe and –HgFc complexes **[2.6]** and **[2.18]** were obtained from dichloromethane-methanol, while the trimetallic **[2.23]** was obtained as orange crystals from benzene.

It would be of interest to see the effect of the three different substituents on the dppm chelates. We have shown that some degree of electronic interaction is present in the molecules. X-ray crystallographic data can provide useful insight into interactions within molecules. Structural parameters such as bond lengths and bond angles are often used in conjunction with spectroscopic data to account for observed interactions within molecules. It is well known that steric and electronic effects have an impact on structural parameters.

A comparison of the crystal data and refinement parameters for **[2.6]**, **[2.18]** and **[2.23]** is given in **Table 2.3** below. Complexes **[2.6]** and **[2.23]** crystallize in the triclinic space group $P\bar{1}$, while **[2.18]** crystallizes in the monoclinic space group $P2_1/c$. Least square refinement of the structures gave final *R* factors of 5.8 **[2.6]**, 10.9 **[2.18]** and 5.1% **[2.23]**. The CIF files for these structures are available on the CD-ROM disk attached to the back cover of this thesis. Selected bond lengths, bond angles and torsion angles are given in **Table 2.3**. The molecular structures are displayed in **Figures 2.10-2.12**, which defines the numbering scheme used in the tables. Packing diagrams are shown in **Figures 2.13-2.15**.

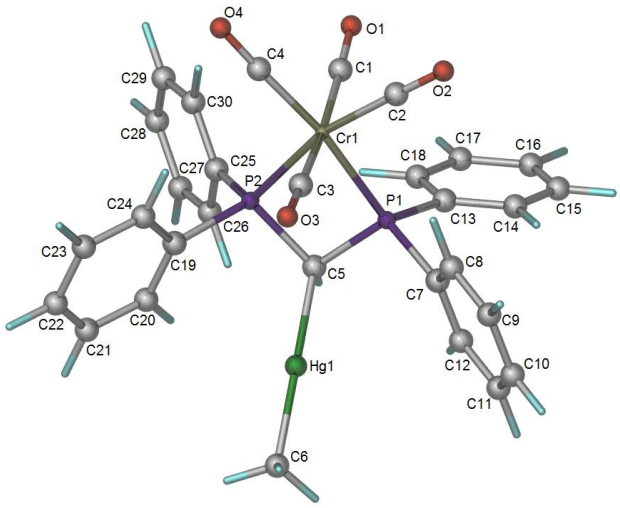

Figure 2.10 Molecular structure of **[2.6]**.

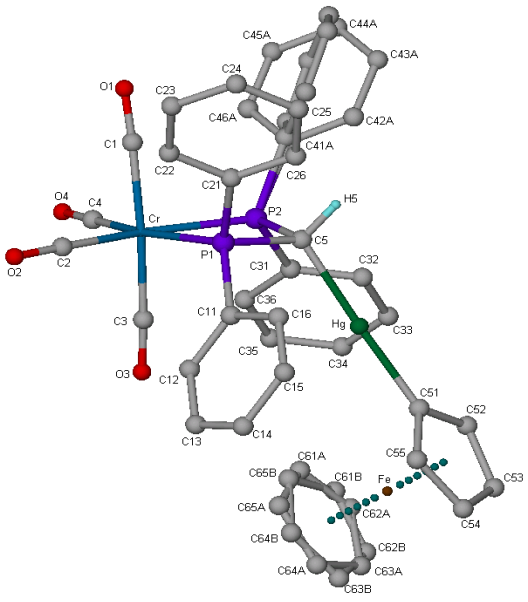

Figure 2.11 : Molecular structure of **[2.18]**

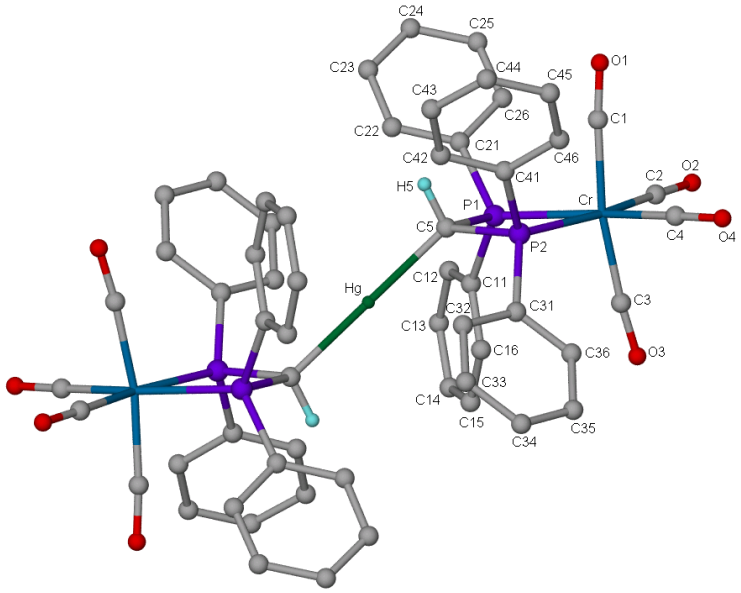

Figure 2.12 : Molecular structure of **[2.23]**

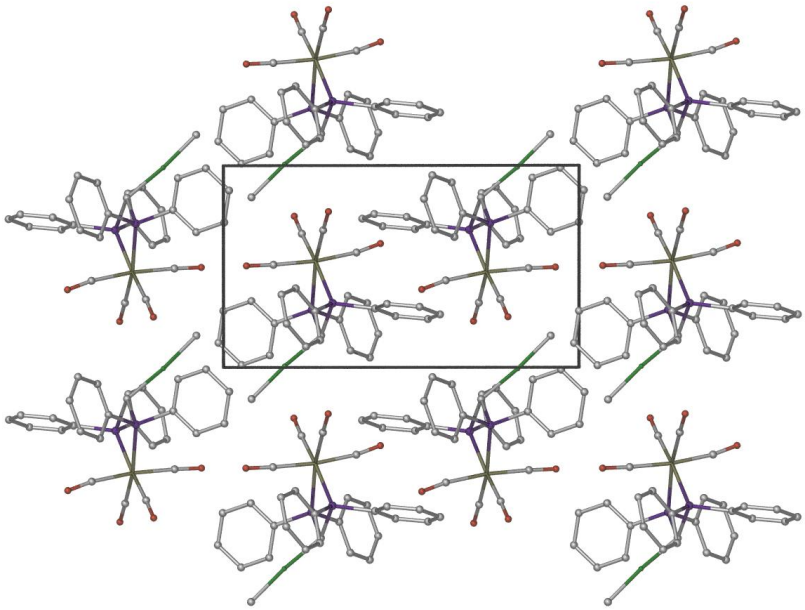

Figure 2.13 Molecular packing diagram of **[2.6]** viewed along [010].

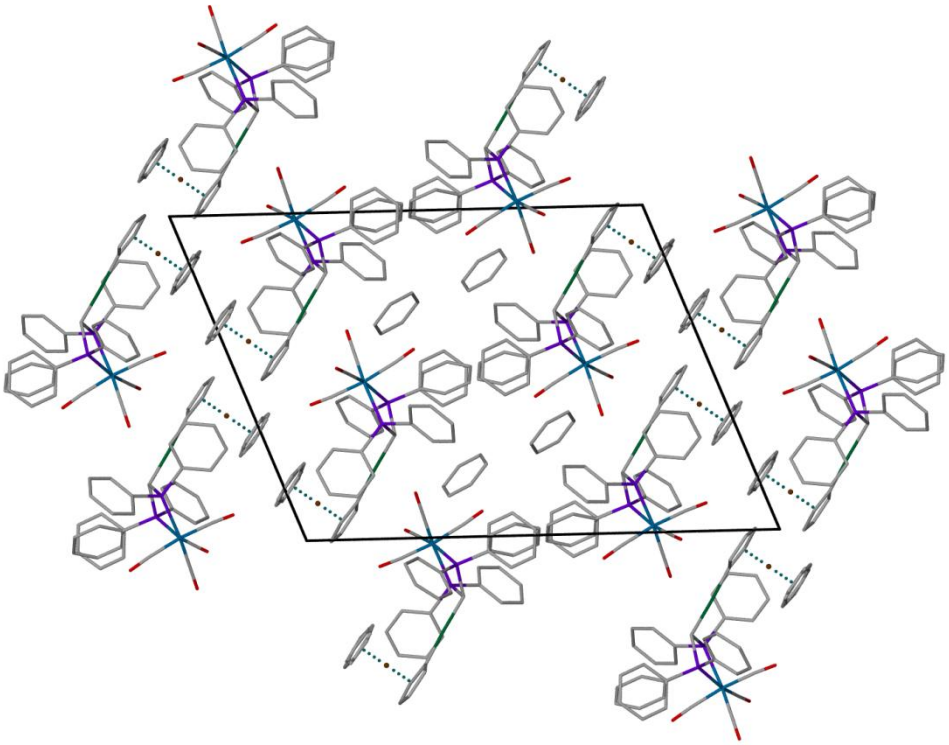

Figure 2.14 Molecular packing diagram of **[2.18]** viewed along [010].

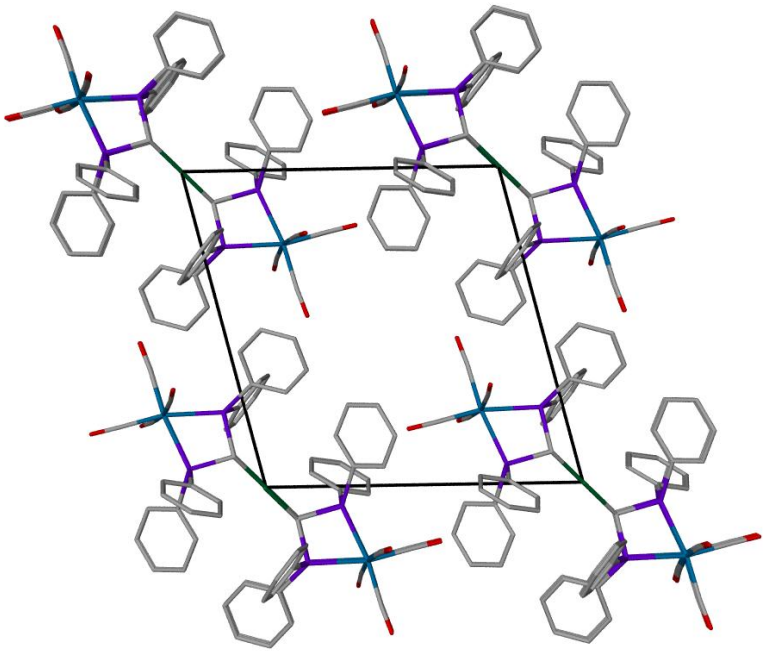

Figure 2.15 Molecular packing diagram of **[2.23]** viewed along [100].

The molecular structures show the dppm ligand bonded in a *P*,*P*-mode to chromium, forming a four-membered chelate ring. This ligand, together with the two axial and two equatorial carbonyls form a distorted octahedral coordination around the chromium atom. The distortion arises chiefly from the restriction of the 'bite' angle, P(1)-Cr-P(2), of the chelated dppm ligand, which ranges from 70.0(1)-70.7(2)°, compared to 89.4(2)-90.8(3)° for chromium hexacarbonyl.[30]

Table 2.3 Crystal data and refinement parameters for **[2.6]**, **[2.18]** and **[2.23]**

	[2.6]	**[2.18]**	**[2.23]**
Molecular formula	$C_{30}H_{24}CrHgO_4P_2$	$C_{39}H_{30}CrFeHgO_4P_2 \cdot C_6H_6$	$C_{58}H_{42}Cr_2HgO_8P_4$
Molecular mass, g mol^{-1}	763.05	1010.38	1295.39
Crystal dimensions, mm	0.40 x 0.25 x 0.20	0.10 x 0.10 x 0.05	0.40 x 0.25 x 0.20
Crystal system	Triclinic	Monoclinic	Triclinic
Space group	$P\bar{1}$	$P2_1/c$	$P\bar{1}$
Unit cell dimensions a, α	8.845(2) Å, 76.92(1)°	23.312(2) Å, 90.00(1)°	9.419(2) Å, 102.79(3)°
b, β	11.322(2) Å, 86.38(2)°	10.650(2) Å, 111.56(3)°	12.643(5) Å, 110.17(3)°
c, γ	15.390(3) Å, 74.08(2)°	17.343(3) Å, 90.00(1)°	13.062(5) Å, 90.96(3)°
*V*olume, Å^3	1444(2)	4005(1)	1416.5(8)
Z, D_C (Mg/m^3)	1.75	4, 1.680	1, 1.519
Absorption coefficient, mm^{-1}	57.8	4.571	3.244
F(000)	740	2000	642
Theta range for data collection		1.88 to 29.96°	1.66 to 24.98°
Limiting indices	-10 ≤ h ≤ 10 -13 ≤ k ≤ 13 0 ≤ l ≤ 18	0 ≤ h ≤ 32 -14 ≤ k ≤ 0 -24 ≤ l ≤ 22	0 ≤ h ≤ 11 -15 ≤ k ≤ 15 -15 ≤ l ≤ 14
Reflections collected / unique	5292 / 4783 [R(int) = 0.030	11895 / 11638 [R(int) = 0.0921]	5298 / 4965 [R(int) = 0.0379]
Completeness to theta = 26.75	-	100.0 %	99.9 %
Max. and min. transmission	-	0.8037 and 0.6579	0.5631 and 0.3569
Refinement method	Full-matrix least-squares on *F*	Full-matrix least-squares on F^2	Full-matrix least-squares on F^2
Data / restraints / parameters	-	11638 / 0 / 165	4965 / 0 / 327
Goodness-of-fit on F^2	0.051	0.540	1.006
Final R indices [I > 2sigma(I)]	0.058	R_1 = 0.1088, wR_2 = 0.2539	R_1 = 0.0513, wR_2 = 0.1273
R indices (all data)	-	R_1 = 0.2316, wR_2 = 0.3055	R_1 = 0.0810, wR_2 = 0.130

The ring angles around the methylene sp^3 carbon and phosphorus atoms further manifest the distortion in the chelate ring and deviate significantly from the ideal tetrahedral geometry. These angles range from 95.5(4) to 96.1(5)° and 96.2(3) to 96.9(3)° for P(1)-C(5)-P(2) and C(5)-P-Cr, respectively. The chelate ring formed by Cr, P(1), C(5) and P(2) for the three complexes is approximately planar, with **[2.23]** having the lowest torsion angles, ranging from -3.4(6) to 3.4(6)°. **[2.18]** deviates most from planarity with angles ranging from -8.0(4) to 8.0(4)°. The P-C(5) distances range from 1.824(8) to 1.851(9) Å and are characteristic of P-C single bonds. This is significant since the only other mercurated dppm structure, as discussed in **Chapter 1**, shows the P-C bonds to possess a degree of double bond character.[31] Whereas mercury did not neutralize the charge on the methylene carbon in the complex **[1.14]**, as described in **Chapter 1**, resulting in a Hg-carbene derivative, it is evident, considering the longer C(5)-P bond distances, that the bonding of mercury to the methylene carbon in these complexes is different.
The Cr-C-O angles fall in the range 171.8(9)–180(1)° and compare well with other chromium carbonyl structures.[32]

The trimetallic complex **[2.23]** adopts an antiparallel (or *trans*) conformation, with the mercury lying on a two-fold axis.

Compounds of the type $[M(CO)_4L_2]$ generally show M-C distances which fall into two distinct groups, where the two mutually *trans* carbonyl groups have longer M-C distances than those *trans* to the phosphorus atoms.[33] This is a result of phosphorus being a poorer π-acceptor than carbonyl and the fact that carbonyl groups have a stronger *trans* influence. The structural data in **Table 2.4** below show the Cr-C(2) and Cr-C(4) bond distances to be marginally shorter than the mutually *trans* distances, Cr-C(1) and Cr-C(3). The carbonyls *trans* to the Cr-P bonds get a greater share of the metal-*d* electrons, while the Cr-P bonds participate in weaker M(d_π)-P(p_{π^*}) back-bonding. The C-O distances *cis* to Cr-P are expected to be longer than their counterparts, since they mainly compete with each other for metal-*d* electrons. This trend is, however, not observed for any of the structures investigated here.

Table 2.4 Comparison of structural parameters for complexes **[2.6], [2.18]** and **[2.23]**

	[2.6]	**[2.18]**	**[2.23]**
Bond lengths (Å)			
Cr-P(1)	2.364(2)	2.371(7)	2.358(2)
Cr-P(2)	2.377(2)	2.375(3)	2.362(2)
Cr-C(1)	1.88(1)	1.85(3)	1.895(8)
Cr-C(2)	1.843(9)	1.83(3)	1.844(8)
Cr-C(3)	1.86(1)	1.85(3)	1.865(8)
Cr-C(4)	1.85(1)	1.84(3)	1.836(7)
C(1)-O(1)	1.15(1)	1.13(4)	1.13(1)
C(2)-O(2)	1.14(1)	1.14(3)	1.14(1)
C(3)-O(3)	1.19(1)	1.14(3)	1.15(1)
C(4)-O(4)	1.16(1)	1.14(3)	1.14(1)
Hg-C(5)	2.118(9)	2.10(2)	2.139(6)
Hg-C(R)	2.06(1)	2.04(1)	2.139(6)
P1-C(5)	1.834(8)	1.81(3)	1.840(6)
P2-C(5)	1.840(8)	1.86(2)	1.831(6)
Bond angles (°)			
P(1)-Cr-P(2)	70.0(1)	70.1(2)	70.7(2)
P(1)-C(5)-P(2)	95.6(4)	95.6(11)	96.1(5)
Cr-P(1)-C(5)	96.9(3)	97.4(8)	96.4(4)
Cr-P(2)-C(5)	96.2(3)	95.9(8)	96.6(4)
Cr-C(1)-O(1)	171.8(8)	176(3)	174.6(7)
Cr-C(2)-O(2)	178.2(8)	178(3)	175.5(8)
Cr-C(3)-O(3)	177(1)	178(2)	175.0(8)
Cr-C(4)-O(4)	177.8(9)	177(3)	177.7(8)
C(5)-Hg-C(6)	174.8(5)	177.6(9)	180.0(2)
Torsion angles (°)			
Cr-P(1)-C(5)-P(2)	9.7(4)	-8.0(4)	-3.3(2)
Cr-P(2)-C(5)-P(1)	-9.6(4)	8.0(4)	3.4(6)
P(1)-Cr-P(2)-C(5)	7.9(3)	6.6(3)	-2.8(5)
P(2)-Cr-P(1)-C(5)	-8.0(3)	-6.5(3)	2.8(5)

The Hg-C(5) (chelate ring) distances are 2.118(9), 2.10(2) and 2.139(6) Å for **[2.6]**, **[2.18]** and **[2.23]**, respectively. This distance is comparable to the Hg-C [2.10(2) Å] distance

found for the Hg-'carbene' complex **[1.14]**, discussed in **Chapter 1**.[10] However, the P(1)-C(5) and P(2)-C(5) bond distances rule out the presence of a Hg-'carbene' bond in these complexes. Distances of 2.06(2)[34] and 2.114(5) Å,[35] for example, have been reported for Hg-carbene bonds. The Hg-C(substituent) distances observed are 2.06(1), 2.043(8) and 2.139(6) Å for **[2.6]**, **[2.18]** and **[2.23]**, respectively. These bond distances are common for organomercury complexes.[36] The slightly longer bond length for **[2.23]** could be ascribed to the greater degree of crowding around the mercury atom.

The coordination at Hg deviates slightly from linearity for molecules **[2.6]** and **[2.18]**, with angles of 174.8 (5) and 176.9(4)°, respectively. Complex **[2.23]** has an equivalent angle of 180° due to the two-coordinate mercury atom lying on a two-fold axis.

The ferrocene moiety shows a degree of disorder in one of its cyclopentadienenyl rings. Disorder was also observed for one of the *P*-phenyl rings. A scan of inter- and intra molecular contacts < 3.5 Å revealed a secondary interaction between the Hg atom of the reference molecule at x, y, z and a carbonyl oxygen of another molecule at x-1, y, z for **[2.6]**. The Hg-O(2) distance of 3.014(7) Å, is 0.01 Å longer than the sum of their van der Waals radii, and thus represents a weak bonding interaction between the metal and the carbonyl group. Weak bonding distances of 2.83[37] Å and 3.08[38] Å have been reported for other mercury compounds. Weak secondary interactions are common for mercury, since it sometimes expand its characteristic linear two-coordination.[39] However, in this instance, it is debatable as to whether the oxygen atom can be considered to lie within the coordination sphere of mercury. The locations of the other molecules participating in the hydrogen bonding interactions are given as a footnote to **Table 2.5**. Compound **[2.18]** was found to be centrosymmetric which precludes it from being used as a NLO material.

Table 2.5 Hydrogen bonding data for **[2.6]** and **[2.18]**

Complex	Hydrogen bond	C-H	H···O, Å	C···O, Å	C-H, °
[2.6]	C(5) - H(5)···O(2)[a]	1.08	2.57(1)	3.35(1)	128.7(8)
	C(34) - H(34)···O(4)[b]	1.08	2.58(1)	3.37(1)	129.5(5)
[2.18]	C(13) - H(13)···O(3)[c]	1.08	2.39(2)	3.43(2)	139(1)
	C(36) - H(36)···O(4)[d]	1.08	2.33(1)	3.23(1)	159(1)

[a]Molecule at *x*-1; *y*; *z* [b]Molecule at -*x*+1; -*y*; -*z*

[c]Molecule at -*x*; -*y*; -*z*+1 [d]Molecule at -*x*; -*y*-1; -*z*

2.7 Electrochemical study of Group 6 metal complexes

Cyclic voltammetry, being sensitive to minute changes in the overall environment on the metal centre, has proven to be an extremely useful tool for measuring electronic effects of ligands on the properties of the accompanying metal centre(s). Various authors have commented on linear relationships of oxidation potentials with parameters such as vibrational frequencies[40], HOMO energies of complexes[41], chemical reactivity[42] and NMR chemical shifts[43] due to electronic effects imparted by the ligand.

We have shown earlier that a significant degree of correlation exists between the phosphorus chemical shift and the substituent group on the mercury atom (see **Section 2.4.3**). This would suggest that an inductive/mesomeric effect is present within the molecule. It would then appear as if the mercury atom acts as a bridge between the four-membered-chelate and the substituent group, facilitating electron flow between these entities. In this section we will attempt to confirm such an interaction by investigating the electrochemical behaviour of these complexes. A key indicator of such an effect would be the resultant oxidation potentials of the Group 6 metal centre. It is well known that the electronic environment around phosphorus influences the availability of electron density on the metal centre through π-backbonding. The fact that the phosphorus atoms experience various degree of deshielding depending on the substituent on the mercury atom would suggest some form of correlation between the electron availability on the Group 6 metal centre. It is well known that the phosphorus ligands can affect the HOMO energy of a molecule by either increasing the electron density on the metal due to σ-donation or decreasing the electron density on the metal centre due to π-backbonding. It therefore follows that good π-acceptor ligands will result in a lowering of the HOMO energy and a corresponding increase in the oxidation potential of the metal centre.

2.7.1 Electrochemistry of the unsubstituted chelates

The electrochemistry of Group 6 metal carbonyls such as $[(CO)_2ML_2]$ where L is a diphosphine (dppm or dppe) is well documented in the literature.[44] The electrochemical behaviour of the unsubstituted dppm compounds was investigated in dichloromethane. The

results of the electrochemical measurements are given in **Table 2.6**. We have found that the oxidation of the chromium complex, $[Cr(CO)_4(dppm)]$, is electrochemically reversible in dichloromethane, which can be attributed to the one electron oxidation process, $[Cr(CO)_4(dppm)]^{0/+1}$, where the oxidation process is metal-based.

The Mo and W analogues, $[M(CO)_4(dppm)]$ (M = Mo or W), on the other hand were electrochemically irreversible exhibiting a single oxidation wave which could be attributed to the process, $[M(CO)_4(dppm)]^0 \rightarrow [M(CO)_4(dppm)]^+$ (M = Mo or W). Cooling of the reaction mixture or faster scan rates did not result in reversibility. It is well known that the M^+ species for Mo and W are unstable, probably due to decomposition or chemical reaction with the solvent.[45] In a study by Ohs *et al*., on Group 6-dppf complexes, the Mo and W analogs showed no reverse reduction waves.[46] From **Table 2.6** it can be seen that the ease of oxidation increases in the order W < Mo < Cr. This is a general trend observed in many studies and is attributed to the increased overlap of metal orbitals with the phosphorus 3*d* orbitals, due to an increase in atomic size, thus resulting in more efficient removal of electron density from the metal-based orbitals. However, a few authors have reported examples where oxidation potentials for Mo and W are similar[47] or where W has a lower[48,49] oxidation potential. The latter was attributed to the higher electron density of tungsten complexes.

2.7.2 Electrochemistry of the metallated derivatives

The electrochemical behaviour of the mercurated complexes was investigated in dichloromethane. The behaviour of the Group 6 metal centres for the bi- and tri-metallic derivatives was similar to that of their unsubstituted precursors. Electrochemical reversibility was observed for the chromium derivatives, while the analogous Mo and W complexes displayed electrochemical irreversibility. The electrochemical data for selected complexes are given in **Table 2.6**.

Very noticeable is the decrease in the oxidation potentials for the Group 6 metal tetracarbonyls on replacing the methylene hydrogen for the HgR^+ fragment. This observation is in agreement with the observed deshielding of the phosphorus atoms on

metallation. The ferrocenyl compound **[2.18]** shows two reversible oxidations, the wave at $E_{½}$ -99 mV being due to the ferrocene couple, $Fc^{0/+1}$, while the redox process at $E_{½}$ +185 mV can be ascribed to the reversible oxidation of the chromium metal centre.

Table 2.6 Electrochemical potentials of selected metallated complexes in dichloromethane in mV

Complex		$E_{½}^{1}$	E_{pa}	$E_{½}^{2}$
$[Cr(CO)_4(PPh_2CH_2PPh_2)]$		+187		
$[Mo(CO)_4(PPh_2CH_2PPh_2)]$			+448	
$[W(CO)_4(PPh_2CH_2PPh_2)]$			+457	
$[Cr(CO)_4(PPh_2CH(HgMe)PPh_2)]$	**[2.6]**	+116		
$[Mo(CO)_4(PPh_2CH(HgMe)PPh_2)]$	**[2.7]**		+326	
$[W(CO)_4(PPh_2CH(HgMe)PPh_2)]$	**[2.8]**		+376	
$[Cr(CO)_4(PPh_2CH(HgEt)PPh_2)]$	**[2.9]**	+89		
$[Mo(CO)_4(PPh_2CH(HgEt)PPh_2)]$	**[2.10]**		+369	
$[W(CO)_4(PPh_2CH(HgEt)PPh_2)]$	**[2.11]**		+383	
$[Cr(CO)_4(PPh_2CH(HgPr)PPh_2)]$	**[2.12]**	+99		
$[Cr(CO)_4(PPh_2CH(HgPh)PPh_2)]$	**[2.14]**	+115		
$[Mo(CO)_4(PPh_2CH(HgPh)PPh_2)]$	**[2.15]**		+350	
$[W(CO)_4(PPh_2CH(HgPh)PPh_2)]$	**[2.16]**		+331	
$[Cr(CO)_4(PPh_2CH(HgFc)PPh_2)]$	**[2.18]**	+185		-96
$[Mo(CO)_4(PPh_2CH(HgFc)PPh_2)]$	**[2.19]**		+403	-101
$[W(CO)_4(PPh_2CH(HgFc)PPh_2)]$	**[2.20]**		+427	-94
$[Cr(CO)_4(PPh_2CH(HgCl)PPh_2)]$	**[2.21]**	+187		
$[Cr(CO)_4(PPh_2CH(Hg(Hdptc))PPh_2)]$	**[2.22]**	+197		
$[Cr(CO)_4(PPh_2CHPPh_2)_2Hg]$	**[2.23]**	+182		
$[Mo(CO)_4(PPh_2CHPPh_2)_2Hg]$	**[2.24]**		+416	
$[Cr(CO)_4(PPh_2CH(AuPPh_3)PPh_2)]$	**[2.33]**	+12		
$[Mo(CO)_4(PPh_2CH(AuPPh_3)PPh_2)]$	**[2.34]**		+305	
$[W(CO)_4(PPh_2CH(AuPPh_3)PPh_2)]$	**[2.35]**		+327	
$[Cr(CO)_4(PPh_2CH(AuPEt_2Ph)PPh_2)]$	**[2.36]**	+10		
$[Mo(CO)_4(PPh_2CH(AuPEt_2Ph)PPh_2)]$	**[2.37]**		+299	
$[W(CO)_4(PPh_2CH(AuPEt_2Ph)PPh_2)]$	**[2.38]**		+330	

The Mo **[2.19]** and W **[2.20]** analogs showed a similar one-electron reversible oxidation for the ferrocenyl moiety at -101 and -94 mV, followed by an irreversible metal-based oxidation at 403 and 427 mV, respectively. Of interest in the complexes **[2.18]**, **[2.19]** and **[2.20]** is the decrease in the oxidation potential of the Fe centre when compared to ferrocene or chloromercuryferrocene (see **Figure 2.16**). This is contrary to what would be expected when adding ferrocene to an electron-rich chelate ring. It is well known that electron-withdrawing substituents increase $E_{1/2}$ values, by removal of electron density from the metal centre.[50]

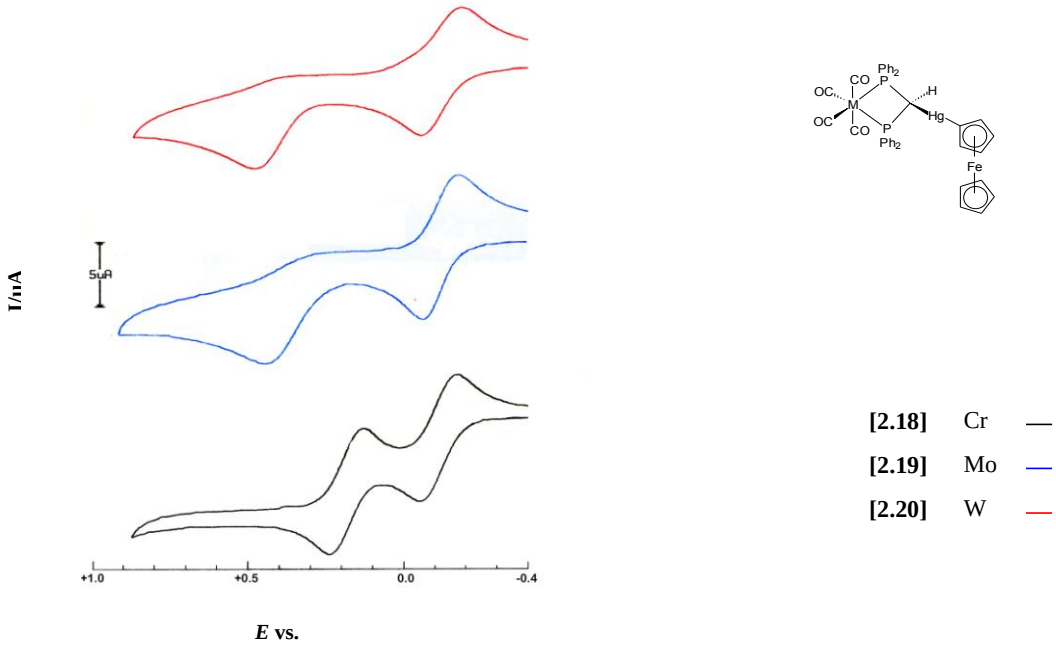

Figure 2.16 Cyclic voltammograms of ferrocenylmercurated derivatives of $M(CO)_4$dppm.

Ferrocene and chloromercuryferrocene show very similar half-wave potentials with the latter being +28 mV more anodic. The slightly more anodic potential for the oxidation of chloromercuryferrocene could be attributed to the electron-withdrawing chlorine. The observed decrease in half-wave potential for the Fe metal centre in the heterotrimetallic complexes could most likely be attributed to the shielding of the ferrocene by the *P*-phenyl groups as observed for the methylmercury complex **[2.6]**. In the X-ray crystallographic

structure the ferrocene appears to be flanked by the *P*-phenyl rings which could affect a 'through-space' shielding resulting in a lowered oxidation potential for the Fe metal centre. From the crystal data, the Fe metal centre has been calculated to be approximately 5.2 Å from the *P*-phenyl rings, slightly more than the 4.6 Å reported by Bach and Weibel to affect significant shielding.[28] 'Through-space' electronic effects have been reported for complexes containing π-systems.[51] It is also evident from the data that $E_{1/2}$ for the ferrocene moiety in **[2.18]**-**[2.20]** is insensitive to the Group 6 metal centre.

A single reversible oxidation peak with $E_{½}$ +182 mV was observed for complex **[2.23]**, indicating that the two chromium centres are completely without interaction and are therefore independently oxidized with a single electron being removed from each metal centre with equal potential. This would be classified as a Class I interaction as defined by Robin and Day.[9] However, results have shown that some degree of electronic interaction is present within the metallated complexes. Other groups have shown that slight peak separation is sometimes achieved when molecules are investigated using, for example, rotating disk techniques, which in such a case would indicate a weak or moderate (Class II) interaction.

The electrochemical data for the isoelectronic Au^{I}-complexes show a similar decrease in oxidation potential for the Group 6 metal centre on metallation. Similar electrochemical behaviour is observed, with electrochemical reversibility for the Cr complexes **[2.33]** and **[2.36]** and irreversible behaviour for the Mo **[2.34]** and **[2.37]** and W **[2.35]** and **[2.38]** complexes. There appears to be no impact on the Group 6 metal oxidation potentials on changing the substitutent on phosphorus.

The oxidation potentials for the aurated complexes are of similar magnitude to the alkyl- and arylmercury complexes. This is to be expected when considering the similarity in the phosphorus chemical shift data. The bonding in mercury(II) and gold(I) complexes has been shown to be comparable, with a slightly increased participation of Au-5*d* orbitals compared to Hg-5*d* orbitals. The bonding in similar mercury complexes has been described in terms of a three-centre two-electron (3*c*-2*e*) bond.[52]

2.7.3 Correlation studies

The most striking feature of the electrochemical data is the sensitivity of the oxidation potential of the Group 6 metal centres to the substituent on mercury. Correlation studies have often been used to verify electrochemical relationships in molecules.

2.7.3.1 Correlation of oxidation potentials with NMR parameters

Table 2.7 summarizes the electrochemical and spectroscopic data for the chromium bi- and trimetallic complexes. In **Figures 2.17** and **2.18** plots of the $E_{1/2}$ values for the chromium metal centre versus δ(P) and ^2J(HgP), respectively, are shown. These plots show a good fit with the linear correlation r^2 = 0.93 and 0.90, respectively. It should be noted that **[2.18]** and **[2.22]** are excluded from the regression analysis. The former complex shows an increased redox potential for the chromium metal centre in **[2.18]**, as displayed in **Figures 2.17** and **2.18**, due to the formation of the electro-generated ferrocenium group, which is comparatively more electron-withdrawing than the ferrocenyl group. While the dithizonate derivative, **[2.22]**, appears to fit the correlation, the difference in the three-coordinate bonding experienced by the Hg atom does influence the degree of electron transfer. This becomes evident when the correlation as depicted in **Figure 2.19** below is considered.

Table 2.7 Correlation data for selected mercurated complexes of $[Cr(CO)_4\{PPh_2CH(HgR)PPh_2\}]$

Complex		$E_{1/2}$ mV	δ(P) ppm	^2J(Hg-P) Hz	$\nu(CO)_{total}$ cm^{-1}
$[Cr(CO)_4(PPh_2CH(HgMe)PPh_2)]$	**[2.6]**	+116	33.1	77	7667
$[Cr(CO)_4(PPh_2CH(HgEt)PPh_2)]$	**[2.9]**	+89	32.7	55	7666
$[Cr(CO)_4(PPh_2CH(HgPr)PPh_2)]$	**[2.12]**	+99	34.5	60	7667
$[Cr(CO)_4(PPh_2CH(HgPh)PPh_2)]$	**[2.14]**	+115	33.8	87	7673
$[Cr(CO)_4(PPh_2CH(HgFc)PPh_2)]$	**[2.18]**	+167	35.5	96	7674
$[Cr(CO)_4(PPh_2CH(HgCl)PPh_2)]$	**[2.21]**	+187	41.7	212	7699
$[Cr(CO)_4(PPh_2CH(Hg(Hdptc))PPh_2)]$	**[2.22]**	+197	40.2	194	7679
$[\{Cr(CO)_4(PPh_2CHPPh_2)\}_2Hg]$	**[2.23]**	+171	40.5	135	7692

The results indicate that the ability of phosphorus to remove electron density from the chromium metal centre is dependent on the substituent on the mercury atom. It also follows the order of electronegativity of the substituent group, i.e. Et < Pr < Me < Ph < Cr(dppm-H) < Cl. The results also show that mercury appears to facilitate electron flow within the molecule. The Hg^{2+} centre is known to have a great tendency to covalency and a substantial polarizing power. The poorer correlation of $E_{1/2}$ with ^{2}J(HgP) could be attributed to possible steric factors present in the trimetallic complex **[2.23]**. The crystal structure of **[2.23]** has shown it to have slightly longer Hg-C bond lengths compared to **[2.6]** and **[2.18]**, possibly due to the proximity of the two large dppm chelates.

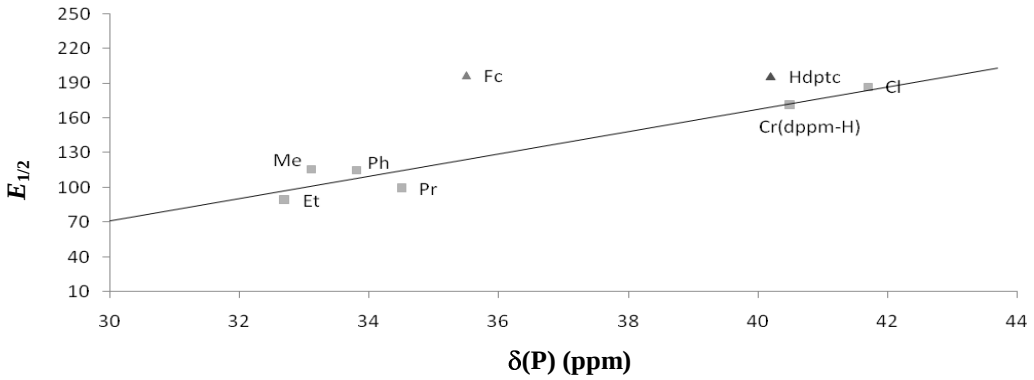

Figure 2.17 Correlation diagram of half-wave potential and NMR chemical shifts of mercurated derivatives of $Cr(CO)_4$dppm.

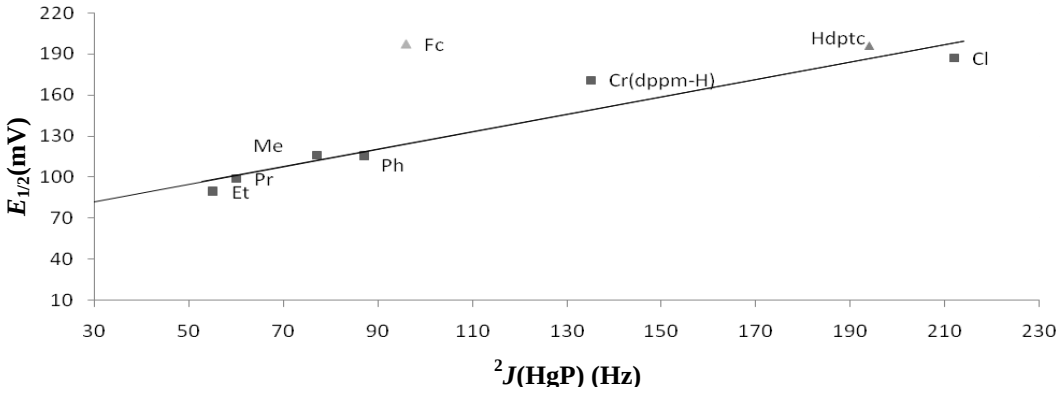

Figure 2.18 Correlation diagram of half-wave potential and NMR coupling constants of mercurated derivatives of $Cr(CO)_4$dppm.

2.7.3.2 Correlation of oxidation potentials with IR parameters

It is well known that the carbonyl stretching frequencies for metal-carbonyl compounds are dependent on the electron density on the metal centre. Moreover, since the oxidation potentials of a complex is a measure of the overall electron density on the transition-metal centre, we expect to find a correlation between carbonyl stretching frequencies and oxidation potential of the metal centre. Milosavljevic *et al.*[53] and Cook *et al.* [54] have, for example, shown a linear relationship to exist between $E_{1/2}$ and ν(CO) for phenyldibenzophosphole and bis(tertiary phosphine) Group 6 metal-tetracarbonyl complexes, respectively. While these and earlier authors used the A_1 stretching frequency in their studies, it has been proposed by Alyea[55] that the sum of all the CO frequencies, rather than a single frequency, provides a better approach to making these correlations, since all of the metal carbonyl groups on the metal centre are affected by electronic changes. Ackermann[56] has, for example, used this method to demonstrate that the carbonyl stretching frequencies provide a more reliable measure of the electronic environment of the metal nucleus. We have also found this method to be more useful in determining the presence of an electronic relationship in this study, since the range of A_1 carbonyl stretching frequency values of 4 cm^{-1} can be considered as insignificant, compared to a range of 33 cm^{-1} for the cumulative frequencies.

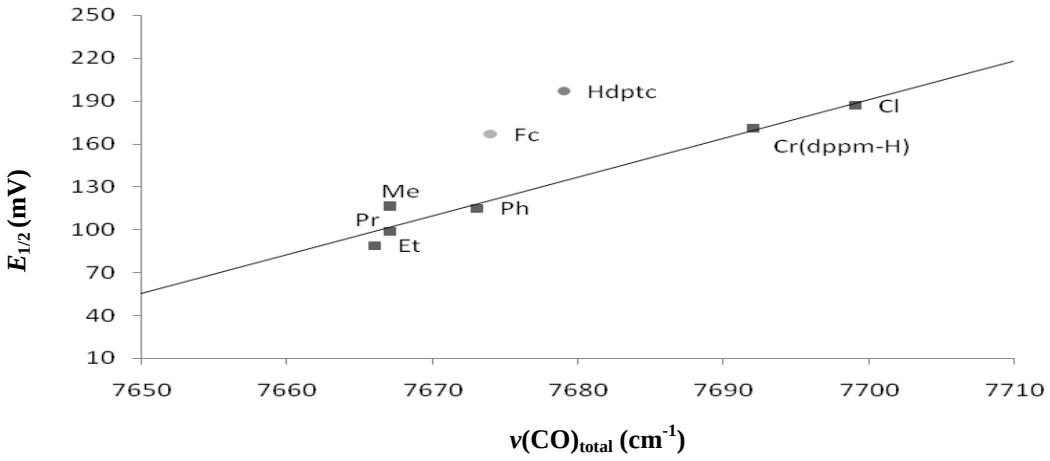

Figure 2.19 Correlation between $E_{1/2}$ and $\nu(CO)_{total}$ for $[Cr(CO)_4(PPh_2CH(HgR)PPh_2\}]$ complexes.

A linear relationship (r^2 = 0.96) was found for the series of compounds. This is clearly illustrated by, for example, the electron-withdrawing chlorine group which would reduce the electron density on the metal centre, which would consequently result in the expected increase in the oxidation potential of the metal centre and strengthening of the CO bond, i.e. increased *v*(CO), as a function of decreased π-backbonding. The inductive methyl group would have the opposite effect as observed. The Fc **[2.18]** and Hdptc **[2.22]** complexes do not fit the correlation. This would imply that the three-coordinate bonding for the mercury atom in **[2.22]** influences the electron density on the metal centre. The formation of the electro-generated ferrocenium group in **[2.18]** is comparatively more electron-withdrawing than the neutral complex. We would consequently expect a shortening of the CO bonds, resulting in an increase in the carbonyl stretching frequencies, *v*(CO).

A series of heterobi- and tri-metallic complexes has been prepared by the metallation of the carbanion derived from the deprotonation of bis(diphenylphosphinomethane) chelates of Cr, Mo and W. Correlation studies of electrochemical potentials with NMR parameters and carbonyl stretching frequencies reveal the ability of Hg to facilitate electron flow within the molecule. The electron-flow has been established to be weak, considering the narrow range in the electrode potentials of the chromium metal centre. Evidence of "through-space" communication was observed in the trimetallic ferrocenyl complexes.

REFERENCES

1 P. Yuan, X. Wu, G. Yu, D. Du and S. H. Liu, *J. Organomet. Chem*, 2007, **692**, 3588.

2 M.-L. Marcos, C. Moreno, R. M. Medina, M.-J. Macazaga, S. Delgado and J. Gonzalez-Velasco, *J. Organomet. Chem.*, 1998, **568**, 185.

3 W.-Y. Wong, K.-H. Choi, G-L. Lu, J-X. Shi, P-Y. Lai, S.-M. Chan and Z. Lin, *Organometallics*, 2001, **20**, 5446.

4 C. J. Sumby and P. J. Steel, *Polyhedron*, 2007, **26**, 5370.

5 T. J. Wedge, A. Herzog, R. Huertas, M. W. Lee, C. B. Knobler and M. F. Hawthorne, *Organometallics*, 2004, **23**, 482.

6 D. Xu, J. Z. Zhang and B. Hong, *J. Phys. Chem. A*, 2001, **105**, 7979.

7 J. V. Ortega, B. Hong, S. Ghosal, J. C. Hemminger, B. Breedlove and C. P. Kubiak, *Inorg. Chem.*, 1999, **38**, 5102.

8 B. Hong, S. R. Woodcock, S. K. Saito and J. V. Ortega, *J. Chem. Soc., Dalton Trans.*, 1998, 2615.

9 M. B. Robin and P. Day, *Adv. Inorg. Chem. Radiochem.*, 1967, **10**, 247.

10 J. Ruiz, R. Aruaz, V. Riera, M. Vivanco, S. Garcia-Granda and E. Perez-Carreno, *J. Chem. Soc., Chem. Commun.*, 1993, 740.

11 B. Bildstein, M. Malaun, H. Kopacka, K.-H. Ongania and K. Wurst, *J. Organomet. Chem.*, 1999, **572**, 177.

12 A. K. Brisdon, I. R. Crossley, R. G. Pritchard and G. Sadiq, *J. Organomet. Chem.*, 2007, **692**, 2125.

13 J. Zheng, J. Ou, Z. Mo and S. Yin, *Sci. Total Environ*., 2011, **412**, 214.

14 Z. Niu, X. Zhang, Z. Wang and Z. Ci, *Environ. Pollution*, 2011, **159**, 2684

15 L. B. Furieri, M. Fioresi, R. F. Ribeiro Junior, M. V. Bartolomé, A. A. Fernandes, V. Cachofeiro, V. Lahera, M. Salaices, I. Stefanon and D. V. Vassallo, *Toxicol. Appl. Pharmacol.*, 2011, **255**, 193.

16 H. Haase, G. Engelhardt, S. Hebel and L. Rink, *Toxicol. Appl. Pharmacol.*, 2011, **250**, 78.

17 D. Vorländer, *Z. Phys. Chem. Stoechiom. Verwandtschaftsl.*, 1923, **105**, 211.

18 A. Itai, Y. Toriumi, H. Kagechika, I. Azumaya and K. Shudo, *Tet. Letters*, 1989, **30**, 6177.

19 M. J. Frisch, G. W. Trucks, H. B. Schlegel, G. E. Scuseria, M. A. Robb, J. R. Cheeseman, G. Scalmani, V. Barone, B. Mennucci, G. A. Petersson, H. Nakatsuji, M. Caricato, X. Li, H. P. Hratchian, A. F. Izmaylov, J. Bloino, G. Zheng, J. L. Sonnenberg, M. Hada, M. Ehara, K. Toyota, R. Fukuda, J. Hasegawa, M. Ishida, T. Nakajima, Y. Honda, O. Kitao, H. Nakai, T. Vreven, J. A. Montgomery, Jr., J. E. Peralta, F. Ogliaro, M. Bearpark, J. J. Heyd, E. Brothers, K. N. Kudin, V. N. Staroverov, R. Kobayashi, J. Normand, K. Raghavachari, A. Rendell, J. C. Burant, S. S. Iyengar, J. Tomasi, M. Cossi, N. Rega, J. M. Millam, M. Klene, J. E. Knox, J. B. Cross, V. Bakken, C. Adamo, J. Jaramillo, R. Gomperts, R. E. Stratmann, O. Yazyev, A. J. Austin, R. Cammi, C. Pomelli, J. W. Ochterski, R. L. Martin, K. Morokuma, V. G. Zakrzewski, G. A. Voth, P. Salvador, J. J. Dannenberg, S. Dapprich, A. D. Daniels, O. Farkas, J. B. Foresman, J. V. Ortiz, J. Cioslowski, Jiband D. J. Fox, *Gaussian, Inc*., Wallingford CT, 2009.

20 A. D. Becke, *J. Chem. Phys*., 1993, **98**, 5648.

21 S. Al-Jibori and B. L. Shaw, *J. Chem. Soc.*, *Chem. Comm.*, 1982, 286.

22 S. Al-Jibori, M. Hall, A. T. Hutton and B. L. Shaw, *J. Chem. Soc.*, *Dalton Trans.*, 1984, 863.

23 M. Ardon, G. Hogarth and D. T. W. Oscroft, *J. Organomet. Chem*., 2004, **689**, 2429.

24 G. Hogarth and J. Kilmartin, *J. Organomet. Chem*., 2007, **692**, 5655.

25 S. Al-Jibori and B. L. Shaw, *Inorg. Chim. Acta*., 1983, **74**, 235.

26 J. Ruiz, V. Riera, M. Vivanco, S. Garcia-Granda and M. R. Diaz, *Organometallics*, 1998, **17**, 4562.

27 J. V. Hatton, W. G. Schneider and W. Siebrand, *J. Chem. Phys*., 1963, **39**, 1330.

28 R. D. Bach, A. T. Weibel, *J. Amer, Chem. Soc*., 1976, **98**, 6241.

29 E. J. Fernandez, M. Concepcion Gimeno, P. G. Jones, A. Laguna, M. Laguna and E. Olmos, *Inorg. Chim. Acta*, 1995, **238**, 173.

30 A. Whitaker and J. W. Jeffery, *Acta. Cryst*., 1967, **23**, 977.

31 J. Ruiz, R. Aruaz, V. Riera, M. Vivanco, S. Garcia-Granda and E. Perez-Carreno, *J. Chem. Soc., Chem. Commun.*, 1993, 740.

32 J. L. Blake, D. J. Cook, P. J. Squattrito and B. A. Howell, *Acta Crystal. C*, 1995, **C51**, 1067.

33 L. F. Tang, Z. H. Wang, Y. M Xu. J. T.Wang, H. G. Wang and X. K. Yao, *Polyhedron*, 1999, **18**, 2383.

34 P. Luger and G. Ruben, *Acta. Crystallogr. Sect. B.*, 1971, **27**, 2276.

35 Q. X. Liu, L. N. Yin and J. C. Feng, *J. Organomet. Chem.*, 2007, **692**, 3655.

36 A. K. Briston, I. R. Crossley, R. G. Pritchard and G. Sadiq, *J. Organomet. Chem.*, 2007, **692**, 2125.

37 N. Ueyama, K. Taniuchi, T. Okamura, A. Nakamura, H. Maeda and S. Emura , *Inorg. Chem.*, 1996, **35**, 1945.

38 H. Barrera, J. C. Bayon, P. Gonzalez-Duarte, J. Sola and J. M. Vinas, *Polyhedron*, 1982, **1**, 647.

39 A. T. Hutton, H. M. N. H. Irving, L. R. Nassimbeni and G. Gafner, *Acta. Crystallogr., Sect. B*, 1980, **26**, 2064.

40 N. G. Connelly and M. D. Kitchen, *J. Chem. Soc., Dalton Trans.*, 1977, 931; E. B. Milosavljevic, L. Solujic, S. Affandi and J. H. Nelson, *Organometallics*, 1988, **7**, 1735.

41 A. C. Serapu and R. F. Fenske, *Inorg. Chem.*, 1975, **14**, 247.

42 R. E. Dessey, R. B. King and M. Waldrop, *J. Am. Chem. Soc.*, 1966, **88**, 5112.

43 M. N. Ackermann, W. G. Fairbrother, N. S. Amin, C. J. Deodene, C. M. Lamborg and P. T. Martin, *J. Organomet. Chem.*, 1996, **523**, 145.

44 J. R. Sowa, J. B Bonanno, V. Zanotti and R. J. Anekici, *Inorg. Chem.*, 1992, **31**, 1370.

45 R. L. Cook and J. G. Morse, *Inorg. Chem.*, 1984, **23**, 2332; S. Ernst and W. Kaim, *J. Am. Chem. Soc.*, 1986, **108**, 3578.

46 A. C. Ohs, A. L. Rheingold, M. J. Shaw and C. Nataro, *Organometallics*, 2004, **23**, 4655.

47 C. M. Alvarez, M. E. Garcia, M. T. Rueda, M. A. Ruiz, D. Saez, and N. G. Connelly, *Organometallics*, 2005, **24**, 650.

48 B. Bildstein, M. Malaun, H. Kopacka, M. Fontani and P. Zanello, *Inorg. Chem. Acta.*, 2000, **300–302**, 16.M.

49 A. Fox, K. A. Campbell and E. P. Kyba, *Inorg. Chem.*, 1981, **20**, 4163.

50 J. C. Kotz, C. L. Nivert and J. M. Lieber, *J. Organomet. Chem.*, 1975, **91**, 87.

51 K. Lee, Y. J. Choi, Y.Cho, C. Y. Lee, H. Song, C. H. Lee, Y. S. Lee, and J. T. Park, *J. Am. Chem. Soc.*, 2004, **126**, 9837.

52 R. L. DeKock, E. J. Baerends, P. M. Boerrigter and R. Hengelmolen, *J. Am. Chem. Soc.*, 1984, **106**, 3387.

53 E. B. Milosavljevic, L. Solujic, S. Affandi and J. H. Nelson, *Organometallics*, 1988, **7**, 1735.

54 R. L. Cook and J. G. Morse, *Inorg. Chem*., 1984, **23**, 2332.

55 E. C. Alyea, R. A. Gossage, J. Malito and Z. A. Munir, *Polyhedron*, 1990, **9**, 1059.

56 M. N. Ackermann, W. G. Fairbrother, N. S. Amin, C. J. Deodene, C. M. Lamborg and P. T. Martin, *J. Organomet. Chem*., 1996, **523**, 145.

CHAPTER 3

Structural and electrochemical study of mercurated Pd-, Pt- and Ru-dppm complexes

3.1 Introduction

In **Chapter 2**, we observed evidence of electronic communication between the two metal centres in the metallated Group 6 metal-dppm complexes. We thought of extending this investigation to include the square-planar Pd- and Pt-dppm compounds, reasoning that the electron flow facilitated by the Hg-chelate system will be enhanced in the square-planar arrangement.

Results from **Chapter 2** have also shown that, as opposed to the findings by Laguna *et al.*,[1] metallation of chelated dppm results in the P-C bonds of the chelate ring adopting bond orders of 1, with the methylene carbon retaining its sp^3 character. It would appear, when considering complex **[1.14]** (see **Figure 1.5**) reported by Laguna *et al.*, that the deprotonated dppm-chelate is partially stabilized by having the metal-dppm complex in a cationic state. This could lead to the formation of a mercury 'carbene' complex on metallation, which should enhance electron flow within the molecule. We therefore extended our investigation to include an electron-rich cationic cyclopentadienyl Ru(II)-dppm complex.

3.2 Preparation of Pd- and Pt dithiolene-dppm complexes

A series of mono-dithiolene metal complexes was prepared by the displacement of the chloride groups from the MCl_2(dppm) precursors by reaction with the disodium salt of the appropriate dithiolene. While mixed dithiolene-dppe complexes are reported in the literature, only the maleonitrile derivative of Pt-dppm is known.[2] In contrast to the

preparation in acetone as reported, we have conducted the preparation of these complexes in ethanol, as shown in **Scheme 3.1**.

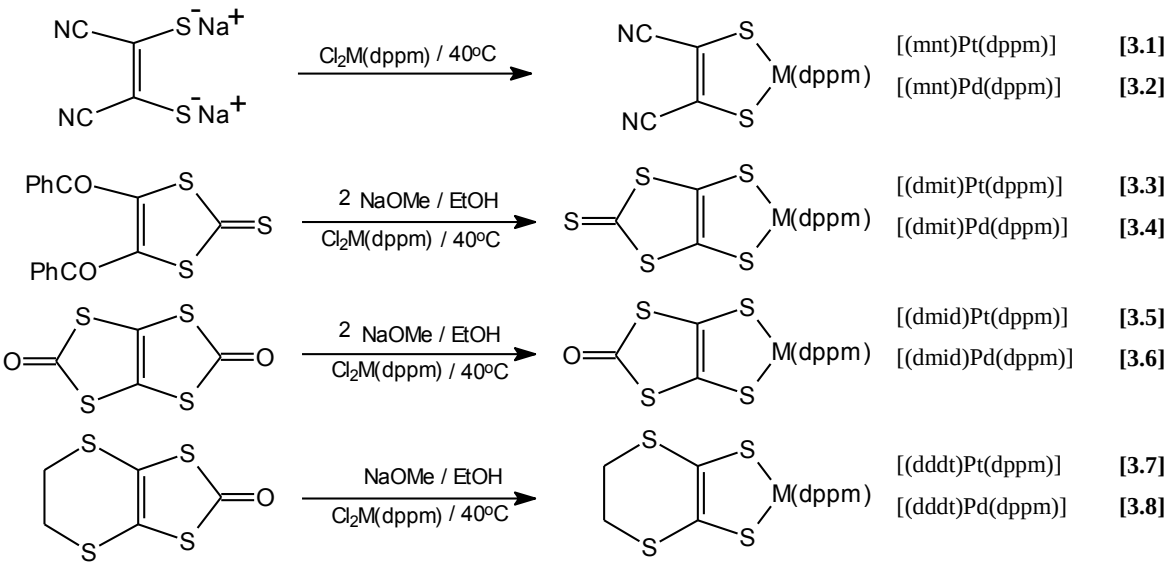

Scheme 3.1 Preparation of (dithiolene)M(dppm) complexes.

The complexes were prepared in good yields by metathesis reactions. The colour of these complexes ranges from light peach for the platinum maleonitrile complexes to black for the dddt complex of palladium. Palladium complexes were generally darker compared to the equivalent platinum complexes.

The infrared spectra for complexes **[3.1]-[3.8]** were recorded as KBr disks and showed the expected *ν*(C=C) vibrations. These vibrations appear to be independent of the dithiolene ligand and unaffected by the specific metal centre the dithiolene is coordinated to, and occur in the narrow range of 1433-1437 cm^{-1}. Complexes **[3.1]** and **[3.2]**, for example, showed the characteristic *ν*(C≡N) vibrations at 2200 and 2198 cm^{-1}, respectively, while the *ν*(C=S) and *ν*(C=O) vibrations lie within the 1612-1660 cm^{-1}range.

The ^{1}H NMR spectra for complexes **[3.1]-[3.8]** (see **Table 3.1**) display a triplet for the methylene hydrogens, with chemical shifts ranging from 4.40 to 4.75 ppm. There appears to be a downfield shift for the methylene protons on going from the MCl_2(dppm) complex to the (dithiolene)M(dppm) derivative, indicating the comparative electron-withdrawing

nature of the dithiolene ligands, and resulting in deshielding of the P_2CH_2 protons. The methylene resonances are generally about 0.3 ppm more downfield for the corresponding platinum complex. The degree of coupling, ^2J(PH), appears to be independent of the substituent dithiolene and is in the narrow range of 10.7 to 10.8 Hz and 9.8 to 10.3 Hz for the platinum and palladium complexes, respectively. The platinum complexes display the characteristic set of satellites due to coupling of the methylene hydrogens with ^{195}Pt. The ^3J(PtH) coupling ranges from 43.9 to 48.0 Hz. The Pt- and Pd-dddt complexes, **[3.7]** and **[3.8],** exhibit a singlet for the four equivalent bridging ethylene hydrogens at 3.06 and 3.11 ppm respectively. The phenyl protons for all complexes show resonances in the chemical shift region ranging from 7.2 to 7.8 ppm.

The ^{31}P NMR spectra are characterized by a singlet for the two equivalent dppm phosphorus atoms. In the case of platinum, the singlet is flanked by two satellites due to coupling with ^{195}Pt. The singlet is found in the range: -37.39 to -39.92 ppm and -47.20 to -48.32 ppm for the palladium and platinum complexes, respectively.

Table 3.1 NMR data of [(dithiolene)M($PPh_2CH_2PPh_2$)] complexes, M = Pd or Pt

Complex		^{1}H-NMR			^{31}P-NMR	
		δ (ppm)		$^2J_{PH}$ (Hz) [$^3J_{PtH}$ (Hz)]	δ (ppm)	J_{Pt-P} (Hz)
[(mnt)Pt($PPh_2CH_2PPh_2$)]	**[3.1]**	4.75	P_2CH_2	10.7 [43.9]	-48.32	2387.5
[(mnt)Pd($PPh_2CH_2PPh_2$)]	**[3.2]**	4.40	P_2CH_2	10.2	-39.37	
[(dmit)Pt($PPh_2CH_2PPh_2$)]	**[3.3]**	4.71	P_2CH_2	10.7 [48.8]	-48.02	2430.5
[(dmit)Pd($PPh_2CH_2PPh_2$)]	**[3.4]**	4.41	P_2CH_2	10.2	-39.92	
[(dmid)Pt($PPh_2CH_2PPh_2$)]	**[3.5]**	4.74	P_2CH_2	10.8 [48.0]	-48.23	2435.8
[(dmid)Pd($PPh_2CH_2PPh_2$)]	**[3.6]**	4.41	P_2CH_2	10.3	-39.67	
[(dddt)Pt($PPh_2CH_2PPh_2$)]	**[3.7]**	4.69 3.07	P_2CH_2 C_2H_4	10.7 [43.9]	-47.20	2411.2
[(dddt)Pd($PPh_2CH_2PPh_2$)]	**[3.8]**	4.33 3.11	P_2CH_2 C_2H_4	9.8	-37.39	

The phosphorus atoms appear to be most shielded when the dithiolene on platinum is mnt^{2-} (-48.32 ppm), and $dmit^{2-}$ (-39.92 ppm) when the metal is palladium. The degree of

shielding increases in the order $dddt^{2-}$ (-47.20) < $dmit^{2-}$ (-48.02) < $dmid^{2-}$ (-48.23) < mnt^{2-} (-48.32 ppm) for the platinum complexes and $dddt^{2-}$ (-37.39) < mnt^{2-} (-39.37) < $dmid^{2-}$ (-39.67) < $dmit^{2-}$ (-39.92 ppm) for the corresponding palladium complexes.

The one bond coupling constant, ^{1}J(PtP), for the platinum complexes increases in the order, mnt^{2-} (2387.5) < $dddt^{2-}$ (2411.2) < $dmit^{2-}$ (2430.5) < $dmid^{2-}$ (2435.8 Hz). From the above data it is evident that the variation of the NMR parameters can be attributed to the difference in the electron-donation or electron-withdrawing ability of the dithiolene ligand. The 1,2-dithiolene ligand can act as either a π-donor or π-acceptor ligand since it has both empty and filled π-orbitals which can interact with Pt-5*d* orbitals. The better the donor ability of the dithiolene ligand, e.g. $dddt^{2-}$, the weaker the phosphorus σ-electron donation of P→M becomes. We therefore expect the ^{31}P NMR resonance at higher field as observed at -47.20 ppm and -37.39 ppm, for the Pt and Pd complexes **[3.7]** and **[3.8]**, respectively. Conversely, the better the electron-withdrawing ability of the ligand, e.g. mnt^{2-} and $dmid^{2-}$, the more phosphorus σ-electron donation, P→M is expected, resulting in the resonances at lower field, as observed at - 48.23 ppm and -39.67 ppm for the Pt and Pd complexes **[3.5]** and **[3.6]**, respectively . The effect of the donor ability of the dithiolene ligand on the degree of Pt-P coupling appears not to be manifested in the case of the mnt^{2-} ligand. All other ligands adhere to the expected trend, with the poorer electron-donor, $dmid^{2-}$, manifesting the stronger Pt-P coupling [J(PtP) = 2435.8 Hz].

3.3 Mercuration of X_2Pd- and X_2Pt-dppm complexes

The preparative route adopted for the preparation of mercurated derivatives of Group 10 dppm compounds was similar to that of the Group 6 metal carbonyls (see **Scheme 2.2**). The only exception was that the bulky, non-nucleophilic base, $LiN(SiMe_3)_2$, was used to effect deprotonation. This was to prevent possible alkylation of the Group 10 metal centre. The insoluble starting compound was solubilized by deprotonation, presumably forming the lithium salt as the intermediate. Surprisingly, an insoluble precipitate formed on addition of the respective organomercury salt. This occurred for both the Pt and Pd chloride-complexes. We attempted the preparation with the Pt-iodide analogue, which

gave similar results. Reaction with the larger ferrocenyl mercury salt gave an orange precipitate **[3.9]** when added to the deprotonated species. The derivatives were insoluble in all common organic solvents and it was decided not to attempt characterization of such intractable materials. It is well known that platinum and palladium dihalides form dimeric compounds, which could be responsible for the insoluble nature of the metallated derivatives.[3,4] The more soluble dithiolene-dppm complexes, as discussed above, were subsequently used as precursors.

Interestingly, sparingly soluble derivatives were isolated using the bulkier, isoelectronic $[(PPh_3)Au^{I}Cl]$ salt.

3.4 Auration of Pd- and Pt-dppm complexes

The reactions with the isoelectronic $[Au^{I}(PPh_3)]^{+}$ salts were carried out in THF as before, with deprotonation effected by the non-nucleophilic base, lithium-tris(trimethylsilyl)amide. Subsequent treatment of the yellow solutions with $(PPh_3)Au^{I}Cl$ yielded sparingly soluble products $[PdCl_2\{PPh_2CH(AuPPh_3)PPh_2\}]$ **[3.10]** and $[PtCl_2\{PPh_2CH(AuPPh_3)PPh_2\}]$ **[3.11]**.

3.4.1 Spectroscopic study

The ^{1}H NMR spectra of the heterobimetallic gold derivatives all gave the characteristic pseudoquartet due to coupling of the methylene hydrogen to the three phosphorus atoms. The Pd and Pt heterobimetallic complexes **[3.10]** and **[3.11]** exhibit resonances at 5.1 ppm [^{2}J(PH) = 9.2 Hz] and 5.3 ppm [^{2}J(PH) = 9.2 Hz], respectively, for the P_2CH proton. The ^{31}P NMR spectrum showed the expected doublet and triplet signals due to coupling of the chelate ring phosphorus atoms to the gold phosphorus atom. The Pd complex **[3.10]** shows a doublet at -42.6 ppm [^{3}J(PP) = 9.9 Hz] and a triplet at 39.2 ppm [^{3}J(PP) = 12.3 Hz]. For the analogous Pt complex **[3.11]**, the doublet and triplet appear at -52.3 ppm [^{3}J(PP) = 9.9 Hz, $^{1}J(^{195}Pt\text{-}^{31}P)$ = 3012 Hz] and 39.3 ppm [^{3}J(PP) = 11.3 Hz], respectively. The coupling

constant, $^{1}J(^{195}Pt\text{-}^{31}P)$, of 3012 Hz appears normal and is typical for one bond coupling of Pt to P. **Figure 3.1** shows the ^{31}P NMR spectrum of **[3.11]**, the satellites due to Pt-P coupling clearly visible.

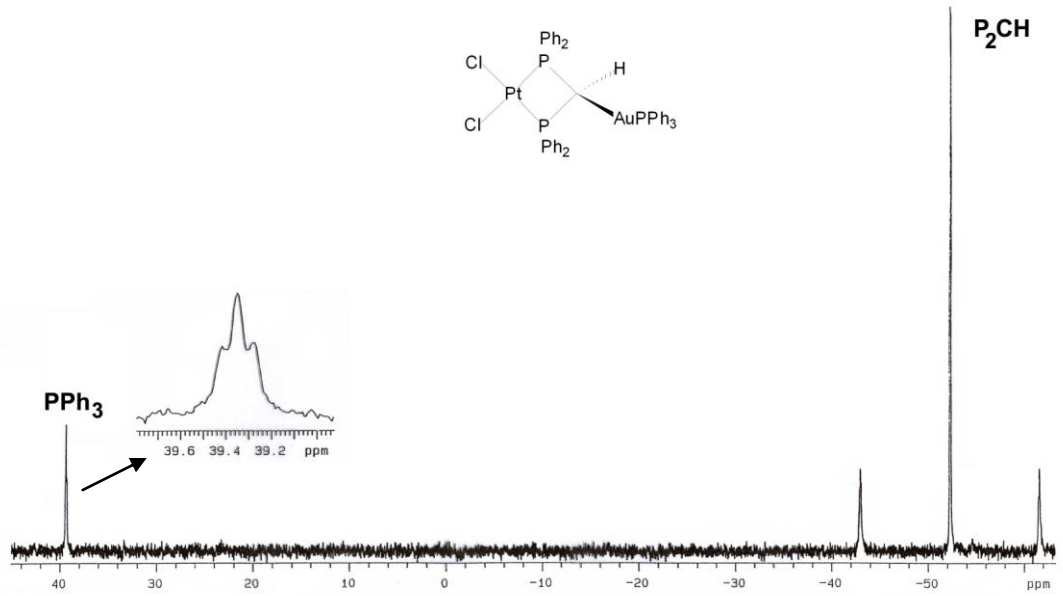

Figure 3.1 ^{31}P NMR spectrum of $[Cl_2Pt((Ph_2P)_2CHAuPPh_3)]$**[3.11]**.

3.5 Mercuration of (dithiolene)Pd- and (dithiolene)Pt-dppm complexes

The preparative route adopted was similar to that of the Group 10 metal-halide precursors discussed above (see **Section 3.3**), and the range of compounds synthesized is listed in **Table 3.2**.

3.5.1 Spectroscopic studies

There appears to be no difference in the characteristic infrared absorptions between the starting complex and the product on metallation. For example, **[3.17]** shows ν(C=C) and ν(C≡N) at 1435 and 2201 cm^{-1}, respectively, compared to 1436 and 2200 cm^{-1} in the starting complex. The fact that both ν(C=C) and ν(C≡N) are unaffected by the presence of

a second metal is surprising, but does not necessarily rule out any interaction between the two metal/redox centres. It does suggest that the interaction is extremely weak or, if such an interaction is present, infrared spectroscopy proves not be a suitable tool to quantify the relationship.

The ^{1}H NMR spectra show that the methylene protons undergo a downfield shift on metallation. The organic substituents on mercury show the expected resonances. The ^{1}H NMR spectrum of **[3.14]**, for example, shows the ethyl resonances at 0.78 and 0.70 ppm, with ^{2}J(HgH) and ^{3}J(HgH) coupling constants of 208.7 and 71.2 Hz, respectively (**Figure 3.2**).

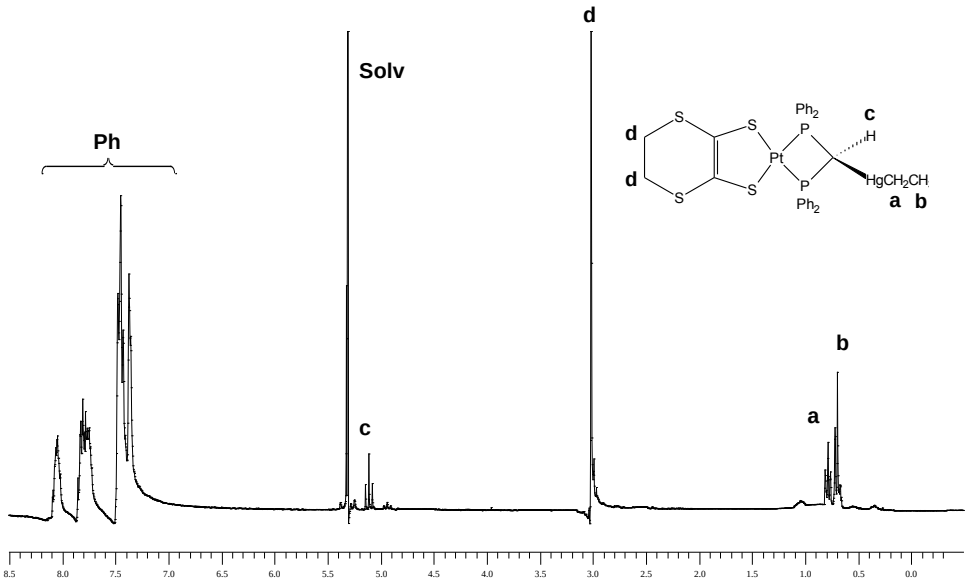

Figure 3.2: ^{1}H NMR spectrum of [(dddt)Pt{$Ph_2PCH(HgEt)PPh_2$}] **[3.14]**.

^{31}P NMR spectra all show that the equivalent phosphorus nuclei shift downfield on metallation, indicating that they are deshielded. The platinum complexes show slightly higher deshielding of the phosphorus nuclei on metallation, as evidenced by the greater downfield shift when compared to the equivalent palladium analogue.

For the platinum complexes, the ^{31}P NMR spectra show a singlet, flanked by two sets of satellites due to coupling to ^{199}Hg and ^{195}Pt. Hg satellites were not observed for all complexes. It is not unusual for HgP satellites to be absent in ^{31}P NMR spectra.[1] In **Figure**

3.3 the ^{31}P NMR spectrum of complex **[3.14]** is shown, with the ^{195}PtP and ^{199}HgP satellites being observed.

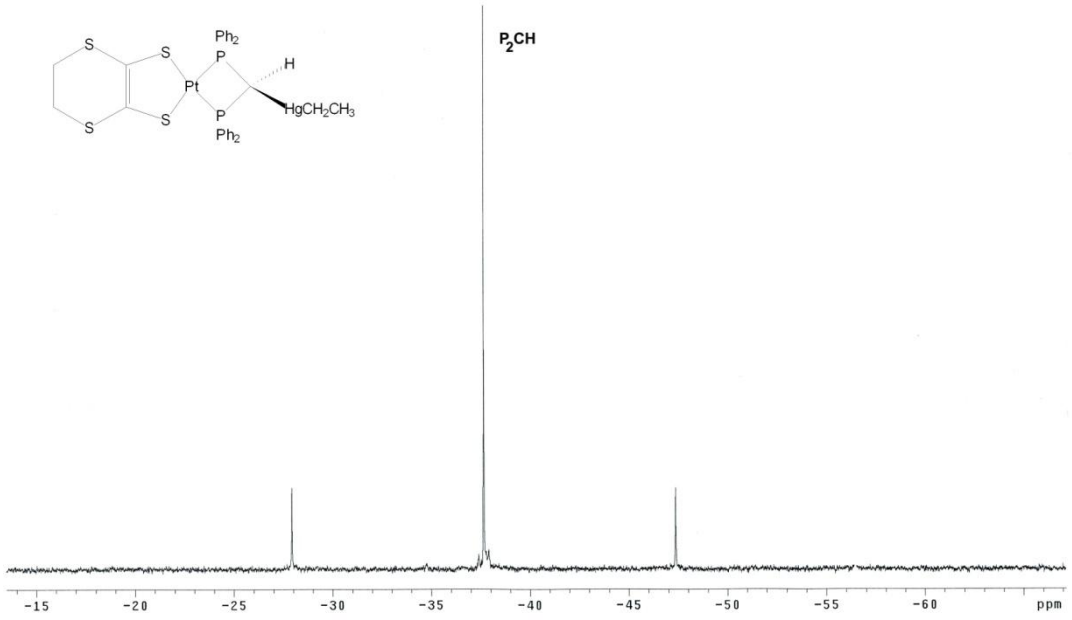

Figure 3.3 ^{31}P NMR spectrum of [(dddt)Pt{$Ph_2PCH(HgEt)PPh_2$}] **[3.14]**, showing both the Pt and Hg satellites.

The ^{31}P NMR data in **Table 3.2** show that the displacement of the phosphorus resonance is less sensitive to the substituent on mercury compared to the Group 6 analogues. For example, the difference in δ(P) between the ethyl- and ferrocenyl-substituted complexes **[3.13]** and **[3.15]** is 0.5 ppm, whereas the corresponding Group 6 complexes differ by 2.8 ppm. Furthermore, the difference in coupling constant between **[3.13]** and **[3.15]**, ^2J(HgP), is 0.1 Hz, whereas the corresponding Group 6 complexes show a difference of 36.7 Hz. Changing the dithiolene ligand also appears to have no significant impact on the phosphorus chemical shift, δ(P). For example, δ(P) differs by 0.1 ppm in going from mnt^{2-} to $dddt^{2-}$ for **[3.16]** and **[3.13]**, respectively. The coupling constant ^1J(PtP) appears to decrease on metallation. The $dddt^{2-}$ complexes **[3.12]**, **[3.13]** and **[3.14]** show values of 2332, 2312 and 2360 Hz, respectively, compared to 2411 Hz for **[3.7]**.

Similarly, the mnt^{2-} complexes gave corresponding values of 2349 **[3.15]** and 2339 Hz **[3.16]**, while the starting complex **[3.1]** adopts a value of 2387 Hz.

Table 3.2 NMR data of [(dithiolene)M($PPh_2CH(HgR)PPh_2$)] complexes, M = Pd or Pt

Complex		^{31}P-NMR		
		δ (ppm)	$J_{Pt\text{-}P}$ (Hz)	$J_{Hg\text{-}P}$ (Hz)
[(dddt)Pt($PPh_2CH(HgPh)PPh_2$)]	**[3.12]**	-39.60	2332	36.8
[(dddt)Pt($PPh_2CH(HgFc)PPh_2$)]	**[3.13]**	-39.77	2312	31.8
[(dddt)Pt($PPh_2CH(HgEt)PPh_2$)]	**[3.14]**	-40.21	2360	31.0
[(mnt)Pt($PPh_2CH(HgPh)PPh_2$)]	**[3.15]**	-40.16	2349	-
[(mnt)Pt($PPh_2CH(HgFc)PPh_2$)]	**[3.16]**	-39.88	2339	31.0
[(mnt)Pd($PPh_2CH(HgFc)PPh_2$)]	**[3.17]**	-31.80		-

3.6 Electrochemical studies

3.6.1 Electrochemistry of the unsubstituted Pd and Pt dithiolene-(dppm) complexes

The electrochemical behaviour of the dithiolene-diphosphine complexes was investigated using cyclic voltammetry in dichloromethane. The redox potentials of these complexes are given in **Table 3.3**, and **Figure 3.4** illustrates typical cyclic voltammograms for the platinum complexes.

Table 3.3 Anodic potentials, E_{pa}, and half-wave potentials, $E_{1/2}$, for [(dithiolene)M(dppm)] complexes (M= Pt or Pd)

Complex		*Electrochemical Process, mV*		
		E_{pa}	$E_{½}$	$E_{½}$
[(mnt)Pt($PPh_2CH_2PPh_2$)]	**[3.1]**	+900		
[(mnt)Pd($PPh_2CH_2PPh_2$)]	**[3.2]**	+827		
[(dmit)Pt($PPh_2CH_2PPh_2$)]	**[3.3]**	+860		+244
[(dmit)Pd($PPh_2CH_2PPh_2$)]	**[3.4]**	+911		+215
[(dmid)Pt($PPh_2CH_2PPh_2$)]	**[3.5]**	+1069		+223
[(dmid)Pd($PPh_2CH_2PPh_2$)]	**[3.6]**			+120
[(dddt)Pt($PPh_2CH_2PPh_2$)]	**[3.7]**		+642	-76
[(dddt)Pd($PPh_2CH_2PPh_2$)]	**[3.8]**	+581		-169

The maleonitrile Pt(II) and Pd(II) complexes **[3.1]** and **[3.2]** showed an irreversible oxidation processes at E_{pa} +900 and +827 mV, respectively. Mono-substituted metal-maleonitrile complexes have been shown to exhibit irreversible electrochemical behaviour.[5]

All other complexes displayed two oxidation processes of which the less anodic oxidation process is reversible for all complexes but for [(dmit)Pd(dppm)]. The half-wave potentials, $E_{1/2}$, for the first oxidation process range from -76 to +215 mV for the palladium complexes and from -76 to +244 mV for the corresponding platinum analogues.

The second oxidation process was only reversible for the [(dddt)Pt(dppm)] complex **[3.7]**. Quasi-reversible behaviour was observed for the platinum dmit **[3.3]** and dmid **[3.5]** complexes at higher scan rates. The palladium complexes displayed oxidation potentials, for the more anodic process, in the region +518 to +911 mV, while the analogous platinum complexes showed oxidation potentials ranging from +642 to +1069 mV.

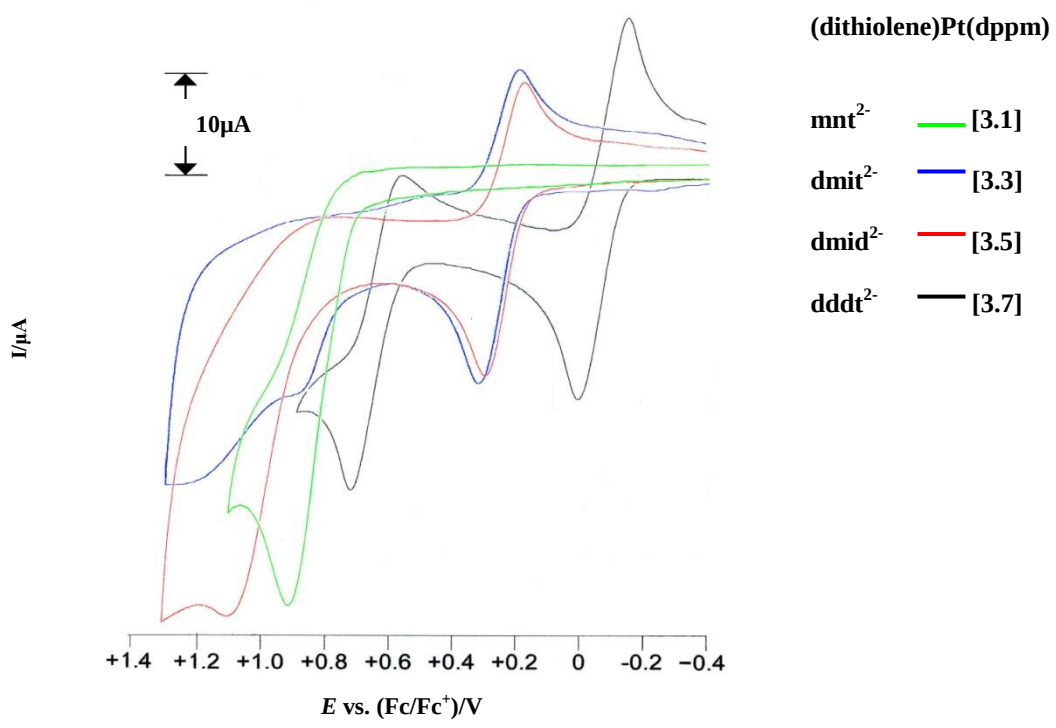

Figure 3.4 Cyclic voltammograms of dithiolene complexes of Pt.

The first and second half-wave potentials for **[3.7]** could be ascribed to the $[(dddt)Pt(dppm)]^{0/+}$ and $[(dddt)Pt(dppm)]^{+/2+}$ redox processes, respectively.
It is clear from the data that the oxidation potentials increase in the order $dddt^{2-} < dmid^{2-} \leq dmit^{2-}$. This is in agreement with the relative donor/acceptor ability of the dithiolene ligands, with dddt being a better donor compared to dmid and dmit. Similar observations have been reported by other authors.[6,7]

3.6.2 Electrochemistry of metallated Pd and Pt dithiolene-dppm complexes

The redox behaviour of the substituted compounds was studied in dichloromethane. The redox potentials are summarized in **Table 3.4**. Representative cyclic voltammograms are shown in **Figure 3.5**.

The cyclic voltammetry of the substituted complexes showed very similar redox behaviour to those of **[3.1]** to **[3.8]**, with a single oxidation for the maleonitrile compounds and two oxidation processes for the $dddt^{2-}$ derivatives. However, a noticeable difference was the appearance of a reversible oxidation process for the ferrocenyl-containing compounds **[3.13]**, **[3.16]** and **[3.17]**, which is ascribed to the one-electron Fc/Fc^{+} redox process for the ferrocenyl moiety. It is clear from the data that the oxidation potentials of the dithiolene moieties underwent a shift to less positive potentials on metallation.

The half-wave potential of the ferrocenyl moiety appears to be independent of the specific dithiolene bonded to the Group 10 metal centre, occurring at around +119 mV, and of similar magnitude to the equivalent process for the analogous Group 6 dppm complexes. However, it appears at a slightly lower potential when the metal is platinum. In the $dddt^{2-}$ complexes, the redox process for the ferrocene moiety coincides with the less anodic process associated of the dithiolene ligand in **[3.7]**. This is observed in **Figure 3.5** by the increased and slightly broader oxidation peak when compared to the other substituted [(dddt)Pt(dppm)] analogues.

Table 3.4 Electrochemical data of complexes **[3.12]-[3.17]** in dichloromethane

Complex		***Electrochemical Process, mV***		
		$E_{½}^{1}$	$E_{½}^{2}$	E_{pa}
[(dddt)Pt($PPh_2CH(HgPh)PPh_2$)]	**[3.12]**	-123	+544	
[(dddt)Pt($PPh_2CH(HgFc)PPh_2$)]	**[3.13]**	-95	+526	
[(dddt)Pt($PPh_2CH(HgEt)PPh_2$)]	**[3.14]**	-138	+545	
[(mnt)Pt($PPh_2CH(HgPh)PPh_2$)]	**[3.15]**			+808
[(mnt)Pd($PPh_2CH(HgFc)PPh_2$)]	**[3.16]**		-95	+787
[(mnt)Pt($PPh_2CH(HgFc)PPh_2$)]	**[3.17]**		-107	+816

When comparing the redox potential of the unmercurated **[3.7]** with its derivatives as reflected in **Table 3.4**, we observe shifts ranging from 19-62 and 97-115 mV for the first and second redox processes, respectively, depending on the nature of the substituent on mercury. From the data it is evident that the second, more anodic, redox process is more sensitive towards metallation, having undergone a greater shift towards a less positive potential. It is however, less sensitive towards the specific substituent on the mercury atom. For example, the most electron-withdrawing substituent, Fc, shows a displacement of the first redox process of 19 mV, while the most inductive substituent, Et, resulted in a corresponding shift of 62 mV towards less positive potentials compared to **[3.7]**, a difference of 43 mV. The second redox process gave corresponding shifts of 116 and 97 mV respectively, a difference of only 19 mV.

A similar decrease in the oxidation potential of the maleonitrile moiety is observed for **[3.16]** and **[3.17]** on metallation. The redox potential for the irreversible oxidation process decreases by 40 and 84 mV, respectively. The data suggest that the platinum complex is more sensitive towards metallation, compared to the analogous palladium complex. No redox processes are observed for the palladium or platinum metal centres.

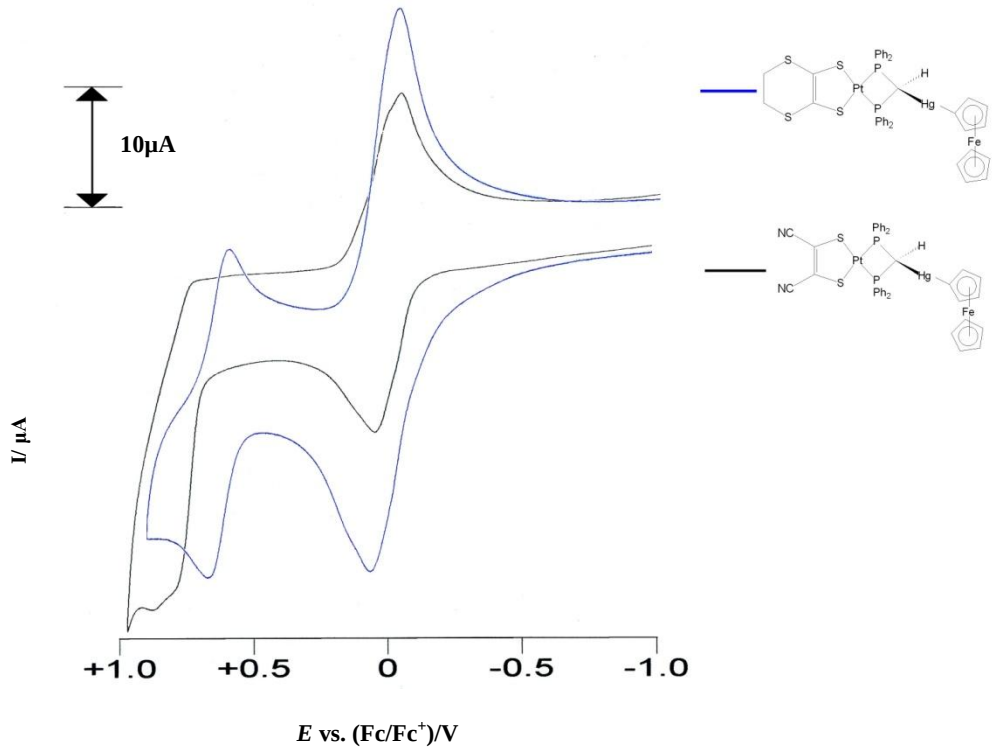

Figure 3.5 Cyclic voltammograms of **[3.13]**. and **[3.17]**.

It is evident from the data in **Table 3.4** that the substituent on the mercury atom does influence the redox behaviour of the dithiolene moiety. We firstly observe a slight decrease of the oxidation potential of the dithiolene moiety on metallation. Secondly, for the dddt^{2-} complexes, we observe a variation of the first and second oxidation potentials of +43 and +18 mV, respectively, depending on the nature of the substituent on mercury. The general trend, as observed in **Chapter 2**, appears to be preserved with the more electronegative substituents resulting in more anodic half-wave potentials. However, the variation appears to be significantly less than that observed for the analogous Group 6 complexes. There is, however, an indication of electronic communication for the trimetallic ferrocenyl complexes **[3.13]**, **[3.16]** and **[3.17]**, with a discernable difference in the oxidation potential of the metal centre when compared to the corresponding potential in the respective starting complex. The Fe^{2+}/Fe^{3+} electrochemical process for these complexes also manifests a significant shift towards lower potentials when compared to the oxidation potentials of ferrocene or ferrocenylmercurychloride (+26 mV). It is however debatable, as for the analogous Group 6 trimetallic complexes, whether the

electronic communication is transmitted entirely through the Hg-chelate ring framework or whether there is a significant contribution affected by a 'through-space' interaction. The 'through-space' contribution is supported by both crystallographic evidence, as discussed in **Chapter 2**, and the expectation that the electron-rich chelate ring would increase the Fe/Fe^{+} potential, as opposed to the observed decrease.

3.7 Ruthenium complexes

We set out to investigate the reactivity of the cationic cyclopentadienyl-ruthenium-dppm compounds based on $[(PPh_3)(Cp)Ru(dppm)]PF_6$ since reported cationic dppm compounds have been shown to be stabilized on deprotonation and retain double bond character in the chelate ring on metallation. It would be of interest to see whether the deprotonated system is nucleophilic enough towards the mercury electrophiles and whether a mercury-'carbene' bond would result, which could favourably impact on the degree of electronic communication between the metal centres, where delocalization across the P_2CHHg framework would facilitate electron-flow between the metal centres.

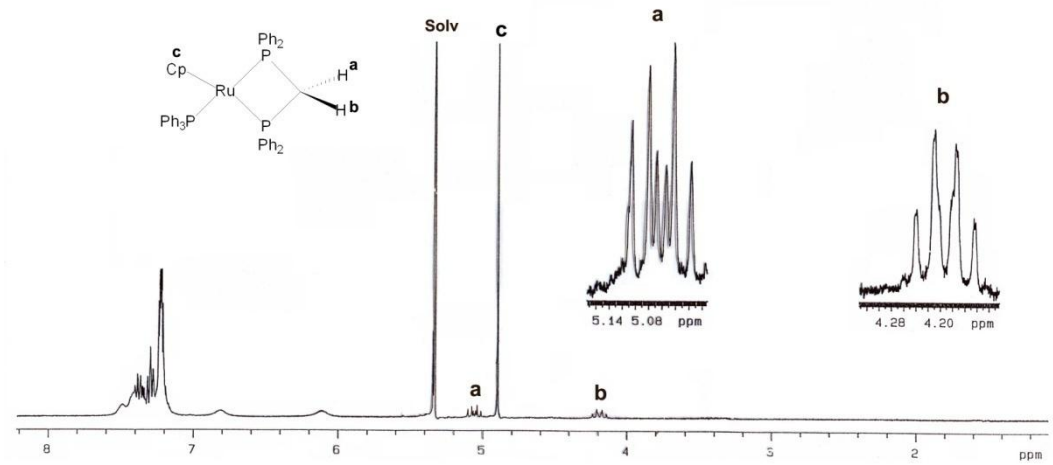

Figure 3.6 ^{1}H-NMR spectrum of $[RuCp(PPh_3)dppm]$.

The ruthenium-dppm complex [(PPh_3)(Cp)Ru(dppm)]PF_6 **[3.18]** was prepared from literature methods.[8] However, the spectroscopic results were significantly different from those reported. We observed no signal at 2.0 ppm that could be ascribed to the methylene hydrogens as reported. The two methylene protons of the dppm moiety turned out to be chemically inequivalent (see **Figure 3.6**) as a result of their fixed spatial arrangement and resulted in two resonances, viz. a doublet of triplets at 5.06 ppm [^2J(HH) = 14.8 Hz, ^2J(PH) = 10.2 Hz] and a quartet (presumably another doublet of triplets that has collapsed into a quartet due to overlapping signals) at 4.20 ppm [^2J(HH) = 13.8 Hz, ^2J(PH) = 11.5 Hz]. These are due to a combination of geminal coupling to the other methylene hydrogen and coupling to the two ring phosphorus atoms. Clearly the tetrahedral arrangement around the metal centre results in different degrees of shielding by the cyclopentadienyl and triphenylphosphine groups on the hydrogens respectively. Non-equivalence of methylene protons in Ru-dppm complexes have been reported by other authors.[9,10] The differentiation between the two methylene protons, labelled **a** and **b** in **Figure 3.6**, was made based on the position of the ferrocene group, relative to the Cp and PPh_3 groups, as shown by the crystal structure of the heterobimetallic complex **[3.20]** (see **Section 3.8**).
A singlet at 4.85 ppm is ascribed to the five equivalent cyclopentadienyl hydrogens.

The ^{31}P NMR spectrum shows the expected doublet at 1.6 ppm [^2J(PP) = 35.4 Hz] and triplet at 49.8 ppm [^2J(PP) = 35.5 Hz] for the chelate ring phosphorus and triphenylphosphine phosphorus atoms, respectively. The PF_6 multiplet occurs at -143.8 ppm.

Deprotonation of the ruthenium complex **[3.18]** was achieved using KOH in CH_2Cl_2. The deprotonated product **[3.19]** was isolated by filtration under nitrogen. The ^{1}H NMR spectrum only showed the resonances due to the cyclopentadienyl, δ 5.0 ppm, and phenyl protons. Interestingly, no clear signal was observed for the P_2CH proton. However, an unresolved signal is observed at 2.25 ppm, which is in the region typically expected for shielded P_2CH^- protons.[11] The ^{31}P NMR spectrum exhibits the expected resonance, viz. a doublet [1.45 ppm, ^2J(PP) = 35.7 Hz] and a triplet [48.12 ppm, ^2J(PP) = 35.2 Hz] for the PPh_3 and P_2CH groups, respectively. The PF_6 resonance is noticeably absent, implying the formation of a neutral molecule.

It is surprising that the phosphorus resonances appear to be unaffected by the removal of the methylene proton, as the resultant delocalized charge is expected to effect some degree of shielding of the chelate phosphorus atoms. **[3.19]** appears to be reasonably stable and there is no indication of decomposition in air or protonation during the workup.

Treatment of **[3.18]** with KOH in CH_2Cl_2 followed by the addition of ferrocenylmercury chloride, yield the trimetallic ferrocenylmercurated complex **[3.20]**. The ^{1}H NMR spectrum of **[3.20]** shows a triplet at 4.37 ppm [^2J(PP) = 10.1 Hz]. The Cp protons appear as a singlet at 4.77 ppm. The ferrocenyl moiety shows three resonances between 3.71 and 4.22 ppm, two triplets, 3.73 ppm [^3J(HH) = 1.8 Hz] and 4.23 ppm [^3J(HH) = 1.7 Hz], for the substituted Cp ring and a singlet at 3.81 ppm for the unsubstituted Cp ring.

Interestingly, when the reaction is repeated with EtHgCl, a mixture of the metallated complex $[(PPh_3)(Cp)Ru\{Ph_2PCH(HgEt)PPh_2\}]PF_6$ **[3.21]**, and the starting compound **[3.19]** is formed. Altering of reaction conditions does not improve the percentage conversion. Attempts at separating the products were unsuccessful, presumably due to their similar solubilities, both existing as PF_6 salts. However, we could perform a complete spectroscopic characterization of **[3.21]**. The ^{1}H NMR spectrum shows the expected triplet for the P_2CH proton at 4.05 ppm. The Cp protons were displaced downfield and appear at 4.84 ppm. The ethyl resonances appear at 0.87 [^3J(HH) = 7.93 Hz, ^3J(HgH) = 87.9 Hz] and 1.01 ppm [^3J(HH) = 7.88 Hz, ^2J(HgH) = 159.9 Hz]. The ^{31}P NMR spectrum shows a triplet, for the PPh_3 group, 48.12 ppm [^2J(PP) = 33.1 Hz] and a doublet at 1.92 ppm [^2J(PP) = 32.2 Hz] for P_2CH, indicting slight deshielding of the chelate ring *P*-atoms.
The above observation could possibly be explained in terms of the decreased reactivity and lower nucleophilicity of the carbanion, due to it being stabilized by the ruthenium metal centre. We have shown that the deprotonated compound can be isolated and that it is reasonably stable. Furthermore, the ethyl group being relatively more inductive compared to the ferrocenyl group, would result in the mercury becoming less electrophilic. Fornies *et al*., for example, experienced a similar inability to alkylate deprotonated dppm when using EtI.[12]

The methanide reacts readily with the isoelectronic $[(PPh_3)Au^{I}Cl]$ salt in CH_2Cl_2 and gave good yields of the heterobimetallic derivative,

$[(PPh_3)(Cp)Ru\{PPh_2CH(AuPPh_3)PPh_2\}]PF_6$ **[3.22]**. The ^1H NMR spectrum gave the characteristic pseudoquartet for the methylene hydrogen at 4.11 ppm [^2J(PH) = 9.9 Hz]. The Cp resonance has moved upfield to 4.64 ppm.

The ^{31}P NMR spectrum shows the expected triplet and quartet patterns, with a doublet at 16.75 ppm [^2J(PP) = 34.8 Hz] and a triplet at 50.31 ppm [^2J(PP) = 34.5 Hz] for the chelate ring and PPh_3 phosphorus atoms respectively.

3.8 Crystal and molecular structure of [3.20]

Crystals suitable for X-ray crystallography were obtained from a mixture of dichloromethane and methanol. Complex **[3.20]** crystallizes in the monoclinic space group $P2_1/n$. The molecular structure and the atomic nomenclature used in its description are shown in **Figure 3.7**. A packing diagram of the molecule is shown in **Figure 3.8**. The intra molecular bond lengths and angles for **[3.20]** are given in **Table 3.5**. Crystal data and refinement parameters are given in **Table 3.6**.

The Ru atom is located in a distorted octahedral environment formed by the chelate ring, the cyclopentadienyl and triphenylphosphine moiety. The PCP bond angle of the chelate ring of 71.0(2)° is less than that for the Group 6 metal complexes discussed in **Chapter 2**, but normal for Ru-dppm structures and compares well with similar structures.[13] The chelate ring is almost planar, with the four torsion angles in the chelate ring being in the range 6.2(4)-7.5(5)°.

The Ru-P(1) and Ru-P(2) bond distances of 2.295(4) and 2.330(4) Å appear normal.[14] The most significant feature of this structure is the P(1)-C(1) and P(2)-C(1) distances of 1.826(13) and 1.859(13) Å, respectively. These are slightly longer than the P-C(Ph) distance found in the same molecule [1.807(14)-1.830(15) Å] and are similar to the distances found in the chromium structures reported earlier. It is thus evident that no double bond character remains in the P_2-CH bonds on metallation.

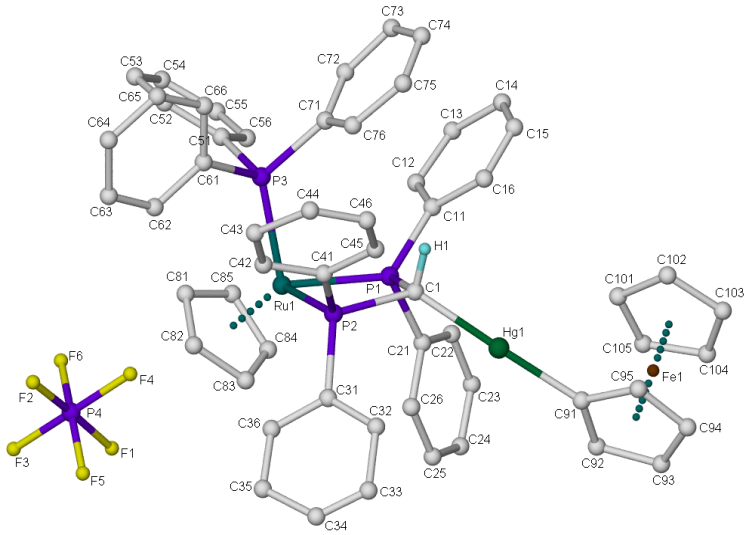

Figure 3.7 Molecular structure of **[3.20]**.

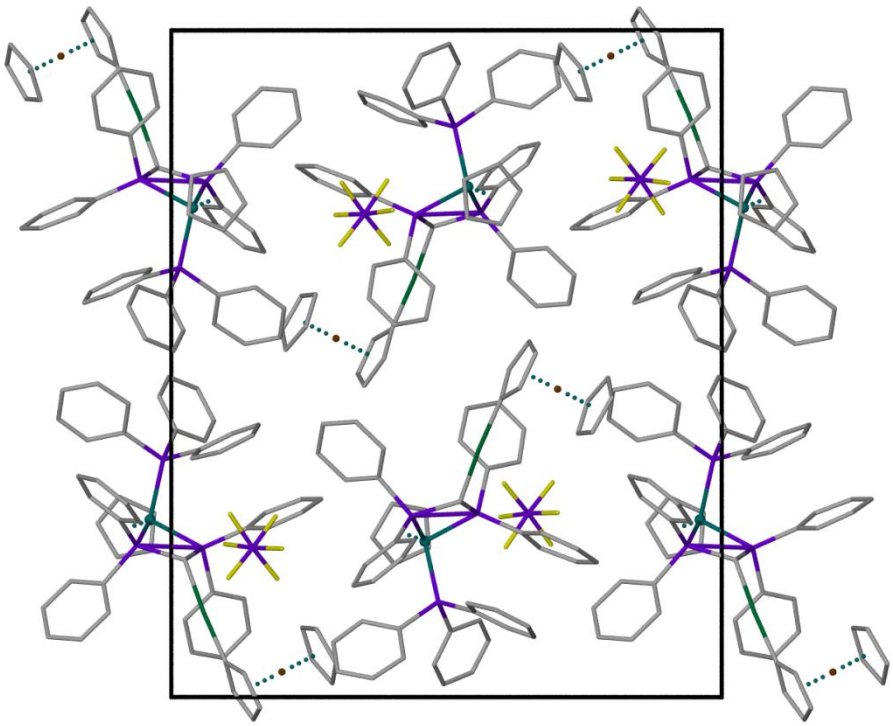

Figure 3.8 Molecular packing for complex **[3.20]** viewed along [100].

Table 3.5 Selected bond lengths (Å) and bond angles (°).

Bond lengths			
Ru - P(1)	2.295(4)	Ru - C(84)	2.201(15)
Ru - P(2)	2.330(4)	Ru - C(85)	2.235(14)
Ru - P(3)	2.327(4)	P(1) - C(1)	1.826(13)
Ru -C(81)	2.235(14)	P(2) - C(1)	1.859(13)
Ru - C(82)	2.233(16)	Hg - C(1)	2.115(13)
Ru – C(83)	2.192(14)	Hg - C(91)	2.049(18)
Bond angles			
P(1) - Ru - P(2)	70.83(13)	P(2) - Ru - P(3)	98.13(14)
P(1) - C(1) - P(2)	93.4(6)	P(2) - C(1) – Hg	127.9(7)
Ru - P(1) - C(1)	98.6(4)	C(91) - Hg - C(1)	173.1(6)
Ru - P(2) - C(1)	96.4(4)	P(1) - C(1) – Hg	113.4(6)
P(1) - Ru - P(3)	97.79(14)		
Torsion angles			
P(2)-Ru(1)-P(1)-C(1)	6.3(5)	C(91)-Hg(1)-C(1)-P(2)	129(5)
Ru(1)-P(1)-C(1)-P(2)	7.5(5)	Hg(1)-C(1)-P(2)-Ru(1)	-130.7(7)
P(1)-C(1)-P(2)-Ru(1)	-7.4(5)	C(81)-C(82)-C(83)-C(84)	0.1(17)
P(1)-Ru(1)-P(2)-C(1)	6.2(4)	C(83)-C(84)-C(85)-C(81)	-1.0(17)
Ru(1)-P(1)-C(1)-Hg(1)	141.7(5)	C(92)-C(91)-C(95)-C(94)	-2(2)
C(91)-Hg(1)-C(1)-P(1)	14(5)	C(105)-C(101)-C(102)-C(103)	2(2)

This feature is significant since, as far as we could ascertain, all reported metallated ionic dppm-methanide complexes retain their double bond character on metallation. As indicated, most metallations of metal-dppm compounds were achieved using either gold or silver electrophiles, the only exception being the mercury carbene complex **[1.14]** discussed in **Chapter 2**, which was shown to retain the sp^2-hybridized methylene carbon centre on metallation. From the crystal data, we can conclude that **[3.20]** does not exist as a Hg-carbene.

Table 3.6 Crystal data and refinement parameters for **[3.20]**

Molecular formula		$C_{58}H_{50}F_6FeP_4FeHgRu$
Molecular mass, g mol^{-1}		1342.37
Crystal dimensions, mm		0.40 x 0.40 x 0.35
Crystal system		Monoclinic
Space group		$P2_1/n$
Unit cell dimensions	a, α	11.413(2) Å, 90°
	b, β	23.971(4) Å, 93.39(2)°
	c, γ	19.802(6) Å, 90°
*V*olume, Å^3		5408(2)
Z, D_C (Mg/m^3)		4, 1.649
Absorption coefficient, mm^{-1}		3.549
F(000)		2648
Theta range for data collection		1.70 to 24.98°
Limiting indices		$-13 \le h \le 13$, $0 \le k \le 28$, $0 \le l \le 23$
Reflections collected / unique		9362 / 9362 [*R*(int) = 0.0000]
Completeness to theta = 24.98		98.5%
Max. and min. transmission		0.3698 and 0.3310
Refinement method		Full-matrix least-squares on F^2
Data / restraints / parameters		9362 / 0 / 611
Goodness-of-fit on F^2		0.922
Final *R* indices [I > 2sigma(I)]		R_1 = 0.0738, wR_2 = 0.1823
R indices (all data)		R_1 = 0.1836, wR_2 = 0.2046

The Hg-C(1) bond distance of 2.115(13) Å compares well with the structures reported in Chapter 2. The geometry around the mercury atom is shown to be near linear at 174.3(8)°. The shorter Hg-C(19) bond distance, 2.049(18) Å, compares well with the earlier structures, which also showed a decreased bond distance for the Hg-C(substituent) bond. The Ru-C bonds of the Cp ring appear normal and range between 2.192(14) and 2.235(14) Å.[15] The Fe-C bond distances in the ferrocene moiety are comparable to the distances found for the earlier and reported structures. The ferrocene rings are observed to exist in an eclipsed conformation. The structure reveals that the ferrocenyl moiety is positioned '*trans*' to the bulky PPh_3 group.

The bond distances and angles for the PF_6 counter-ion appear normal. A search for intermolecular interactions revealed the presence of four weak C-H···F hydrogen bonds between the counter-ion fluorine atoms and phenyl and cyclopentadienyl carbon atoms.

Complex **[3.20]** was found to be centrosymmetric which precludes it from being used as a NLO material.

3.9 Electrochemistry of ruthenium complexes

The electrochemical behaviour of the ruthenium complexes was investigated in dichloromethane. The electrochemical data are given in **Table 3.7**. Representative voltammograms are shown in **Figure 3.9**.

The unsubstituted ruthenium compound **[3.18]** gave a reversible wave at $E_{1/2}$ = +841 mV, which is attributed to the one electron reversible oxidation of ruthenium, $Ru^{2+/3+}$.

Table 3.7 Oxidation potentials of ruthenium complexes in dichloromethane

Complex		***Electrochemical Proces, mV***	
		$E_{1/2}$	$E_{1/2}$
$[(PPh_3)(Cp)Ru(dppm)]PF_6$	**[3.18]**		+841
$[(PPh_3)(Cp)Ru(PPh_2CH(HgFc)PPh_2)]PF_6$	**[3.20]**	-34	+809
$[(PPh_3)Ru(Cp)\{PPh_2CH(AuPPh_3)PPh_2\}]PF_6$	**[3.22]**		+835

The trimetallic complex **[3.20]** showed two one-electron reversible processes. The less anodic process at -34 mV is attributed to the reversible oxidation of Fe in the ferrocenyl moiety, while the wave at +809 mV is attributed to the reversible oxidation of the ruthenium metal centre.

The aurated derivative **[3.22]** gave a one-electron reversible oxidation at +835 mV.

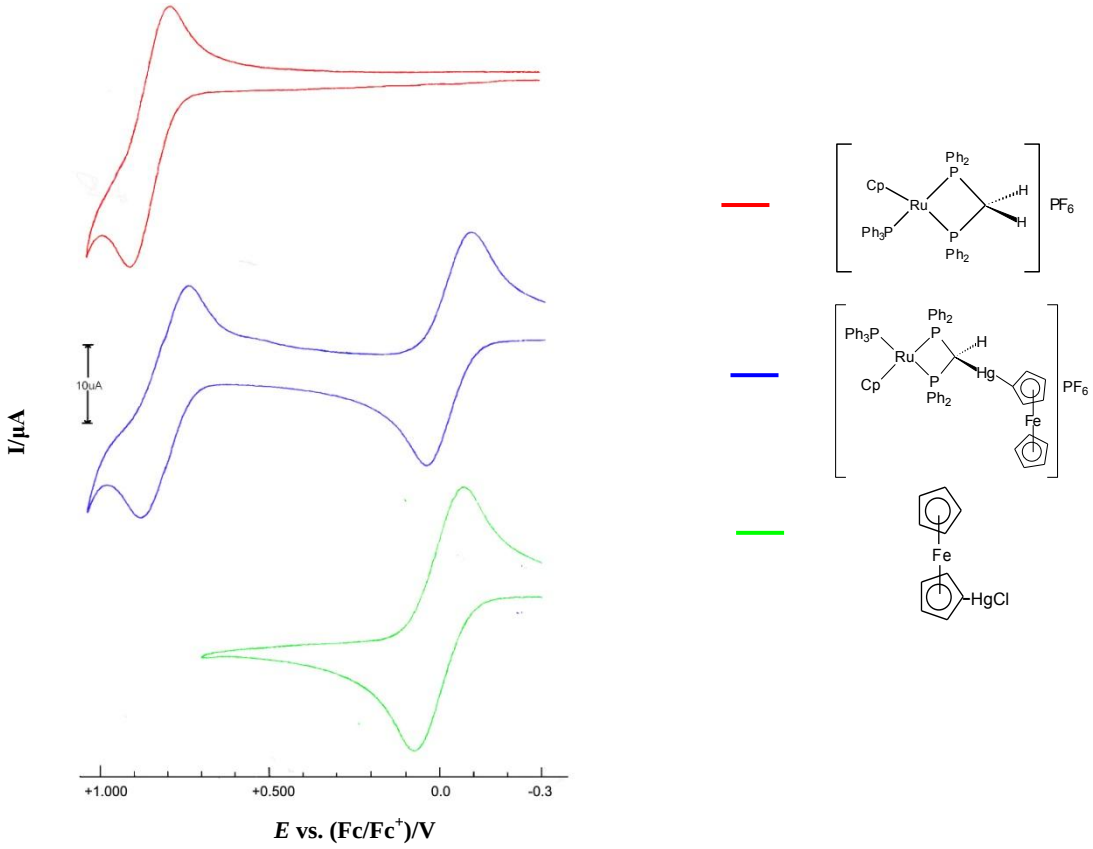

Figure 3.9 Cyclic voltammogram of **[3.18]**, **[3.20]** and ferrocenylmercurychloride.

There is a shift of 32 mV towards a less anodic potential of the ruthenium metal centre on metallation. The oxidation attributed to the ferrocenyl moiety is 40 mV less anodic than the Fc/Fc^+ couple but more anodic compared to the potentials recorded previously for the analogous Group 6 Pt- and Pd-trimetallic ferrocenylmercury complexes. This could be a result of the different background electrolyte used. However, the oxidation potentials for the ferrocene reference compound and chloromercuryferrocene appear at similar potentials, as reported earlier with [*n*-Bu_4N][ClO_4] as background electrolyte (see **Section 3.6**). The oxidation potential for complex **[3.22]** appears at slightly more anodic potential, which is contrary to the observation made for the Group 6 metal complexes, where the aurated derivatives showed lower oxidation potentials (see **Section 2.7**).

It is evident from the electrochemical results that the trimetallic complex **[3.20]** does exhibit some degree of electronic communication. However, based on the relatively small shift in the redox potential of the starting complex **[3.18]** compared to **[3.20]**, the

interaction could be classified as weak. The larger and more significant shift observed in the redox potential of the Fc/Fc^+ couple in the ferrocenylmercury moiety is more difficult to define, due to the possibility of 'through-space' electronic interactions. The communication is therefore not necessarily transmitted through the Hg-chelate framework and the shift being towards a lower potential favours the former interaction.

REFERENCES

1 E. J. Fenandez, M. C. Gimeno, P. G. Jones, A. Laguna, M. Laguna and E. Olmos, *Inorg. Chim. Acta.*, 1995, **238**, 173.

2 C. E. Johnson, R. Eisenberg, T. R. Evans and M. S. Burberry, *J. Am. Chem. Soc*., 1983, **105**, 1795.

3 I. G. Phillips, R. G. Ball and R. G. Cavell, *Inorg. Chem.*, 1988, **27**, 4038.

4 M. C. Cornock and T. A. Stephenson, *J. Chem. Soc., Dalton Trans.*, 1977, 683.

5 R. Prasad, A. Kumar and R. Kumar, *J. Mol. Struc.*, 2006, **786**, 68.

6 M. Fourmique, C. Lenoir, C. Coulon, F. Guyon and J. Amaudrut, *Inorg. Chem.*, 1995, **34**, 4979.

7 D.-Y. Noh, E.-M. Seo, H.-J. Lee, H.-Y. Jang, M.-G. Choi, Y.-H. Kim and J. Hong, *Polyhedron*, 2001, **20**, 1939.

8 G. S. Ashby, M. I. Bruce, I. B. Tumkins and R. C. Wallis, *Aust. J. Chem.*, 1979, **32**, 1003.

9 V. Cadierno, M. P. Gamasa, J. Gimeno and B. M. Martin-Vaca, *J. Organomet. Chem.*, 2001, **617**, 261.

10 M. P. Gamasa, J. Gimeno, C. Gonzalez-Bernardo, B. M. Martin-Vaca, D. Monti and M. Bassetti, *Organometallics*, 1996, **15**, 302.

11 V. Riera, J. Ruiz, X. Solans and E. Tauler, *J. Chem. Soc., Dalton Trans.*, 1990, 1607.

12 L. R. Falvello, J. Fornies, R. Navarro, A. Rueda and E. P. Urriolabeitia, *Organometallics*, 1996, **15**, 309.

13 I. W. Wyman, T. J. Burchell, K. N. Robertson, T. S. Cameron and M. A. S. Aquino, *Organometallics*, 2004, **23**, 5353.

14 M. I. Bruce, P.A. Humphrey, M. Jevric, B. W. Skelton and A. H. White, *J. Organomet. Chem.*, 2007, **692**, 2564.

15 D. Serra, K. A. Abboud, C. R. Hillard and L. McElwee-White, *Organometallics*, 2007, **26**, 3085.

CHAPTER 4

Structural and computational studies of dithizone and its anion

4.1 General introduction

Since its preparation in 1878 by Fischer, dithizone has established itself as a useful ligand in many branches of chemistry. The molecular structure of dithizone has intrigued chemists for decades. Many authors have sought to shed light on the structure of dithizone, both in the solid state and in solution, using spectroscopic, crystallographic and computational techniques. Almost 100 years after its preparation the molecular structure of dithizone was first investigated when Alsop[1] and Laing[2] determined the X-ray crystallographic structure of dithizone in the 1970s. Laing proposed a slightly different molecular structure as was initially determined by Alsop, the difference being the position of the two protons on the dithizone backbone. Alsop placed the two protons on neighbouring nitrogens, i.e. N(4) and N(5) [alternatively N(5) and S] (**Figure 4.1b** and **Figure 4.1c**), while Laing suggested positions N(1) and N(5) (**Figure 4.1a**). The preferred structure (**Figure 4.5c**) proposed by Alsop was shown to be highly unlikely as the geometry centred around N(4) and N(5) would adopt a trigonal pyramidal arrangement which is contrary to the near planar geometry found for the dithizone molecule.

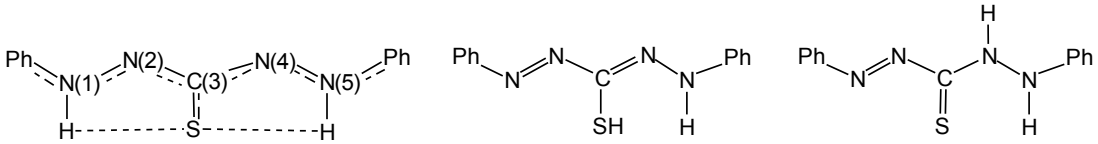

Figure 4.1 Molecular structures of dithizone as proposed by Laing (**a**) and Alsop (**b** and **c**).

Both the keto and enol structures, as proposed by Alsop and Laing, received support in the literature. The geometric structure of dithizone in solution has similarly received much

attention over the years. Coleman[3] and Hutton[4], for example, observed a single N*H* resonance in the ^{1}H NMR spectra of dithizone derivatives and deduced the existence of a single symmetrical thione species as proposed by Laing. Nabilsi[5] suggested dithizone to exist in a tautomeric equilibrium after observing a second resonance at δ = 0.97 ppm which he attributed to the presence of a S*H* group. The symmetrical keto form of dithizone has also been proposed based on molecular orbital calculations. Recent quantum mechanical calculations showed the symmetrical form (**Figure 4.1a**) to be most stabilized in the gas phase. However, it was found that this conclusion is highly dependent on the chosen method of calculation. DFT calculations favour the former, while semi-empirical methods stabilize the enol form (**Figure 4.1b**).[6] The proton transfer barrier was calculated to be 3 kcal mol^{-1}. The same study suggests that dithizone exists in a tautomeric equilibrium in solution.

Of interest is the fact that dithizone only forms *S,N*-coordinated complexes (opposed to *N,N*) with metal ions, which can best be explained by the existence of a sulfur nucleophile, derived from the deprotonation of the thiol group. From the resonance structure of the dithizonate ion, we expect it to be ambidentate with the possibility of forming linkage isomers. However, all reported primary dithizonate complexes bond through the sulfur atom. Furthermore, there are three examples reported in the literature where dithizone acts as a monodentate ligand, forming *S*-coordinated metal complexes.[7,8,9]

4.2. Preparation of 1,5-diphenylthiocarbazonate salt

In the preparation of dithizonate complexes, the dithizone ligand is usually deprotonated by the presence of a base, such as NH_3(aq) or Et_3N. We found it useful to prepare dithizone in its ionic form as the terabutylammonium or tetraphenylarsonium salt. The salt offers better solubility and the base might interfere where precursors with labile ligands are used. The potassium salt of dithizone has been previously prepared by Noda *et al.*[10] While this work was in progress, the tetrabutylammonium salt of dithizone was prepared by cation exchange from potassium dithizonate.[11] We prepared the desired salt by the addition of sodium hydroxide to a suspension of dithizone in water as shown in **Scheme 4.1**.

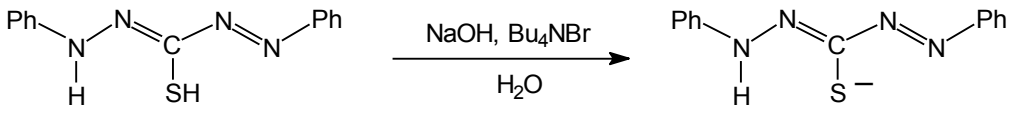

Scheme 4.1 Sample preparation of the 1.5-diphenylthiocarbazonate salt.

The suspension disappears on addition of the base, giving a red solution. The desired product was obtained as red microcrystalline material from the solution by the addition of a solution of tetrabutylammonium bromide or tetraphenylarsonium bromide. The thiocarbazonate salts **[4.1]** and **[4.2]** gave the desired microanalytical data, with melting points of 101°C and 99°C, respectively. This is significantly higher than the melting point of 71°C for the tetrabutylammonium salt reported by von Eschwege *et al.*[11], which coincidently is also the melting point reported for the potassium salt of dithizone reported by Noda.[10] A higher melting point is expected when exchanging a smaller cation such as potassium for a larger cation.

Of interest were the ^{1}H NMR spectra of **[4.1]** and **[4.2]**, which show a singlet at δ 10.43 and 10.59 ppm, respectively, assigned to the N*H* proton (see **Figure 4.2**). However, on closer inspection, we found that the signals integrate for less than one proton.

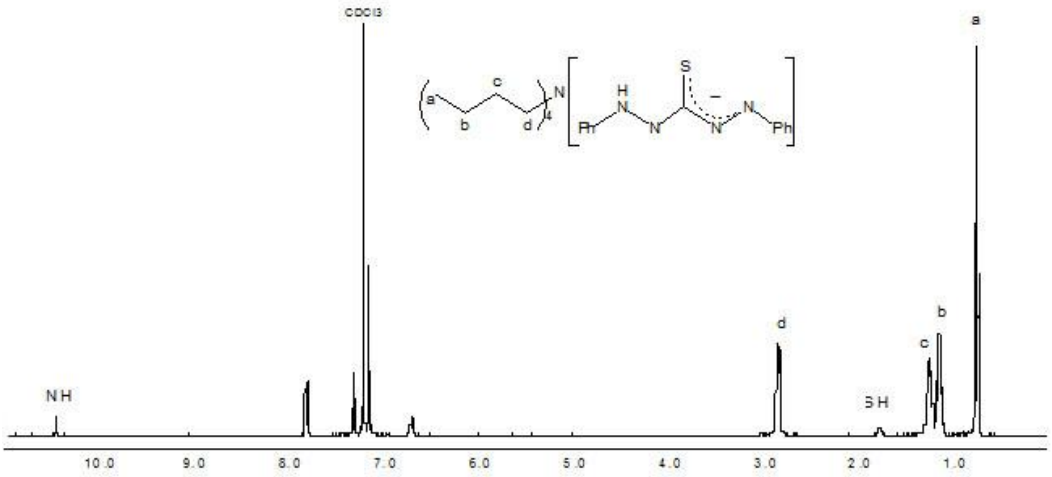

Figure 4.2 ^{1}H NMR spectrum of the dithiocarbazonate salt, Bu_4N[Hdptc] **[4.1]**.

We observed another weak, broad singlet at δ = 1.80 and 1.91 ppm, respectively, which is in the region expected for S*H* protons. The combined resonances accounted for one proton, with the N*H*/S*H* resonances occurring in a 1:1.5 ratio. The N*H* signals are significantly more upfield than the corresponding signal (12.59 ppm) in the parent dithizone molecule, which could be attributed to possible shielding by the residual negative charge present in the molecule. Both resonances disappear in the ^{1}H NMR spectrum on performing a D_2O wash. Neither Noda *et al.*[10] nor von Eschwege *et al.*[11] provided any spectroscopic data for the N*H* or S*H* resonances for comparison. While von Eschwege *et al*. only reported the resonances for the counter-ion and phenyl protons, Noda *et al*. reported no spectroscopic data at all.

All the evidence would suggest an exchange of a proton between the sulfur and the nitrogen atoms, giving rise to resonance structure as shown in **Figure 4.3**. The ^{13}C NMR spectrum of **[4.1]** appears to favour the thiol structure (see **Section 4.6**). No resonances downfield from 135 ppm in **[4.2]** are observed, presumably due to their lower intensities compared to the phenyl resonances.

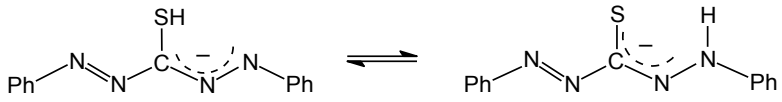

Figure 4.3 Proton exchange in the thiocarbazonate anion.

4.3 Crystal and molecular structure of Bu_4N[Hdptc]

The molecular structure of the potassium salt of dithizone has been reported on previously.[10] It is well known that molecules could be stabilized by π-interactions and hydrogen bonding. Counter-ions are also known to influence the packing of the molecule in the crystal cell, which could impact on the possible electronic interactions within a molecular unit or between neighbouring molecules.

Red crystals of **[4.1]** suitable for crystallographic studies were obtained from recrystallisation in water. An ORTEP representation of the molecular structure is shown in **Figure 4.4**, with a

molecular packing diagram displayed in **Figure 4.5**. Selected bond lengths and angles are given in **Table 4.2**.

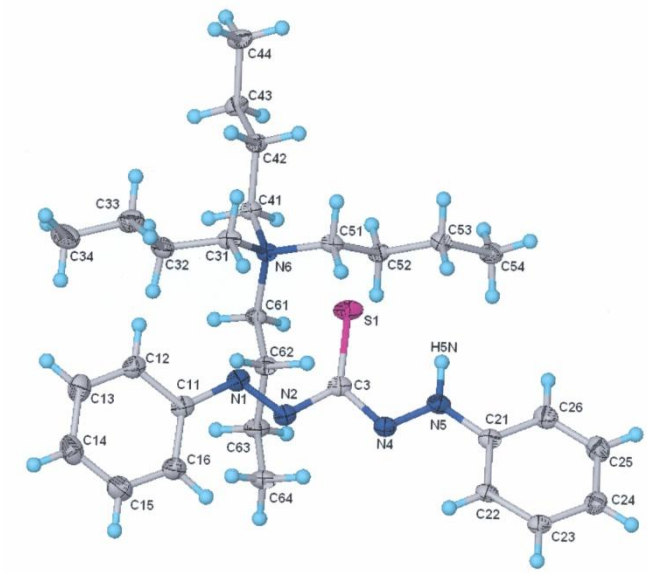

Figure 4.4 Molecular structure and atom numbering system of **[4.1]**. Thermal ellipsoids are drawn at the 50% probability level.

The molecule has been shown to crystallize in the monoclinic space group $P2_1$ with two molecules per unit cell. The potassium analogue crystallizes in the orthorhombic space group *P*bca with eight molecules per unit cell. Crystal data and refinement parameters are given in **Table 4.1**. Selected bond lengths and bond angles for **[4.1]** and the potassium analogue are provided in **Table 4.2**.

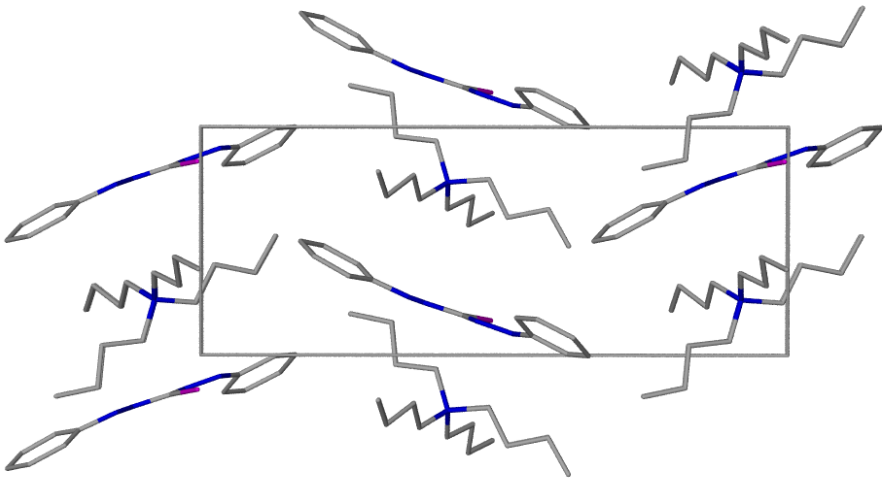

Figure 4.5 Molecular packing diagram of **[4.1]** viewed along [010].

The molecule is shown to be near planar, with the phenyl rings twisted slightly out of the mean plane, adopting an *anti*, *s-trans-trans* configuration similar to the parent dithizone molecule. The *S*-methyl derivative has been shown to adopt a near planar *syn*, *s-trans-trans* arrangement.[12] The N(1)-N(2) and N(4)-N(5) distances are 1.299(3) and 1.313(4) Å, respectively, which are comparable to distances reported for the potassium analogue, parent dithizone molecule and metal complexes of dithizone and are intermediate between *NN* single and double bonds. Distances of 1.40 and 1.43 Å have been reported for diphenylthiocarbazide.[13] The N-C(Ph) distances of 1.413(4) and 1.394(4) Å are comparable to the equivalent bonds in dithizone and its *S*-methyl derivative, but shorter than 1.43 Å, which is typical for N-C(Ph) single bonds. The corresponding C(3)-N(2) and C(3)-N(4) bond distances of 1.382(4) and 1.353(4) Å are indicative of a degree of double bond character, suggesting the delocalized nature of the thiocarbazone backbone.

Table 4.1 Crystal data and structure refinement for **[4.1]**

Empirical formula	$C_{29}H_{47}N_5S$
Formula weight	497.78 amu
Temperature	133(2) K
Wavelength	0.71073 Å
Crystal system, space group	Monoclinic, $P2_1$
Unit cell dimensions	a = 8.6354(1) Å, $\alpha = 90°$
	b = 20.0899(4) Å, $\beta = 114.9°$
	c = 9.5951(2) Å, $\gamma = 90°$
Volume	1509.29(5) $Å^3$
Z, Calculated density	2, 1.095 Mg/m^3
Absorption coefficient	0.132 mm^{-1}
F(000)	544
Crystal size	0.11 x 0.07 x 0.05 mm
Theta range for data collection	2.55 to 26.36°
Limiting indices	$-10 \leq h \leq 10$, $-24 \leq k \leq 24$, $-11 \leq l \leq 11$
Reflections collected / unique	37910 / 5508 [R(int) = 0.0549]
Completeness to theta = 26.75	99.5 %
Max. and min. transmission	0.9935 and 0.9857
Refinement method	Full-matrix least-squares on F^2
Data / restraints / parameters	5508 / 2 / 325
Goodness-of-fit on F^2	1.070
Final R indices [I > 2sigma(I)]	$R_1 = 0.0524$, $wR_2 = 0.1342$
R indices (all data)	$R_1 = 0.0748$, $wR_2 = 0.1479$

The C(3)-S(1) bond distance of 1.720(2) Å is comparable to the distance of 1.71(1) Å reported for dithizone, but shorter than the 1.76(3) Å in the *S*-methyldithizone molecule, being intermediate between 1.82 Å for a C-S single bond and 1.56 Å for a C=S double bond.[14]

Laing, by considering the graphical relationship of bond length of a S-C(sp^2) bond with bond order, concluded that the delocalization in the N(1)-N(2)-C(3)-N(4)-N(5) backbone is less for *S*-methyldithizone compared to the parent dithizone. From this it would then appear that the delocalization in the anionic dithizone compound is intermediate between *S*-methyldithizone and the more delocalized dithizone.

The amine hydrogen atom, H(5N), was located in the difference electron density maps and refined with simple bond length constraints. No other hydrogen atoms could be located, as to be expected for the deprotonated species.

Table 4.2 Comparison of bond lengths (Å) and bond angles (°)

	This work	***Potassium dithizonate***[10]
Bond lengths		
S(1) – C(3)	1.720(3)	1.719(5)
N(1) – N(2)	1.299(3)	1.276(6)
N(1) – C(11)	1.413(4)	1.434(7)
N(2) – C(3)	1.382(4)	1.410(7)
N(4) – N(5)	1.313(4)	1.346(6)
N(4) – C(3)	1.353(4)	1.320(7)
N(5) – C(21)	1.394(4)	1.382(7)
N(5) – H(N5)	0.938(10)	0.90(5)
Bond angles		
N(2) – N(1) – C(11)	115.0(3)	113.3(4)
N(1) – N(2) – C(3)	114.2(3)	114.6(4)
N(5) – N(4) – C(3)	113.9(3)	114.9(4)
N(4) – N(5) – C(21)	119.2(3)	121.8(5)
N(4) – C(3) – N(2)	109.2(3)	108.6(4)
N(4) – C(3) – S(1)	125.4(3)	125.5(4)
N(2) – C(3) – S(1)	125.3(3)	125.9(4)

From a comparison of crystallographic parameters with reported dithizonate structures, as summarized in **Table 4.3**, it is apparent that the delocalization is more prominent on the side of the backbone containing the NH group. This is consistent with the structure reported by Noda et al.[10] It is surprising that this is manifested in the title compound considering the presence of additional electron density.

The bond distances and bond angles for the tetrabutylammonium counter-ion all appear normal. An intramolecular hydrogen bond was found to exist between N(5) and the S atom.

It can be seen from **Table 4.2** that there is significant agreement between the structural parameters for the two structures. The largest deviations in bond length (0.03 Å) occur on the side of the backbone containing the NH group. It is clear from the data that the counter-ion does influence the packing of the molecule in the crystal. There are no close contacts within the title compound whereas the potassium analogue exhibits stacking of molecules within the unit cell.

Table 4.3 Comparative bond lengths (Å) in the dithizone salt with dithizone and related compounds

Compounds	**Bond lengths**						
	C(11)–N(1)	**N(1)–N(2)**	**N(2)–C(3)**	**C(3)–S(1)**	**C(3)–N(4)**	**N(4)–N(5)**	**N(5)–C(21)**
[4.1]	1.413(4)	1.299(3)	1.382(4)	1.720(3)	1.353(4)	1.313(4)	1.394(4)
K[Hdptc]	1.434(7)	1.276(6)	1.410(7)	1.719(5)	1.320(7)	1.346(6)	1.382(7)
H_2dptc[a, b]	1.38	1.30	1.34	1.71	1.35	1.29	1.39
H_2dptc[a, c]	1.48	1.20	1.41	1.74	1.39	1.34	1.36
$[Ru(bipy)_2(Hdptc)_2]$[d]	1.436(7)	1.256(6)	1.412(7)	1.737(5)	1.310	1.343(6)	1.385
$[In(Hdptc)_3]$[e]	1.437(9)	1.27(1)	1.410(9)	1.761(8)	1.305(11)	1.324(9)	1.409(12)

[a] Probable errors in bond lengths estimated to be 0.01 Å
[b] Structure reported by Laing[2]
[c] Structure reported by Alsop[1]
[d] Dithizonate ligand in monodentate coordination[9]
[e] Details for the monodentate dithizone ligand only[8]

4.4 Crystal and molecular structure of dithizone

The quality of the dithizone crystals appears to have greatly influenced the accuracy of the structure reported by Alsop, who used a twinned crystal of dimensions 1.0 x 0.04 x 0.01

mm.[1] Laing, in an attempt to obtain structural parameters of greater accuracy and locating the two protons on the dithizone backbone, reported on having obtained "by good chance, one relatively good single crystal" of dimensions 0.9 x 0.3 x 0.1 mm.[2]

Current X-ray diffractometers have the ability to perform measurements on significantly smaller crystals with greater accuracy. With this in mind, we reasoned that by isolating a relatively small, good quality crystal, a more accurate molecular description of dithizone could be provided should the protons be located on the difference map.

Blue-gray crystals suitable for X-ray crystallography were grown by slow evaporation of a saturated ether solution. The crystal used for data collection was of dimensions 0.28 x 0.11 x 0.02 mm. An ORTEP representation of the molecular structure is shown in **Figure 4.6**. A molecular packing diagram is shown in **Figure 4.7**. Selected bond lengths and angles are given in **Table 4.5**.

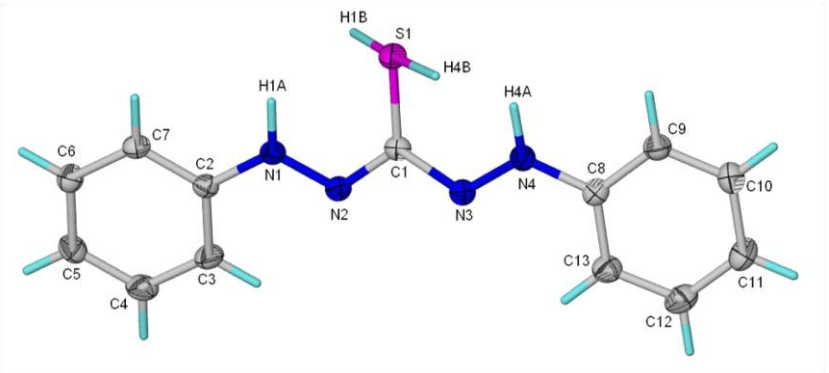

Figure 4.6 Molecular structure and atom numbering system of dithizone. Thermal ellipsoids are drawn at the 40% probability level.

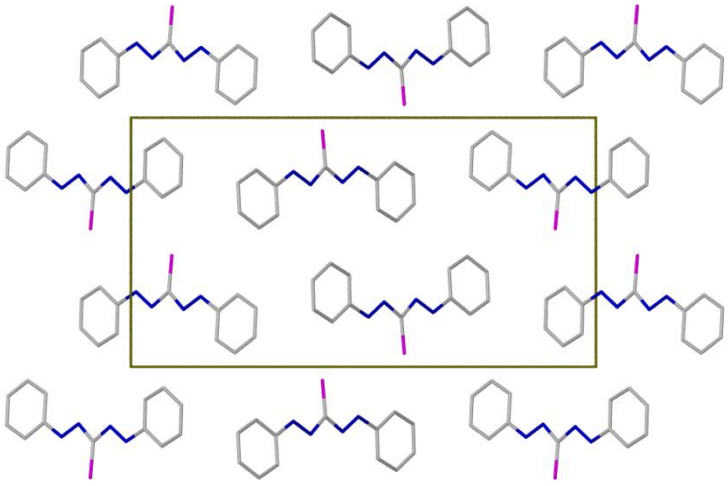

Figure 4.7 Molecular packing diagram of dithizone viewed along a.

The molecule has been shown to crystallize in the monoclinic space group $P2_{1/}n$ with four molecules per unit cell. The crystal parameters, viz. space group and crystal dimensions, are in agreement with those reported by Laing[2]. While the space group is in agreement to that reported by Alsop, the β angle is significantly different at 91.8(1)°. Crystal data and refinement parameters are given in **Table 4.4**.

Table 4.4: Crystal data and structure refinement for dithizone

Empirical formula	$C_{13}H_{12}N_4S$
Formula weight	256.33 amu
Temperature	173(2) K
Wavelength	0.71073 Å
Crystal system, space group	Monoclinic, $P2_{1/}n$
Unit cell dimensions	a = 4.6814(5) Å, α = 90°
	b = 22.016(3) Å, β = 98.181(2)°
	c = 11.9509(14) Å, γ = 90°
Volume	1219.2(2) $Å^3$
Z, Calculated density	4, 1.396 Mg/m^3
Absorption coefficient	0.252 mm^{-1}
F(000)	536
Crystal size	0.28 x 0.11 x 0.02 mm
Theta range for data collection	1.85 to 28.44°
Limiting indices	$-5 \leq h \leq 6$, $-29 \leq k \leq 29$, $-15 \leq l \leq 15$
Reflections collected / unique	13030 / 3043 [R(int) = 0.0437]
Completeness to theta = 26.75	99.1 %
Max. and min. transmission	0.9950 and 0.9328
Refinement method	Full-matrix least-squares on F^2
Data / restraints / parameters	3043 / 4 / 176
Goodness-of-fit on F^2	1.023
Final R indices [I > 2sigma(I)]	R_1 = 0.0419, wR_2 = 0.0958
R indices (all data)	R_1 = 0.0672, wR_2 = 0.1059

The nitrogen and sulfur hydrogen atoms were located from a difference Fourier map and their fractional site occupancies were assigned according to their relative peak heights. The hydrogen atoms located on N(1) and N(4) were assigned a fractional site occupancy of 69% while those on S(1) were assigned a fractional site occupancy of 31%, suggesting the

existence of tautomers. The co-existence of tautomers in a unit cell has been shown to be possible, either as two discrete molecules[15] or as a single molecule,[16,17] as is the case here.

Table 4.5 Comparison of bond lengths (Å) and bond angles (°) of dithizone with previously reported and calculated structures.

	This work	**Alsop**[1]	**Laing**[2]	**DFT**[a]	
Bond lengths				**keto**	**enol**
S(1)-C(1)	1.7123(17)	1.74	1.71	1.719	1.785
S(1)-H(4B)	1.253(10)	-	-	-	1.354
S(1)-H(1B)	1.250(10)	-	-	-	-
N(1)-N(2)	1.297(2)	1.20	1.29	1.288	1.255
N(1)-C(2)	1.405(2)	1.48	1.39	1.396	1.411
N(1)-H(1A)	0.963(10)	-	-	1.033	-
N(2)-C(1)	1.355(2)	1.41	1.34	1.354	1.386
N(3)-N(4)	1.301(2)	1.34	1.30	1.288	1.320
N(3)-C(1)	1.356(2)	1.39	1.34	1.354	1.294
N(4)-C(8)	1.398(2)	1.36	1.38	1.396	1.397
N(4)-H(4A)	0.964(10)	-	-	1.033	1.014
Bond angles					
C(1)-S(1)-H(4B)	91(2)	-	-	-	90.47
C(1)-S(1)-H(1B)	92(2)	-	-	-	-
H(4B)-S(1)-H(1B)	175(3)	-	-	-	-
N(2)-N(1)-C(2)	121.28(14)	115	122	123.38	116.04
N(2)-N(1)-H(1A)	117.9(19)	-	-	115.72	-
C(2)-N(1)-H(1A)	120.9(19)	-	-	120.90	-
N(1)-N(2)-C(1)	114.19(14)	108	112	114.44	116.47
N(4)-N(3)-C(1)	113.17(14)	106	117	114.44	119.73
N(3)-N(4)-C(8)	122.63(14)	117	122	123.39	121.91
N(3)-N(4)-H(4A)	115.6(19)	-	-	115.73	120.29
C(8)-N(4)-H(4A)	121.8(19)	-	-	120.88	117.80
N(2)-C(1)-N(3)	109.04(14)	105	-	108.81	114.44
N(2)-C(1)-S(1)	125.78(13)	134	126	125.59	121.72
N(3)-C(1)-S(1)	125.17(13)	120	124	125.60	123.83

[a]6-311++G(2df,2p) basis set

The bond angles and bond lengths are in close agreement with the findings of Laing[2], but as can be seen in **Table 4.5**, differ in some instances significantly from the parameters reported by Alsop[1]. Furthermore, the structural parameters presented show greater accuracy compared to the structures reported previously with esd's for bond lengths having been estimated to be 0.01 Å.

The torsion angles, C(2)-N(1)-N(2)-C(1)[179.0(2)°], C(1)-N(3)-N(4)-C(8)[-178.7(2)°], N(1)-N(2)-C(1)-S(1)[-2.5(2)°] and N(4)-N(3)-C(1)-N(2)[-180.0(1)°], indicate that the molecule is near planar. Both phenyl rings appear to retain the planarity of the molecule. The bond lengths in the dithizone backbone, PhNNC(S)NNPh, indicate significant delocalization of electron density. The N(1)-N(2) and N(3)-N(4) bond distances are 1.297(2) and 1.301(2) Å, respectively, while the C(1)-N(2) and C(1)-N(3) bond lengths appear similar at 1.355(2) and 1.356(2) Å, respectively. The N(1)-C2 [1.405(2) Å] and N(4)-C(8) [1.398(2) Å] bond lengths are typical of NC bonds with single bond character. The C(1)-S(1) bond length of 1.712(2) Å is shorter than CS single bonds and is evidence that the delocalization is extended into the CS bond. It is of interest to note that the N-N bond distances appear to be unaffected by the presence of the hydrogen atoms, both retaining their double bond character. Similarly, the torsion angles, as indicated above, suggest that the presence of the hydrogen atoms on N(1) and N(4) have no influence on the geometry around these atoms. We would expect that the presence of hydrogen atoms would result in a trigonal pyramidal geometry around N(1) and N(4).

The four hydrogen atoms on the nitrogen and sulfur atoms were constrained at bond lengths of 0.97 and 1.25 Å, for N-H and S-H, respectively. It is interesting to note that H(1B) and H(4B) are located at an angle with respect to the molecular plane.
The molecular packing is in agreement with that reported by Alsop and Laing.[1,2]

4.5 DFT calculations

Geometry optimizations were performed on the tautomeric forms of the parent dithizone molecule and its corresponding anion. While dithizone has been shown to exist in more than 20 conformers, only the three most commonly accepted forms, as depicted in **Figure 4.1**, will

be discussed. Optimized structures were verified to be minima through vibrational frequency analysis.

4.5.1 Calculations based on the parent dithizone molecule

The energy differences for the three conformers in the gas phase at the HF and B3LYP levels of theory, using the 6-31+G(2d,p) and 6-311++G(2df,2p) basis sets, respectively, are shown in **Table 4.6**. As shown in **Figure 4.1**, conformers are labelled as being either **[4.1a]**(C_{2v}), **[4.1b]**(C_s) or **[4.1c]**(C_1).

From these results it can be seen that the lowest energy is dependent on the chosen level of theory. While DFT calculations show conformer **[4.1a]** to be most stabilized, HF calculations stabilize conformers **[4.1b]** and **[4.1c]**. Similar findings were made by Schonherr *et al*.[6] The energy difference, using DFT, between conformer **[4.1a]** and **[4.1b]** was found to be 3.1 kcal mol^{-1} (12.9 kJ mol^{-1}), and 9.5 kcal mol^{-1} (39.0 kJ mol^{-1}) between **[4.1a]** and **[4.1c]**. HF shows the difference in energy between **[4.1b]** and **[4.1a]** to be 9.2 kcal.mol^{-1} (38.4 kJ mol^{-1}). Energies of similar magnitude were reported by Schonherr *et al*.[6] There appears to be no significant difference in energy between **[4.1b]** and **[4.1c]**, with energy differences being 0.7 kcal mol^{-1} (2.8 kJ mol^{-1}). Schonherr *et al*. did not report any optimisation energy for the latter conformer. The DFT findings are supportive of the co-existence of the two conformers as observed in the solid state structure due to the extremely low proton transfer barrier of 3.1 kcal mol^{-1} between the enol and keto forms.

Table 4.6 Energies of optimized geometries for the three conformers of dithizone in hartrees.

Method	**[4.1a]**	**[4.1b]**	**[4.1c]**
B3LYP/6-311++G(2df,2p)	-1119.780534	-1119.775634	-1119.765343
RHF/6-31+G(2d,p)	-1114.301704	-1114.316315	-1114.317364

4.5.2 Calculations based on the dithizone anion

Calculations were performed on the enol and keto forms using the B3LYP and HF functionals and with various basis sets in attempt to: (i) understand the tautomeric nature of the anion in the gas phase and in solution, and (ii) describe the nucleophilicity of the anion. Structures of the anion as well as the neutral species protonated at either N(4), N(2) or S were determined, all as isolated molecules in the gas phase. The two tautomers associated with the anion were also optimized in solution using the polarized continuum model (PCM).

Table 4.7 Energies in hartrees of optimized geometries for enol and keto tautomers of the dithizone anion in the gas phase. Corresponding optimizations in solution are given in parentheses.

Level of theory/basis set	Tautomers		ΔE kJ.mol^{-1}(kcal mol^{-1})
	keto	enol	
B3LYP/6-311++G(2df,2p)	-1119.25981 (-1119.32380)	-1119.25529 (-1119.31127)	11.9 (2.8) 32.9 (7.9)
B3LYP/6-311+G(d,p)	-1119.21005 (-1119.27511)	-1119.20501 (-1119.26203)	13.2 (3.2) 34.3(8.2)
RHF/6-31++G(2d,p)	-1113.79660 (-1113.86600)	-1113.77529 (-1113.83499)	55.9 (13.4) 81.4 (19.5)

A comparison of experimental and calculated structural parameters (**Table 4.8**) reveals that DFT favours the keto conformer. While the experimental bond lengths show excellent agreement with the enol (r^2 = 0.98) and keto (r^2 = 0.97) empirical bond lengths, bond angles for the keto form (r^2=0.94) show significantly better correlation with experimental data than the enol form (r^2 = 0.45).

When considering the protonation of the anion at the sulfur and the nitrogen atom, we found that the species protonated at S is 17 kJ mol^{-1} lower in energy than the N(4)-protonated analogue, indicating that the favoured protonation site of the anion will be the S atom. This was further verified by looking at the Highest Occupied Molecular Orbital (HOMO) of the anionic species and determining the Fukui index[18] of the S and N(4) atoms.

Table 4.8 Comparison of experimental and calculated bond lengths (Å) and bond angles (°) for complex **[4.1]**

	[4.1]	**enol**	**keto**
Bond lengths			
C(1)-S(1)	1.720(3)	1.799	1.725
N(1)-N(2)	1.299(3)	1.293	1.256
N(3)-N(4)	1.313(4)	1.289	1.337
C(2)-N(1)	1.413(4)	1.391	1.417
N(2)-C(1)	1.382(4)	1.333	1.407
N(3)-C(1)	1.353(4)	1.337	1.327
N(4)-C(8)	1.394(4)	1.394	1.369
S(1)-H(1)	-	1.351	-
N(4)-H(1)	-	-	1.028
Bond angles			
C(2)-N(1)-N(2)	115.0(3)	114.4	113.9
N(2)-C(1)-N(3)	109.2(3)	116.2	107.9
N(1)-N(2)-C(1)	114.2(1)	118.6	116.9
C(1)-N(3)-N(4)	113.9(3)	116.4	114.2
N(3)-N(4)-C(8)	119.2(3)	114.4	122.5
N(2)-C(1)-S(1)	125.3(3)	123.5	126.4
N(3)-C(1)-S(1)	125.4(3)	120.3	125.7

The composition of the HOMO can be used to indicate the regioselectivity to electrophilic attack. The atom that contributes most (in terms of its contribution to the HOMO composition as summed over all the basis functions centred on the atom) is the most nucleophilic site, which appears to be the S atom, as shown in **Figure 4.5a**. We also considered the Fukui function which is related to frontier molecular orbital theory and is a representation of the electron density of the normal species (with N_0 electrons) minus that of the species with one electron removed (with N_0-1 electrons).

This difference indicates the region where electron density is “most labile”, i.e. the region most susceptible to electrophilic attack. Being linked to the concept of frontier molecular orbital theory it is expected to give the same conclusion as inspecting the HOMO, which is

observed in this case. The Fukui function[18] is depicted in **Figure 4.5b**. Numerically this can be verified by doing a population analysis of the N_0 and (N_0-1) species condensed to individual atoms. Therefore, a Mulliken population analysis was done to obtain individual Fukui indexes, which were found to be 1.134 for the S and 0.370 for the N(4) atom. The largest index corresponds to the atom most susceptible to electrophilic attack. The results are unambiguous in their identification of the *S*-atom as the preferred site of deprotonation.

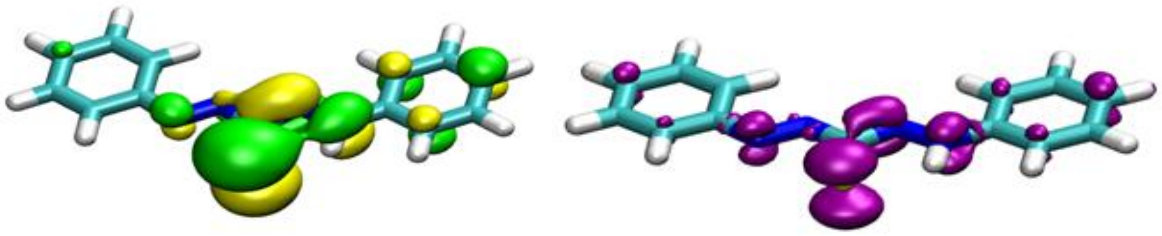

(a) HOMO **(b) Fukui function**

Figure 4.5 Molecular orbital structures for the dithizonate anion.

4.6 NMR Spectra

The ^{1}H NMR spectrum of the anion (**Figure 4.2**) shows that the tautomeric interconversion of the anion is slow enough for the N*H* and S*H* resonances of both forms to be observed.
NMR spectra were calculated for the DFT/6-311++G(2df,2p) optimized structures, using the 6-31++G(2d,p) basis set. Chemical shift results at the HF and DFT levels of theory are shown in **Table 4.9**. Chemical shifts for TMS [δ_0 = 31.57 ppm (DFT) and δ_0 = 31.90 ppm (RHF)] were calculated at the same level of theory, using the same basis set.

From the results it can be seen that the DFT method provides the better approximation of the N*H* chemical shift for the keto form, being 1.0 ppm lower than the experimental value. Calculated chemical shifts for the enol form is significantly less accurate at 7.92 ppm (2.5 ppm lower than the experimental value). The values obtained for the phenyl resonances using either level of theory are reasonably accurate. None of the two methods provided reasonable parameters for the S*H* chemical shifts. Similar difficulty in calculating chemical shift values for S*H* protons has been reported.[6]

Table 4.9 Calculated ^{1}H chemical shift values for **[4.1]** in ppm.

	DFT/6-31++G(2d,p)		RHF/6-31++G(2d,p)		Observed
	keto	**enol**	**keto**	**enol**	
	N*H*	**S*H***	**N*H***	**S*H***	
-N*H* / S*H*	11.44	6.47	7.92	5.36	10.43/1.80
Ph	6.77-8.14	6.95-7.87	6.70-8.61	6.85-7.99	6.65-7.82

A comparison between experimental and calculated ^{13}C chemical shifts, using the same level of theory and basis sets as discussed before, is given in **Table 4.10**. Chemical shift values for TMS [δ_0 = 191.4 ppm (DFT) and δ_0 = 183.8 ppm (RHF)] were calculated at the same level of theory, using the same basis set. The two C(Ph) [C11 (144.2 ppm) and C21 (153.4ppm)] and the C-S [C3 (170.3 ppm)] (see **Figure 4.4**) resonances are in close agreement with the keto conformer, irrespective of the level of theory used. The calculated phenyl resonances appear between 107.3 and 128.1 ppm, in close agreement with the observed resonances appearing between 113.5 and 129.1 ppm.

Table 4.10 Calculated and experimental ^{13}C chemical shift values for **[4.1]** in ppm

	DFT/6-31++G(2d,p)		RHF/6-31++G(2d,p)		Observed
	keto	**enol**	**keto**	**enol**	
C21	150.6	151.9	147.4	153.5	153.4
C3	171.4	142.6	167.2	118.0	170.3
C11	140.6	152.3	140.9	156.3	144.2
C22-C26	111.45-129.1	110.7-124.2	113.6-131.3	109.5-127.5	113.5-129.1
C12-C16	109.2-125.4	109.9-124.1	107.3-130.6	114.7-128.1	

Based on the data in **Table 4.9**, it would appear as if DFT better approximates the experimental chemical shifts. Unlike the ^{1}H NMR spectrum where the S*H* resonance confirms the presence of both conformers in solution, the ^{13}C NMR spectrum appears to be less conclusive in this respect. It would appear from the ^{13}C NMR data of **[4.1]** and the data contained in the table that the keto conformer is the only form in solution.

As can be seen from **Table 4.7**, both DFT and HF levels of theory favour stabilization of the keto form in solution (chloroform). Solution calculations using the PCM method show the keto form to be 32.8 kJ mol^{-1} (7.9 kcal mol^{-1}) [DFT] and 81.4 kJ mol^{-1} (19.5 kcal mol^{-1}) [HF], lower in energy compared to the enol form. A frequency calculation allowed the determination of the equilibrium constant. Using the thermochemical data, in conjunction with the equilibrium equation, $\Delta G = -RT\ln K$, gave an equilibrium constant, K of 0.93. This shows that the tautomers are in near equilibrium conditions, slightly favouring the reverse reaction, i.e. the keto form. This appears to be in contrast with the ^{1}H NMR spectroscopic data, which indicates a 1:1.5 ratio of the two tautomers in chloroform, favouring the enol form.

REFERENCES

1 P. A. Alsop, *Ph.D. Thesis*, University of London, 1971.

2 M. Laing, *J. Chem. Soc., Perkin Trans.*, 1977, 1248.

3 R. A. Coleman, W. H. Foster, J. Kazan and M. Mason, *J. Org. Chem.*, 1970, **35**, 2039.

4 A. T. Hutton, *Polyhedron*, 1987, **6**, 13.

5 A. H. Nabilsi, *Ph.D. Thesis*, University of Leeds, 1972.

6 T. Schonherr, R. Linder, U. Rosellen and V. Schmid, *Int. J. Quant. Chem.*, 2002, **86**, 90.

7 G. L. Seamans, J. L. Walsh, M. Krawiec and W. T. Pennington, *Acta. Cryst.*, 2003, C59.

8 J. M. Harrowfield, C. Pakawatchai and A. H. White, *J. Chem. Soc., Dalton Trans.*, 1983, 1109.

9 F. S. Kong and W. T. Wong, *J. Chem. Soc., Dalton Trans.*, 1999, 2497.

10 H. Noda, L. M. Engelhardt, J. M. Harrowfield, C. Pakawatchai, J. M. Patrick and A. H. White, *Bull. Chem. Soc. Jpn*, 1985, **58**, 2385.

11 K. G. von Eschwege and J. C. Swarts, *Polyhedron*, 2010, **29**, 1727.

12 J. Preuss and A. Gieren, *Acta. Cryst.*, 1975, **B31**, 1276.

13 M. Harding, M. J. Adams, P. A. Alsop and H. M. N. H. Irving, *Analyt. Chim. Acta.*, 1973, **67**, 204.

14 H. Cheng, D. Chun-ying, F. Chen-jie, L. Yong-jiang and M. Qing-jin, *J. Chem. Soc., Dalton Trans.*, 2000, 1207.

15 B. Kosar, C. Albayrak, M. Odabasoglu and O. Buyukgungor, *Internat. J. Quant. Chem.*, 2010, **12**, 22.

16 M. G. B. Drew, D. Das, S. De, J. P. Naskar and D. Datta, *J. Chem. Crystallogr.*, 2008, **38**, 507.

17 R. Novotna, Z. Travnicek and I. Popa, *J. Mol. Struct.*, 2010, **963**, 202.

18 P. W. Ayers, S. Lui and T. Li, *Chem Phys. Lett*., 2009, **480**, 318.

CHAPTER 5

Structural, spectrochemical and electrochemical studies of Pd and Pt dithizone-phosphine complexes

5.1 General introduction

In an attempt at preparing the dithizone derivative of 1,5-cycloocatdiene-platinum(II) as a precursor for the preparation of mixed dithiolene-dithizonate complexes (see **Chapter 6**), we instead isolated the unexpected secondary dithizonate derivative. The formation of this complex led us to investigate the reactivity of dithizone towards platinum and palladium complexes containing various stabilizing ligands.

Since the phenomenon of photochromism has predominantly been investigated in disubstituted palladium- and platinum-dithizonate complexes, i.e., $M(Hdptc)_2$,[1,2] we considered that it would be of interest to see whether coordination of the Group 10 metal centre with other coordinating ligands would impact on the photochromism reported for the bis-dithizonate complexes. Even though many monosubstituted-dithizonate complexes have been prepared, very little, if any, mention is made regarding the presence of photochromism in these complexes. The most extensive work on the photochromism of mono-substituted dithizonates has been reported by Hutton.[3,4,5,6]

5.2 Reaction of $X_2Pt(COD)$ with dithizone

The organometallic platinum-dithizonate complex **[5.1]** was prepared according to **Scheme 5.1**. The reaction of $(COD)PtCl_2$ (X = Cl or Br) with dithizone, in the presence of Et_3N, or $Bu_4N[Hdptc]$ **[4.1]** led to the precipitation of an orange precipitate. Mass spectral data suggested that both halogens have been displaced. The integrity of the organic coordinating ligand, 1,5-cyclooctadiene, was confirmed by the characteristic singlets, with Pt-satellites, in the ^1H NMR spectrum. The singlets resonate at 4.89 [$^2J(^{195}Pt\text{-}H)$ 26.37 Hz]

and 5.42 ppm [$^{2}J(^{195}$Pt-H) 27.10 Hz], irrespective of which halide precursor was used, confirming the displacement of both halogens.

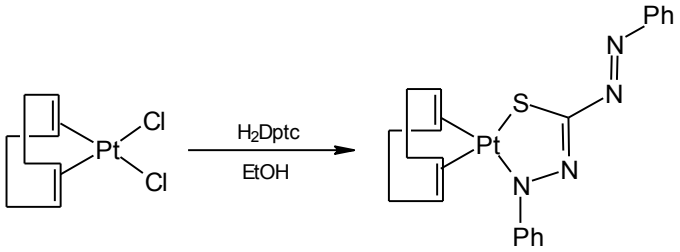

Scheme 5.1 Preparation of the cyclooctadiene platinum dithizonate complex **[5.1]**.

All spectroscopic evidence suggested that the dithizone ligand was doubly deprotonated. The characteristic -NH stretch for the dithizone moiety was also absent in the infrared spectrum of **[5.1]**, supporting the formation of a secondary dithizonate complex. What was more surprising was that the same complex was formed in the absence of a base. This reactivity of dithizone with the organoplatinum halides was of interest, since as far as we could ascertain, all recorded reactions of dithizone to form organometallic dithizonate complexes were performed in the presence of a base. Singh,[7,8] for example, has prepared organometallic titanium complexes using Et_3N as a base. Subsequent treatment with Et_3N or using an excess base resulted in the formation of the secondary metal-dithizonates. No crystal structure was reported to confirm this observation. Moreover, there are, as far as we could ascertain, only two crystal structures of secondary dithizonate complexes in the literature.[9,10]

Complex **[5.1]** has been shown to readily displace COD on reaction with phosphine ligands in ethanol as shown in **Scheme 5.2**. The resultant phosphine complexes are formed almost quantitatively when the selected phosphine is reacted with a suspension of the secondary metal-dithizonate complexes in ethanol. PPh_3, dppe and dppp have been shown to displace cyclooctadiene to form the corresponding mono and bidentate dithizone-phosphine complexes.

The ^{1}H NMR spectra of the phosphine derivatives show the expected resonances and are summarized in the experimental section.

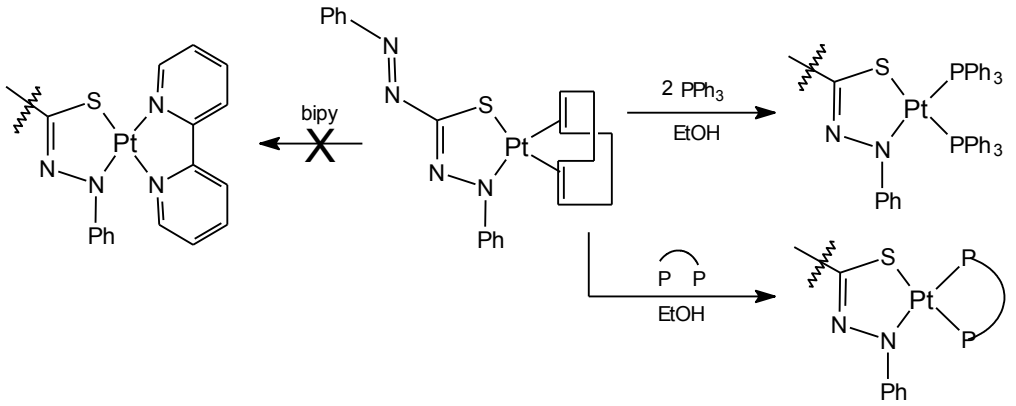

Scheme 5.2 Reactivity of **[5.1]**.

The ^{31}P NMR spectra exhibit two resonances for two inequivalent phosphorus atoms. Each resonance is flanked by satellites due to coupling with ^{195}Pt. Chemical shift and coupling constant values are summarized in **Table 5.1**.

No displacement was found to take place when an *N*-heterocycle, such as bipy, was reacted with **[5.1]**, even when refluxed in dichloromethane. This is generally observed with attempts at displacing COD with weaker *N*-donor ligands (see **Scheme 5.2**).

5.3 Platinum and palladium dithizone-phosphine complexes

Due to the unexpected reactivity of dithizone towards the organoplatinum halides, we further investigated its reactivity with platinum and palladium complexes containing other stabilizing ligands.

5.3.1 Reaction of dithizone with platinum and palladium phosphine precursors

The mixed Group 10 dithizonate-phosphine complexes were prepared according to **Scheme 5.3**.

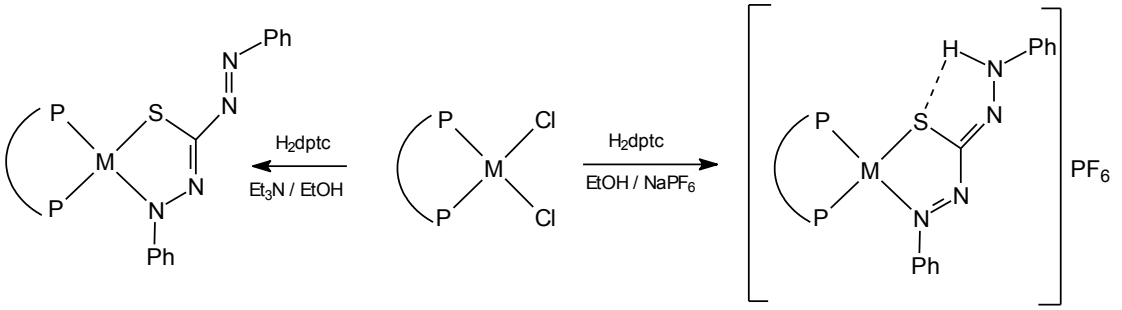

Scheme 5.3 Preparation of Group 10 dithizonate-phosphine complexes.

The reactivity of the metal-phosphines with dithizone initially appeared to be similar to that of the organometallic precursor, [(COD)$PtCl_2$], with an immediate colour change on addition of dithizone. However, unlike the reaction of dithizone with [(COD)$PtCl_2$], where the product precipitated on addition of dithizone, the resultant dithizonate-phosphine complexes were completely soluble in ethanol, indicating the formation of a salt. This was confirmed by the addition of either Na[PF_6] or Na[Ph_4B], to yield crimson to purple coloured precipitates. The formation of the ionic complexes suggested the displacement of both halogens and the formation of the primary dithizonate complexes. Interestingly, in the presence of an equimolar amount of a base, Et_3N, precipitates are formed, suggesting the formation of secondary dithizonate complexes.

The characteristic proton resonances are observed in the ^{1}H NMR spectra of the Pt- and Pd dithizonate-phosphine complexes. The coupling constants are in agreement with those reported in **Chapter 3** and are summarized in the experimental section.

The ^{31}P NMR data are given in **Table 5.1**. The ^{31}P NMR spectra show two signals for the two inequivalent phosphorus nuclei. Each signal is split into a doublet due to the coupling between the two inequivalent phosphorus nuclei. There appears to be a slight upfield shift in going from the primary to the corresponding secondary dithizonate. This observation is in line with the expected deshielding effect of the electron-deficient metal centre. The two-bond coupling constant, ^2J(PP), is in the range 8.3-94.6 Hz for the Pd complexes and 10.9-72.3 for the platinum complexes. The highest coupling constant for both metals are due to the primary dppm-dithizonate complexes.

Table 5.1 ^{31}P NMR data for complexes primary and secondary Pd and Pt phosphine dithizonate complexes

Complex		^{31}P NMR		
		δ (ppm)	J_{Pt-P} (Hz)	J_{P-P} (Hz)
[(dppm)Pd(Hdptc)]PF_6	**[5.2]**	-29.4		94.6
		-49.4		91.1
[(dppm)Pd(dptc)]	**[5.3]**	-24.8		72.9
		-44.2		75.3
[(dppm)Pt(Hdptc)]PF_6	**[5.4]**	-50.7	2538	72.3
		-48.2	2564	72.2
[(dppm)Pt(dptc)]	**[5.5]**	-48.3	2666	70.1
		-46.7	2306	70.2
[(dppe)Pd(Hdptc)]Ph_4B	**[5.6]**	59.2		20.0
		64.5		20.2
[(dppe)Pd(dptc)]	**[5.7]**	48.5		32.7
		56.8		32.9
[(dppe)Pt(dptc)]	**[5.8]**	38.5	2880	10.9
		47.1	2943	11.9
[(dppp)Pd(Hdptc)]Ph_4B	**[5.9]**	5.4		60.2
		12.2		60.1
[(dppp)Pd(dptc)]	**[5.10]**	4.9		60.6
		7.2		60.5
[(dppp)Pt(dptc)]	**[5.11]**	-13.0	2776	37.5
		1.4	2826	36.6
[(dppf)Pd(Hdptc)]Ph_4B	**[5.12]**	30.6		10.9
		38.1		10.8
[(dppf)Pd(dptc)]	**[5.13]**	23.1		8.3
		23.9		8.4
[(dppf)Pt(Hdptc)]Ph_4B	**[5.14]**	-0.7	3288	18.4
		23.5	3317	18.2
[(dppf)Pt(dptc)]	**[5.15]**	-9.3	3100	26.5
		11.4	3167	26.5
[(PPh_3)Pt(dptc)]	**[5.16]**	6.3	3073	25.6
		19.3	3098	24.7
[($P(Me_2Ph)$)$_2$Pt(dptc)]	**[5.17]**	-23.5	2889	27.3
		-14.1	2958	27.5
[($P(Et_3)$)$_2$Pt(Hdptc)]Ph_4B	**[5.18]**	0.0	2967	25.4
		5.6	2943	25.8

For the Pt complexes, the phosphorus resonances are flanked by satellites due to coupling with ^{195}Pt as depicted in **Figure 5.1**. The $^1J(^{195}PtP)$ coupling constants range from 2306-3317 Hz. The $^1J(^{195}PtP)$ coupling constants appear to be higher for the primary complexes, which is in line with coupling of the phosphorus atom with the metal centre.

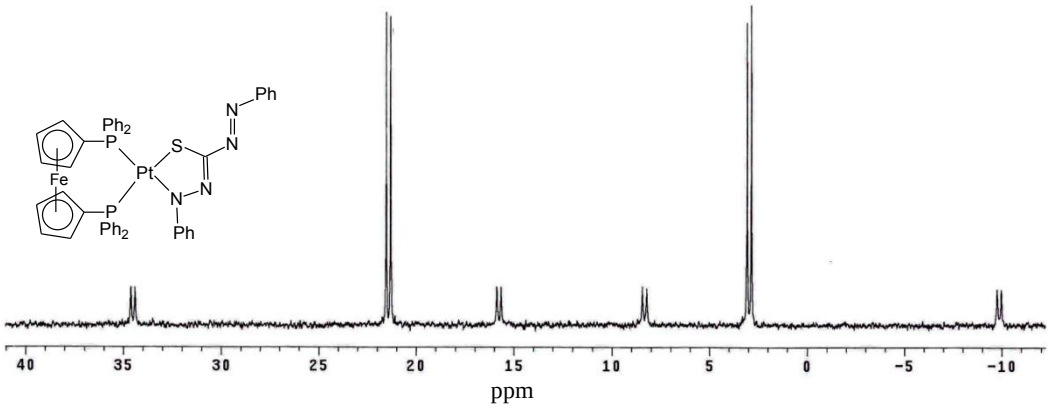

Figure 5.1 ^{31}P NMR spectrum of **[5.16]** showing the chemically inequivalent phosphorus atoms with corresponding $^{1}J(^{195}\text{PtP})$ coupling.

5.4 Crystal and molecular structure of complex [5.1]

Orange-red crystals of **[5.1]** suitable for crystallographic studies were obtained from dichloromethane/methanol. An ORTEP representation of the molecular structure is shown in **Figure 5.2**, while the molecular packing diagram is given in **Figure 5.3**. The crystal data and refinement parameters are given in **Table 5.2**, while selected bond lengths and angles are provided in **Table 5.3**. The molecule was shown to crystallize in the $P2_1/c$ space group. Least squares refinement gave a final *R* value of 2.92%.

The crystal structure shows platinum bonded to the η^4-cyclooctadiene and dithizone ligands in a distorted square-planar environment. The dithizone backbone is reasonably planar, with the phenyl ring attached to the chelate nitrogen atom being twisted slightly against the coordination plane, presumably to minimize interaction with the cyclooctadiene residue.

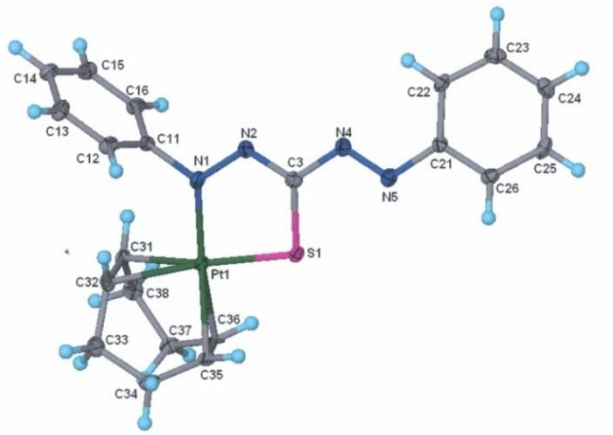

Figure 5.2 Molecular structure and atom numbering system of **[5.1]**. Thermal ellipsoids are drawn at the 50% probability level.

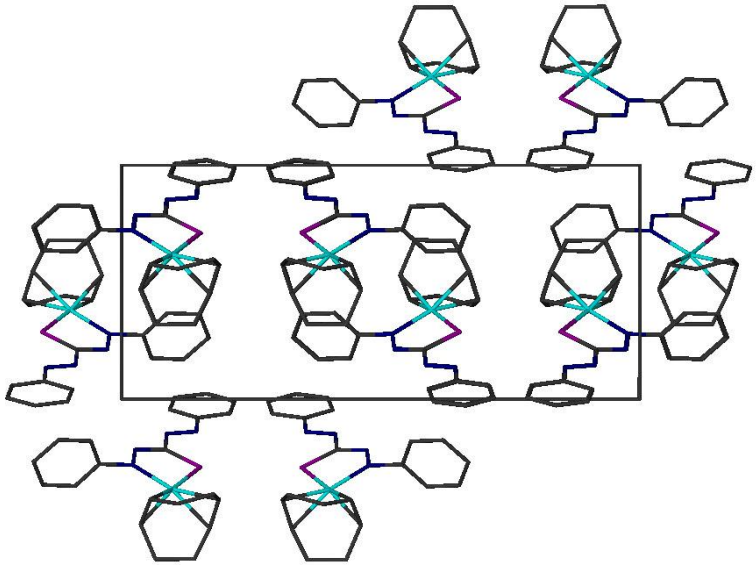

Figure 5.3 Molecular packing diagram for **[5.1]** viewed along [100].

The bond distances between Pt and the olefinic C atoms of the cyclooctadiene differ slightly. The distance to the C atoms *trans* to S, C(31) and C(32), is slightly longer with an average of 2.206 Å compared with an average of 2.184 Å for the C atoms *trans* to the N atom. This is consistent with the weaker bonding of *N*-donor compared with *S*-donor atoms. The olefinic bond lengths of 1.388(7) and 1.393(7) Å are consistent with those found in cyclooctadiene complexes.[11,12]

The PtS and PtN distances of the dithizone moiety are 2.267(1) and 1.998(4) Å, respectively. The longer bond length of Pt-S is to be expected for the larger S atom. The Pt-N(1) bond distance is shorter than that found in complexes where N bonds in a dative covalent manner to Pt. The bond length is consistent with Pt-N single bonds.[13]

Table 5.2 Crystal data and structure refinement for **[5.1]**

Empirical formula	$C_{21}H_{22}N_4PtS$
Formula weight	557.58 amu
Temperature	113(2) K
Wavelength	0.71073 Å
Crystal system, space group	Monoclinic, $P2_1/c$
Unit cell dimensions	a = 9.9266(2) Å, α = 90°
	b = 20.6521(2) Å, β = 110.0°
	c = 9.9386(5) Å, γ = 90°
Volume	1914.3(1) $Å^3$
Z, Calculated density	4, 1.935 Mg/m^3
Absorption coefficient	7.452 mm^{-1}
F(000)	1080
Crystal size	0.08 x 0.07 x 0.05 mm
Theta range for data collection	2.18 to 26.75°
Limiting indices	$-12 \leq h \leq 12$, $-26 \leq k \leq 25$, $-11 \leq l \leq 11$
Reflections collected / unique	26126 / 3925 [R(int) = 0.0622]
Completeness to theta = 26.75	96.4 %
Max. and min. transmission	0.7070 and 0.5870
Refinement method	Full-matrix least-squares on F^2
Data / restraints / parameters	3925 / 0 / 244
Goodness-of-fit on F^2	1.074
Final R indices [I>2sigma(I)]	R_1 = 0.0292, wR_2 = 0.0492
R indices (all data)	R_1 = 0.0484, wR_2 = 0.0542

In Hg dithizonate structures the metal-nitrogen bond is shorter than the sum of the van der Waals radii of the two atoms and is classified as a weak bond. This supports the existence of dithizonate in its secondary form. This is further supported by the increased bond length of N(1)-N(2) in the chelate ring from a typical length of 1.31 Å to 1.353(5) Å for this structure, denoting single bond character.

Table 5.3 Selected bond lengths (Å), bond- and torsion angles (°) for **[5.1]**

Bond lengths			
Pt – N(1)	1.998(4)	N(4) – N(5)	1.275(6)
Pt – S(1)	2.267(1)	N(3) – C(3)	1.394(6)
Pt – C(31)	2.196(4)	C(31) – C(32)	1.388(7)
Pt – C(32)	2.216(4)	C(31) – C(38)	1.516(7)
Pt – C(35)	2.186(5)	C(32) – C(33)	1.514(7)
Pt – C(36)	2.182(4)	C(33) – C(34)	1.533(7)
S(1) – C(3)	1.749(5)	C(34) – C(35)	1.519(7)
N(4) – C(3)	1.394(6)	C(35) – C(36)	1.393(7)
N(1) – C(11)	1.437(6)	C(36) – C(37)	1.523(7)
N(1) – N(2)	1.353(5)	C(37) – C(38)	1.540(7)
N(2) – C(3)	1.307(6)		
Bond angles			
N(1) – Pt – S(1)	83.7(1)	N(4) – C(3) – S(1)	122.5(4)
C(3) –S(1) – Pt	95.8(2)	N(2) – N(1) – C(11)	111.4(4)
N(5) – N(4) – C(3)	113.6(4)	N(2) – N(1) – Pt	121.6(3)
N(2) – C(3) – N(4)	114.1(4)	C(11) – N(1) – Pt	126.7(3)
N(2) – C(3) – S(1)	123.4(4)	C(3) – N(2) – N(1)	114.9(4)
Torsion angles			
N(1) – N(2) – C(3) – N(4)	-179.9(4)	N(1) – N(2) – C(3) – S(1)	0.3(6)
C(3) – N(4) – N(5) – C(21)	176.6(4)	N(1) – Pt(1) – S(1) – C(3)	-5.3(2)
N(5) – N(4) – C(3) – N(2)	176.3(4)	S(1) – Pt(1) – N(1) – N(2)	7.5(3)
N(5) – N(4) – C(3) – S(1)	-3.9(5)	S(1) – Pt(1) – N(1) – C(11)	-179.2(4)
N(1) – N(2) – C(3) – N(4)	-179.0(2)	C(11) – N(1) – N(2) – C(3)	179.3(4)

Furthermore, the decreased bond distances for C(3)-N(4) and N(1)-N(2) of 1.394(6) and 1.353(5) Å, respectively, are typical of bonds with double bond character, whereas primary dithizonates would have single bond character. The geometric parameters are in agreement with other secondary dithizonate complexes as shown in **Table 5.4**.

There is no indication of any intermolecular interactions in the molecule.

Table 5.4. Comparison of crystal parameters for **[5.1]** with other secondary metal-dithizonates

Bond lengths (Å)	**Compounds**		
and angles (°)	**[4.1]**	**[Au(Hdamp-C){dptc}L][a, 14]**	**$Bu_4N[MoO_2(dptc)(Hdptc)]$[15]**
M-S(3)	2.267(1)	2.283(1)	2.513(1)
M-N(1)	1.998(4)	2.054(5)	2.108(4)
N(1)–N(2)	1.353(5)	1.335(6)	1.345(7)
N(2)–C(3)	1.307(6)	1.314(7)	1.300(7)
C(3)–S(1)	1.749(5)	1.770(6)	1.740(7)
C(3)–N(4)	1.394(6)	1.370(7)	1.380(9)
N(4)–N(5)	1.275(6)	1.279(6)	1.275(7)
S(3) - M - N(1)	83.7(1)	84.0(1)	75.1(1)
N(2) – C(3) – N(4)	114.1(4)	114.5(5)	

[a] L = 2-methylmercaptotertrazole,
Hdamp-C = 2-(dimethylammonium-methyl)phenyl

5.5 UV/Vis spectrophotometry

The electronic spectra of the palladium and platinum dithizonate complexes were obtained in dichloromethane in the range 200 - 800 nm. None of the complexes showed any evidence of photochromism in solution. The mixed metal dithizonate complexes exhibit similar absorption characteristics compared to the dithizonate salt **[4.1]**, with two absorption peaks in the region 200-800 nm. The bimetallic ferrocenyl complexes show an additional long wave absorption between 600 and 730 nm, presumably due to the absorption by the ferrocene moiety. The molar extinction coefficients, ε, are in accordance with literature data and range from 4555 to 36759 $mol^{-1}\ dm^3\ cm^{-1}$.

The spectrophotometric data in **Table 5.5** show that there is a hypsochromic shift for the longer wavelength absorption of approximately 30 nm in going from the primary to the secondary complex. Furthermore, it appears as if the shorter wavelength absorption shows greater sensitivity with respect to the charge on the complex, with a shift of approximately 100 nm in going from the neutral secondary to the cationic primary complex.

Table 5.5 Spectroscopic data for palladium and platinum primary and secondary dithizonate complexes in dichloromethane

Complex		λ nm	ε mol^{-1} dm^3 cm^{-1}
[(dppm)Pd(Hdptc)]PF_6	**[5.2]**	516 390	31320 4650
[(dppm)Pd(dptc)]	**[5.3]**	491	29772
[(dppm)Pt(Hdptc)]PF_6	**[5.4]**	512 345	32550 4568
[(dppm)Pt(dptc)]	**[5.5]**	492 350	32556 4552
[(dppe)Pd(Hdptc)]Ph_4B	**[5.6]**	515 387	32796 4555
[(dppe)Pd(dptc)]	**[5.7]**	486	29862
[(dppe)Pt(dptc)]	**[5.8**	490 342	32570 7470
[(dppp)Pd(Hdptc)]Ph_4B	**[5.9]**	519 393	27448 4516
[(dppp)Pd(dptc)]	**[5.10]**	487	29620
[(dppp)Pt(dptc)]	**[5.11]**	494 335	31791 7483
[(dppf)Pd(Hdptc)]Ph_4B	**[5.12]**	632 505	2536 39641
[(dppf)Pd(dptc)]	**[5.13]**	635 500	4789 24738
[(dppf)Pt(Hdptc)]Ph_4B	**[5.14]**	721 537 436	2454 27055 10513
[(dppf)Pt(dptc)]	**[5.15]**	724 518	4214 13246
[(PPh_3)Pt(dptc)]	**[5.16]**	506 323	26986 8371
[($P(Me_2Ph))_2$Pt(dptc)]	**[5.17]**	503 325	36759 11463
[($P(Et_3))_2$Pt(Hdptc)]Ph_4B	**[5.18]**	544 445	22100 13446

The hypsochromic shift could be attributed to the slightly higher HOMO which is to be expected for the cationic complexes, resulting in a lower energy of absorption for the primary complexes.

The absorption due to ferrocene is shown to be at a longer wavelength when the metal is Pt compared to Pd. The dppf based absorptions occur at 721, 724 nm and at 632, 635 nm for the Pt and Pd complexes, respectively. The absorptions are not significantly different from that of the [(dffp)MCl_2] precursors. There appears to be no significant difference in the absorption wavelength of the metal-based transition between Pd and Pt complexes for a given ligand. However, it would appear as if the ligand-based transition is more sensitive towards the particular metal centre, with Pd complexes exhibiting absorption between 50 and 60 nm towards shorter wavelength.

5.6 Crystal and molecular structure of complex [5.15]

Red crystals of **[5.15]** suitable for X-ray crystallographic analysis were grown from a solution of dichloromethane/methanol. The molecule was shown to crystallize in the $P2_1/c$ space group, with eight molecules per unit cell. The unit cell was shown to contain two crystallographic independent molecules. Least squares refinement gave a final *R* value of 3.69%.

An ORTEP representation of the molecular structure is shown in **Figure 5.4**, while the molecular packing diagram is given in **Figure 5.5**. Selected bond lengths and angles, of one of the two crystallographic independent molecules, are given in **Table 5.6**. Crystal data and refinement parameters are shown in **Table 5.7**.

The molecule shows the expected coordination of the dppf and the dithizone moieties as bidentate ligands to the Pt metal centre, resulting in a distorted square-planar geometry around the central metal ion. The P(2A)-Pt-P(2B) and N(1A)-Pt-S(1A) 'bite' angles are 96.21(5) and 82.47(12)°, respectively. The P(1A)-Pt-S(1A) and P(2A)-Pt-N(1A) angles of 164.22(5) and 165.27(13)°, respectively, deviate slightly from the expected linear geometry expected in square planar geometry. The Pt-P bond lengths of 2.298(1) Å [Pt-P(1A)] and 2.296(1) Å [Pt-P(2A)] appear similar and are characteristic of Pt-P bond lengths, while the Pt-N(1A) and Pt-S(1A) bond lengths differ at 2.053(4) Å and 2.310(1) Å, respectively. The longer bond length for the latter is expected due to larger S atom.

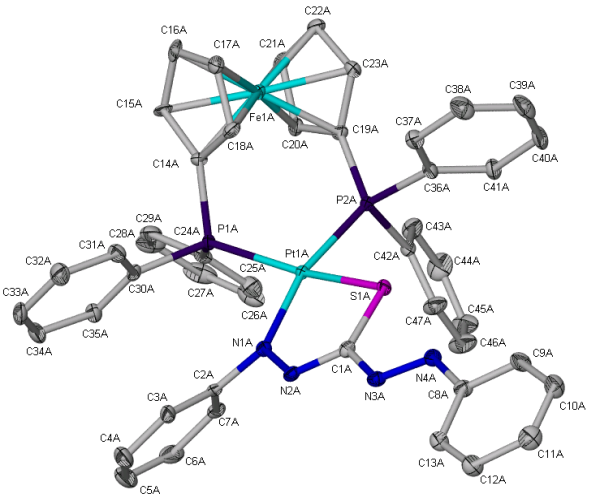

Figure 5.4 Perspective view of the molecular structure of **[5.15]** with atomic nomenclature. Thermal ellipsoids are drawn at the 40% probability level.

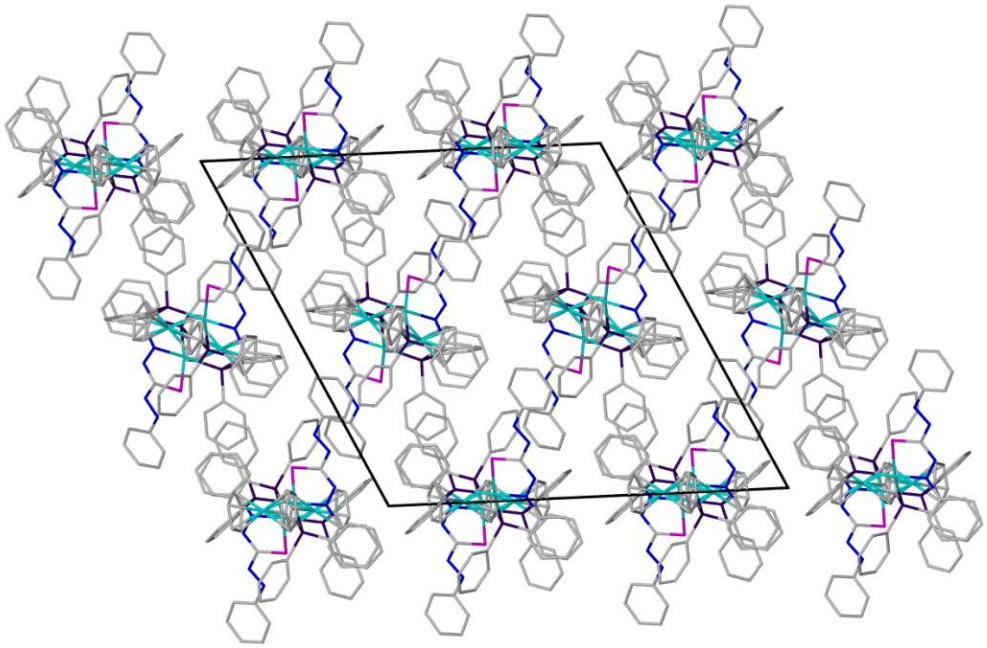

Figure 5.5 Molecular packing diagram of **[5.15]** viewed along [010].

The bond lengths within the five-membered chelate confirms the bonding of dithizonate in its secondary form, with bond angles of 1.346(6) and 1.316(6)° for the N(1A)-N(2A) and N(2A)-C(1A) bonds, respectively, the former showing single bond character, while the

latter show double bond character. The C(1A)-N(3A) [1.388(7) Å] and N(3A)-N(4A) [1.283(6) Å] bonds show the expected double and single bond character of secondary dithizonates.

Table 5.6: Comparison of bond lengths (Å) and bond angles (°) for **[5.15]**

Bong lengths			
Pt(1A)-N(1A)	2.053(4)	Pt(1A)-P(1A)	2.2963(14)
Pt(1A)-P(2A)	2.2979(14)	Pt(1A)-S(1A)	2.3100(13)
S(1A)-C(1A)	1.758(5)	P(1A)-C(14A)	1.807(6)
P(1A)-C(24A)	1.818(6)	P(1A)-C(30A)	1.835(5)
P(2A)-C(19A)	1.820(5)	P(2A)-C(36A)	1.820(6)
P(2A)-C(42A)	1.842(6)	N(1A)-N(2A)	1.346(6)
N(1A)-C(2A)	1.440(6)	N(2A)-C(1A)	1.316(6)
N(3A)-N(4A)	1.283(6)	N(3A)-C(1A)	1.388(7)
N(4A)-C(8A)	1.426(7)	C(2A)-C(7A)	1.385(8)
Bond angles			
N(1A)-Pt(1A)-P(1A)	95.76(12)	N(1A)-Pt(1A)-P(2A)	165.27(13)
P(1A)-Pt(1A)-P(2A)	96.21(5)	N(1A)-Pt(1A)-S(1A)	82.47(12)
P(1A)-Pt(1A)-S(1A)	164.22(5)	P(2A)-Pt(1A)-S(1A)	88.29(5)
C(14A)-P(1A)-C(24A)	109.5(3)	C(14A)-P(1A)-C(30A)	100.1(3)
C(24A)-P(1A)-C(30A)	104.8(3)	C(14A)-P(1A)-Pt(1A)	106.45(18)
C(24A)-P(1A)-Pt(1A)	117.01(19)	C(30A)-P(1A)-Pt(1A)	117.47(18)
C(19A)-P(2A)-C(36A)	99.4(3)	C(19A)-P(2A)-C(42A)	104.5(3)
C(36A)-P(2A)-C(42A)	105.0(3)	C(19A)-P(2A)-Pt(1A)	124.83(17)
C(36A)-P(2A)-Pt(1A)	113.77(19)	C(42A)-P(2A)-Pt(1A)	107.42(17)
N(2A)-N(1A)-C(2A)	109.8(4)	N(2A)-N(1A)-Pt(1A)	121.8(3)
C(2A)-N(1A)-Pt(1A)	127.2(3)	C(1A)-N(2A)-N(1A)	115.5(4)
N(4A)-N(3A)-C(1A)	113.1(4)	N(3A)-N(4A)-C(8A)	113.3(4)
N(2A)-C(1A)-N(3A)	113.8(5)	N(2A)-C(1A)-S(1A)	123.7(4)
N(3A)-C(1A)-S(1A)	122.3(4)	C(7A)-C(2A)-C(3A)	119.8(5)

The ferrocene moiety appears to exist in a staggered conformation. The Fe-C(cyclopentadiene) bond lengths appear normal with bond lengths ranging from 2.011(5) to 2.076(5) Å. The C-C bond lengths of the cyclopentadienyl rings also appear normal, ranging from 1.403(8) to 1.451(8) Å.

Table 5.7 Crystal data and structure refinement for **[5.15]**

Empirical formula	$C_{47}H_{38}N_4P_2PtS$
Formula weight	1003.75 amu
Temperature	173(2) K
Wavelength	0.71073 Å
Crystal system, space group	Monoclinic, $P2_1/c$
Unit cell dimensions	a = 22.192(3) Å α = 90°
	b = 18.587(2) Å β = 115.722(3)°
	c = 22.433(3) Å γ = 90°
Volume	8336.3(19) $Å^3$
Z, Calculated density	8, 1.600 Mg/m^3
Absorption coefficient	3.866 mm^{-1}
F(000)	3984
Crystal size	0.35 x 0.07 x 0.03 mm
Theta range for data collection	1.49 to 27.07°
Limiting indices	$-28 \leq h \leq 28$, $-23 \leq k \leq 12$, $-28 \leq l \leq 28$
Reflections collected / unique	112673 / 18296 [R(int) = 0.0756]
Completeness to theta = 25.35	99.7 %
Max. and min. transmission	0.8928 and 0.3448
Absorption correction	Semi-empirical from equivalents
Refinement method	Full-matrix least-squares on F^2
Data / restraints / parameters	18296 / 0 / 1009
Goodness-of-fit on F^2	1.134
Final R indices [I>2sigma(I)]	R_1 = 0.0369, wR_2 = 0.0638
R indices (all data)	R_2 = 0.0749, wR_2 = 0.0767

The 5-membered chelate appears to be reasonably planar with dihedral angles ranging from 0.1(7) to 5.89(4)°. However, it appears as if the coordination of the dppf moiety causes a deviation from planarity around the central metal ion, resulting in dihedral angles ranging from 57.4(7) to 80.4(3)°.

5.7 Electrochemistry of complexes

The electrochemistry of the ferrocenyl derivatives was investigated by cyclic voltammetry in dichloromethane. The redox potentials are supplied in **Table 5.8**. The redox behaviour

of the bis(diphenylphosphino)ferrocene-metal dithizonates **[5.12]-[5.15]** closely resembles that of [PhHg(Hdptc)].[16] The voltammograms are characterized by three irreversible reduction processes and four oxidation processes (**Figure 5.6**). One of the oxidation processes is reversible and attributed to the ferrocenyl moiety. All other redox processes are attributed to the dithizone ligand. Based on the redox behaviour of [PhHg(Hdptc)], the most anodic wave E_{pa}^{1} is due to the ligand-centred oxidation of the complex. Wave E_{pc}^{1} represents the reduction of the former species back to the neutral complex. E_{pc}^{2} and E_{pc}^{3} correspond to the successive ligand-based reductions. E_{pa}^{3} and E_{pc}^{2} represent the two sequential ligand-based re-oxidations back to the neutral complex.

The oxidation peak appearing in the range +0.326 to +0.460 V can be attributed to the reversible oxidation of the Fe metal centre ($Fc^{0/+}$) of the dppf ligand.

Table 5.8 Electrochemical data for ferrocenyl palladium and platinum dithizonate complexes

Complex		Redox potentials, V						
		Hdptc ligand			Fc	Hdptc ligand		
		E_{pa}^{1}	E_{pa}^{2}	E_{pa}^{3}	$E_{1/2}$	E_{pc}^{1}	E_{pc}^{2}	E_{pc}^{3}
[FcPd(Hdptc)]Ph_4B	**[5.12]**	+ 0.584	-0.010	-1.205	+ 0.326	-0.615	- 1.030	-1.736[a]
[FcPd(dptc)]	**[5.13]**	+ 0.643	-0.034	-1.215	+ 0.413	-0.465	- 1.035	-1.576
[FcPt(Hdptc)]Ph_4B	**[5.14]**	+ 0.459	+ 0.052	-1.343	+ 0.219	a	- 1.032	- 1.525
[FcPt(dptc)]	**[5.15]**	+ 0.739	+ 0.010	-1.281	+ 0.460	-0.630	- 1.040	- 1.460

[a]not visible

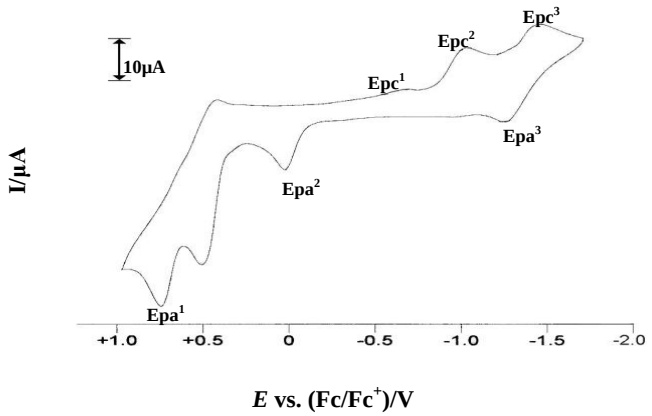

Figure 5.6 Cyclic voltammogram of **[5.14]**.

REFERENCES

1 L. S. Meriwether, E. C. Brietner and N. B. Colthup, *J. Am. Chem. Soc.*, 1965, **87**, 4448.

2 N. Sertova, I. Petkov and J. M. Nunzi, *J. Photochem. Photobio. A Chem.*, 2000, **134**, 163.

3 A. T. Hutton, *Ph.D. Thesis*, University of Cape Town, 1980.

4 A. T. Hutton, *Polyhedron*, 1987, **6**, 13.

5 N. L. Cromhout and A. T. Hutton, *Appl. Organomet. Chem.*, 2000, **14**, 66.

6 N. L. Cromhout and A. T. Hutton, *J. Coord. Chem*., 2000, **52**, 169.

7 Y. Singh, R. Sharan and R. N. Kapoor, *Transition Met. Chem.*, 1986, **11**, 321.

8 Y. Singh, M. P. Singh and R. Swarup, *Synthetic Met.*, 1993, **56**, 1878.

9 S. Liu and J. Zubieta, *Polyhedron*, 1989, **8**, 677.

10 K. Ortner and U. Abram, *Polyhedron*, 1999, **18**, 749.

11 N. D. Jones, G. Lin, R. A. Gossage, R. McDonald and R. G. Cavell, *Organometallics*, 2003, **22**, 2832.

12 Y. Suzaki, T. Yagyu, Y. Yamamura, A. Mori and K. Osakada, *Organometallics*, 2002, **21**, 5254.

13 J. A. Weinstein, M. T. Tierney, E. S. Davies, K. Base, A. A. Robeiro and M. W. Grinstaff, *Inorg. Chem.*, 2006, **45**, 4544.

14 K. Ortner and U. Abram, *Polyhedron*, 1999, **18**, 749.

15 S. Liu and J. Zubieta, *Polyhedron*, 1989, **8**, 677.

16 K. G. von Eschwege, L. van As and J. C. Swarts, *Electrochim. Acta*, 2011, in press.

CHAPTER 6

Structural, spectroscopic and electrochemical studies of mixed dithiolene-dithizone complexes of Hg and Pt

6.1. Introduction

Dithiolene ligands have predominantly been investigated in complexes exhibiting one type of physical behaviour, either as conducting, superconducting, magnetic or as NLO material. A few authors have explored the possibility of using dithiolenes as precursors in the preparation of complexes exhibiting a co-existence of the above properties. The combination of conducting and magnetic properties is, for example, exhibited by the α-(perylene)$_2$[M(mnt)$_2$] (M = Ni, Pt or Pd) complexes. The perylene cation chains provide the metallic property, while the segregated [M(mnt)$_2$]$^{2-}$ chains provide the magnetic property.[1]

Malfant *et al.*[2,3] combined the conducting properties of [Ni(dmit)$_2$]$^{2-}$ anions with the NLO properties of systems such as DAMS$^+$ (4-[2-(4,4-dimethylaminophenyl)ethenyl]-1-methylpyridium) and DAMP$^+$ (4-dimethylamino-1-methylpyridium). The (DAMP)[Ni(dmit)$_2$] structure has been shown to consist of layers of [Ni(dmit)$_2$]$^-$ anions separated by layers of DAMP$^+$ cations with short *S*···*S* contacts within a layer. While conductivity was observed for these complexes, the NLO property was absent due to the structure being centrosymmetric, non-centrosymmetry, being a prerequisite for NLO behaviour.

Photochromic complexes, widely studied for their application as photo-optical switches, optical memory devices and sensors,[4,5,6] have also received attention in the preparation of multifunctional materials. The photochromic complex, [Fe(CN)$_5$NO]$^{2-}$, for example, was combined with highly electro-active conducting tetrathiofulvalene (TTF) salts as a way of producing molecular conductors with optical properties.[7] Research activities in our

laboratory are focusing on the preparation of ferrocene substituted dithizonates as a potential sensor towards heavy metals.[8] Other attempts focused on combining the photochromic properties of dithizone with mesogenic long-chain mercury complexes to produce molecules with both photochromic and liquid crystalline properties.[9]

In this chapter we will investigate the preparation of mixed dithiolene-dithizone complexes, thereby combining the known electro-active dithiolene moiety with the photochromic dithizone moiety as shown in **Figure 6.1**.

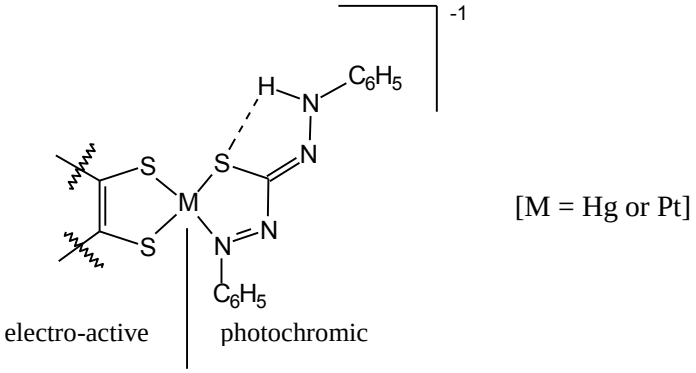

Figure 6.1 Generic example of a mixed dithiolene-dithizone- complex, showing the electro-active and photochromic moieties.

6.2 Mixed dithiolene-dithizone complexes of mercury

The hybrid dithiolene-dithizonate complexes were prepared according to **Scheme 6.1** outlined below. The chloromercury(II)dithizonate **[6.1]** was prepared from the reaction of mercury(II)chloride and dithizone in ether to yield an orange-red precipitate. This differs from the route followed by Webb.[10] All dithiolene salts, except for the maleonitrile derivative, were prepared in situ from the ethoxide cleavage of the relevant dithiolene in ethanol to yield the corresponding sodium dithiolene salts. **[6.1]** was reacted with an equimolar quantity of the appropriate dithiolene salt in ethanol at room temperature as outlined in **Scheme 6.1**. Any unreacted chloromercurydithizonate was removed by filtration.

Addition of a bulky counter-ion such as $[Bu_4N]^+$ or $[Ph_4As]^+$ to the respective filtrates yielded the desired mixed dithiolene-dithizonate ionic complexes,

Bu_4N[(mnt)Hg(Hdptc)]**[6.2],** Ph_4As[(mnt)Hg(Hdptc)]**[6.3],** Ph_4As[(dmit)Hg(Hdptc)]**[6.4]**, and Ph_4As[(dmid)Hg(Hdptc)]**[6.5].** All mixed dithiolene-dithizonate complexes are dark red in colour.

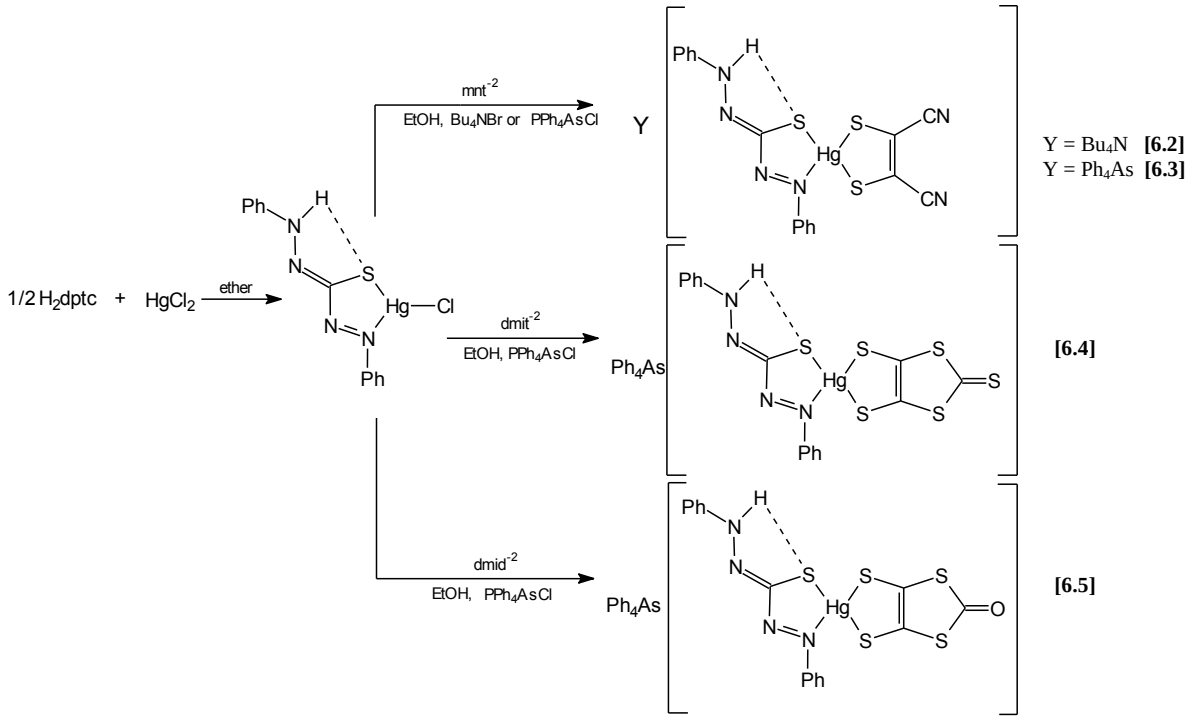

Scheme 6.1 Synthetic route to mixed mercury(II) dithiolene-dithizone complexes.

The derivatives all show the N*H* resonance in the ^{1}H NMR spectra occurring at about 9.4 ppm, with the phenyl resonances between 7.2 and 7.8 ppm. The NMR resonances for the tetraphenyl arsonium counter-ion also occur in the phenyl region as indicated above. For **[6.2]**, the tetrabutylammonium counter-ion is present as the characteristic set of multiplets between 0.9 and 3.1 ppm.

6.3 Spectroscopic studies

6.3.1 Infrared spectroscopy

The infrared spectra of all complexes were recorded as KBr pellets and are reflected in **Table 6.1**. All complexes displayed peaks for the characteristic absorptions in the

following regions: 3199-3223 cm^{-1} (N-H stretching), 1516-1530 cm^{-1} (N-H bending), 1305-1368 cm^{-1} (N-Ph modes) and 1478-1496 cm^{-1} (C-S stretching).

While ν(CS)(thio-amidic) and ν(N-Ph) occur as single vibrations in free dithizone at 1490 and 1312 cm^{-1}, respectively, they are split into two bands in the metal-dithizonate complexes. The two bands assigned to the N-Ph vibrations are attributed to the two non-equivalent N-Ph moieties, the higher frequency vibration being due to ν[N(H)-Ph], while the lower frequency vibration is due to ν[N(Hg)-Ph].[11]

Each of the mixed ligand complexes displayed additional absorptions characteristic of the respective dithiolene moiety. The mnt^{2-}, $dmid^{2-}$ and $dmit^{2-}$ derivatives displayed unique absorptions at 2196, 1661 and 1055 cm^{-1} due to the vibration of the C≡N, C=O and C=S functionalities, respectively.

All complexes, except **[6.2]**, showed the NH stretch at lower wavenumber compared to the unsubstituted chloromercury(II)dithizonate precursor **[6.1]**. It is of interest to note that the NH stretching frequency, *ν*(NH), is shifted 46 cm^{-1} towards lower wavenumber on changing the counter-ion from $[Bu_4N]^+$ to $[Ph_4As]^+$ in the maleonitrile derivative.

Table 6.1 Infrared absorption bands for mixed mercury dithiolene-dithizone complexes

Complex		Infrared absorptions, KBr (cm^{-1})					
		ν(N-H)	δ(N-H)	N-Ph	ν(C-S)	ν(C=C)	Other
H_2dptc		absent	-	1312m	1490m	-	-
ClHg(Hdptc)	**[6.1]**	3232s	1530s	1351s 1310s	1494s 1477m	-	-
Bu_4N[(mnt)Hg(Hdptc)]	**[6.2]**	3245w	1523s	1351s 1309s	1485s 1455s	1429s	2190s C≡N
Ph_4As[(mnt)Hg(Hdptc)]	**[6.3]**	3199s	1516s	1361s 1305m	1495s 1479s	1428s	2196s C≡N
Ph_4As[(dmit)Hg(Hdptc)]	**[6.4]**	3214w	1519m	1368m 1307sh	1496m 1480m	1455m	1679m C=S
Ph_4As[(dmid)Hg(Hdptc)]	**[6.5]**	3221w	1519m	1360m 1308m	1496m 1482m	1447m	1661s C=O

The shift could be attributed to the different counter-ion present in the two complexes. In the crystal structure of **[6.3]** (see **Section 6.4**) we observed the presence of an intermolecular hydrogen bonding interaction of the N-H group with an S atom of a neighbouring molecule. This is in addition to an intramolecular N-H···S hydrogen bond by the same group, which is typical of primary dithizonates. We therefore expect this multiple hydrogen bonding interaction to lower *ν*(NH), as observed. It is also evident from **Table 6.1** that all dithizonate-related bands, except for N-Ph, are towards a lower wavenumber for compounds **[6.2]-[6.5]**.

Hutton has observed a significant shift for ν(N-H) in chloroform for organomercury derivatives of dithizone.[12] We, for example, observed a similar shift on irradiation of a chloroform solution of complex **[6.3].** The irradiated complex displayed an absorption of 53 cm^{-1} to higher wavenumber, compared to an average of 70 cm^{-1} as observed by Hutton. This is a consequence of the weakening of the hydrogen bond in the activated blue form and is consistent with the formation of a N-H···N hydrogen bond, the weakening being due to the lower basicity of the azo nitrogen, compared to the sulfur atom. While there is no crystallographic data of the blue form, recent quantum computational studies support the isomerisation as depicted in **Figure 6.2** below.[13]

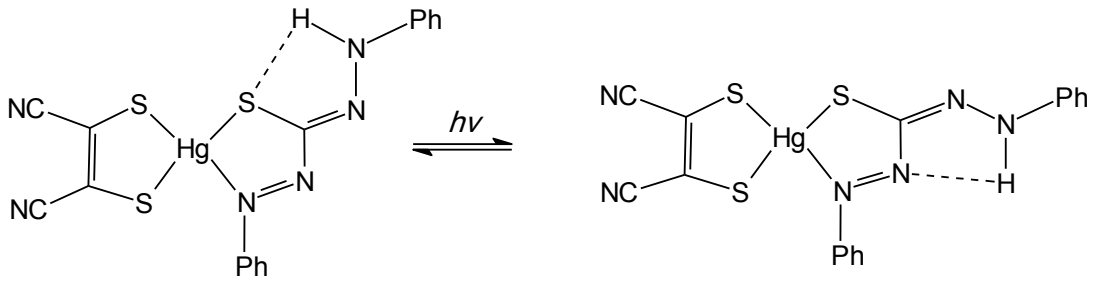

orange blue

Figure 6.2 An example of the isomerisation of dithizonate complexes on irradiation.

6.3.2 Electronic spectroscopy

The electronic spectra of the mixed ligand complexes were obtained in the range 400-700 nm in dichloromethane for the normal (yellow) and activated (blue) forms and are summarized in **Table 6.3**.

Complexes **[6.2]-[6.5]** exhibit similar spectral properties to mercury(II)dithizonate[14] and organomercury(II)dithizonates[12], indicating that the dithizonate ligand is essentially unaffected by the replacement of the second dithizonate or the organo group by a dithiolene ligand '*trans*' to the dithizonate ligand. There appears to be a small bathochromic shift in the visible spectra of the normal yellow mixed complexes when compared to the absorption of the chloromercury(II)dithizonate complex **[6.1]**.

The latter compound shows a maximum absorption at 481 nm, while the dithiolene complexes gave equivalent absorptions at 482, 487 and 488 nm for the mnt, dmit and dmid complexes, respectively. This small bathochromic shift can be attributed to electronic effects being transmitted from the one side of the mercury atom to the other.

Table 6.2 Electronic spectroscopic data for complexes **[6.1]-[6.5]** in dichloromethane

Complex		**Orange**		**Blue**
		Wavelength, λ nm	**Extinction coefficient, ε mol^{-1} dm^3 cm^{-1}**	**Wavelength, λ nm**
(Hdptc)HgCl[a]	**[6.1]**	481		
Bu_4N[(mnt)Hg(Hdptc)]	**[6.2]**	482	23 442	599
Ph_4As[(mnt)Hg(Hdptc)]	**[6.3]**	482	23 391	599
Ph_4As[(dmit)Hg(Hdptc)]	**[6.4]**	487	32 359	608
Ph_4As[(dmid)Hg(Hdptc)]	**[6.5]**	488	33 113	600

[a] molar extinction coefficient not determined due to poor solubility

There appears to be no significant difference in the absorption wavelength between the different dithiolene-substituted dithizonate complexes, with the more substituted dithiolene complexes exhibiting a small bathochromic shift of between 5 and 6 nm. The molar extinction coefficients appear to be slightly higher for the more conjugated dithiolene complexes, dmit and dmid, compared to the maleonitrile derivatives. The latter complex has an average value of 23 417 $mol^{-1}.dm^3.cm^{-1}$, compared to 32 359 and 33 113 mol^{-1} dm^3 cm^{-1} for the former complexes, respectively.

The data in **Table 6.2** also show that there is no variation in either the absorption wavelength or the molar extinction coefficient on changing the counter-ion, as exemplified by the maleonitrile derivatives.

On irradiation of solutions of the mixed complexes, the colour changes to blue indicating the formation of the isomerised form. The absorption maxima for the blue forms range from 599 to 608 nm for the mixed complexes. The photochromic behaviour exhibited is similar to that of organomercury(II) complexes of dithizone.[15] The presence of a single isosbestic point between the absorption maxima of the normal (yellow) and photo-activated (blue) forms indicates the absence of reaction intermediates or side reactions (**Figure 6.3**). The extinction coefficients for the blue forms could not be determined because of the difficulty of maintaining a steady-state concentration of 100% of the activated blue form.

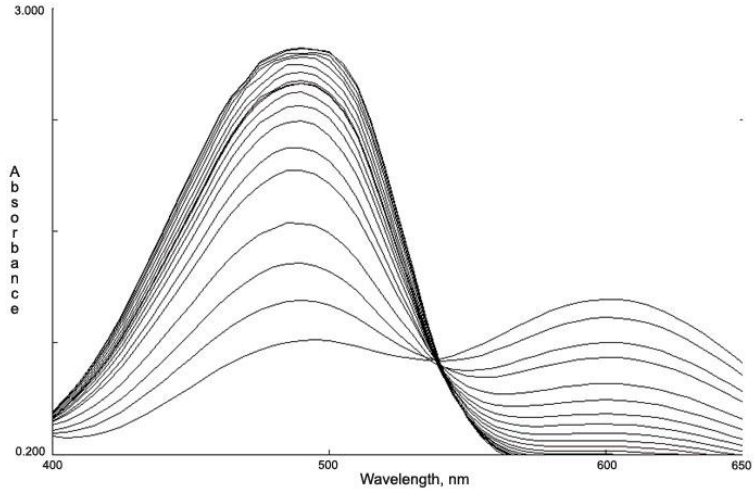

Figure 6.3 Electronic absorption spectrum of **[6.3]**, showing the equilibrium between the yellow and blue forms.

6.4 Crystal and molecular structure of [6.4]

Crystals of **[6.4]** suitable for crystallographic studies were obtained from dichloromethane/methanol. An ORTEP representation of the molecular structure is shown in **Figure 6.4**, with a packing diagram displayed in **Figure 6.5**. Selected bond lengths, bond angles and torsion angles are given in **Table 6.3**. Crystal data and refinement parameters are displayed in **Table 6.4**. A molecular packing diagram showing the inter- and intra-molecular interactions is shown in **Figure 6.6**.

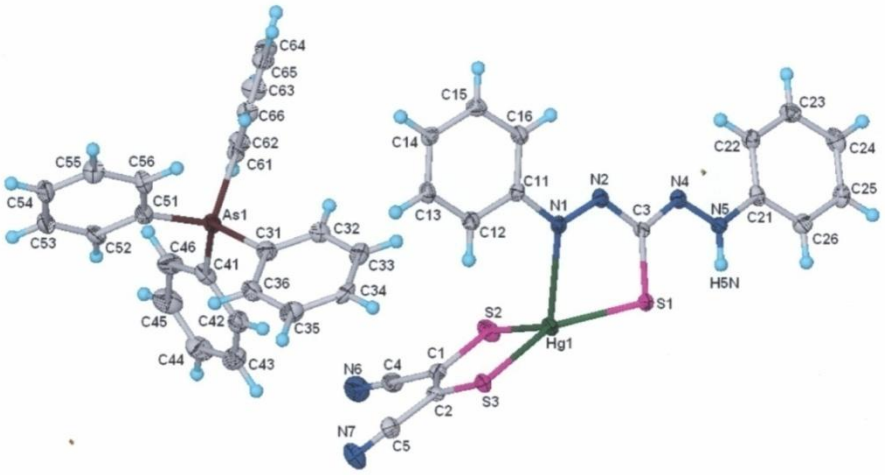

Figure 6.4 Perspective view of the molecular structure of **[6.4]** with atomic nomenclature. Thermal ellipsoids are drawn at the 50% probability level.

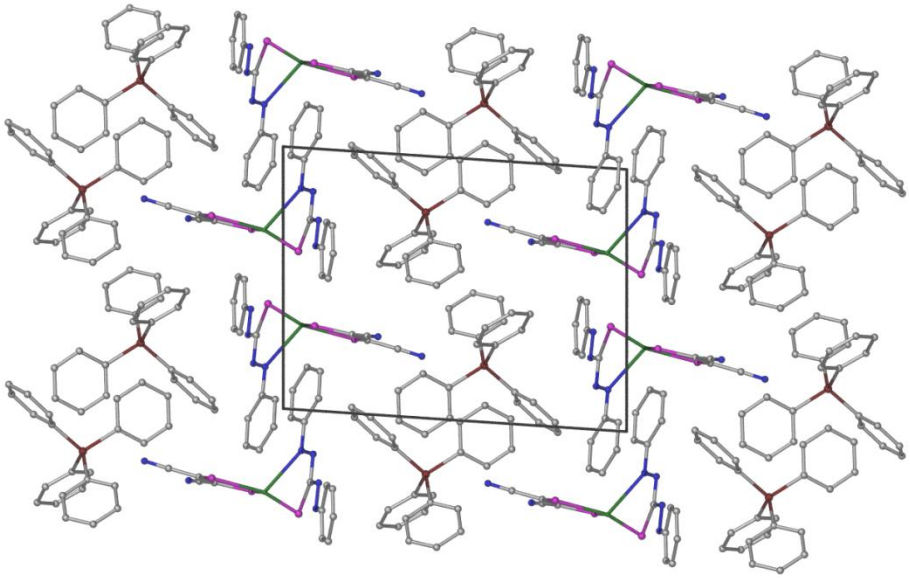

Figure 6.5 Molecular packing diagram of structure of **[6.4]** viewed along [010].

Table 6.3 Selected bond lengths (Å), bond and torsion angles (°) for **[6.4]**

Bond lengths			
Hg1(1) – S(1)	2.402(1)	S(1) – C(3)	1.751(3)
Hg(1) – S(3)	2.446(1)	S(2) – C(1)	1.737(4)
Hg(1) – S(2)	2.528(1)	S(3) – C(2)	1.748(4)
Hg(1) – N(1)	2.636(3)	N(1) – N(2)	1.272(5)
N(6) – C(4)	1.145(6)	N(2) – C(3)	1.396(5)
N(7) – C(5)	1.153(6)	N(4) – C(3)	1.309(5)
C(1) – C(2)	1.363(6)	N(4) – N(5)	1.339(5)
C(1) – C(4)	1.443(6)	N(5) – C(21)	1.405(5)
C(2) – C(5)	1.428(6)	N(5) – H(5N)	0.95(5)
Bond angles			
S(1) – Hg(1) – S(3)	141.94(4)	N(5) – N(4) – C(3)	116.6(3)
S(1) – Hg(1) – S(2)	125.21(4)	N(4) – N(5) – C(21)	120.2(4)
S(3) – Hg(1) – S(2)	88.89(4)	N(4) – N(5) – H(5N)	121(3)
S(3) – Hg(1) – N(1)	113.64(8)	C(21) – N(5) – H(5N)	119(3)
S(2) – Hg(1) – N(1)	111.49(8)	N(4) – C(3) – N(2)	111.7(3)
C(3) – S(1) – Hg(1)	101.0(1)	N(4) – C(3) – S(1)	123.2(3)
C(1) – S(2) – Hg(1)	97.1(2)	N(2) – C(3) – S(1)	125.1(3)
C(2) – S(3) – Hg(1)	98.99(14)	N(6) – C(4) – C(1)	177.7(5)
N(2) – N(1) – C(11)	115.2(3)	N(7) – C(5) – C(2)	177.0(5)
N(1) – N(2) – C(3)	115.7(3)		
Torsion angles			
S(1) – Hg(1) – S(2) – C(1)	160.8(2)	C(3) – N(4) – N(5) – C(21)	174.4(4)
S(1) – Hg(1) – S(3) – C(2)	-153.8(2)	N(5) – N(4) – C(3) – N(2)	-177.8(3)
S(3) – Hg(1) – S(2) – C(1)	-1.0(2)	N(5) – N(4) – C(3) – S(1)	3.6(5)
S(2) – Hg(1) – S(3) – C(2)	1.9(1)	N(1) – N(2) – C(3) – N(4)	-169.5(3)
S(2) – C(1) – C(4) – N(6)	-29(14)	N(1) – N(2) – C(3) – S(1)	-12.0(5)
S(3) – C(2) – C(5) – N(7)	-8(10)	N(2) – N(1) – C(11) – C(12)	179.5(4)
C(2) – C(1) – C(4) – N(6)	150(14)	N(2) – N(1) – C(11) – C(16)	-0.7(6)
C(1) – C(2) – C(5) – N(7)	173(10)	N(4) – N(5) – C(21) – C(26)	172.1(4)
C(11) – N(1) – N(2) – C(3)	-179.7(3)	N(4) – N(5) – C(21) – C(22)	-7.8(6)

Complex **[6.4]** crystallizes in the triclinic space group $P\bar{1}$. The molecule has both the dithizone and maleonitrile residues acting as bidentate ligands coordinating through N-S and S-S atoms, respectively, resulting in mercury assuming a four-coordinate geometry,

which can at best be described as distorted tetrahedral. While mercury has been shown to adopt other four coordinate geometries, such as square-planar[16] and see-saw,[17] four-coordinate distorted tetrahedral geometry for mercury is by far the most common.

The bond angles around mercury range from 72.39(7) to 141.94(4)°. The S(2)-Hg-S(3) and N(1)-Hg-S(1) bond angles being 88.89(4) and 72.39(7)°, respectively, deviating significantly from ideal tetrahedral bond angles and being imposed by the restricted 'bite' angle of the two chelate rings. The two chelate rings are reasonably planar with torsion angles of between -1.0(2)-1.9(1)° and -1.0(2)-1.9(1)° for the mnt^{2-} and Hdptc chelate rings, respectively.

The Hg-S bond length of 2.402(1) Å for the dithizone residue is in agreement with Hg-S distances in truly two-coordinate mercury compounds which lie in the range 2.32-2.42 Å.[11] This bond distance is however longer than corresponding length of 2.33(1), 2.372(7) and 2.389(4) Å found in $[Hg(Hdptc)_2]$[18], [PhHg(Hdptc)][12] and [MeHg(Hdptc)][12], respectively. The Hg-S bond distances of 2.446(1) and 2.528(1) Å for the maleonitrile residue are in agreement with distances in reported mercury-dithiolene compounds.[19] The S(2)-Hg-S(3) bond angle of 88.89(4)° is in agreement with that found in mercury-dithiolene complexes.[18,20] The Hg-N distance of 2.636(3) Å is 0.514 Å shorter than the sum of the van der Waals radii[21] and thus constitutes a weak bond. Bond lengths of 2.1 Å are usually found in compounds containing covalent Hg-N bonds.[22] It compares well with Hg-N distances in mercury(II) compounds with similar coordination numbers for mercury.[17]

The S(2)-C(1) [1.737(4) Å] and S(3)-C(3) [1.748(4) Å] bond lengths of the dithiolene moiety are in the range found in other metal-maleonitrile complexes.[23,24,25]
The C=C [1.363(6) Å] and C≡N [1.145(6) and 1.153(6) Å] bond lengths are consistent with formal double and triple bonds [i.e. 1.32 Å for C(sp^2)-C(sp^2) bonds and 1.14 Å for N(*sp*)-C(*sp*) bonds, respectively[26]] and agree well with other structures containing the maleonitrile ligand.[23-25] The C(1)-C(4) and C(2)-C(5) bond lengths of 1.443(6) and 1.428(6) Å respectively, are shorter than localised C(sp^3)-C(sp^3) single bonds, indicating some form of delocalisation of the maleonitrile ligand. Delocalisation within the

maleonitrile chelate ring is a well known phenomenon[22] and is ascribed to the presence of both the α,β-dithiolate or α,β-dithione resonance forms, of which the former is more dominant as evidenced by the crystallographic data.

The tetraphenylarsonium counter-ion has arsenic in a tetrahedral environment. As-C bond distances range from 1.906(5)-1.917(4) Å. The bond angles around As are in the range 108.1(2)-111.3(2)°. All bond lengths and bond angles appear normal.

Table 6.4 Crystal data and structure refinement for **[6.4]**

Empirical formula	$C_{41}H_{32}AsN_6S_3Hg$
Formula weight	979.41 amu
Temperature	133(2) K
Wavelength	0.71073 Å
Crystal system, space group	Triclinic, $P\bar{1}$
Unit cell dimensions	a = 10.2474(1) Å, α = 92.662(1)°
	b = 12.1700(2) Å, β = 94.662(1)°
	c = 15.7023(2) Å, γ = 102.584(1)°
Volume	1900.66(4) $Å^3$
Z, Calculated density	2, 1.711 Mg/m^3
Absorption coefficient	5.117 mm^{-1}
F(000)	960
Crystal size	0.08 x 0.06 x 0.05 mm
Theta range for data collection	3.46 to 25.35°
Limiting indices	$-12 \le h \le 12$, $-14 \le k \le 14$, $-18 \le l \le 18$
Reflections collected / unique	67941 / 6925 [R(int) = 0.0807]
Completeness to theta = 25.35	99.6 %
Max. and min. transmission	0.7840 and 0.6850
Refinement method	Full-matrix least-squares on F^2
Data / restraints / parameters	6925 / 0 / 474
Goodness-of-fit on F^2	1.044
Final R indices [I>2sigma(I)]	R_1 = 0.0301, wR_2 = 0.0690
R indices (all data)	R_1 = 0.0446, wR_2 = 0.0690

Two hydrogen bonding interactions were found for **[6.4]**. The intramolecular N(5)-H(5N)···S(1) and the intermolecular N(5)-H(5N)···S(3) hydrogen bonding interactions, symmetry operation: 1-*x*+2, -*y*+1, -*z*, as shown in **Table 6.5**, are depicted in **Figure 6.6**. It

is evident from the diagram that the discrete molecules are located around a centre of symmetry.

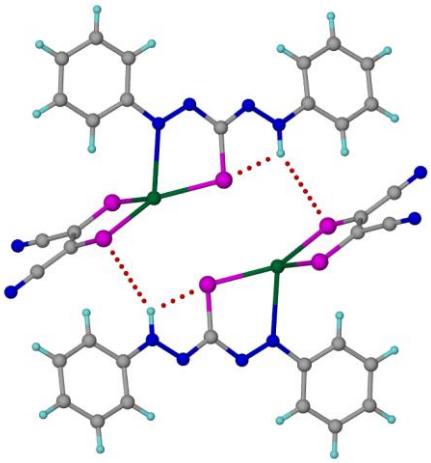

Figure 6.6 Diagram depicting both intra- and inter-molecular hydrogen bonding in **[6.4]**.

While both the dithiolene and dithizone ligands are reasonably planar, we can attribute the absence of π-π or S···S interactions, and therefore the absence of stacking, to a combination of the distorted tetrahedral environment around the mercury metal centre and the presence of the bulky tetraphenylarsonium counter-ion.

Table 6.5 Hydrogen bonds for **[6.4]**

Hydrogen bond	N – H (Å)	H···S (Å)	N···S (Å)	NHS (°)
N(5) – H(5N) ··· S(1)	0.95(5)	2.42(5)	2.882(4)	110(3)
N(5) – H(5N) ··· S(3)[a]	0.95(5)	2.92(5)	3.769(4)	150(3)

[a] *molecule at: –x + 2, -y + 1, z*

6.5 ELECTROCHEMISTRY

The redox behaviour of the dithiolene-dithizonate complexes **[6.2]**–**[6.5]** was investigated by cyclic voltammetry in dichloromethane using a platinum disk working electrode. The oxidation and reduction potentials are summarized in **Table 6.6**. The cyclic voltammograms show two irreversible reduction processes for all complexes ranging from -628 to -1360 mV. Three irreversible oxidation processes are also observed for all

complexes, except the maleonitrile derivatives, where only two irreversible oxidation processes are observed. Cyclic voltammetric analysis of phenylmercurydithizonate and chloromercurydithizonate **[6.1]** reveals that the irreversible reduction processes and the oxidation processes centred around +800 mV and the one at approximately +100 mV could be ascribed to the dithizonate moiety. These observations have been confirmed by a recent electrochemical study of dithizonatophenylmercury(II), where the two irreversible cathodic and two irreversible anodic processes have been ascribed to the ligand. [27]

This would attribute the remaining oxidation processes for **[6.4]** and **[6.5]** at +1225 and +1460 mV, respectively, to be centred on the dithiolene moiety. The presence of only one oxidation process in **[6.2]** and **[6.3]** could be attributed to two independent oxidation processes with equal potential, one dithizone centred with the second being ascribed to the dithiolene moiety.

The absence of rich redox behaviour commonly associated with dithiolenes, has been observed for other mercury-dithiolene complexes. Wen[19], Guo[28] and Narvor[29], for example, observed a single oxidation for mercury complexes containing an extended tetrathiafulvalene ligand. Baundron also observed irreversible behaviour for a mercury dithiolene complex, while the analogous Ni complex displayed reversible behaviour.[30]

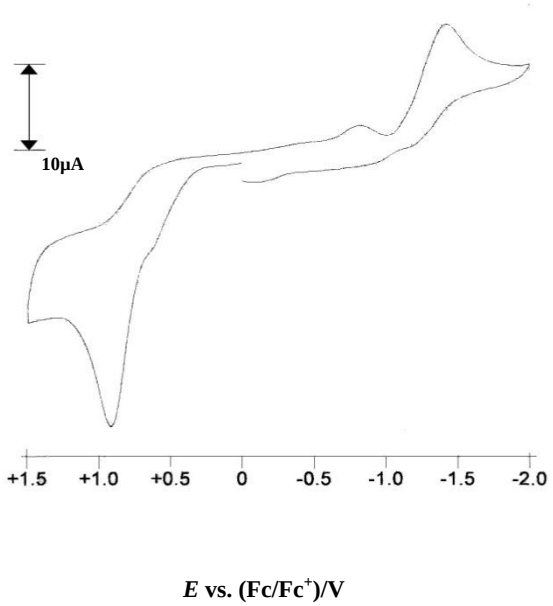

Figure 6.7 Cyclic voltammogram of **[6.5]**.

The redox behaviour of the irradiated complexes was also investigated. However, cyclic voltammetric data of the irradiated complexes show no difference in redox potentials from the corresponding non-irradiated complexes. This would imply that the isomerisation of the dithizone moiety on irradiation has no discernable electronic impact on the dithiolene moiety. Recent electrochemical studies on ferrocenylmercurydithizonate, conducted in this laboratory, showed similar results, with no shift in the oxidation potential of ferrocene on irradiation.[8] This is further supported by a recent comparative electrochemical study on the blue photo-excited and the orange ground state of dithizonatophenylmercury(II). Cyclic voltammetry showed that the voltammogram of the blue form is identical to that of the orange form.[27]

Table 6.6 Electrochemical data in mV for complexes **[6.2]-[6.5]** in dichloromethane

Complex		Electrochemical process, mV				
		Oxidation			Reduction	
		E_{pa}^{1}	E_{pa}^{2}	E_{pa}^{3}	E_{pc}^{1}	E_{pc}^{2}
ClHg(Hdptc)	**[6.1]**		+864		-835	-1427
Bu_4N[(mnt)Hg(Hdptc)]	**[6.2]**		+833		-724	-1047
Ph_4As[(mnt)Hg(Hdptc)]	**[6.3]**		+840		-729	-1052
Ph_4As[(dmit)Hg(Hdptc)]	**[6.4]**	+1225	+846	+57	-628	-1325
Ph_4As[(dmid)Hg(Hdptc)]	**[6.5]**	+1460	+852	+145	-731	-1360

6.6 Mixed dithiolene-dithizonate complexes of platinum

We have shown in **Section 6.2** that mixed dithiolene-dithizonate complexes of mercury can be prepared from chloromercury(II)dithizonate and the appropriate dithiolene salt. An X-ray crystallographic study of the maleonitrile derivative revealed that the geometry around the mercury atom is distorted tetrahedral, therefore inhibiting the stacking of molecules in the solid state. Four-coordinate platinum complexes are known for adopting a square-planar geometry, making them amenable to stacking in the solid state, often responsible for conferring novel properties to the resultant molecule.

The synthetic methodology to obtain mixed platinum dithiolene-dithizone complexes could adopt a number of approaches. The envisaged routes are outlined in **Scheme 6.2** below.

6.6.1 Reaction of metal halides with dithizone

In Route 1, the appropriate metal salt is reacted with equimolar quantities of dithizone and maleonitrile in a water/ethanol (1:1) mixture, in the presence of a base.

Route 1

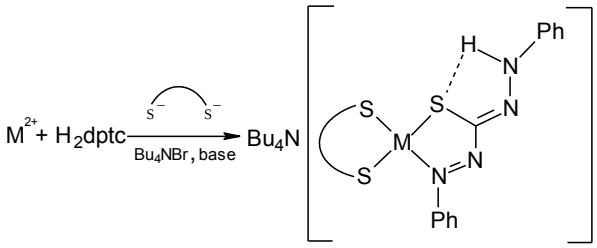

Route 2

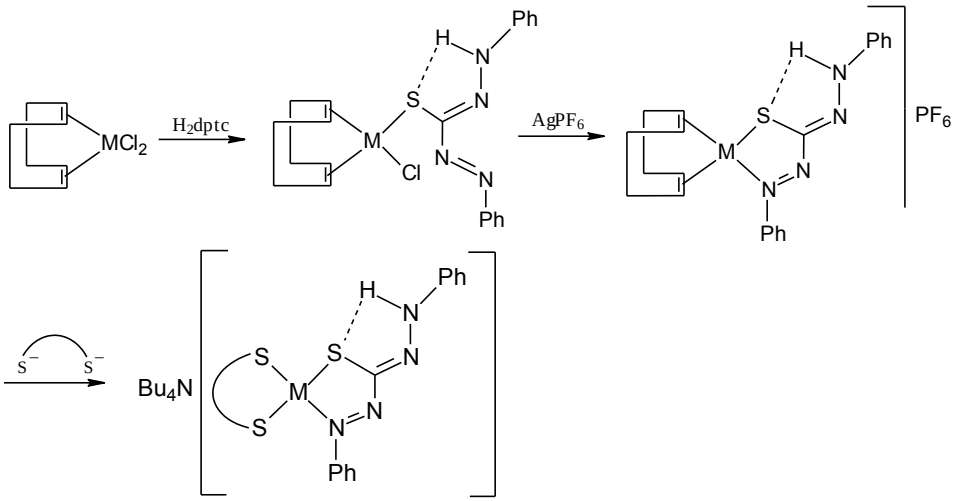

Route 3

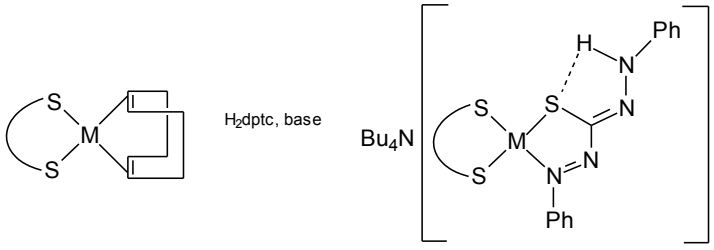

Scheme 6.2 Envisiged approaches for the preparation of mixed dithiolene-dithizone complexes of platinum and palladium.

The disadvantage of this approach is the tendency of both ligands to form disubstituted complexes. This was confirmed, as the reaction with the palladium chloride salt, afforded a black precipitate, which was identified as the disubstituted dithizonate complex, $[Pd(Hdptc)_2]$.[31] The addition of tetrabutylammonium bromide to the filtrate gave a dark-green precipitate of the bis-maleonitrile complex, $(Bu_4N)_2[Pd(mnt)_2]$.[32] Similar results were obtained when K_2PtCl_4 was used, with the formation of the dark red salt $(Bu_4N)_2[Pt(mnt)_2]$.[32]

6.6.2 Reaction of cyclooctadiene platinum salt with dithizone

For Route 2, we anticipated the formation of two possible complexes. The first complex, being the desired cationic primary dithizonate complex, $[Pt(Hdptc)(COD)]PF_6$, or the neutral dithizonate complex, $[PtCl(\eta^1\text{-}Hdptc)(COD)]$, with the dithizone moiety in a monodentate bonding mode. The latter is based on work done by Manzer, in which he has shown that the complex $[PtCH_3Cl(COD)]$, readily displaces the labile chlorine by the addition of silver salts such as $AgPF_6$. The addition of a Lewis base results in a cationic complex, in which the COD ligand showed increased lability and could be displaced by, for example, sulfur nucleophiles.[33] We envisaged that for the anticipated target complex, $[PtCl(\eta^1\text{-}Hdptc)(COD)]$, after removal of the chlorine, the nitrogen of dithizone would serve as the Lewis base which would result in dithizone adopting the preferred bidentate coordination mode, giving the cationic complex, $[Pt(Hdptc)(COD)]PF_6$. Subsequent treatment of the cationic complex with a 1,2-dithiolene salt will result in the displacement of COD and the formation of the target complex. However, as discussed in **Chapter 5**, reaction of the cyclooctadienylplatinum(II)chloride with dithizone resulted in the formation of the unexpected secondary platinum dithizonate derivative.

6.6.3 Reaction of (dithiolene)Pt(COD) with dithizonate salt

Route 3 involved the reaction of the dithizonate salt **[4.1]** with the appropriate platinum-dithiolene derivative, (dithiolene)Pt(COD) (see **Scheme 6.3**).

The [(mnt)Pt(COD)] **[6.6]** complex was prepared from the reaction of [(COD)$PtCl_2$] with the mnt^{2-} salt in EtOH. Refluxing **[6.6]** with the tetrabutylammonium dithizonate salt **[4.1]** in ethanol afforded green crystalline material which was identified as the desired product, Bu_4N[(mnt)Pt(Hdptc)]**[6.7]**.

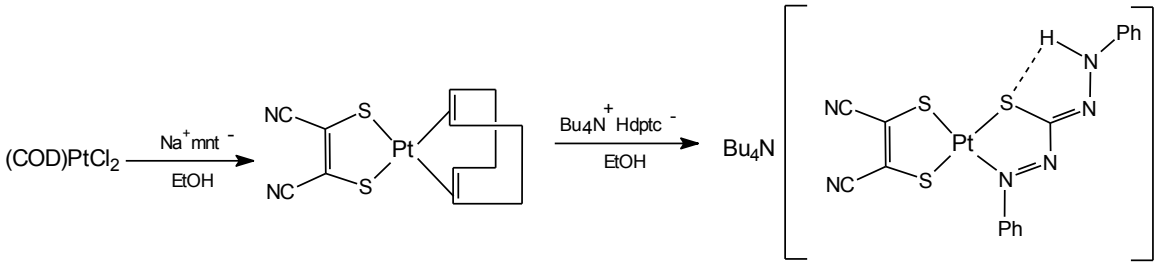

Scheme 6.3 Preparative route to mixed platinum dithiolene-dithizone complex **[6.7]**.

The infrared spectrum of **[6.7]** shows a NH absorption at 3201 cm^{-1}, which is typical for primary dithizonates. The maleonitrile CN stretch at 2199 cm^{-1} for **[6.7]** is 12 cm^{-1} lower than *ν*(CN) in the maleonitrile precursor **[6.6]**.

The ^{1}H NMR spectrum of **[6.7]** shows the expected resonance for the N*H* group at 8.9 ppm. The tetrabutylammonium signals are observed as multiplets between 0.96 and 3.1 ppm.

The electronic absorption spectrum of **[6.7]** in dichloromethane reveals two absorptions in the 400-800 nm range, i.e., at 699 and 456 nm, with corresponding molar extinction coefficients of 12800 and 22164.

The two absorptions in the ultraviolet spectra of the mixed dithiolene-dithizone platinum complex are in agreement with those previously observed for the platinum phosphine-dithizonate complexes reported in **Chapter 5**. The shorter wavelength band is attributed to a ligand-centred transition, while the absorption at the longer wavelength is either a metal-to-ligand (MLCT) or a ligand-to-metal (LMCT) charge transfer transition. This, however, differs from the mercury dithiolene-dithizone complexes, where only one absorption is observed in the 300-800 nm region.

Unlike the mixed mercury complexes, no photochromic behaviour was observed on irradiation of a solution of the mixed dithiolene-dithizone platinum complex.

6.7 Crystal and molecular structure of [6.7]

Crystals suitable for X-ray crystallography were grown from chloroform/ethanol. The molecule crystallized in the orthorhombic space group $P2_12_12_1$. The molecule showing the numbering system is given in **Figure 6.8**, with a packing diagram being shown in **Figure 6.9**., with Representative bond lengths and bond angles shown in **Table 6.7,** while crystal data and refinement parameters are given in **Table 6.8**

The molecule shows the bidentate dithizone and maleonitrile ligands coordinating to the platinum metal centre through *N,S* and *S,S* atoms, respectively, resulting in the expected square-planar geometry around the metal centre. The bite-angles around the central metal ion are 82.85(5) and 90.04(2)° for the former and latter ligands, respectively. The two chelate rings are shown to be reasonably planar with torsion angles for the dithizonate residue ranging between 0.3(2) to -0.7(2) and -3.8(2) to 4.6(2) for the dithiolene residue.

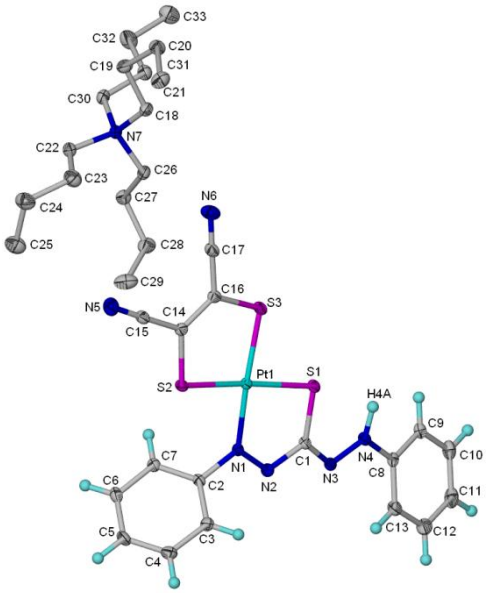

Figure 6.8 Perspective view of the molecular structure of **[6.7]** with atomic nomenclature. Thermal ellipsoids are drawn at the 40% probability level.

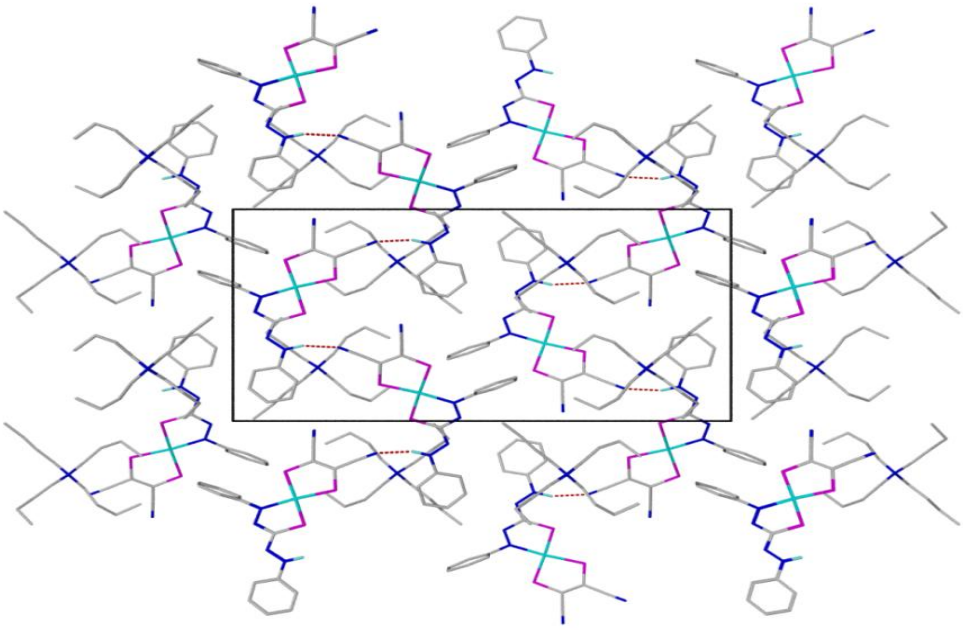

Figure 6.9 Molecular packing diagram of structure of **[6.7]** viewed along [ ]**.**

The Pt-S bond length of the dithizone residue of 2.3067(5) Å is in agreement with the Pt-S distances reported for the platinum dithizonate complexes reported in **Chapter 5**. The Pt-N bond length of 2.024(2) Å appears short, falling between the bond distances of 1.998(4) and 2.053(4) Å, reported for the two secondary platinum dithizonate complexes discussed in **Chapter 5**. The Pt-S bond lengths of the dithiolene residue of 2.2841(5) and 2.2605(5) Å agree with bond distances reported for platinum dithiolene complexes.
The N(1)-N(2) bond length of 1.286(2) Å, being shorter than the N(3)-N(4) bond of 1.331(2) Å is as expected for the primary bonding mode of the dithizonate chelate.

The S(2)-C(14) and S(3)-C(16) distances of 1.733(2) and 1.741(2) Å of the dithiolene moiety are in agreement with the mercury derivative discussed above. The C≡N [1.148(3) and 1.144(3) Å] and C=C [1.358(3) Å] bond distances of the maleonitrile ligand are consistent with formal triple and double bonds.

Table 6.7 Selected bond lengths (Å), bond and torsion angles (°) for **[6.7]**

Bond lengths			
Pt(1) - N(1)	2.024(2)	Pt(1) - S(3)	2.2605(5)
Pt(1) - S(2)	2.2841(5)	Pt(1) - S(1)	2.3067(5)
S(1) - C(1)	1.746(2)	S(2) - C(14)	1.733(2)
S(3) - C(16)	1.741(2)	N(1) - N(2)	1.286(2)
N(1) - C(2)	1.448(2)	N(2) - C(1)	1.376(2)
N(3) - C(1)	1.322(3)	N(3) - N(4)	1.331(2)
N(4) - C(8)	1.411(3)	N(4) - H(4A)	0.990(10)
N(5) - C(15)	1.148(3)	N(6) - C(17)	1.144(3)
N(7) - C(30)	1.518(3)	N(7) - C(26)	1.519(3)
N(7) - C(18)	1.521(3)	N(7) - C(22)	1.529(3)
Bond angles			
N(1) - Pt(1) - S(2)	95.11(5)	S(3) - Pt(1) - S(2)	90.04(2)
N(1) - Pt(1) - S(1)	82.85(5)	S(3) - Pt(1) - S(1)	92.14(2)
S(2) - Pt(1) - S(1)	175.46(2)	C(1) - S(1) - Pt(1)	95.87(7)
C(14) - S(2) - Pt(1)	102.34(7)	C(16) - S(3) - Pt(1)	103.00(7)
N(2) - N(1) - C(2)	111.4(2)	N(2) - N(1) - Pt(1)	123.7(1)
C(2) - N(1) - Pt(1)	124.9(1)	N(1) - Pt(1) - S(3)	174.58(4)
C(1) - N(3) - N(4)	116.2(2)	N(3) - N(4) - C(8)	118.7(2)
N(3) - N(4) - H(4A)	123(2)	C(8) - N(4) - H(4A)	118(2)
N(1) - N(2) - C(1)	115.4(2)	N(2)-C(1)-S(1)	122.1(2)
N(3)-C(1)-N(2)	111.8(2)	N(3)-C(1)-S(1)	126.0(2)
Torsion angles			
N(1)-Pt(1)-S(1)-C(1)	0.73(8)	S(3)-Pt(1)-S(1)-C(1)	-177.20(7)
S(2)-Pt(1)-S(1)-C(1)	64.2(3)	N(1)-Pt(1)-S(2)-C(14)	-177.64(8)
S(3)-Pt(1)-S(2)-C(14)	0.66(7)	S(1)-Pt(1)-S(2)-C(14)	119.3(2)
N(1)-Pt(1)-S(3)-C(16)	161.1(5)	S(2)-Pt(1)-S(3)-C(16)	-0.56(7)
S(1)-Pt(1)-S(3)-C(16)	-176.57(7)	S(3)-Pt(1)-N(1)-N(2)	24.0(6)
S(2)-Pt(1)-N(1)-N(2)	-174.4(1)	S(1)-Pt(1)-N(1)-N(2)	1.5(1)
Pt(1)-N(1)-N(2)-C(1)	-3.8(2)		
N(1)-N(2)-C(1)-N(3)	-171.7(2)	N(1)-N(2)-C(1)-S(1)	4.6(2)
Pt(1)-S(1)-C(1)-N(3)	172.7(2)	Pt(1)-S(1)-C(1)-N(2)	-3.0(2)
Pt(1)-S(2)-C(14)-C(16)	-0.7(2)	Pt(1)-S(2)-C(14)-C(15)	176.0(2)
Pt(1)-S(3)-C(16)-C(14)	0.3(2)	S(2)-C(14)-C(15)-N(5)	-118(8)
Pt(1)-S(3)-C(16)-C(17)	-178.1(2)	S(2)-C(14)-C(16)-C(17)	178.7(2)
S(3)-C(16)-C(17)-N(6)	31(9)	S(2)-C(14)-C(16)-S(3)	0.3(3)

The tetrabutylammonium counter-ion shows the nitrogen in a tetrahedral environment with N-C bond distances and bond angles around nitrogen all appearing normal.

Table 6.8 Crystal data and structure refinement for **[6.7]**

Empirical formula	$C_{33}H_{47}N_7S_3Pt$
Formula weight	833.05 amu
Temperature	173(2)K
Wavelength	0.71073 Å
Crystal system, space group	Orthorhombic, $P2_12_12_1$
Unit cell dimensions	a = 8.7972(5)Å, $\alpha = 90°$
	b = 14.8635(8) Å, $\beta = 90°$
	c = 27.2072(14) Å, $\gamma = 90°$
Volume	3557.5(3) $Å^3$
Z, Calculated density	4, 1.555 Mg/m^3
Absorption coefficient	4.154 mm^{-1}
F(000)	1680
Crystal size	0.21 x 0.21 x 0.19 mm
Theta range for data collection	2.03 to 28.28°
Limiting indices	$-11 \leq h \leq 11$, $-19 \leq k \leq 19$, $-36 \leq l \leq 36$
Reflections collected / unique	86381 / 8818 [R(int) = 0.0318]
Completeness to theta = 25.35	100.0 %
Max. and min. transmission	0.5058 and 0.4758
Absorption correction	Semi-empirical from equivalents
Refinement method	Full-matrix least-squares on F^2
Data / restraints / parameters	8818 / 1 / 401
Goodness-of-fit on F^2	1.059
Final R indices [I>2sigma(I)]	R_1 = 0.0138, wR_2 = 0.0311
R indices (all data)	R_1 = 0.0145, wR_2 = 0.0313

An intermolecular hydrogen bond between H(4A) and the nitrogen atom, N(6) belonging to the nitrile functionality, was observed (**Table 6.9**). This results in a one-dimensional hydrogen bonding chain along [010] as depicted in **Figure 6.10**.

Table 6.9 Hydrogen bonds for **[6.7]**

Hydrogen bond	N – H (Å)	H···N (Å)	N···N (Å)	NHN (°)
N(4)-H(4A)...N(6)[a]	0.990(10)	2.172(17)	3.078(3)	151(2)

[a] molecule at -x,y-1/2,-z+1/2

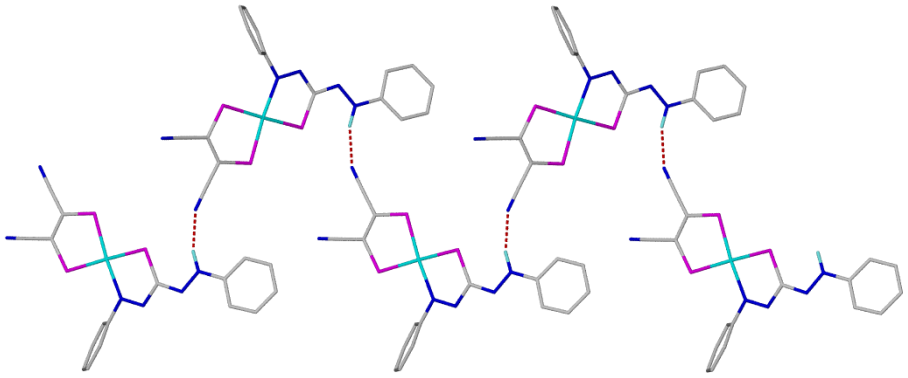

Figure 6.10 One-dimensional hydrogen bonding chain along [010].

6.8 Cyclic voltammetry

The electrochemical behaviour of **[6.7]** was investigated in dichloromethane. The cyclic voltammogram of **[6.7]** is shown in **Figure 6.11**.

We observed similar redox behaviour as seen for the mixed Hg complexes **[6.2]**-**[6.5]**, i.e. three irreversible reduction processes at -450, -674 and -1410 mV, which are attributed to the dithizone moiety. Two reversible oxidation peaks are also observed. As for the Hg complexes, the two anodic processes at +203 and +500 mV could be attributed to the dithizonate moiety, as discussed in **Chapter 5**. The corresponding reverse reduction waves at +260 and +110 mV would indicate that there could be two one-electron oxidation processes overlapping with the two dithizonate oxidations discussed above, due to the process:

$$[Pt(mnt)(Hdptc)]^{-1} \rightarrow [Pt(mnt)(Hdptc)]^{0} \rightarrow [Pt(mnt)(Hdptc)]^{+1}$$

which is presumably dithiolene based. It is interesting to note that both oxidation processes are reversible, whereas the analogous processes observed for the Hg complexes

were irreversible, which is consistent with the studies by Wen[19], Guo[28] and Narvor[29], discussed above, showing an absence of reversibility for dithiolene ligands attached to mercury.

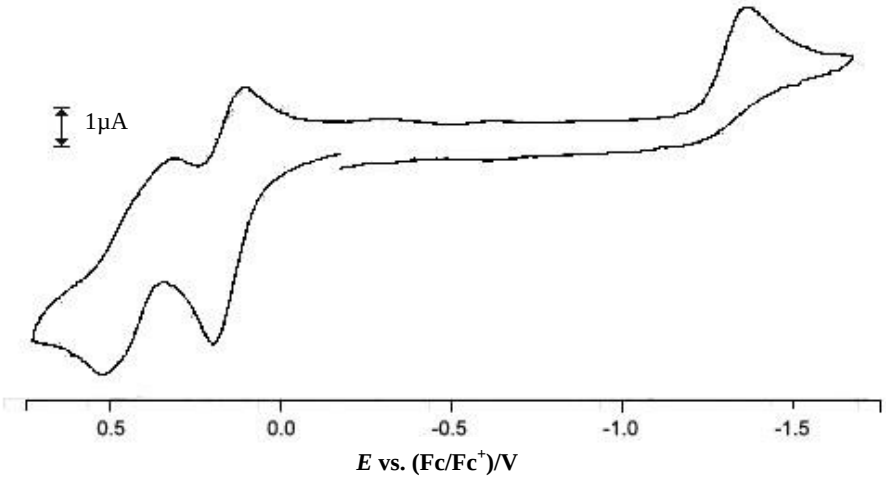

Figure 6.11 Cyclic voltammogram of **[6.7]**.

REFERENCES

1 M. Almeida and R. Henriques, *Handbook of Organic Conductive Molecules and Polymers, Vol. 1, Wiley, New York*, 1997, 87.

2 I. Malfant, R. Andreu, P. G. Lacroix, C. Faulmann and P. Cassoux, *Inorg. Chem.*, 1998, **37**, 3361.

3 S. R. Marder, J. W. Perry and W. P. Schaefer, *Science*, 1989, **245**, 626.

4 J. N. Yao, K. Hashimoto and A. Fujishima, *Nature*, 1992, **335**, 624.

5 P. Fernando, J. M. Maria, M. Mauro, B. Roberto and B. Vincenzo, *J. Am. Chem. Soc.*, 1997, **119**, 5556.

6 M. Xu, Y. Li, W. Li, C. Sun and L. Wu, *J. Coll. Interface Sc.*, 2007, **315**, 753.

7 M. Clemente-Leon, E. Coronado, J. R. Galan-Mascaros, C. Gimenez-Saiz, C. J. Gomez-Garcia, J. M. Fabre, G. A. Mousdis and G. C. Papavassiliou, *J. Solid State Chem.*, 2002, **168**, 616.

8 P. Malatji, *MSc. Thesis*, University of Cape Town, 2008.

9 N. L. Cromhout and A. T. Hutton, *J. Coord. Chem*., 2000, **52**, 169.

10 J. L. A. Webb, I. Singh Bhatia, A. H. Corwin and A. G. Sharp, *J. Am. Chem. Soc*., 1950, 72, 91.

11 A. C. Fabretti and G. Peyronel, *J. Inorg. Nucl. Chem.*, 1975, **37**, 603.

12 A. T. Hutton, *PhD. Thesis*, University of Cape Town, 1980.

13 K. G. von Eschwege, J. Conradie and J. C. Swarts, *J. Phys. Chem. A*, 2008, **112**, 2211.

14 M. M. Harding, *J. Chem. Soc*., 1958, 4136.

15 N. L. Cromhout and A. T. Hutton, *Appl. Organomet. Chem.*, 2000, **14**, 66.

16 R. Haid, R. Gutmann, G. Czermak, C. Langes, W. Oberhauser, H. Kopacka, K.-H. Ongania and P. Bruggeller, *Inorg. Chem. Comm.*, 2003, **6**, 61.

17 H.-Y. Hsieh, C.-W. Cheng, F.-A. Yang, J.-H. Chen, J.-Y. Tung, S.-S Wang and L.-P. Hwang, *Polyhedron*, 2007, **26**, 4915.

18 P. A. Alsop, *PhD. Thesis*, University of London, 1971.

19 H.-R. Wen, J.-L. Zuo, T. A. Scott, H.-C. Zhou and X.-Z. You, *Polyhedron*, 2005, **24**, 671.

20 W. F. Guo, D. Xu, W. T. Yu, Q. Wang and G. H. Zhang, 2006, *Acta. Cryst*., **E62**, E62, m2345.

21 A. Bondi, *J. Phys. Chem.*, 1964, **68**, 441.

22 D. Grdenic, *Q. Rev. Chem. Soc.*, 1965, **19**, 303.

23 J. R. Stork, M. M. Olmstead, J. C. Fettinger and A. L. Balch, *Inorg. Chem*., 2006, **45**, 849.

24 M. Nomura, T. Fujii and M. Kajitani, *Organometallics,* 2009, **28**, 3776.

25 P. Banerjee, S. Sproules, T. Weyhermuller, S. DeBeer George and K. Wieghardt, *Inorg. Chem.,* 2009, **48**, 5829.

26 F. H. Allen, O. Kennard, D. G. Wilson, L. Brammer, A. G. Orpen and R. Taylor, *Typical Interatomic Distances: Organic Compounds*, A. J. C. Wilson (ed.), International Tables for Crystallography, Vol. C: Mathematical, Physical and Chemical Tables, Kluwer, Dordrecht, 1995, 685-706.

27 K. G. von Eschwege, L. van As and J. C. Swarts, *Electrochim. Acta*, 2011, **56**, 10064.

28 W. F. Guo, D. Xu, W. T. Yu, X. Q. Wang and G. H. Zhang, *Acta, Cryst.*, 2006, **E62**, 222.

29 N. L. Narvor, N. Robertson, E. Wallace, J. D. Kilburn, A. E. Underhill, P. N. Bartlett and M. Webster, *J. Chem. Soc., Dalton Trans.*, 1996, 823.

30 S. A. Baudron and M. W. Hosseini, *Inorg. Chem*., 2006, **45** 5260.

31 Y. Sueishi, Y. Takashima and S. Yamamoto, *Int. J. Chem Kinetics*, 2000, **32**, 542.

32 E. Billig, R. Williams, I. Bernal, J. H. Waters and H. B. Gray, *Inorg. Chem*, 1964, **3**, 663.

33 L. E. Manzer, *J. Chem. Soc., Dalton Trans.*, 1974, 1535.

CHAPTER 7

Concluding remarks

A series of heterobi- and tri-metallic complexes has been prepared by the metallation of the carbanion derived from the deprotonation of bis(diphenylphosphinomethane) chelates of Cr, Mo, W, Ru, Pd and Pt.

^{31}P NMR spectroscopy revealed the presence of electronic communication within the Group 6 dppm derivatives which is influenced by the substituent on the mercury atom. The presence of electronic communication between the metal centres linked via the dppm-chelate was investigated by cyclic voltammetry, which showed that the mercury atom in conjunction with the four-membered chelate ring does to a certain degree facilitate electron flow. This is supported by the presence of linear relationships between the redox potentials, $E_{½}$, of the chelate metal centre with parameters such as, ν(CO), $\delta(^{31}P)$ and $^{2}J(^{199}Hg\text{-}^{31}P)$. The communication can at best be described as weak, considering a range of 33 mV in the oxidation potential of the chromium metal centre in going from the most electron-withdrawing chlorine substituent to the most inductive ethyl substituent. The trimetallic ferrocenyl complexes exhibited what could be described as a "through-space" communication resulting in a decreased oxidation potential of the Group 6 metal centre as opposed to the expected increased potential.

X-ray crystallographic structures revealed that mercuration results in the complete neutralisation of electron density in the four-membered chelate moiety, as manifested by the P-C(methylene) bond distances. This is noteworthy, since the only reported structure where the dppm chelate is mercurated, shows the P-C(methylene) bonds to have double bond character. An X-ray structure of the ferrocenylmercury derivative of the electron-rich $[RuCp(PPh_3)dppm]PF_6$ complex showed similar features to the zero-valent chromium analogues on mercuration.

A series of long chain alkoxybenzyladine complexes was prepared in an attempt to produce mercury containing mesogenic material. None of the complexes showed any liquid crystalline behaviour.

A series of mixed diphosphine-dithiolene complexes of Pd and Pt were prepared and investigated for their electrochemical behaviour, which showed an increase in oxidation potential in the order $dddt^{2-} < dmid^{2-} \leq dmit^{2-}$, which is in agreement with the relative donor/acceptor ability of the dithiolene ligands.

Mixed diphosphine-dithizone complexes of Pd and Pt were prepared and investigated for photochromism. None of the mixed complexes showed any photochromic behaviour in solution. Dithizone was shown to form a secondary complex when reacted with the organometallic platinum precursor $[Pt(COD)Cl_2]$ and primary complexes when reacted with the phosphine platinum or palladium precursors $[M(diphosphine)Cl_2]$ (M = Pd or Pt].

The X-ray crystal structure of 1,5-diphenylthiocarbazone or dithizone, which had been previously reported, was re-determined. The structure reported in the literature was inconclusive with regards to the tautomeric nature of dithizone. Both spectroscopic and computational studies were conducted to resolve the structural aspects pertaining to dithizone in the solid state. This study has been successful in locating the elusive protons in the electron Fourier difference map, showing the molecule to exist as a tautomer in the solid state, where the keto/enol ratio is approximately 2:1. This was supported by computational studies. Density functional theory, employing the B3LYP level of theory and the 6-311++G(2df,2p) basis set, showed the symmetrical keto form to be most stabilized in the gas phase. The ground-state energy of the enol form was shown to be approximately 3.1 kJ mol^{-1} or 12.9 kJ mol^{-1} higher.

The ^1H NMR spectrum of the dithizonate anion showed it to exhibit proton transfer in solution, resulting in both enol and keto forms being present. While the anion has been prepared previously, no supporting spectroscopic data was reported. NMR spectra were

calculated for the DFT/6-311++G(2df,2p) optimized structures, using the 6-31++G(2d,p) basis set. DFT calculations showed that the keto form is preferred in solution, with an energy difference of 7.9 kcal mol^{-1} between the two forms. DFT was shown to provide a better approximation, relative to HF methods, of chemical shift values for the keto form compared to the enol form.

Mixed dithiolene-dithizone complexes of Hg and Pt were prepared. Only the Hg complexes exhibited photochromism in solution. Electrochemical studies showed a difference in electrochemical behaviour between the analogous Pt and Hg complexes. X-ray crystallographic structures of the two maleonitrile analogues showed the absence of any π···π or *S*···*S* interactions, often required for conferring novel properties to molecules. Nevertheless, it was shown that incorporation of the dithiolene ligand did not impede the photochromism shown by the Hg dithizonate complexes. Conversely, the dithizonate ligand did not impede the electrochemical activity of the dithiolene ligands.

The solution chemistry and reactivity of dithizone appears still to be unresolved. Experimental results show that the enol tautomer is the dominant species in solution. However, there is as yet no evidence in the literature of any *N*,*N*-coordinated dithizonate complexes. The sulfur atom has been shown to be the preferred nucleophile, based on computational calculations. Since sulfur has an affinity for softer Lewis acids, it would be of interest to investigate, both experimentally and theoretically, the reaction with harder Lewis acids.

CHAPTER 8

Experimental

8.1 General procedures

All glassware were thoroughly dried at about 120°C overnight prior to use. Syringes and cannulas were stored at 60°C. All reactions, unless otherwise stated, were carried out under inert atmosphere conditions.

Solvents were all AR grade and were dried and distilled before use using standard literature procedures (see **Table 8.1**).

Table 8.1: Drying procedures for relevant solvents

Solvent/Reagent	Drying agent
Acetone	Drierite® 4 mesh
Acetonitrile	CaH_2
Chloroform	CaH_2
Dichloromethane	P_2O_5
Diethyl ether	Sodium
Ethanol	Iodine/Mg
Methanol	Iodine/Mg
N-methylanaline	Drierite® 4 mesh
Tetrahydrofuran	Sodium

n- Butyllithium (1.6 M in hexanes) and lithium tris(dimethylsilyl)amide (1.0 M in hexanes) were purchased from Sigma Aldrich. All other reagents were used as obtained. Various precursors were prepared following literature procedures.

8.2 Instrumentation

8.2.1 Molecular Spectroscopy

Infrared spectra were recorded on a PerkinElmer FTIR spectrometer. Spectra were recorded as solutions in sodium chloride solution cells, as Nujol mulls between sodium chloride plates or as KBr pellets. Ultraviolet-visible spectra were recorded on a SpectroScan 80DV UV-Vis spectrophotometer. NMR spectra were recorded on either a Varian-VXR (^{1}H: 200 MHz; ^{13}C: 100 MHz; ^{31}P: 80 MHz), Varian-300 (^{1}H: 300 MHz; ^{13}C: 75.5 MHz; ^{31}P: 121.5 MHz) or a Varian Unity-400 (^{1}H: 400 MHz; ^{13}C: 100.6 MHz; ^{31}P: 121.5 MHz) spectrometer.

8.2.2 Cyclic Voltammetry

Cyclic voltammetric studies were conducted using a BAS 100A or BAS 100B electrochemical analyzer with a one compartment three-electrode system consisting of a Ag/Ag^{+} (0.01 M) reference electrode, platinum wire auxiliary electrode and either a platinum disk or glassy carbon working electrode. The complexes were run in dichloromethane, containing tetrabutylammonium perchlorate or tetrabutylammonium hexafluorophosphate as background electrolyte. The scan rate was generally 100 mV s^{-1}. All voltammograms were run against the ferrocene/ferrocenium (Fc/Fc^{+}) couple as reference.

8.2.3 X-ray crystallography

X-ray crystallographic data were collected using on a Nonius Kappa CCD diffractometer using 1.5 kW graphite monochromated MoKα radiation. Temperature was controlled by an Oxford Cryostream cooling system. Data were scaled and reduced using DENZO-SMN software.[1] Unit cell dimensions were refined for all data. Structures were solved by direct methods and refined by full-matrix least-squares on F^2 using SHELX97.[2,3]

Molecular graphics were produced using X-Seed.[4] The CIF files for all the structures solved are available on the CD-ROM disk attached to the back cover of this thesis.

For all structures, the non-H atoms were refined anisotropically, unless otherwise indicated. For **[2.6]**, **[2.18], [2.23]** and **[3.22]**, all hydrogen atoms excepts the chelate-ring methylene proton were included in idealised positions in a riding model with U_{iso} set at 1.2 or 1.5 times those of the parent atoms. The dppm chelate-ring proton for all structures was located in the difference electron density maps and refined independently.

For compound **[2.18]**, all non-H atoms, except the ferrocene ring C61-C65, the phenyl ring C41-C46 and the carbons of the benzene solvent molecule, were refined anisotropically. The ferrocene ring was found to be distorted over two geometries with ring C61A-C65A and ring C61B-C65B rotating anti-clockwise about 44-48°, with site occupancy factors of 50%. The phenyl ring C41-C46 was also found to be disordered and was modeled with two rings C41A-C46A and C41B-C46B, with an inter-planar angle of 51(1)° and a site occupancy factor of 50%.
The benzene ring C1B-C6B exhibited high thermal motions with minimum U_{iso}=0.114 and was therefore refined isotropically.
All the phenyl rings were fixed to idealized hexagons and all the ferrocene rings were fitted to pentagons.

For compound **[3.22]** one phenyl ring, C31-C36, was fitted to an idealised hexagon and refined with the same anisotropic displacement parameters. The phosphorus atom P4 of the PF_6^- anion was refined anisotropically while the fluorine atoms were refined with the same isotropic parameters due to their high thermal motion.

8.2.4 Computational methods

All calculations were performed by way of Density Functional Theory (DFT)[5] using the B3LYP functional (Becke's three parameter exchange functional combined with the Lee, Yang and Parr correlation functional[6,7]) or ab-initio methods for comparison. All

calculations were performed with the Gaussian 09 program.[8] Input geometries were either obtained from related X-ray crystal data or were artificially generated. Geometry optimizations were performed using the levels of theory as stated above using standard 6-31G or 6-311G basis sets with diffusion and polarization functions. Effective core potential (ECP) basis sets were used for heavy atoms. The LANL2DZ core potential was used for calculations involving heavy atoms. Calculations in solution were done using the Polarized Continuum Model (PCM). ^{1}H NMR and ^{13}C NMR chemical shifts were calculated with the GIAO method.[9,10] The shielding constant of TMS was calculated at the same level of theory, using the same basis sets as the reference.

8.3 Preparations pertaining to Chapter 2

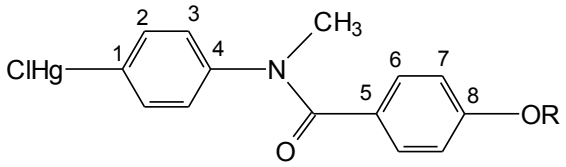

$ClHgC_6H_4N(CH_3)CO\text{-}C_6H_4\text{-}p\text{-}OC_2H_5$ [2.1]

4-(4-ethyloxybenzylidene-N-methylanilino)mercury(II) chloride

p-Ethoxybenzoic acid (0.40 g; 2.4 mmol) was gently refluxed in $SOCl_2$ (ca. 0.5 cm^3) as solvent for 30 min. The excess $SOCl_2$ was removed under reduced pressure to leave a pale yellow oil. This was further dried under high vacuum for 10 min and dissolved in THF (10 cm^3). Triethylamine (0.2 cm^3; 2.4 mmol) was added, followed by the appropriate mercury salt, *p-N*-methylaminephenylmercury(II)chloride[11] (0.71 g; 2.4 mmol). The immediate formation of a white precipitate was observed, presumably that of triethylamine-hydrochloride. The reaction mixture was allowed to stir for 20 min at room temperature. The white precipitate was filtered and washed with THF (5 cm^3). The filtrate was removed under reduced pressure and the residue recrystallised from CH_2Cl_2/MeOH to give a colourless product.

(0.89 g, 76%), m.p. 197-198°C; (Found: C, 39.4; H, 3.3; N, 3.1%; $C_{16}H_{16}ClNO_2Hg$ requires C, 39.19; H, 3.26; N, 2.86 %); ^{1}H NMR δ_H (200 MHz; $CDCl_3$): 1.36 [3 H, t, ^3J(HH) 6.98 Hz, OCH_2CH_3], 3.47 [3 H, s, $NHCH_3$], 3.96 [2 H, q, ^3J(HH) 6.8 Hz, OCH_2CH_3], 6.66 [2 H, d, $^3J_{ab}$ 8.91 Hz, ^4J(HgH) 44.0 Hz, H_a], 7.08 [2 H, d, $^3J_{ab}$ 8.62 Hz, H_b], 7.20 (2 H, d, ^3J(HH) 8.91 Hz, ^3J(HgH) 190.0 Hz H_b], 7.24 [2 H, d, ^3J(HH) 8.62 Hz, H_a]; ^{13}C NMR δ_C (100 MHz; $CDCl_3$): 14.66 (CH_3-), 38.45(N-CH_3) , 63.43 (-OCH_2CH_3), 113.59 (C_7), 127.37 (C_2 or C_3), 127.46 (C_5), 130.86 (C_6), 136.44 (C_3 or C_2), 146.56 (C_1 or C_4), 146.87 (C_4 or C_1), 160.20 (C_8), 170.33 (-NCO).

$ClHgC_6H_4N(CH_3)CO\text{-}C_6H_4\text{-}p\text{-}OC_5H_{11}$ [2.2]

4-(4-pentyloxybenzylidene-N-methylanilino)mercury(II) chloride

(0.99 g, 78%), m.p. 195-196°C; (Found: C, 42.7; H, 4.2; N, 4.5%; $C_{19}H_{22}ClNO_2Hg$ requires C, 42.86; H, 4.13; N, 2.63 %); ^{1}H NMR δ_H (200 MHz; $CDCl_3$): 0.87 (3 H, t CH_3-), 1.28 (6 H, m, -$(CH_2)_3$ -), 1.75 (2 H, q, -OCH_2CH_2), 3.46 (3 H, s, NH-CH_3), 3.88 (2 H, t, OCH_2-), 6.66 (2 H, d, $^3J_{ab}$ 8.9, H_a), 7.07 (2 H, d, $^3J_{ab}$ 8.6, H_a), 7.21 (2 H, d, $^3J_{ab}$ 8.6, H_a), 7.24 (2 H, d, $^3J_{ab}$ 8.8, H_b); ^{13}C NMR δ_C (100 MHz; $CDCl_3$): 13.96 (*C*H_3-), 22.52 (CH_3*C*H_2-), 25.61 (CH_3CH_2*C*H_2-), 29.06 ($CH_3CH_2CH_2$*C*H_2-), 31.49 (-OCH_2*C*H_2-), 38.47 (-NH-*C*H_3), 67.98 (-O*C*H_2-), 113.59 (*C*$_7$), 127.32 (*C*$_2$ or *C*$_3$), 127.40 (*C*$_5$), 130.85 (*C*$_5$), 136.48 (*C*$_3$ or *C*$_2$), 146.48 (*C*$_1$ or *C*$_4$), 146.95 (*C*$_4$ or *C*$_1$), 160.40 (*C*$_8$), 170.33 (-N*C*O).

$ClHgC_6H_4N(CH_3)CO\text{-}C_6H_4\text{-}p\text{-}OC_7H_{15}$ [2.3]

4-(4-heptyloxybenzylidene-N-methylanilino)mercury(II) chloride

(0.87 g, 65%), m.p. 194-195°C; (Found: C, 45.3; H, 4.3; N, 2.8%; $C_{21}H_{26}ClNO_2Hg$ requires C, 45.00; H, 4.63; N, 2.50 %); ^{1}H-NMR δ_H (200 MHz; $CDCl_3$): 0.87 (3 H, t, CH_3), 1.30 (8 H, m, -$(CH_2)_4$-), 1.82 (2 H, q, -OCH_2CH_2), 3.46 (3 H, s, NH-CH_3), 3.89 (2 H, t, OCH_2-), 6.65 (2 H, d, $^3J_{ab}$ 8.8, H_a), 7.06 (2 H, d, $^3J_{ab}$ 8.5, H_a), 7.20 (2 H, d, $^3J_{ab}$ 8.5, H_a), 7.24 (2 H, d, $^3J_{ab}$ 8.7, H_b); ^{13}C NMR δ_C (100 MHz; $CDCl_3$): 14.04 (*C*H_3-), 22.55 (CH_3*C*H_2-), 25.92 (CH_3CH_2*C*H_2-), 28.99 ($CH_3CH_2CH_2$*C*H_2-), 29.11 ($CH_3CH_2CH_2CH_2$*C*H_2-), 31.71 (-OCH_2*C*H_2-), 38.48 (-NH-*C*H_3) , 68.01 (-O*C*H_2-), 113.61 (*C*$_7$), 127.36 (*C*$_2$ or *C*$_3$), 130.87 (*C*$_5$), 136.45 (*C*$_3$ or *C*$_2$), 146.56 (*C*$_1$ or *C*$_4$), 146.87 (*C*$_4$ or *C*$_1$), 160.43 (*C*$_8$), 170.34 (-N*C*O).

$ClHgC_6H_4N(CH_3)CO\text{-}C_6H_4\text{-}p\text{-}OC_9H_{19}$ [2.4]

4-(4-nonyloxybenzylidene-N-methylanilino)mercury(II) chloride

p-Hexyloxybenzoylchloride (0.28 cm^3; 1.2 mmol) was added to a solution of $ClHgC_6H_4NH(CH_3)$ (0.4g; 1.2 mmol) and Et_3N (0.1 cm^3; 1.2 mmol) in THF (10 cm^3). Observations and work-up were similar to **[2.1]** described above.

(0.47 g, 66 %), m.p. 193-195°C; (Found: C, 46.7; H, 5.1; N, 2.6%; $C_{23}H_{30}ClNO_2Hg$ requires C, 46.94; H, 5.10; N, 2.38%); ^{1}H NMR δ_H (200 MHz; $CDCl_3$): 0.87 [3 H, t, ^3J(HH) 6.22 Hz, CH_2CH_3], 1.26 [12 H, m, $(CH_2)_6$], 1.71 [2 H, sep, ^3J(HH) 6.80 Hz, $CH_2CH_2CH_3$], 3.47 [3 H, s, $NHCH_3$], 3.87 [2 H, t, ^3J(HH) 6.59 Hz OCH_2CH_2], 6.65 [2 H, d, $^3J_{ab}$ 8.88 Hz, H_a], 7.07 (2 H, d, $^3J_{ab}$ 8.54 Hz, H_b], 7.20 [2 H, d, $^3J_{ab}$ 8.51 Hz, H_b], 7.23 [2 H, d, $^3J_{ab}$ 8.88 Hz, H_a]; ^{13}C NMR δ_C (100 MHz; $CDCl_3$): 13.96 (CH_3-), 22.52 (CH_3CH_2-), 25.61 ($CH_3CH_2CH_2$-), 29.06- 29.57 [$(CH_2)_4$], 31.49 (-OCH_2CH_2-), 38.47 (-NH-CH_3), 67.98 (-OCH_2-), 113.59 (C_7), 127.32 (C_2 or C_3), 127.46 (C_5) 130.85 (C_6), 136.48 (C_3 or C_2), 146.48 (C_1 or C_4), 146.95 (C_4 or C_1), 160.40 (C_8), 170.33 (-NCO).

$ClHgC_6H_4N(CH_3)CO\text{-}C_6H_4\text{-}p\text{-}OC_{12}H_{25}$ [2.5]

4-(4-dodecyloxybenzylidene-N-methylanilino)mercury(II) chloride

This was prepared using the method as described for **[2.4]** above using using *p-N*-methylphenylmercury(II)chloride and *p*-dodecyloxybenzoylchloride.

(0.47 g, 63%), m.p. 185-187°C; (Found: C, 49.08; H, 5.70; N, 2.0%; $C_{26}H_{36}ClNO_2Hg$ requires C, 49.52; H, 5.71; N, 2.22%); ^{1}H NMR δ_H (200 MHz; $CDCl_3$): 0.87 [3 H, t, ^3J(HH) 6.13 Hz, CH_2CH_3], 1.26 [18 H, m, $(CH_2)_9$], 1.73 [2 H, sep, ^3J(HH) 7.08 Hz, $CH_2CH_2CH_3$], 3.46 [3 H, s, $NHCH_3$], 3.87 [2 H, t, ^3J(HH) 6.60 Hz OCH_2CH_2], 6.65 [2 H, d, $^3J_{ab}$ 8.90 Hz, Ha], 7.07 (2 H, d, $^3J_{ab}$ 8.56 Hz, H_b], 7.20 [2 H, d, $^3J_{ab}$ 8.51 Hz, H_b], 6.67 [2 H, d, ^{3} J_{ab} 8.87 Hz, H_a], 7.09 [2 H, d, ^{3} J_{ab} 8.57 Hz, H_c], 7.20 [2 H, d, ^{3} J_{ab} 8.60 Hz, H_d], 7.23 [2 H, d, ^{3} J_{ab} 8.62 Hz, H_b]; ^{13}C NMR δ_C (100 MHz; $CDCl_3$): 13.96 (CH_3-), 22.52 (CH_3CH_2-), 25.61 ($CH_3CH_2CH_2$-), 29.06-29.68 [$(CH_2)_7$], 31.49 (-OCH_2CH_2),

38.47 (-NH-*C*H_3) , 67.98 (-O*C*H_2-), 113.59 (*C*$_7$), 127.32 (*C*$_2$), 127.45 (*C*$_5$), 130.85 (*C*$_6$), 136.48 (*C*$_3$), 146.48 (*C*$_1$ or *C*$_4$), 146.95 (*C*$_4$ or *C*$_1$), 160.41 (*C*$_8$), 170.33 (-N*C*O).

[Cr(CO)$_4${PPh$_2$CH(HgCH$_3$)PPh$_2$}] [2.6]

[Bis(diphenylphosphino)methine][methylmercury(II)]-tetracarbonylchromium(0)

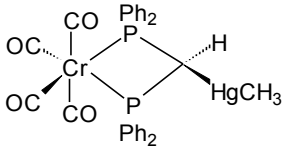

BuLi^n (0.69 cm^3; 1.10 mmol) was added to a solution of tetracarbonyl-bis(diphenylphosphinomethane)chromium(0)[12] (0.40 g; 0.73 mmol) in THF (15 cm^3) at 0°C. The solution was stirred for 1.5 hours at 0°C, followed by the addition of methylmercury(II)chloride (0.22 g; 0.87 mmol). The resulting yellow solution was allowed to warm to room temperature and stirred for 2 hours. The solution was evaporated under reduced pressure. The crude material was recrystallised from CH_2Cl_2/MeOH, to yield a yellow crystalline product

(0.47 g, 85%); m.p. 171-172°C; (Found: C, 47.15; H, 3.2%; $C_{30}H_{24}O_4P_2CrHg$ requires C, 47.22; H, 3.14%); FTIR *ν*(CO)(THF)/cm^{-1} 2001s, 1912s, 1884s, and 1870s; ^{1}H NMR δ_H (200 MHz; $CDCl_3$): -0.12 [3 H, s, ^2J(HHg) 146.0 Hz, C*H*$_3$], 4.61 [1 H, t, ^2J(PH) 8.0 Hz, P_2C*H*], 7.31-7.82 [20 H, m, Ph]; ^{31}P NMR δ_P (80 MHz; $CDCl_3$): 33.08 [s, ^2J(PHg) 76.8 Hz, P_2Cr].

[Mo(CO)$_4${PPh$_2$CH(HgCH$_3$)PPh$_2$}] [2.7]

[Bis(diphenylphosphino)methine][methylmercury(II)]-tetracarbonylmolybdenum(0)

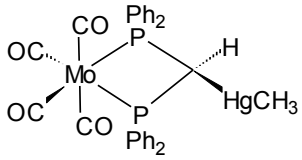

(0.44 g, 76%); m.p. 164-165°C; (Found: C, 44.6; H, 2.9%; $C_{30}H_{24}O_4P_2HgMo$ requires C, 44.65; H, 2.97%); FTIR ν(CO)(THF)/cm^{-1} 2016m, 1915s, 1900s, and 1880s; ^{1}H NMR δ_H (200 MHz; $CDCl_3$): -0.13 [3 H, s, ^2J(HHg) 144 Hz, C*H*$_3$], 4.69 [1 H, t, ^2J(PH) 7.50], 7.28-7.82 [20 H, m, Ph]; ^{31}P NMR δ_P (80 MHz; $CDCl_3$): 11.31 [s, ^2J(PHg) 70.0 Hz, P_2Mo].

$[W(CO)_4\{PPh_2CH(HgCH_3)PPh_2\}]$ [2.8]

[Bis(diphenylphosphino)methine][methylmercury(II)]-tetracarbonyltungsten(0)

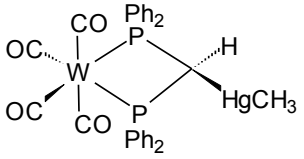

(0.45 g, 69%); m.p. 160-161°C; (Found: C, 40.3; H, 2.7%; $C_{30}H_{24}O_4P_2HgW$ requires C, 40.26; H, 2.68%); FTIR ν (CO)(THF)/cm^{-1} 2010m, 1910s, 1888s, and 1867s; ^{1}H NMR δ_H (200 MHz; $CDCl_3$): -0.13 [3 H, s, ^2J(HHg) 142 Hz, CH_3], 5.61 [1 H, t, ^2J(PH) 8.1 Hz, P_2C*H*], 7.32-7.80 [20 H, m, Ph]; ^{31}P NMR δ_P (80 MHz; $CDCl_3$): -13.47 [s, ^2J(PHg) 70.5 Hz, ^1J(PW), 197.4, P_2W].

$[Cr(CO)_4\{PPh_2CH(HgCH_2CH_3)PPh_2\}]$ [2.9]

[Bis(diphenylphosphino)methine][ethylmercury(II)]-tetracarbonylchromium(0)

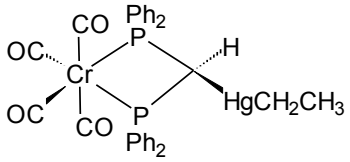

(0.32 g, 67%); m.p. 178-180°C; (Found: C, 47.7; H, 3.3%; $C_{31}H_{26}O_4P_2CrHg$ requires C, 47.91; H, 3.35%); FTIR ν(CO)(THF) 2001s, 1912s, 1884s and 1869s; ^{1}H NMR δ_H (400 MHz; $CDCl_3$): 0.61 [3 H, t, ^3J(HH) 7.79 Hz, ^3J(HHg) 199.9 Hz, CH_2CH_3], 0.71 [2 H, q, ^3J(HH) 8.39 Hz, ^2J(HHg) 143.2 Hz, CH_2CH$_3$], 4.55 [1 H, t, ^2J(PH) 8.59 Hz, P_2C*H*], 7.25-7.82 [20 H, m, Ph]; ^{31}P NMR δ_P (80 MHz; $CDCl_3$): 32.68 [s, ^2J(PHg) 58.9 Hz, P_2Cr].

$[Mo(CO)_4\{PPh_2CH(HgCH_2CH_3)PPh_2\}]$ [2.10]

[Bis(diphenylphosphino)methine][ethylmercury(II)]-tetracarbonylmolybdenum(0)

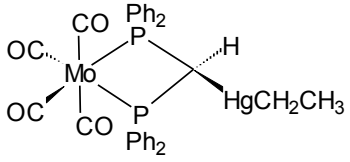

(0.32 g, 65%); m.p. 172-174°C; (Found: C, 45.5; H, 3.2%; $C_{31}H_{26}O_4P_2HgMo$ requires C, 45.35; H, 3.12%); FTIR ν(CO)(THF)/cm^{-1} 2014s, 1917s, 1896s and 1876s; ^{1}H NMR δ_H (400 MHz; $CDCl_3$): 0.61 [3 H, t, ^3J(HH) 7.78 Hz, ^3J(HHg) 199.9 Hz, CH_2CH_3], 0.69 [2 H, q, ^3J(HH) 7.79 Hz, ^2J(HHg) 143.2 Hz, CH_2CH$_3$], 4.62 [1 H, t, ^2J(PH) 7.64 Hz,

P_2CH], 7.21-7.81 [20 H, m, Ph] ; ^{31}P NMR δ_P (80 MHz; $CDCl_3$): 8.77 [s, ^2J(PHg), 50.3 Hz, P_2Mo].

$[W(CO)_4\{PPh_2CH(HgCH_2CH_3)PPh_2\}]$ [2.11]
[Bis(diphenylphosphino)methine][ethylmercury(II)]-tetracarbonyltungsten(0)

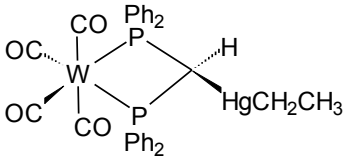

(0.34 g, 63%); m.p. 171-172°C; (Found: C, 40.7; H, 2.9%; $C_{31}H_{26}O_4P_2HgW$ requires C, 40.96; H, 2.86%); FTIR ν(CO)(THF) 2010s, 1910s, 1887s and 1869s; ^1H NMR δ_H (400 MHz; $CDCl_3$): 0.69 [3 H, t, ^3J(HH) 7.99 Hz, ^3J(HHg) 199.9 Hz, CH_2CH_3], 0.61 [2 H, q, ^3J(HH) 7.59 Hz, ^2J(HHg) 143.2 Hz, CH_2CH_3], 5.50 [1 H, t, ^2J(PH) 7.79 Hz, P_2CH],], 7.31-7.83 [20 H, m, Ph]; ^{31}P NMR δ_P (80 MHz; $CDCl_3$): -15.95 [s, ^2J(PHg), 51.8 Hz, ^1J(PHg) 196.8 Hz, P_2W].

$[Cr(CO)_4\{PPh_2CH(HgCH_2CH_2CH_3)PPh_2\}]$ [2.12]
[Bis(diphenylphosphino)methine][propylmercury(II)]-tetracarbonylchromium(0)

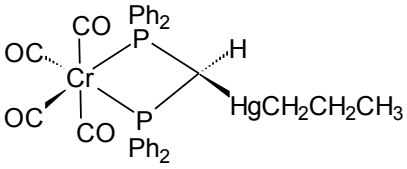

(0.33 g, 70%); mp. 178-181°C; (Found: C, 48.2; H, 3.2%; $C_{32}H_{28}O_4P_2CrHg$ requires C, 48.58; H, 3.54%); FTIR ν(CO)(THF)/cm^{-1} 2001s, 1912s, 1884s and 1868s; ^1H NMR δ_H (400 MHz; $CDCl_3$) 0.40 [3 H, t, ^3J(HH) 7.27 Hz, $CH_2CH_2CH_3$], 0.80 [2 H, t, ^3J(HH) 7.13 Hz, ^2J(HHg) 139.9 Hz, $CH_2CH_2CH_3$], 1.15 [2 H, sext, ^3J(HH) 7.18 Hz, ^3J(HHg) 187.9 Hz, $CH_2CH_2CH_3$], 4.55 [1 H, t, ^2J(PH) 8.59 Hz, P_2CH]; ^{31}P NMR δ_P (80 MHz; $CDCl_3$) 34.54 [s, ^2J(PHg) 60.3 Hz, P_2Cr].

$[Cr(CO)_4\{PPh_2CH(HgCH_2(CH_2)_6CH_3)PPh_2\}]$ [2.13]

[Bis(diphenylphosphino)methine][octylmercury(II)]-tetracarbonylchromium(0)

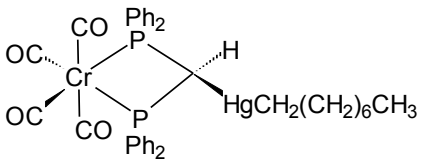

(0.34 g, 65%); mp. 131-133°C; (Found: C, 51.9; H, 4.6%; $C_{37}H_{38}O_4P_2CrHg$ requires C, 51.60; H, 4.41%); FTIR ν(CO)(THF)/cm^{-1} 2001s 1911vs, 1884vs and 1870sh; ^{1}H NMR δ_H (400 MHz; $CDCl_3$): 0.40 [3 H, t, ^3J(HH) 7.27 Hz, $CH_2CH_2CH_3$], 0.80 [2 H, t, ^3J(HH) 7.13 Hz, ^2J(HHg) 139.9 Hz, $CH_2CH_2CH_3$], 1.15 [2 H, sext, ^3J(HH) 7.18 Hz, ^3J(HHg) 187.9 Hz, $CH_2CH_2CH_3$], 4.55 [1 H, t, ^2J(PH) 8.52 Hz, P_2CH]; ^{31}P NMR δ_P (80 MHz; $CDCl_3$): 34.57 [s, ^2J(PHg) 59.7 Hz, P_2Cr].

$[Cr(CO)_4\{PPh_2CH(HgCH_2(CH_2)_8CH_3)PPh_2\}]$ [2.14]

[Bis(diphenylphosphino)methine][decylmercury(II)]-tetracarbonylchromium(0)

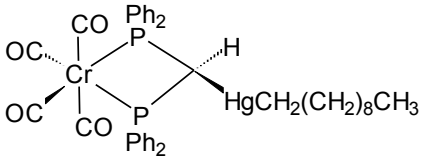

(0.36 g, 68%); m.p. 123-127°C; (Found: C, 52.8; H, 4.8%; $C_{39}H_{42}O_4P_2CrHg$ requires C, 52.67; H, 4.72%); ν(CO)(THF)/cm^{-1} 2002s, 1912vs, 1901vs and 1875s; ^{1}H NMR δ_H (400 MHz; $CDCl_3$): 0.40 [3 H, t, ^3J(HH) 7.27 Hz, $CH_2CH_2CH_3$], 0.80 [2 H, t, ^3J(HH) 7.13 Hz, ^2J(HHg) 139.9 Hz, $CH_2CH_2CH_3$], 1.15 [2 H, sext, ^3J(HH) 7.18 Hz, ^3J(HHg) 187.9 Hz, $CH_2CH_2CH_3$], 4.55 [1 H, t, ^2J(PH) 8.59 Hz, P_2CH]; ^{31}P NMR δ_P (80 MHz; $CDCl_3$): 34.56 [s, ^2J(PHg) 59.5 Hz, P_2Cr].

$[Cr(CO)_4\{PPh_2CH(HgC_6H_5)PPh_2\}]$ [2.15]

[Bis(diphenylphosphino)methine][phenylmercury(II)]-tetracarbonylchromium(0)

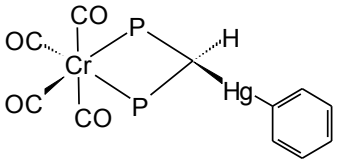

(0.34 g, 69%); m.p. 168-170°C; (Found: C, 51.1; H, 3.4%; $C_{35}H_{26}O_4P_2CrHg$ requires C, 50.95; H, 3.15%); FTIR ν(CO)(THF)/cm^{-1} 2002m, 1912m, 1887s and 1872s; ^{1}H NMR δ_H (200 MHz; $CDCl_3$): 4.6 [1 H, t, ^2J(PH) 8.50 Hz, P_2CH], 6.33 [2 H, d, ^2J(ab) 7.64 Hz,

^{3}J(HHg) 138.0 Hz, Ha], 7.09 [3 H, m, Hb], 7.35-7.88 [20 H, m, Ph]; ^{31}P NMR δ_P (80 MHz; $CDCl_3$): 33.84 [s, ^{2}J(PHg) 87.4 Hz, P_2Cr].

$[Mo(CO)_4\{PPh_2CH(HgC_6H_5)PPh_2\}]$ [2.16]

[Bis(diphenylphosphino)methine][phenylmercury(II)]-tetracarbonylmolybdenum(0)

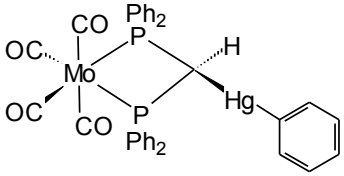

(0.35 g, 67%); m.p. 161-162°C; (Found: C, 47.8; H, 3.05%; $C_{35}H_{26}O_4P_2HgMo$ requires C, 48.37; H, 2.99%); FTIR ν(CO)(THF)/cm^{-1} 2015s, 1917s, 1900s and 1878s; ^{1}H NMR δ_H (200 MHz; $CDCl_3$): 5.05 [1 H, t, ^{2}J(PH) 7.48 Hz, P_2CH], 6.30 [2 H, d, ^{2}J(ab) 7.64 Hz, ^{3}J(HHg) 138.0 Hz, Ha], 7.10 [3 H, m, Hb], 7.36-7.88 [20 H, m, Ph]; ^{31}P NMR δ_P (80 MHz; $CDCl_3$): 11.52 [s, ^{2}J(PHg) 79.3 Hz, P_2Mo].

$[W(CO)_4\{PPh_2CH(HgC_6H_5)PPh_2\}]$ [2.17]

[Bis(diphenylphosphino)methine][phenylmercury(II)]-tetracarbonyltungsten(0)

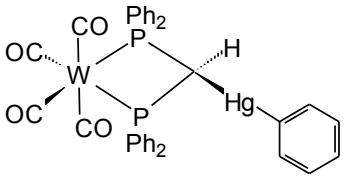

(0.41 g, 71%); m.p. 160 °C; (Found: C, 43.7; H, 2.8%; $C_{35}H_{26}O_4P_2HgW$ requires C, 43.93; H, 2.72%); FTIR ν(CO)(THF)/cm^{-1} 2011s 1911s 1893s 1872s; ^{1}H NMR δ_H (200 MHz; $CDCl_3$): 5.91 [1 H, t, ^{2}J(PH) 7.88 Hz, P_2CH], 6.40 [2 H, d, ^{2}J(ab) 7.55 Hz, ^{3}J(HHg) 140 Hz, Ha], 7.10 [3 H, m, Hb], 7.31-7.89 [20 H, m, Ph]; ^{31}P NMR δ_P (80 MHz; $CDCl_3$): -13.36 [s, ^{2}J(PHg) 81.3 Hz, ^{1}J(PW) 198.7 Hz, P_2W].

$[Cr(CO)_4\{PPh_2CH(Hg(C_5H_4)Fe(C_5H_5))PPh_2\}]$ [2.18]

[Bis(diphenylphosphino)methine][ferrocenylmercury(II)]-tetracarbonylchromium(0)

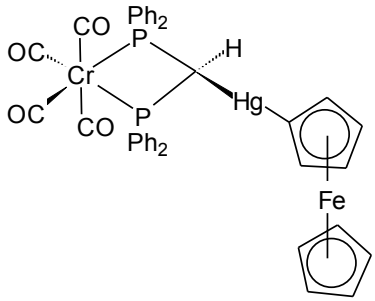

$BuLi^n$ (0.69 cm^3; 1.10 mmol) was added to a solution of tetracarbonyl-bis(diphenylphosphinomethane)chromium(0) (0.40 g; 0.73 mmol) in THF (15 cm^3) at 0°C. The solution was stirred for 1.5 hours at 0°C; followed by the addition of ferrocenenylmercury(II)choride (0.37 g, 0.86 mmol). The resulting orange solution was allowed to warm to room temperature and stirred for a further 2 hours. The orange solution was evaporated to dryness under reduced pressure. The crude orange material was recrystallised from CH_2Cl_2/MeOH, to yield orange crystals

(0.52 g, 76%); m.p. 215°C(dec); (Found: C, 50.1; H, 3.1%; $C_{39}H_{30}O_4P_2CrFeHg$ requires C, 50.20; H, 3.22%); FTIR ν(CO)(THF)/cm^{-1} 2002s, 1912s, 1888s, and 1872s; ^{1}H NMR δ_H (200 MHz; $CDCl_3$): ^{1}H, δ, 3.26 [2 H, t, Jab 3.35 Hz, Ha], 3.71 [5 H, s, C_5H_5], 4.16 [2 H, t, Jab 3.35 Hz, Hb], 5.02 [1 H, t, ^2J(PH) 8.4 Hz, P_2CH], 7.34-7.96 [20 H, m, Ph]; ^{31}P NMR δ_P (80 MHz; $CDCl_3$): δ 35.52 [s, ^2J(PHg) 95.6 Hz, P_2Cr].

$[Mo(CO)_4\{PPh_2CH(Hg(C_5H_4)Fe(C_5H_5))PPh_2\}]$ [2.19]

[Bis(diphenylphosphino)methine] [ferrocenylmercury(II)]-tetracarbonylmolybdenum(0)

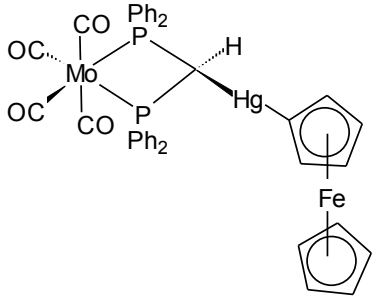

(0.55 g, 77%); m.p. 193-196°C; (Found: C, 48.13; H, 3.16 %; $C_{39}H_{30}O_4P_2FeHgMo$ requires C, 47.95; H, 3.07%); FTIR ν(CO)(THF)/cm^{-1} 2018s, 1912s, and 1881s; ^{1}H-NMR δ_H (200 MHz; $CDCl_3$); 3.24 [2 H, t, Jab 3.35 Hz, Ha], 3.72 [5 H, s, C_5H_5], 4.14 [2 H, t, Jab 3.35 Hz, Hb], 5.09 [1 H, t, ^2J(PH) 7.78 Hz, P_2CH], 7.31-7.98 [20 H, m, Ph]; ^{31}P NMR δ_P (80 MHz; $CDCl_3$): 11.41 [s, ^2J(PHg) 88.0 Hz, P_2Cr].

$[W(CO)_4\{PPh_2CH(Hg(C_5H_4)Fe(C_5H_5))PPh_2\}]$ [2.20]

[Bis(diphenylphosphino)methine] [ferrocenylmercury(II)]-tetracarbonyltungsten(0)

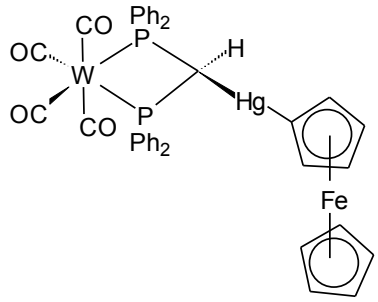

(0.54 g, 69%); m.p. 182-185°C; (Found: C, 44.15; H, 2.81 %; $C_{39}H_{30}O_4P_2FeHgW$ requires C, 43.99; H, 2.82%); FTIR ν(CO)(THF)/cm^{-1} 2011s, 1903s, 1893s, and 1873s; ^{1}H NMR δ_H (200 MHz; $CDCl_3$): 3.25 [2 H, t, Jab 3.35 Hz, Ha], 3.72 [5 H, s, C_5H_5], 4.16 [2 H, t, Jab 3.34 Hz, Hb], 5.89 [1 H, t, ^2J(PH) 8.26 Hz, P_2CH], 7.35-7.90 [20 H, m, Ph]; ^{31}P NMR δ_P (80 MHz; $CDCl_3$): -14.09 [t, ^2J(PHg), 89.9, ^1J(PW) 198.4 Hz, P_2W].

$[Cr(CO)_4\{PPh_2CH(HgCl)PPh_2\}]$ [2.21]

[Bis(diphenylphosphino)methine][chloromercury(II)]-tetracarbonylchromium(0)

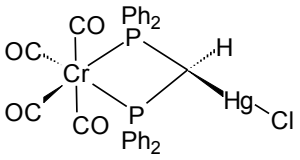

Method 1

$BuLi^n$ (0.77 cm^3; 1.10 mmol) was added to a solution of tetracarbonyl-bis(diphenylphosphinomethane)chromium(0) (0.40 g; 0.73 mmol) in THF (15 cm^3) at 0° C. The solution was stirred for 2 hours at 0°C. The resulting lithiated derivative was transferred via a canula into a solution of mercurychloride (0.39 g; 1.46 mmol) in THF (20 cm^3) at 0°C over a period of 30 minutes. The resulting solution was warmed to room temperature and allowed to stir for 2 hours. The solvent was evaporated under reduced pressure, the residue washed with water and dried. It was then chromatographed on silica gel using CH_2Cl_2/hexane (30% CH_2Cl_2/hexane) and finally 50% CH_2Cl_2/hexane to give the desired product.

Method 2

Mercurychloride (0.15 g; 1.46 mmol) was added to a solution of **[2.23]** (0.71 g, 0.55 mmol) in THF (20 cm^3). The resultant mixture was gently refluxed for 1 hour. The

solution was allowed to cool and the solvent concentrated under reduced pressure to precipitate the desired product. The product was washed with water (2 x 5 cm^3) and ethanol (2 x 5 cm^3).

(0.39 g, 91%); m.p. 184-186°C; (Found: C, 44.2; H, 2.3 %; $C_{29}H_{21}ClO_4P_2CrHg$ requires C, 44.46; H, 2.68 %); FTIR ν(CO)(THF)/cm^{-1} 2006, 1906, 1884 and 1824; ^{1}H NMR δ_H (200 MHz; $CDCl_3$): 5.75 [1 H, t, ^2J(PHg) 8.50 Hz, P_2CH], 7.36-7.78 [20 H, m, Ph]; ^{31}P NMR δ_P (80 MHz; $CDCl_3$): 41.7 [s, ^2J(PHg) 212.4 Hz, P_2Cr].

$[Cr(CO)_4\{PPh_2CH(HgHdptc)PPh_2\}]$ [2.22]

[Bis(diphenylphosphino)methine][1,5-diphenylthio-carbazonemercury(II)]tetracarbonylchromium(0)

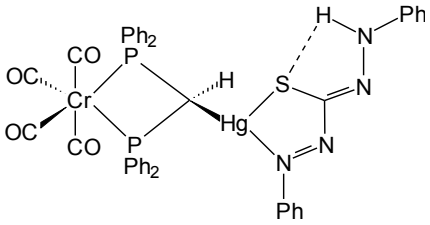

Solid H_2dptc (0.03 g, 0.13 mmol) was added to a solution of **[2.21]** (0.1 g; 0.13 mmol) in CH_2Cl_2. This was followed by the addition of triethylamine (0.04 cm^3; 0.26 mmol). The resulting brick-red solution was stirred for 1 hour at room temperature, thereafter it was filtered to remove any triethylammonium-hydochloride formed during the reaction. The filtrate was evaporated under reduced pressure and the residue recrystallised from CH_2Cl_2/MeOH to yield a dark red product.

(0.11 g, 85%); m.p. 163°C; (Found: C, 50.1; H, 3.1; N, 5.5; S, 3.0%; $C_{42}H_{32}N_4O_4P_2SCrHg$ requires C, 50.28; H, 3.19; N, 5.58; S, 3.19%); FTIR ν(CO)(THF)/cm^{-1} 2003s, 1913m, 1889s, and 1874s; ^{1}H NMR δ_H (200 MHz; $CDCl_3$): ^{1}H, δ 5.75 [1 H, t, ^2J(PH) 8.24 Hz, P_2CH], 7.01-7.90 [30 H, m, Ph], 8.96 [1 H, s, NH]; ^{31}P NMR δ_P (80 MHz, $CDCl_3$): δ 40.21 [s, ^2J(PHg) 194.2 Hz, P_2Cr].

$[Cr(CO)_4(PPh_2CHPPh_2)]_2Hg$ [2.23]

Bis[bis(diphenylphosphino)methine][tetracarbonyl-chromium(0)]mercury(II)

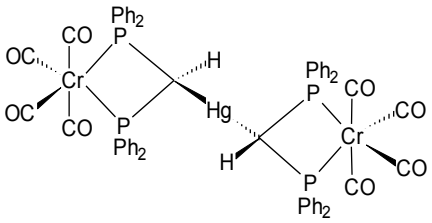

$BuLi^n$ (0.77 cm^3; 1.10 mmol) was added to a solution of tetracarbonyl-bis(diphenylphosphinomethane)chromium(0) (0.40 g; 0.73 mmol) in THF (15 cm^3) at 0°C. The solution was stirred for 1.5 hours. Mercury(II)chloride (0.098.g; 0.36 mmol) was added to the solution. The resulting solution was then allowed to stir for 2 hours. The solvent was concentrated under reduced pressure to precipitate the product. The product was filtered and washed with water (2 x 5 cm^3) and ethanol (2 x 5 cm^3). Recrystallisation from dichloromethane/methanol yield yellow crystalline material.

(0.31 g, 68%); m.p. 210°C(dec); (Found: C, 53.6; H, 3.2%; $C_{58}H_{42}O_8P_4Cr_2Hg$ requires C, 53.77; H, 3.24%); FTIR ν(CO)(THF)/cm^{-1} 2006, 1906, 1884 and 1824; ^{1}H NMR δ_H (200 MHz; $CDCl_3$): 4.17 [2 H, t, ^2J(PH) 9.21 Hz, P_2CH], 7.16-7.51 [40 H, m, Ph]; ^{31}P NMR δ_P (80 MHz; $CDCl_3$): 40.5 [s, ^2J(PHg) 135.1 Hz, P_2Cr].

$[Mo(CO)_4(PPh_2CHPPh_2)]_2Hg$ [2.24]

Bis[bis(diphenylphosphino)methine][tetracarbonyl-molybdenum(0)]mercury(II)

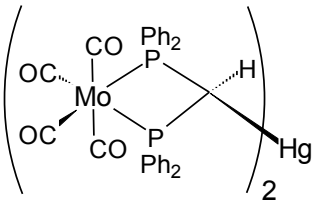

(0.32 g, 70%); m.p. 201-202°C(dec); (Found: C, 54.4; H, 3.1%; $C_{58}H_{42}O_8P_4Cr_2Hg$ requires C, 54.06; H, 3.26%); FTIR ν_{max}(CO)(THF)/cm^{-1} 2015, 1907, 1883; ^{1}H NMR δ_H (200 MHz; $CDCl_3$): 4.2 [2 H, t, ^2J(PH) 8.8 Hz, P_2CH], 7.12-7.61 [40 H, m, Ph]; ^{31}P NMR δ_P (80 MHz; $CDCl_3$): 16.9 [s, ^2J(PHg) 123.8 Hz, P_2Cr].

$[Cr(CO)_4\{PPh_2CH(HgC_6H_4)$-*p*$OCH_3)PPh_2\}]$ [2.25]

[Bis(diphenylphosphino)methine][(4-methyloxybenzylidene)-mercury(II)]tetracarbonylchromium(0)

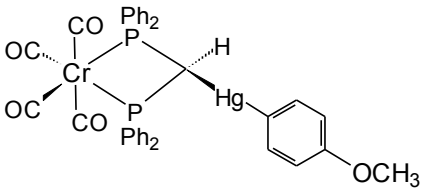

This was prepared in a similar fashion to the methyl analog using *p*-methoxybenzylmercury(II)chloride. (0.31 g, 72%); m.p. 189-190°C; (Found: C, 50.5; H, 3.2%; $C_{36}H_{28}O_5P_2CrHg$ requires C, 50.56; H, 3.27%); ν(CO)(THF)/cm^{-1} 2002, 1913, 1888 and 1872; ^{1}H NMR δ_H (200 MHz; $CDCl_3$); 3.68 [3 H, s, OCH_3], 4.95 [1 H, t, ^2J(PHg) 8.39 Hz, P_2CH], 6.25 [2 H, d, ^2Jab 8.58 Hz, Ha], 6.69 [2 H, d, ^2Jab 8.64 Hz, Hb]; ^{31}P NMR δ_P (80 MHz; $CDCl_3$): 35.55 [s, ^2J(PHg) 88.4 Hz, P_2Cr]

$[W(CO)_4\{PPh_2CH(HgC_6H_4)$-*p*-$OCH_3)PPh_2\}]$ [2.26]

Bis(diphenylphosphinomethine)(4-methyloxybenzylidene)-mercury(II)]tetracarbonyltungsten(0)

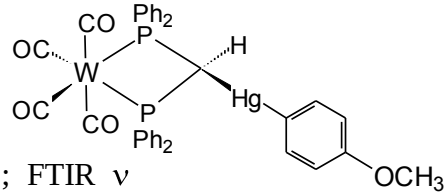

(0.34 g, 69%); m.p. 181-182°C; (Found: C, 43.8; H, 2.7%; $C_{36}H_{28}O_5P_2HgW$ requires C, 43.81; H, 2.84%); FTIR ν (CO)(THF)/cm^{-1} 2011, 1910, 1893 and 1872; ^{1}H NMR δ_H (200 MHz; $CDCl_3$): 3.69 [3 H, s, OCH_3], 5.89 (1 H, t, ^2J(PH) 7.83 Hz, P_2CH], 6.25 [2 H, d, ^3Jab 11.54 Hz, Ha], 6.68 [2 H, d, ^3Jab 8.62 Hz, Hb], 7.34-7.85 [20 H, m, Ph]; ^{31}P NMR δ_P (80 MHz; $CDCl_3$): -13.42 [s, ^2J(PHg) 81.9 Hz, ^1J(PW) 198.5 Hz, P_2W].

$[Cr(CO)_4\{PPh_2CH(HgC_6H_4)$-*p*-$N(CH_3)_2)PPh_2\}]$ [2.27]

[Bis(diphenylphosphino)methine][(4-N-dimethylbenzylidene)-mercury(II)]tetracarbonylchromium(0)

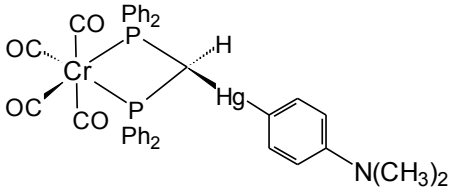

Tetracarbonyl-bis(diphenylphosphinomethane)chromium(0) (0.35 g; 0.63 mmol) was dissolved in THF (15 cm^3). The solution was cooled to 0°C and BuLi^n (0.59 cm^3; 0.94 mmol) was added. The resulting solution was stirred for 1.5 hours, followed by the addition of p-*N*-dimethylmercury(II)chloride (0.49 g; 0.88 mmol).The mixture was allow to stir for 2 hours. The yellow precipitate obtained was filtered, washed with water (5 cm^3), ethanol (5 cm^3) and THF (5 cm^3) and dried in vacuo.

(0.45 g, 82%); m.p. >250°C ; (Found: C, 51.15; H, 3.51; N, 1.48%; $C_{37}H_{31}NO_4P_2CrHg$ requires C, 51.19; H, 3.57; N, 1.62%); FTIR ν(CO)(THF)/cm^{-1} 1993, 1900, 1878 and 1857; ^{1}H NMR δ_H (200 MHz; DMSO- d_6): 2.86 [6 H, s, $N(CH_3)_2$], 5.19 [1 H, t, ^2J(PH) 7.9 Hz, P_2CH], 6.68 [2 H, d, ^2Jab 8.24 Hz, Ha], 7.24 [2 H, d, ^2Jab 8.46 Hz, Hb]; ^{31}P NMR δ_P (80 MHz; DMSO- d_6): 37.18 [s, ^2J(PHg) 80.9 Hz, P_2Cr].

$[W(CO)_4\{PPh_2CH(HgC_6H_5)$-*p*-$N(CH_3)_2)PPh_2\}]$ [2.28]

[Bis(diphenylphosphino)methine][(4-N-dimethylbenzylidene)-mercury(II)]tetracarbonyltungsten(0)

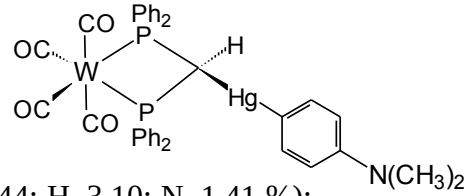

(0.53 g, 83%); m.p. >250(dec)°C; (Found: C,44.2; H, 3.2; N, 1.3 %; $C_{37}H_{31}NO_4P_2HgW$ requires C, 44.44; H, 3.10; N, 1.41 %); ν(CO)(THF)/cm^{-1} 2011, 1910, 1893 and 1869; ^{1}H NMR δ_H (200 MHz; DMSO- d_6): 2.77 [6 H, s, $N(CH_3)_2$], 5.25 [1 H, t, ^2J(PH) 7.9 Hz, P_2CH], 6.21 [2 H, d, ^2Jab 8.44 Hz, Ha], 6.46 [2 H, d, ^2Jab 8.54 Hz, Hb]; ^{31}P NMR δ_P (80 MHz; DMSO- d_6): -10.46 [s, ^2J(PHg) 76.0 Hz, ^2J(PW) 192.8 Hz P_2W]

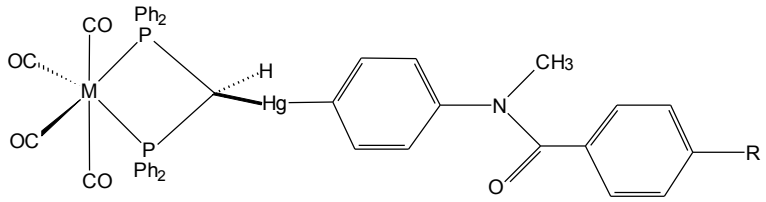

$[Cr(CO)_4\{PPh_2CH(HgC_6H_4N(CH_3)CO\text{-}C_6H_4\text{-}OC_2H_5)PPh_2\}]$ [2.29]

[Bis(diphenylphosphino)methine][4-(4-ethyloxybenzylidene-N-methylanilino)mercury(II)]tetracarbonylchromium(0)

(0.43 g, 69%); m.p. 223-224°C; (Found: C, 53.81; H, 3.71; N, 1.28%; $C_{45}H_{37}NO_6P_2CrHg$ requires C, 53.92; H, 3.69; N, 1.40 %); FTIR ν(CO)(THF)/cm^{-1} 2001s, 1911s, 1884b and 1860sh; ^{1}H NMR δ_H (200 MHz; $CDCl_3$): 1.19 [3 H, t, ^3J(HH) 7.18 Hz, OCH_2CH_3], 3.29 [3 H, s, $NHCH_3$], 3.05 [2 H, q, ^3J(HH) 7.14 Hz, OCH_2 CH_2], 4.90 [1 H, t, ^2J(PH) 8.90 Hz, P_2CH], 6.12 [2 Hz, d, $^3J_{ab}$ 8.21 Hz, ^3J(PHg) 126 Hz, H_a], 6.58 [2 H, d, $^3J_{ab}$ 8.73 Hz, H_b], 6.76 [2 H, d, $^3J_{ab}$ 8.27 Hz, H_a], 7.07 [2 H, d, $^3J_{ab}$ 8.74 Hz, H_b], 7.22-7.83 [20 H, m, Ph]; ^{31}P NMR δ_P (80 MHz; $CDCl_3$): 35.93 [s, ^2J(PHg) 90.3 Hz, P_2Cr].

$[Cr(CO)_4\{PPh_2CH(HgC_6H_4N(CH_3)CO\text{-}C_6H_4\text{-}OC_5H_{11})PPh_2\}]$ [2.30]

[Bis(diphenylphosphino)methine][4-(4-pentyloxybenzylidene-N-methylanilino)mercury(II)]tetracarbonylchromium(0)

(0.44 g, 71%); m.p. 194-195°C; (Found: C, 55.15; H, 4.37; N, 1.28%; $C_{48}H_{43}NO_6P_2CrHg$ requires C, 55.20; H, 4.12; N, 1.34 %); FTIR ν(CO)(THF)/cm^{-1} 2002s, 1910s, 1884b and 1860sh; ^{1}H NMR δ_H (200 MHz; $CDCl_3$): 0.81 [2 H, t, ^3J(HH) 5.67 Hz, CH_2CH_3], 1.21 [4 H, m, $(CH_2)_2$], 1.65 [2 H, sext, ^3J(HH) 6.52 Hz, $CH_2CH_2CH_3$], 3.29 [3 H, s, $NHCH_3$], 3.83 [2 H, t, ^3J(HH) 5.24 Hz, OCH_2 CH_2], 4.91 [1 H, t, ^2J(PH) 8.60 Hz, P_2CH], 6.14 [2 Hz, d, $^3J_{ab}$ 8.06 Hz, ^3J(PHg) 126 Hz, H_a], 6.55 [2 H,

d, $^{3}J_{ab}$ 8.74 Hz, H_b], 6.72 [2 H, d, $^{3}J_{ab}$ 8.21 Hz, H_a], 7.08 [2 H, d, $^{3}J_{ab}$ 8.75 Hz, H_b], 7.22-7.83 [20 H, m, Ph]; ^{31}P NMR δ_P (80 MHz; $CDCl_3$): 35.94 [s, ^{2}J(PHg) 90.7 Hz, P_2Cr].

$[Cr(CO)_4\{PPh_2CH(HgC_6H_4N(CH_3)CO\text{-}C_6H_4\text{-}OC_7H_{15})PPh_2\}]$ [2.31]

[Bis(diphenylphosphino)methine][4-(4-heptyloxybenzylidene-N-methylanilino)mercury(II)]tetracarbonylchromium(0)

(0.38 g, 59%); m.p. 189-190°C; (Found: C, 55.8; H, 4.4; N, 1.2 %; $C_{50}H_{47}NO_6P_2CrHg$ requires C, 56.00; H, 4.38; N, 1.31 %); FTIR ν(CO)(THF)/cm^{-1} 2002s, 1911s, 1884b and 1859sh; ^{1}H NMR δ_H (200 MHz; $CDCl_3$): 0.87 [2 H, t, ^{3}J(HH) 5.87 Hz, CH_2CH_3], 1.26 [12 H, m, $(CH_2)_6$], 1.71 [2 H, sext, ^{3}J(HH) 6.62 Hz, CH_2 CH_2CH_3], 3.35 [3 H, s, $NHCH_3$], 3.88 [2 H, t, ^{3}J(HH) 5.33 Hz, OCH_2 CH_2], 4.98 [1 H, t, ^{2}J(PH) 8.33 Hz, P_2CH], 6.20 [2 H, d, $^{3}J_{ab}$ 7.79 Hz, ^{3}J(PHg) 126 Hz, H_a], 6.62 [2 H, d, $^{3}J_{ab}$ 8.48 Hz, H_b], 6.79 [2 H, d, $^{3}J_{ab}$ 7.73 Hz, H_a], 7.14 [2 H, d, $^{3}J_{ab}$ 8.20 Hz, H_b], 7.24-7.88 [20 H, m, Ph]; ^{31}P NMR δ_P (80 MHz; $CDCl_3$): 35.97 [s, ^{2}J(PHg) 90.8 Hz, P_2Cr].

$[Cr(CO)_4\{PPh_2CH(HgC_6H_4N(CH_3)CO\text{-}C_6H_4\text{-}OC_9H_{19})PPh_2\}]$ [2.32]

[Bis(diphenylphosphino)methine][4-(4-nonyloxybenzylidene-N-methylanilino)mercury(II)]tetracarbonylchromium(0)

(0.59 g, 59%); m.p. 183-184°C; (Found: C, 56.88; H, 4.62; N, 1.37%; $C_{52}H_{51}NO_6P_2CrHg$ requires C, 56.75; H, 4.64; N, 1.27%); FTIR ν(CO)(THF)/cm^{-1} 2001s, 1910s, 1885b and 1860sh; ^{1}H-NMR δ_H (200 MHz; $CDCl_3$): 0.87 [2 H, t, ^{3}J(HH) 5.87 Hz, CH_2CH_3], 1.26 [18 H, m, $(CH_2)_6$], 1.71 [2 H, sext, ^{3}J(HH) 6.62 Hz, CH_2 CH_2CH_3], 3.35 [3 H, s, $NHCH_3$], 3.88 [2 H, t, ^{3}J(HH) 5.33 Hz, OCH_2 CH_2], 4.98 [1 H, t, ^{2}J(PH) 8.33 Hz, P_2CH], 6.20 [2 H, d, $^{3}J_{ab}$ 7.79 Hz, ^{3}J(PHg) 126 Hz, H_a], 6.62 [2 H, d, $^{3}J_{ab}$ 8.48 Hz, H_b], 6.79 [2 H, d, $^{3}J_{ab}$ 7.73 Hz, H_a], 7.14 [2 H, d, $^{3}J_{ab}$ 8.20 Hz, H_b], 7.24-7.88 [20 H, m, Ph]; ^{31}P NMR δ_P (80 MHz; $CDCl_3$): 35.97 [s, ^{2}J(PHg) 90.8 Hz, P_2Cr].

$[Cr(CO)_4\{PPh_2CH(HgC_6H_4N(CH_3)CO\text{-}C_6H_4\text{-}OC_{12}H_{25})PPh_2\}]$ [2.33]

[Bis(diphenylphosphino)methine][4-(4-dodecyloxybenzylidene-N-methylanilino)mercury(II])tetracarbonylchromium(0)

(0.38 g, 55%); mp. 169-170°C; (Found: C, 57.64; H, 5.01; N, 1.23%; $C_{55}H_{57}NO_6P_2CrHg$ requires C, 57.82; H, 4.99; N, 1.23 %); FTIR ν(CO)(THF)/cm^{-1}; 2001s, 1911s, 1884b and 1860sh; ^{1}H NMR δ_H (200 MHz; $CDCl_3$): 0.88 [2 H, t, ^3J(HH) 5.88 Hz, CH_2CH_3], 1.26 [18 H, m, $(CH_2)_9$], 1.72 [2 H, sext, ^3J(HH) 6.61 Hz, CH_2 CH_2CH_3], 3.35 [3 H, s, $NHCH_3$], 3.90 [2 H, t, ^3J(HH) 5.60 Hz, OCH_2 CH_2], 4.99 [1 H, t, ^2J(PH) 8.0 Hz, P_2CH], 6.21 [2 H, d, $^3J_{ab}$ 7.27 Hz, ^3J(PHg) 126 Hz, H_a], 6.25 [2 H, d, $^3J_{ab}$ 7.88 Hz, H_b], 6.80 [2 H, d, $^3J_{ab}$ 6.69 Hz, H_a], 7.16 [2 H, d, $^3J_{ab}$ 8.06 Hz, H_b], 7.24-7.89 [20 H, m, Ph]; ^{31}P NMR δ_P (80 MHz; $CDCl_3$): 35.94 [s, ^2J(PHg) 90.8 Hz, P_2Cr].

$[Cr(CO)_4\{PPh_2CH(AuPPh_3)PPh_2\}]$[13] **[2.34]**

[Bis(diphenylphosphino)methine][triphenylphosphine-aurate(I)]tetracarbonylchromium(0)

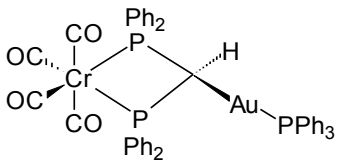

A solution of BuLi in hexane (0.34 cm^3; 0.54 mmol) was added to a solution of $[Cr(CO)_4(dppm)]$ (0.2 g; 0.36 mmol) in THF (15 cm^3) at 0°C. The mixture was stirred for 1.5 hours, whereafter triphenylphosphirylauric(I) chloride (0.21 g; 0.43 mmol) was added. The resulting solution was allowed to warm to room and stirred for a further 1.5 hours. The solvent was removed under reduced pressure and the resulting yellow crude material recrystallised from CH_2Cl_2/MeOH to a give yellow crystalline product.

(0.28 g, 76%); m.p. 119°C(dec); (Found: C, 56.2; H, 3.6 %; $C_{47}H_{36}O_4P_3AuCr$ requires C, 56.08; H, 3.58 %); FTIR ν(CO)(THF)/cm^{-1}; 1997s, 1902s, 1885s, and 1859s; ^{1}H NMR δ_H (200 MHz; $CDCl_3$): 5.20 [1 H, q, ^2J(HP) 9.3 Hz, ^2J(HP) 9.3 Hz, P_2CH], 6.81-7.89 [35 H, m, Ph]; ^{31}P NMR δ_P (80 MHz; $CDCl_3$): 35.81 [d, ^2J(PP) 9.9 Hz, P_2Cr]; 40.13 [t, ^3J(PP) 22.0 Hz, PPh_3].

$[Mo(CO)_4\{PPh_2CH(AuPPh_3)PPh_2\}]$[13] **[2.35]**

[Bis(diphenylphosphino)methine][triphenylphosphine-aurate(I)]tetracarbonylmolybdenum(0)

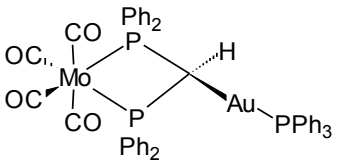

(0.28 g, 73%); m.p. 142-143°C; (Found: C, 53.5; H, 3.3 %; $C_{47}H_{36}O_4P_3AuMo$ requires C, 53.73; H, 3.43 %); FTIR ν(CO)(THF)/cm^{-1}; 2011s, 1909s, 1900sh, and 1863s; ^{1}H NMR δ_H (200 MHz; $CDCl_3$): 5.24 [1 H, q, ^2J(PH) 8.7 Hz, ^2J(PH) 8.7 Hz, P_2CH], 6.81-7.90 [35 H, m, Ph]; ^{31}P NMR δ_P (80 MHz; $CDCl_3$): 12.61 [d, ^3J(PP) 10.38 Hz, P_2Mo], 40.19 [t, ^3J(PP) 21.9 Hz, PPh_3].

$[W(CO)_4\{PPh_2CH(AuPPh_3)PPh_2\}]$[13] **[2.36]**

[Bis(diphenylphosphino)methine][triphenylphosphine-aurate(I)]tetracarbonyltungsten(0)

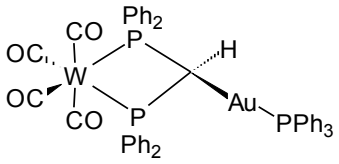

(0.32 g, 77%); m.p 130°C(dec); (Found: C, 49.7; H, 3.1 %; $C_{47}H_{36}O_4P_3AuW$ requires C, 49.58; H, 3.16 %); FTIR ν(CO)(THF)/cm^{-1}; 2005s, 1902s, 1875s 1859s; ^{1}H NMR δ_H (200 MHz; $CDCl_3$): 6.10 [1 H, q, ^2J(PH) 8.9 Hz, ^3J(PH) 8.9 Hz , P_2CH] 6.85-7.90 [30 H, m, Ph]; ^{31}P NMR δ_P (80 MHz; $CDCl_3$): -11.93 [d, ^3J(PP) 10.1 Hz, ^1J(PW) 192.9 Hz, P_2W], 40.26 [t, ^3J(PP) 22.0 Hz, PPh_3].

$[Cr(CO)_4\{PPh_2CH(AuPEtPh_2)PPh_2\}]$ [2.37]

[Bis(diphenylphosphino)methine][ethyldiphenyl-phosphineaurate(I)]tetracarbonylchromium(0)

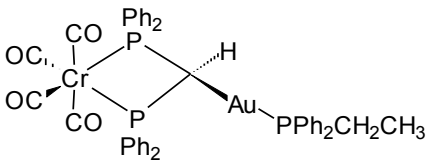

(0.25 g, 0.71%); m.p. 84-85°C (Found: C, 53.7; H, 3.7 %; $C_{43}H_{36}O_4P_3AuCr$ requires C, 53.88; H, 3.76 %); FTIR ν(CO)(THF)/cm^{-1} 1998s, 1903s, 1885s, and 1860s; ^{1}H-NMR δ_H (200 MHz; $CDCl_3$) 0.60 [3 H, dt, ^3J(PH) 17.6 Hz, -CH_3] 1.90 [dq, 2 H, ^2J(PH) 13.6 Hz, -CH_2-] 5.09 [1 H, q, ^2J(PH) 9.3 Hz, ^3J(PH) 9.3, P_2CH] 7.05-7.98 [30 H, m, Ph]; ^{31}P NMR δ_P (80 MHz; $CDCl_3$) 12.26 [d, ^3J(PP) 10.38 Hz, P_2Cr], 40.19 [t, ^3J(PP) 21.9 Hz, PPh_3].

$[Mo(CO)_4\{PPh_2CH(AuPEtPh_2)PPh_2\}]$ [2.38]

[Bis(diphenylphosphino)methine][ethyldiphenyl-phosphineaurate(I)]tetracarbonylmolybdenum(0)

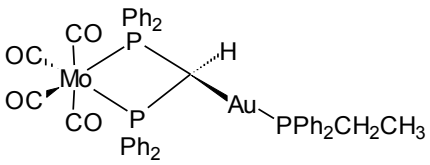

(0.26 g, 0.73%); m.p. 86-87°C (Found: C, 51.5; H, 3.7 %; $C_{43}H_{36}O_4P_3AuMo$ requires C, 51.51; H, 3.59 %); FTIR ν(CO)(THF)/cm^{-1} 2010s, 1909s, 1898s, and 1860s; ^{1}H-NMR δ_H (200 MHz; $CDCl_3$) 0.61 [3 H, dt, ^3J(PH) 17.8 Hz, -CH_3] 1.90 [dq, 2 H, ^2J(PH) 16.2 Hz, -CH_2-] 5.19 [1 H, q, ^2J(PH) 8.7 Hz, ^3J(PH) 8.7 Hz, P_2CH] 7.01-8.90 [30 H, m, Ph]; ^{31}P NMR δ_P (80 MHz; $CDCl_3$) 12.26 [d, ^3J(PP) 10.38 Hz, P_2Mo], 40.19 (t, ^3J(PP) 21.9 Hz, PPh_3].

$[W(CO)_4\{PPh_2CH(AuPEtPh_2)PPh_2\}]$ [2.39]

[Bis(diphenylphosphino)methine][ethyldiphenyl-phosphineaurate(I)]tetracarbonyltungsten(0)

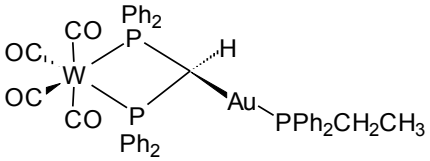

(0.27 g, 69%); m.p. 90°C; (Found: C, 47.1; H, 3.2 %; $C_{43}H_{36}AuCO_4P_3W$ requires C, 47.36; H, 3.30 %); FTIR ν(CO)(THF)/cm^{-1} 2005s, 1905s, 1876s, and 1863s; ^{1}H-NMR δ_H (200 MHz; $CDCl_3$) 0.61 [3 H, dt, ^3J(PH) 17.9 Hz, -CH_3] 1.90 [dq, 2 H, ^2J(PH) 16.2 Hz, -CH_2-] 6.01 [1 H, q, ^2J(PH) 8.9 Hz, ^3J(PH) 8.9 Hz, P_2CH] 6.95-7.90 [30 H, m, Ph]; ^{31}P NMR δ_P (80 MHz; $CDCl_3$) -12.26 [d, ^3J(PP) 10.85 Hz, ^1J(PW) 192.3 Hz, P_2W]; 39.07 [t, ^3J(PP) 21.9 Hz, PPh_3].

$[Cr(CO)_4\{PPh_2CH(AuAsPh_3)PPh_2\}]$ [2.40]

[Bis(diphenylphosphino)methine][triphenylarsenate-

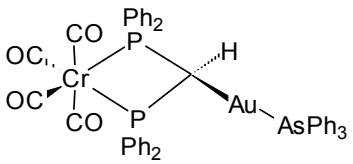

aurate(I)]tetracarbonylchromium(0)

(0.25 g, 67%); m.p. 174°C(dec); (Found: C, 53.6; H, 3.3 %; $C_{47}H_{36}AsO_4P_2AuCr$ requires C, 53.73; H, 3.42 %); FTIR ν(CO)(THF)/cm^{-1} 1998s, 1903s, 1885s, and 1860s; ^{1}H-NMR δ_H (200 MHz; $CDCl_3$) 5.29 [1 H, t, ^2J(PH) 8.9 Hz, P_2CH] 6.91-7.90 [35 H, m, Ph]; ^{31}P NMR δ_P (80 MHz; $CDCl_3$) 35.9 [s, P_2Cr].

$[W(CO)_4\{PPh_2CH(AuAsPh_3)PPh_2\}]$ [2.41]

[Bis(diphenylphosphino)methine][triphenylarsenate-aurate(I)]tetracarbonyltungsten(0)

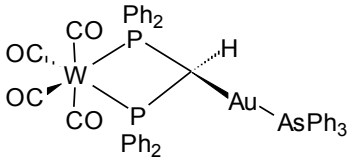

(0.29 g, 69%); m.p. 137°C(dec); (Found: C, 47.6; H, 3.0 %; $C_{47}H_{36}AsO_4P_2AuW$ requires C, 47.74; H, 3.04 %); FTIR ν(CO)(THF)/cm^{-1} 2006s, 1905s, 1876s, and 1860s; ^{1}H-NMR δ_H (200 MHz; $CDCl_3$) 6.20 [1 H, q, ^2J(PH) 8.4 Hz, P_2CH] 6.91-7.90 [35 H, m, Ph]; ^{31}P NMR δ_P (80 MHz; $CDCl_3$) -11.8 [s, ^1J(PW) 193.0 Hz, P_2W].

8.4 Preparations pertaining to Chapter 3

[Pt(mnt)dppm][14] [3.1]

[Bis(diphenylphosphino)methane](1,2-maleonitrile-1,2 dithiolato)platinum(II)

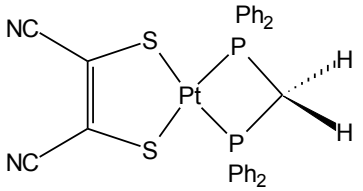

Maleonitrile[15] (0.15 g; 0.8 mmol) was added to a suspension of $PtCl_2$dppm[16] (0.42 g; 0.65 mmol) in methanol. The solution was stirred at 40°C for 6 hrs. The faint pink precipitate was filtered, washed with water (5 cm^3) and ethanol (5 cm^3) and dried in vacuo.

(0.45 g, 79%); m.p. >250°C; (Found: C, 48.12; H, 3.10; N, 3.65; S, 8.49 %; $C_{29}H_{22}N_2P_2S_2Pt$ requires C, 48.40; H, 3.06; N, 3.91; S, 8.91%); FTIR (KBr)/cm^{-1} 2201vs (CN) 1478vs 1436vs 1352m 1334w 1307w 1187m 1153s 1101vs 997m 732vs 714vs 692vs 547vs 488vs 475m 463w; ^{1}H NMR δ_H (300 MHz; $CDCl_3$) 4.72 [2 H, t, ^2J(PH) 10.2 Hz, ^3J(PtH) 46.8 Hz, P_2CH], 7.40-7.80 [20 H, m, Ph], ^{31}P NMR δ_P(121 MHz; $CDCl_3$) -48.32 [s, ^1J(PtP) 2387.5 Hz, P_2CH_2].

[Pd(mnt)dppm] [3.2]

[Bis(diphenylphosphino)methane](1,2-maleonitrile-1,2 dithiolato)palladium(II)

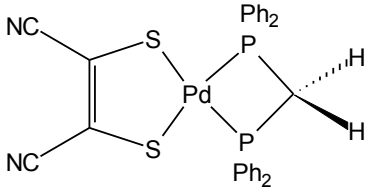

(0.38 g, 75%); m.p. 246-247°C; (Found: C, 55.12; H, 3.41; N, 4.22; S, 9.83 %; $C_{29}H_{22}N_2P_2S_2Pt$ requires C, 55.20; H, 3.49; N, 4.46; S, 10.16%); FTIR (KBr)/cm^{-1} 2198vs (CN) 1477vs 1438vs 1348m 1187m 1146s 1100vs 997m 730vs 714s 691vs 663s 537s 500vs 472m 459m; ^{1}H NMR δ_H (300 MHz; $CDCl_3$) 4.40 [2 H, t, ^2J(PH) 9.9 Hz, P_2CH], 7.44-7.74 [20 H, m, Ph], ^{31}P NMR δ_P(121 MHz; $CDCl_3$) -39.37 [s, P_2CH_2].

[Pt(dmit)dppm] [3.3]

[Bis(diphenylphosphino)methane](1,3-dithiole-2-thione-4,5-dithiolato)platinum(II)

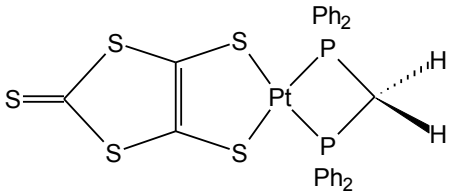

Dmit[17] (0.2 g, 0.6 mmol) was added to a solution of NaOMe (0.065 g; 1.2 mmol) in 20 cm^3 MeOH. The solution was stirred for 30 minutes. $PtCl_2$dppm (0.33 g; 0.5 mmol) was slowly added to the dark red solution and stirred overnight. The yellow/brown precipitate which formed was filtered and washed with water (5 cm^3) and ethanol (5 cm^3).

(0.31 g, 68%); m.p. >250°C; (Found: C, 43.22; H, 2.79; S, 20.58 %; $C_{28}H_{22}P_2S_5Pt$ requires C, 43.35; H, 2.84; S, 20.67%); FTIR (KBr)/cm^{-1} 1481m 1434s 1457vs 1341w 1306w 1187w 1100s 1025s 904m 770m 730vs 687vs 548vs 511vs 469s; ^{1}H NMR δ_H (300 MHz; $CDCl_3$) 4.2 [2 H, t, ^2J(PH) 10.1 Hz, ^3J(PtH) 47.3 Hz, P_2CH], 7.40-7.80 [20 H, m, Ph], ^{31}P NMR δ_P(121 MHz; $CDCl_3$) -48.02 [s, ^1J(PtP) 2430.5 Hz, P_2CH_2].

[Pd(dmit)dppm] [3.4]

[Bis(diphenylphosphino)methane](1,3-dithiole-2-thione-4,5-dithiolato)palladium(II)

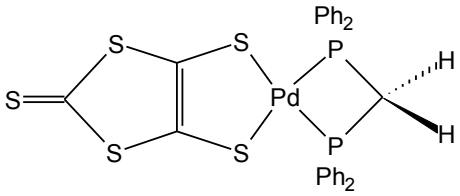

(0.28 g, 68%); m.p. 247°C; (Found: C, 48.79; H, 3.18; S, 23.01 %; $C_{28}H_{22}P_2S_5Pd$ requires C, 48.94; H, 3.20; S, 23.33%); ^{1}H NMR δ_H (300 MHz; $CDCl_3$) 4.3 [2 H, t, ^2J(PH) 10.4 Hz, P_2CH], 7.46-7.80 [20 H, m, Ph], ^{31}P NMR δ_P(121 MHz; $CDCl_3$) -39.92 [s, P_2CH_2].

[Pt(dmid)dppm] [3.5]

[Bis(diphenylphosphino)methane](1,3-dithiole-2-one-4,5-dithiolato)platinum(II)

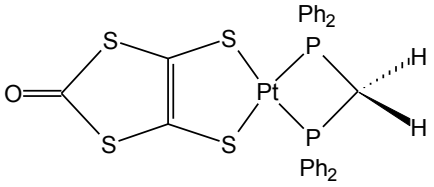

(0.3 g, 65%); m.p. >250°C; (Found: C, 44.11; H, 2.82; S, 16.54 %; $C_{28}H_{22}OP_2S_4Pt$ requires C, 44.27; H, 2.90; S, 16.88%); FTIR (KBr)/cm^{-1} 1726m 1659vs 1614vs 1482s

1435vs 1337m 1307w 1331s 1099vs 997m 881m 899m 729vs 679vs 547s 509vs 468s; ^{1}H NMR δ_H (300 MHz; $CDCl_3$) 4.5 [2 H, t, ^{2}J(PH) 10.3 Hz, ^{3}J(PtH) 46.5 Hz, P_2CH], 7.40-7.85 [20 H, m, Ph], ^{31}P NMR δ_P (121 MHz; $CDCl_3$) -48.23 [s, ^{1}J(PtP) 2435.8 Hz, P_2CH_2].

[Pd(dmid)dppm] [3.6]

[Bis(diphenylphosphino)methane](1,3-dithiole-2-one-4,5-dithiolato)palladium(II)

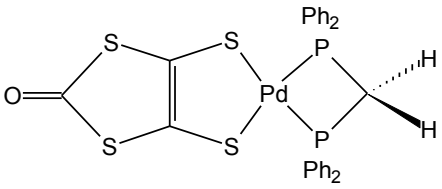

(0.25 g, 62%); m.p. 177°C(dec); (Found: C, 49.98; H, 3.22; S, 18.87 %; $C_{28}H_{22}OP_2S_4Pd$ requires C, 50.11; H, 3.28; S, 19.11%); FTIR (KBr)/cm^{-1} 1725m 1660vs 1610vs 1483m 1434vs 1309w 1188s 1138vs 1099vs 998m 894m 772m 738vs 688vs 580w 518m 501m 478m; ^{1}H NMR δ_H (300 MHz; $CDCl_3$) 4.6 [2 H, t, ^{2}J(PH) 10.3 Hz, P_2CH], 7.40-7.80 [20 H, m, Ph], ^{31}P NMR δ_P (121 MHz; $CDCl_3$) -39.67 [s, P_2CH_2].

[Pt(dddt)dppm] [3.7]

[Bis(diphenylphosphino)methane](5,6-dihydro-1,4-dithiine-2,3-dithiolato)platinum(II)

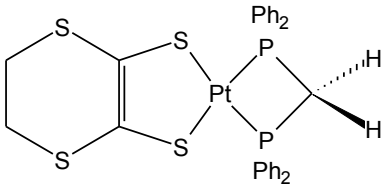

(0.26 g, 58%); m.p. >250°C; (Found: C, 45.95; H, 3.39; S, 16.56 %; $C_{29}H_{26}P_2S_4Pt$ requires C, 45.84; H, 3.42; S, 16.88%); ^{1}H NMR δ_H (300 MHz; $CDCl_3$) 3.07 [4 H, s, CH_2CH_2], 4.69 [2 H, t, ^{2}J(PH) 9.9 Hz, ^{3}J(PtH) 45.9 Hz, P_2CH], 7.38–7.84 [20 H, m, Ph], ^{31}P NMR δ_P (121 MHz; $CDCl_3$) -47.20 [s, ^{1}J(PtP) 2411.2 Hz, P_2CH_2].

[Pd(dddt)dppm] [3.8]

[Bis(diphenylphosphino)methane](5,6-dihydro-1,4-dithiine-2,3-dithiolato)palladium(II)

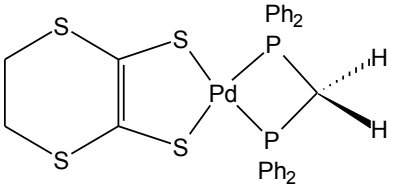

(0.23 g, 56%); m.p. >250°C; (Found: C, 51.85; H, 3.81; S, 18.87 %; $C_{29}H_{26}P_2S_4Pd$

requires C, 51.90; H, 3.87; S, 19.11%); ^{1}H NMR δ_H (300 MHz; $CDCl_3$) 3.11 [4 H, s, CH_2CH_2], 4.6 [2 H, t, ^{2}J(PH) 10.2 Hz, P_2CH], 7.42-7.82 [20 H, m, Ph], ^{31}P NMR δ_P (121 MHz; $CDCl_3$) -37.39 [s, P_2CH_2].

$[PdCl_2\{PPh_2CH(AuPPh_3)PPh_2\}]$ [3.10]

[Bis(diphenylphosphino)methine][(triphenylphosphine-aurate(I)]dichloropalladium(II)

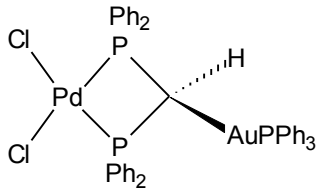

A solution of $LiN[SiMe_2]_3$ in THF (0.19 cm^3, 0.19 mmol) was added to a suspension of $[PdCl_2(dppm)]$[18] (0.1 g, 0.17 mmol) in THF at 0°C. The solution gradually becomes orange with disappearance of the suspension. The mixture was stirred at this temperature for ca. 1.5 hr. $[AuClPPh_3]$ (0.11 g, 0.23 mmol) was added to this orange solution, with an immediate formation of a precipitate. The reaction was allowed to warm up to room temperature and stirred for 30min. The cream precipitate was filtered, washed with THF, followed by methanol and dried in vacuo.

(0.12 g, 69%); m.p. 158-161°C; (Found: C, 50.3; H, 3.4 %; $C_{43}H_{36}Cl_2P_3AuPd$ requires C, 50.64; H, 3.53 %); ^{1}H NMR δ_H (200 MHz; $CDCl_3$); 4.64 [1 H, q, ^{2}J(PH) 9.16 Hz, ^{3}J(PH) 9.16 Hz, P_2CH], 6.84-8.30 [35 H, m, Ph]; ^{31}P NMR δ_P(80 MHz; $CDCl_3$); -42.56 [d, ^{3}J(PP) 9.9 Hz, P_2CH], 39.23 (t, ^{3}J(PP) 12.3 Hz, PPh_3].

$[PtCl_2\{PPh_2CH(AuPPh_3)PPh_2\}]$ [3.11]

[Bis(diphenylphosphino)methine][triphenylphosphine-aurate(I)]dichloroplatium(II)

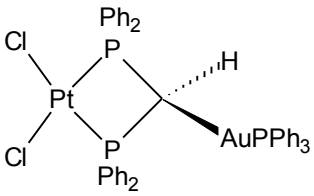

This was prepared in a similar fashion to the palladium analog. A precipitate forms immediately on addition of $[ClAuPPh_3]$. The light brown precipitate was filtered under nitrogen, washed with THF followed by methanol and dried in vacuo.

(0.15 g, 78%); m.p. 167-168°C; (Found: C, 46.3; H, 3.1 %; $C_{43}H_{36}Cl_2P_3AuPt$ requires C, 46.59; H, 3.25 %); ^{1}H NMR δ_H (200 MHz; CD_2Cl_2) 5.30 [1 H, q, ^{2}J(PH) 9.60 Hz, ^{3}J(PH)

9.60 Hz, ^{3}J(HPt) 149.6 Hz, P_2CH], 6.82-8.25 [35 H, m, Ph]; ^{31}P NMR δ_P (80 MHz; CD_2Cl_2); -52.29 [d, ^{3}J(PP) 9.9 Hz, ^{1}J(PPt) 3011.6, P_2CH], 39.35 [t, ^{3}J(PP) 10.6 Hz, PPh_3].

[(dddt)Pt{$PPh_2CH(HgPh)PPh_2$}] [3.12]

[Bis(diphenylphosphino)methine][phenylmercury(II)]-(5,6-dihydro-1,4-dithiine-2,3-dithiolato)platinum(II)

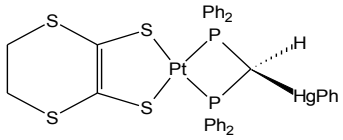

(0.11 g, 55%); m.p. 205°C; (Found: C, 40.52; H, 2.89; S, 12.35%; $C_{35}H_{30}P_2S_4HgPt$ requires C, 40.24; H, 3.03; S, 12.65%); FTIR (KBr)/cm^{-1} 2909w 1480m 1434vs 1310w 1282w 1185w 1099vs 1023m 997m 926m 841m 786s 730vs 691vs 595s 548s 511s 481m ^{1}H-NMR δ_H (300 MHz; CD_2Cl_2) 3.02 [4 H, s, CH_2CH_2], 5.36 [2 H, t, P_2CH], 6.39 [2 H, d, Ph], 7.12 [3 H, m, Ph], 7.41-8.18 [20 H, m, Ph], ^{31}P NMR δ_P (121 MHz; CD_2Cl_2)

-39.60 [s, ^{2}J(HgP) 36.8 Hz, ^{1}J(PtP) 2312.0 Hz, P_2CH].

[(dddt)Pt{$PPh_2CH(Hg(C_5H_4)Fe(C_5H_5))PPh_2$}] [3.13]

[Bis(diphenylphosphino)methine][ferrocenylmercury(II)]-(5,6-dihydro-1,4-dithiine-2,3-dithiolato)platinum(II)

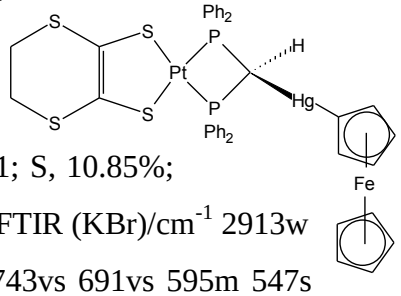

(0.14 g, 66%); m.p. 195°C(dec); (Found: C, 40.86; H, 2.91; S, 10.85%; $C_{39}H_{34}P_2S_4FeHgPt$ requires C, 40.89; H, 2.97; S, 11.18%); FTIR (KBr)/cm^{-1} 2913w (CH_2) 1481m 1435vs 1311w 1099vs 1020m 997m 779s 743vs 691vs 595m 547s 510vs 441w; ^{1}H-NMR δ_H (400 MHz; CD_2Cl_2) 2.97 [4 H, s, CH_2CH_2] 3.25 [2 H, s, C_5H_5] 3.41 [5 H, s, C_5H_5] 3.58 [2 H, s, C_5H_5], 5.6 [1 H, t, PCH_2], 7.41-8.62 [20 H, m, Ph]; ^{31}P NMR δ_P (121 MHz; CD_2Cl_2) -39.77 [s, ^{2}J(HgP) 31.8, ^{1}J(PtP) 2312.0 Hz, P_2CH].

[(dddt)Pt{$PPh_2CH(HgCH_2CH_3)PPh_2$}] [3.14]

[Bis(diphenylphosphino)methine][ethylmercury(II)]-(5,6-dihydro-1,4-dithiine-2,3-dithiolato)platinum(II)

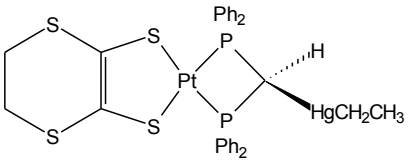

A solution of $LiN[SiMe_2]_3$ in THF (0.19 cm^3, 0.19 mmol) was added to a solution of Pt(dddt)(dppm) (0.13 g, 0.17 mmol) in THF at 0°C. The mixture was stirred at this temperature for ca. 1.5 hr. This was followed by the addition of ethylmercurychloride (0.053 g, 0.20 mmol). The reaction was allowed to warm up to room temperature and stirred for 30 min. The solvent was then removed under reduced pressure. The residue was recrystallised from dichloromethane/methanol to yield a yellow product.

(0.13 g, 69%); m.p. 212°C(dec); (Found: C, 37.64; H, 3.03; S, 12.92%; $C_{31}H_{30}P_2S_4HgPt$ requires C, 37.52; H, 2.89; S, 12.45%); ^{1}H NMR δ_H (300 MHz; CD_2Cl_2) 0.65 [3 H, t, -CH_2CH_3] 0.79 [2 H, q, CH_2CH_3] 3.06 [4 H, s, CH_2CH_2] 5.10 [1 H, t, PCH_2] 7.30-8.02 [20 H, m, Ph]; ^{31}P NMR δ_P (121 MHz; CD_2Cl_2) -40.21 [s, ^2J(HgP) 31.0, ^1J(PtP) 2359.8 Hz, P_2CH].

[(mnt)Pt{$PPh_2CH(HgPh)PPh_2$}] [3.15]

[Bis(diphenylphosphino)methine][phenylmercury(II)](1,2-maleonitrile-1,2-dithiolato)platinum(II)

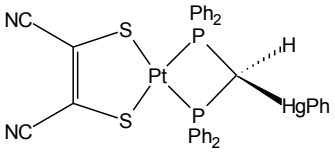

(0.13 g, 68%); m.p. >250°C; (Found: C, 42.01; H, 2.56; S, 2.55%; $C_{35}H_{26}N_2P_2S_2HgPt$ requires C, 42.15; H, 2.61; N, 2.81; S, 6.42%); ^{1}H NMR δ_H (400 MHz; CD_2Cl_2) 5.45 [1 H, t, PCH_2] 7.2-8.1 [25 H, m, Ph]; ^{31}P NMR δ_P (121 MHz; CD_2Cl_2) -40.16 [s, ^1J(PtP) 2348.5 Hz, P_2CH].

[(mnt)Pt{$PPh_2CH(Hg(C_5H_4)Fe(C_5H_5))PPh_2$}] [3.16]

[Bis(diphenylphosphino)methine][η^5-ferrocenyl-mercury(II)]-(1,2-maleonitrile-1,2-dithiolato)platinum(II)

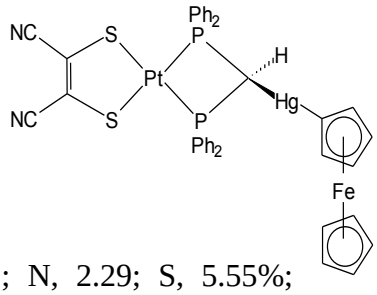

(0.12 g, 68%); m.p. >250°C; (Found: C, 42.01; H, 2.71; N, 2.29; S, 5.55%; $C_{39}H_{30}N_2P_2S_2FeHgPt$ requires C, 42.31; H, 2.72; N, 2.54; S, 5.80%); FTIR (KBr)/cm^{-1} 2201 (CN) 1483s 1435vs 1309w 1186m 1151m 1099vs 1021m 998m 815m 833m 745s 741s 689vs 593m 548s 452vs; ^{1}H NMR δ_H (300 MHz; CD_2Cl_2) 3.24 [2 H, s, C_5H_5] 3.82 [5 H, s, C_5H_5] 4.11 [2 H, s, C_5H_5], 5.5 [1 H, t, PCH_2], 7.45-8.22 [20 H, m, Ph]; ^{31}P NMR δ_P (121 MHz; CD_2Cl_2) -39.88 [s, ^1J(PtP) 2339.1 Hz, ^2J(HgP), P_2CH].

[(mnt)Pd{$PPh_2CH(Hg(C_5H_4)Fe(C_5H_5))PPh_2$}] [3.17]

[Bis(diphenylphosphino)methine][η^5-ferrocenyl-mercury(II)](1,2-maleonitrile-1,2-dithiolato)palladium(II)

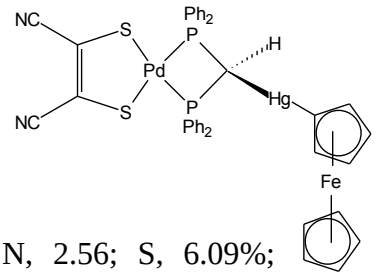

(0.10 g, 59%); m.p. >250; (Found: C, 46.11; H, 2.90; N, 2.56; S, 6.09%; $C_{39}H_{30}N_2P_2S_2FeHgPd$ requires C, 46.08; H, 2.95; N, 2.76; S, 6.30%); FTIR (KBr)/cm^{-1} 2198s (CN) 1481s 1435vs 1307w 1186m 1146m 1098s 1022m 998s 817m 781s 739s 689vs 687m 538m 505vs; ^{1}H NMR δ_H (300 MHz; CD_2Cl_2) 3.26 [2 H, s, C_5H_4] 3.86 [5 H, s, C_5H_4] 4.15 [2 H, s, C_5H_4] 4.80 [1 H, t, PCH_2] 7.40-8.11 [20 H, m, Ph]; ^{31}P NMR δ_P (121 MHz; CD_2Cl_2) -31.80 [s, P_2CH].

[Ru(η-C_5H_5)(PPh_3){$PPh_2CH_2PPh_2$}]PF_6[19] [3.18]

Bis(diphenylphosphinomethane)(η^5-cyclopentadienyl) (triphenylphosphine)ruthenium(II) hexafluorophosphate

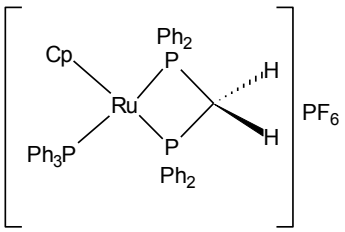

A mixture of $RuCl(PPh_3)_2(\eta^5$-$C_5H_5)$ (0.29 g, 0.40 mmol), dppm(0.15 g, 0.40 mmol) and $NaPF_6$(0.20 g, 1.2 mmol) was refluxed in methanol for about 45 min. The yellow

precipitate was filtered, washed with water (5 cm^3) and ethanol (5 cm^3) and recrystallised from CH_2Cl_2/MeOH to give a yellow crystalline product.

(0.25 g, 65%); m.p. >250°C; (Found: C, 60.3; H, 4.4 %; $C_{48}H_{42}F_6P_4Ru$ requires C, 60.19; H, 4.39%); ^{1}H NMR δ_H (200 MHz; CD_2Cl_2): 4.20 [1 H, q, ^2J(PH) 11.49 Hz, ^2J(HH) 13.8 Hz, CHH_b] 5.06 [1 H, dt, ^2J(PH) 10.2 Hz, ^2J(HH) 14.8 Hz, CH_aH], 7.18-7.58 [35 H, m, Ph]; ^{31}P NMR δ_P (121 MHz; $CDCl_3$) 1.61 [d, ^2J(PP) 35.4 Hz, P_2CH], 49.77 [t, ^2J(PP), 35.5, PPh_3], 143.8 [sep, PF_6].

[Ru(η-C_5H_5)(PPh_3){PPh_2CHPPh_2}] [3.19]

Bis(diphenylphosphinomethine)ruthenium (II)

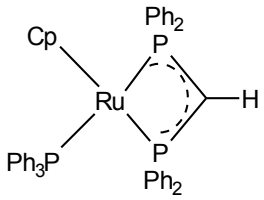

Powdered KOH (0.18 g, 0.30 mmol) was added to a stirred solution of [Ru(η-C_5H_5)(PPh_3){$PPh_2CH_2PPh_2$}]PF_6 (0.22 g, 0.22 mmol) in CH_2Cl_2 (20 cm^3). After stirring for 2 hrs., the solution was filtered under a nitrogen atmosphere. The filtrate was evaporated to dryness to yield a yellow oily residue. This was triturated with diethyl ether (20 cm^3) to yield a bright yellow solid, which was filtered, washed with diethyl ether and dried in vacuo.

(0.15 g, 88%); m.p. >250°C; (Found: C,60.3; H, 4.4 %; $C_{48}H_{41}P_3Ru$ requires C, 71.03; H, 5.06%); ^{1}H NMR δ_H (200 MHz; $CDCl_3$): 4.91 [1 H, s, P_2CH], 7.08-7.41 [35 H, m, Ph]; ^{31}P NMR δ_P (121 MHz; $CDCl_3$) 1.45 [d, ^2J(PP) 35.7 Hz, P_2CH], 48.12 [t, ^2J(PP), 35.2, PPh_3].

[Ru(η-C_5H_5)(PPh_3){$PPh_2CH(Hg(C_5H_4)Fe(C_5H_5))PPh_2$}]$PF_6$ [3.20]

Bis(diphenylphosphinomethine)[ferrocenylmercury(II)](cyclopentadienyl)-(triphenylphosphine)ruthenium(II) hexafluorophosphate

Powdered KOH (0.09 g, 0.15 mmol) was added to a stirred solution of [Ru(η-C_5H_5)(PPh_3){$PPh_2CH_2PPh_2$}]PF_6 (0.11 g, 0.11 mmol) in CH_2Cl_2 (10 cm^3). This was followed by

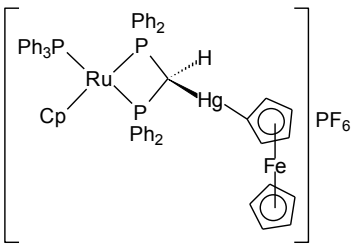

the addition of $ClHg(C_5H_4)Fe(C_5H_5)$(0.05 g, 0.13 mmol). The resulting orange solution was stirred for 2 hrs. The orange solution was concentrated under reduced pressure. Addition of hexane gave an orange solid. The product was filtered and washed with water (2 x 5 cm^3) and ethanol (2 x 5 cm^3). Recrystallisation from dichloromethane/methanol gave orange crystals.

(0.10 g, 68%); m.p. 225-227°C; (Found: C,60.3; H, 4.4 %; $C_{58}H_{50}F_6P_4FeHgRu$ requires C, 51.93; H, 3.66%); ^{1}H NMR δ_H (200 MHz; CD_2Cl_2): 3.71 [2 H, t, ^2J(Hab) 1.8 Hz, Ha], 3.81 [5 H, s, $Fe(C_5H_5)$], 4.22 (1 H, t, ^2J(PH) 10.1 Hz, P_2CH], 4.23 [2 H, t, ^2J(Hab) 1.7 Hz, Ha], 4.77 [5 H, s, (C_5H_5)], 7.18-7.56 [35 H, m, Ph]; ^{31}P NMR δ_P (121 MHz; $CDCl_3$) 4.01 [d, ^2J(PP) 35.5 Hz, P_2CH], 39.77 [t, ^2J(PP), 35.3, PPh_3], -143.7 [sep, PF_6].

$[Ru(\eta\text{-}C_5H_5)(PPh_3)\{PPh_2CH(Hg(C_2H_5)PPh_2\}]PF_6$ [3.21]

[Bis(diphenylphosphino)methane][ethylmercury(II)]-ruthenium(II) hexafluorophosphate

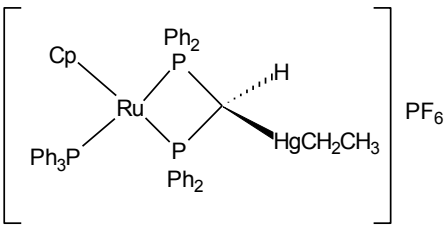

Powdered KOH (0.09 g, 0.15 mmol) was added to a stirred solution of $[Ru(\eta\text{-}C_5H_5)(PPh_3)\{PPh_2CH_2PPh_2\}]PF_6$ (0.11 g, 0.11 mmol) in CH_2Cl_2 (10 cm^3). This was followed by the addition of ethylmercurychloride (0.034 g, 0.13 mmol). The resulting orange solution was stirred for 2 hrs. The orange solution was concentrated under reduced pressure to yield a yellow solid. The product was filtered and washed with water (2 x 5 cm^3) and ethanol (2 x 5 cm^3).

(Found: C, 46.55; H, 4.4 %; $C_{50}H_{46}F_6P_4HgRu$ requires C, 47.67; H, 3.88%); ^{1}H NMR δ_H (200 MHz; CD_2Cl_2) 0.87 [2 H, t, ^3J(HH) 7.88 Hz, ^2J(HgH) 159.9 Hz, CH_3], 1.10 [3 H, t, ^3J(HH) 7.93 Hz, ^3J(HgH) 87.9 Hz, CH_3], 3.82 [2 H, q, -CH_2CH$_3$], 4.09 (1 H, t, ^2J(PH) 12.75 Hz, P_2CH]; 7.18-7.56 [35 H, m, Ph]; ^{31}P NMR δ_P (121 MHz; $CDCl_3$) 1.92 [d, ^2J(PP) 32.2 Hz, P_2CH], 48.12 [t, ^2J(PP), 33.1, PPh_3], -143.9 [sep, PF_6].

[Ru(η-C_5H_5)(PPh_3){$PPh_2CH(AuPPh_3)PPh_2$}]PF_6 [3.22]

[Bis(diphenylphosphino)methine][triphenylphosphine-aurate(I)](cyclopentadienyl)(triphenylphosphine)-ruthenium(II) hexafluorophosphate)

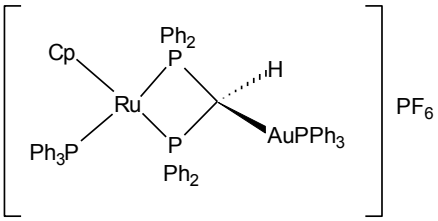

$ClAuPPh_3$ (0.10 g; 0.22 mmol) and KOH (0.012 g; 0.22 mmol) were added to a solution of [Ru(η-C_5H_5)(PPh_3){$PPh_2CH_2PPh_2$}]PF_6 (0.14 g; 0.18 mmol) in CH_2Cl_2(10 cm^3). The resulting orange solution was stirred in CH_2Cl_2 for 3 hrs. The reaction mixture was filtered to remove the excess KOH. The yellow filtrate was concentrated under reduced pressure. Addition of hexane yielded a yellow solid.

(0.20 g, 80%); m.p. 219°C(dec); (Found: C, 56.03; H, 4.91%; $C_{66}H_{56}F_6P_5AuRu$ requires C, 55.97; H, 3.96%); ^{1}H-NMR δ_H (200 MHz; $CDCl_3$): ^{1}H, δ 4.11 [1 H, q, ^2J(PH) 9.9 Hz, P_2CH], 4.64 [5 H, s, C_5H_5], 6.96-7.68 [50 H, m, Ph]; ^{31}P NMR δ_P (121 MHz; $CDCl_3$) 16.75 [d, ^2J(PP) 34.8 Hz, P_2CH], 50.31 [t, ^2J(PP), 35.3, PPh_3] -144.1 [sep, PF_6].

8.5 Preparations pertaining to Chapter 4

Bu_4[NHdptc] [4.1][20]

Tetrabutylammonium 1,5-diphenylthiocarbazonate

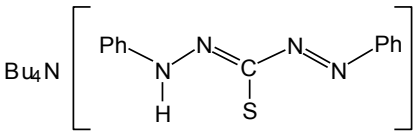

Dithizone (0.50 g, 1.95 mmol) was suspended in water (50 cm^3). To this was slowly added 25 cm^3 of an 0.1 M NaOH solution with stirring. The suspension disappeared with the formation of a red solution. The solution was filtered to remove any unreacted material. The desired product was precipitated from the filtrate as a red salt by the addition of tetrabutylammonium bromide (0.94 g, 2.93 mmol) and washed with cold water (3 x 10 cm^3).

(0.91 g, 91%); m.p. 101°C; (Found: C, 69.41; H, 9.49; N, 13.78; S, 5.96 %; $C_{29}H_{47}N_5S$ requires C, 69.91; H, 9.44; N, 14.06; S, 6.43%); FTIR (KBr)/cm^{-1} 3401m (NH) 1599vs (Ph) 1505vs (δNH) 1454vs (CS) 1423vs 1347vs (Ph) 1262s 1146vs 1096br 882s 755s 776vs 712s 695vs 507s; ^{1}H NMR δ_H (300 MHz; $CDCl_3$) 0.79 [12 H, s, -CH_3], 1.19 [8 H, m, $CH_3C\mathit{H}_2$-], 1.24 [8 H, m, $CH_3CH_2C\mathit{H}_2$-], 2.84 [8 H, m, -CH_2-N], 7.19-7.82 [12 H, m, Ph], 10.43 [1 H, s, -NH]; ^{13}C NMR δ_C (75 MHz; $CDCl_3$) 13.6 (-$CH_2\mathit{C}H_3$) 19.6 (-$\mathit{C}H_2CH_3$) 23.8 (-$\mathit{C}H_2CH_2\mathit{C}H_3$) 58.4 (-N$\mathit{C}H_2CH_2CH_2\mathit{C}H_3$) 113.5 119.2 122.5 128.4 129.1 144.2 153.4 170.3(CS).

Ph_4As[Hdptc] [4.1]

Tetraphenylarsonium 1,5-diphenylthiocarbazonate

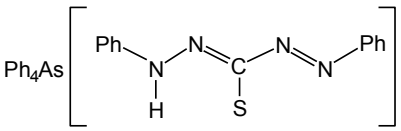

(1.2 g, 92%); m.p. 98-99°C; (Found: C, 64.56; H, 4.38; N, 8.26; S, 4.34 %; $C_{37}H_{31}N_4AsS$ requires C, 64.94; H, 4.43; N, 8.19; S, 4.68%); FTIR (KBr)/cm^{-1} UV-Vis (CH_2Cl_2); ^{1}H NMR δ_H (400 MHz; $CDCl_3$) 7.19-7.79 [36 H, m, Ph] 10.56 [1 H, s, -NH]; ^{13}C NMR δ_C (100 MHz; $CDCl_3$) 121.1 128.3 131.5 132.8 134.9.

8.6 Preparations pertaining to Chapter 5

[Pt(dptc)(COD)] [5.1]

(1,5-cyclooctadiene)(1,5-diphenylthiocarbozonato) platinum(II)

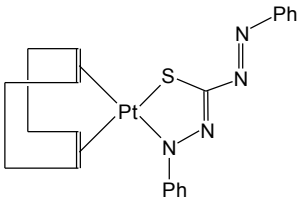

Dithizone (0.08 g, 0.31 mmol) was added as a solid to a suspension of platinumcyclooctadienechloride[21] (0.15 g, 0.31 mmol) in methanol (10 cm^3). The mixture turned orange on addition. The resulting solution was stirred for 1.0 hr. The orange product was filtered and washed with water (5 cm^3) and ethanol (5 cm^3). The orange material was recrystallised from dichloromethane/methanol to give red crystals. (0.14 g, 82%); m.p. 212°C (dec); (Found: C, 45.11; H, 3.89; N, 9.82; S, 5.46%; $C_{21}H_{22}N_4PtS$ requires C, 45.24; H, 3.98; N, 10.05; S, 5.75%); FTIR (KBr)/cm^{-1} 1587s (C=N) 1489vs 1478vs 1332vs (NPh) 1302m 1181s 1146vs 1127vs 1068s 1000s 951w 924w 881 s 845w 823w 789s 770s 718s 690vs 596s 523vs 469m; ^{1}H NMR δ_H (400 MHz; $CDCl_3$) 2.32 [2 H, m, COD-CH_2], 2.59 [6 H, m, COD-CH_2], 4.89 [2 H, s, ^2J(^{195}Pt-H) 82 Hz, COD-CH], 5.42 [2 H, s, ^2J(^{195}Pt-H) 81 Hz, COD-CH_2], 7.20-7.40 [8 H, m, Ph], 7.9 [2 H, m, Ph].

[Pd(Hdptc)dppm]PF_6 [5.2]

[Bis(diphenylphosphino)methane](1,5-diphenylthio-carbazonato)palladium(II) hexafluorophosphate

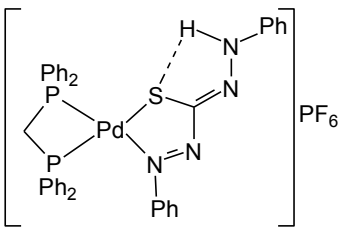

Dithizone (0.06 g, 0.23 mmol) was added as a solid to a suspension of diphenylphosphinomethanepalladiumchloride (0.13 g, 0.23 mmol) in ethanol (15 cm^3). The resulting solution turned red on addition, with disappearance of the suspension. The solution was stirred for 1.0 hr, filtered, followed by the addition of Na[PF_6] (0.058 g, 0.34 mmol) to the filtrate. The resulting dark red precipitate was filtered and washed with water (2 x 5 cm^3), followed by cold ethanol (5 cm^3).

(0.14 g, 70%); m.p. 212°C; (Found: C, 51.19; H, 3.69; N, 6.12; S, 3.46%; $C_{38}H_{33}F_6N_4P_3SPd$ requires C, 51.22; H, 3.70; N, 6.31; S, 3.60%); FTIR (KBr)/cm^{-1} 3218w (NH) 1590m 1533m 1473m 1436s 1318s 1215s 1100s 998m 845vs 735s 688s 557s 547s 504s 479m; UV-Vis (CH_2Cl_2) (λ_{max}, nm; ε, $mol^{-1}cm^{-1}$) 390(4650), 516(31320); ^{1}H NMR δ_H (300 MHz; $CDCl_3$) 4.67 [2 H, t, P_2CH], 6.96-8.0 [20 H, m, Ph], 9.59 [1 H, s, NH]; ^{31}P NMR δ_P (121 MHz; $CDCl_3$) -49.40 [d, ^2J(PP) 91.1 Hz, PdP_2], -29.38 [d, ^2J(PP) 94.6 Hz, PdP_2], -143.9 [sep, PF_6].

[Pd(dptc)dppm] [5.3]

[Bis(diphenylphosphino)methane](1,5-diphenylthio-carbazone)(palladium(II)

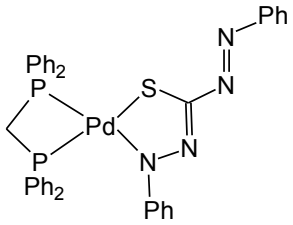

A solution of the dithizonate salt in methanol, prepared by addition of Et_3N (0.026 cm^3, 0.18 mmol) to dithizone (0.047 g, 0.18 mmol) in methanol (5 cm^3), was slowly added to a yellow suspension of [dppmPdCl_2] (0.10 g, 0.18 mmol) in methanol (5 cm^3). The mixture underwent an immediate colour change, yielding a red precipitate. The resulting mixture was stirred for 30 min, filtered and washed with small quantity of water (2 x 5 cm^3) and cold ethanol (5 cm^3).

(0.10 g, 77%); m.p. 186-188°C; (Found: C, 61.01; H, 4.28; N, 7.12; S, 4.02%; $C_{38}H_{32}N_4P_2SPd$ requires C, 61.25; H, 4.29; N, 7.56; S, 4.30%); UV-Vis (CH_2Cl_2) (λ_{max}, nm; ε, $mol^{-1}cm^{-1}$) 491 (29772); ^{1}H NMR δ_H (400 MHz; $CDCl_3$) 4.09 [2 H, t, ^2J(PH) 10.1 Hz P_2CH], 6.71-7.82 [20 H, m, Ph]; ^{31}P NMR δ_P (121 MHz; $CDCl_3$) -44.20 [d, ^2J(PP) 75.3 Hz, PdP_2], -24.80 [d, ^2J(PP) 72.9 Hz, PdP_2].

[Pt(Hdptc)dppm]PF_6 [5.4]

[Bis(diphenylphosphino)methane](1,5-diphenylthio-carbazonato)platinum(II) hexafluorophosphate

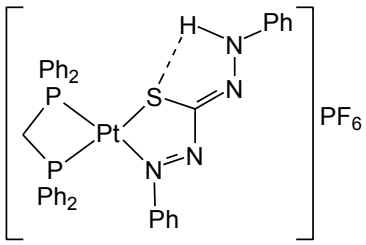

(0.14 g, 73%); m.p. 250°C; (Found: C, 46.61; H, 3.35; N,

5.65; S, 3.15 %; $C_{38}H_{33}F_6N_4P_3SPt$ requires C, 46.59; H, 3.37; N, 5.75; S, 3.27%); FTIR (KBr)/cm^{-1} 3248w (NH) 1589m 1523m 1471s 1436s 1338vs 1285s 1185m 1143vs 1118vs 1101s 999m 916m 785m 733s 689s 588m 547s 506s 479m; UV-Vis (CH_2Cl_2) (λ_{max}, nm; ε, $mol^{-1}cm^{-1}$) 345 (4568), 512 (32550); ^{1}H NMR δ_H (300 MHz; $CDCl_3$) 4.72 [2 H, t, P_2CH], 6.90-7.90 [20 H, m, Ph], 9.89 [1 H, br s, NH]; ^{31}P NMR δ_P (121 MHz; $CDCl_3$) -50.57 [d, ^2J(PP) 72.1 Hz, ^1J(Pt-P_B) 2538.4 Hz, PtP_2], -48.13 [d, ^2J(PP) 72.0 Hz, ^1J(Pt-P_A) 2563.8 Hz, PtP_2], -144.0 [sep, PF_6].

[Pt(dptc)dppm] [5.5]

[Bis(diphenylphosphino)methane](1,5-diphenylthio-carbazone)platinum(II)

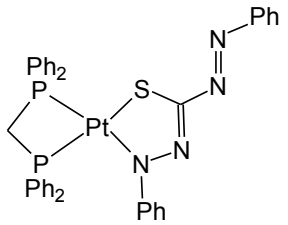

(0.12 g, 75%); m.p. 196°C; (Found: C, 54.29; H, 3.78; N, 6.29; S, 3.55 %; $C_{38}H_{32}N_4P_2SPt$ requires C, 54.74; H, 3.83; N, 6.75; S, 3.85%); UV-Vis (CH_2Cl_2) (λ_{max}, nm; ε, $mol^{-1}cm^{-1}$) 350 (4552), 492 (32556); ^{1}H NMR δ_H (300 MHz; $CDCl_3$) 4.45 [2 H, t, P_2CH], 6.79-7.89 [20 H, m, Ph]; ^{31}P NMR δ_P (121 MHz; $CDCl_3$) -48.29 [d, ^2J(PP) 70.2 Hz, ^1J(Pt-P_A) 2666.3 Hz, PtP_2], -46.68 [d, ^2J(PP) 70.1 Hz, ^1J(Pt-P_B) 2305.5 Hz, PtP_2].

Method 2

As an alternative preparative route to the method described in the preparation of **[5.3]** above, dppm (0.10 g, 0.26 mmol) was added to a suspension of [(COD)Pt(dptc)] (0.15 g, 0.26 mmol) in ethanol (20 cm^3). The resultant mixture was stirred for 3 hrs, after which the precipitate was filtered and washed with ethanol (2 x 5 cm^3) and dried. The resultant material was recrystallised from dichloromethane/ethanol.

(0.17 g, 81%); m.p. 196°C.

^{1}H NMR δ_H (300 MHz; $CDCl_3$) 4.46 [2 H, t, P_2CH], 6.79-7.89 [20 H, m, Ph]; ^{31}P NMR δ_P (121 MHz; $CDCl_3$) -48.28 [d, ^2J(PP) 70.2 Hz, ^1J(Pt-P_A) 2666.1 Hz, PtP_2], -46.68 [d, ^2J(PP) 70.1 Hz, ^1J(Pt-P_B) 2305.1 Hz, PtP_2].

[Pd(Hdptc)dppe]Ph_4B [5.6]

[Bis(diphenylphosphino)ethane](1,5-diphenylthio-carbazonato)palladium(II) tetraphenylborate

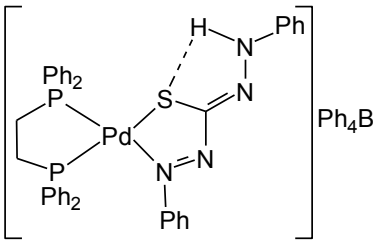

(0.13 g, 76%); m.p. 193°C(dec); (Found: C, 69.98; H, 5.08; N, 5.01; S, 2.77 %; $C_{63}H_{55}BN_4P_2SPd$ requires C, 70.04; H, 5.10; N, 5.19; S, 2.96%); FTIR (KBr)/cm^{-1} 3213m (NH) 1595m 1579m (Ph_4B) 1526s 1479s 1435s 1318vs 1211vs 1100vs 1029m 998s 930m 879m 842m 746s 732s 703vs 686vs 610s 530s 480s; UV-Vis (CH_2Cl_2) (λ_{max}, nm; ε, $mol^{-1}cm^{-1}$) 486 (29862); ^1H NMR δ_H (300 MHz; $CDCl_3$) 1.79 [4 H, m, PCH_2CH_2P], 6.75-7.60 [50 H, m, Ph], 9.27 [1 H, s, NH]; ^{31}P NMR δ_P (121 MHz; $CDCl_3$) 59.16 [d, ^2J(PP) 20.0 Hz, PdP_2], 64.54 [d, ^2J(PP) 20.2 Hz, PdP_2].

[Pd(dptc)dppe] [5.7]

[Bis(diphenylphosphino)ethane](1,5-diphenylthio-carbazone)palladium(II)

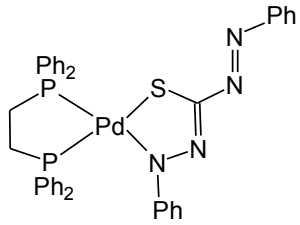

(0.12 g, 79%); m.p. >250°C; (Found: C, 61.54; H, 4.41; N, 7.45; S, 4.11 %; $C_{39}H_{34}N_4P_2SPd$ requires C, 61.65; H, 4.47; N, 7.56; S, 4.30%); FTIR (KBr)/cm^{-1} 1589m 1470s 1435s 1334vs 1298s 1279vs 1219m 1182s 1139vs 1120vs 1025m 995m 913m 867m 878m 822m 770m 749s 714s 688vs 573m 519s 482s; UV-Vis (CH_2Cl_2) (λ_{max}, nm; ε, $mol^{-1}cm^{-1}$) 387(4555), 515(32796); ^1H NMR δ_H (300 MHz; $CDCl_3$) 2.22 [4 H, m, PCH_2CH_2P], 6.51-7.90 [30 H, m, Ph]; ^{31}P NMR δ_P (121 MHz; $CDCl_3$) 48.54 [d, ^2J(PP) 32.9 Hz, PdP_2], 56.79 [d, ^2J(PP) 32.9 Hz, PdP_2].

[Pt(dptc)dppe] [5.8]

[Bis(diphenylphosphino)ethane](1,5-diphenylthio-carbazone)platinum(II)

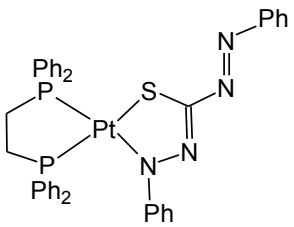

(0.11 g, 80%); m.p. >250°C; (Found: C, 55.28; H, 3.98; N, 6.19; S, 3.31 %; $C_{39}H_{34}N_4P_2SPt$ requires C, 55.25; H, 4.01; N, 6.64; S, 3.78%); FTIR (KBr)/cm^{-1} 1590m 1465s 1434s 1335vs 1284vs 1182m 1142vs 1123vs 996m 881m 823m 786m 770m 750m 687vs 583m 531s 485s; UV-Vis (CH_2Cl_2) (λ_{max}, nm; ε, $mol^{-1}cm^{-1}$) 342(7470), 490(32570); ^{1}H NMR δ_H (300 MHz; $CDCl_3$) 2.19 [4 H, m, PCH_2CH_2P], 6.58 –7.86 [30 H, m, Ph]; ^{31}P NMR δ_P (121 MHz; $CDCl_3$) 38.49 [d, ^2J(PP) 10.9 Hz, ^1J(Pt-P_A) 2879.8 Hz, PtP_2], 47.14 [d, ^2J(PP) 11.9 Hz, ^1J(Pt-P_B) 2942.8 Hz, PtP_2].

[Pd(Hdptc)dppp]Ph_4B [5.9]

[Bis(diphenylphosphino)propane](1,5-diphenylthio-carbazonato)palladium(II) tetraphenylborate

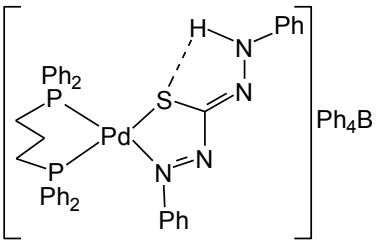

(0.13 g, 76%); m.p. 131°C (dec); (Found: C, 70.02; H, 5.14; N, 4.89; S, 2.66 %; $C_{64}H_{57}BN_4P_2SPd$ requires C, 70.24; H, 5.21; N, 5.12; S, 2.93%); FTIR (KBr)/cm^{-1} 3217w (NH) 1595m 1579m (Ph_4B) 1527s 1480s 1432s 1322vs 1270s 1213vs 1099vs 1029s 998m 972s 972m 928m 834m 783w 731s 702vs 686vs 610s 534w 507s; UV-Vis (CH_2Cl_2) (λ_{max}, nm; ε, $mol^{-1}cm^{-1}$) 393(4516), 519(27448); ^{1}H NMR δ_H (300 MHz; $CDCl_3$) 1.40 [2 H, m, $CH_2CH_2CH_2$], 1.89 [4 H, m, PCH_2], 6.62 –7.65 [50 H, m, Ph], 9.15 [1 H, s, NH]; ^{31}P NMR δ_P (121 MHz; $CDCl_3$) 5.42 [d, ^2J(PP) 60.2 Hz, PdP_2], 12.21 [d, ^2J(PP) 60.1 Hz, PdP_2].

[Pd(dptc)dppp] [5.10]

[Bis(diphenylphosphino)propane](1,5-diphenylthio-carbazone)palladium(II)

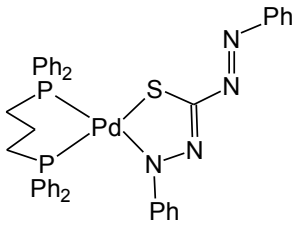

(0.13 g, 85%); m.p. >250°C; (Found: C, 62.18; H, 5.01; N, 7.18; S, 4.01%; $C_{40}H_{36}N_4P_2SPd$ requires C, 62.08; H, 5.04; N, 7.24; S, 4.14%); FTIR (KBr)/cm^{-1} 1586s 1481s 1451s 1435vs 1334vs 1299s 1278vs 1216m 1183s 1146vs 999m 915w 866w 767s 740s 716s 690vs 658s 616w 572w 497vs; UV-Vis (CH_2Cl_2) (λ_{max}, nm; ε, $mol^{-1}cm^{-1}$)

487(29620); ^{1}H NMR δ_H (300 MHz; $CDCl_3$) 1.80 [2 H, m, $CH_2CH_2CH_2$], 2.31 [4 H, m, PCH_2], 6.41–7.65 [30 H, m, Ph]; ^{31}P NMR δ_P (121 MHz; $CDCl_3$) 4.95 [d, ^{2}J(PP) 60.6 Hz, PdP_2], 7.15 [d, ^{2}J(PP) 60.5 Hz, PdP_2].

[Pt(dptc)dppp] [5.11]

[Bis(diphenylphosphino)propane](1,5-diphenylthiocarbazone)platinum(II)

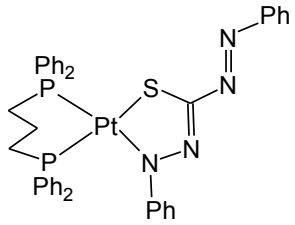

(0.15 g, 82%); m.p. >250°C; (Found: C, 55.33; H, 3.85; N, 6.18; S, 3.25 %; $C_{40}H_{36}N_4P_2SPt$ requires C, 55.75; H, 4.18; N, 6.53; S, 3.72%); FTIR (KBr)/cm^{-1} 1587s 1482s 1453s 1335vs 1300s 1283s 1216m 1183s 1146vs 1130vs 1099vs 976s 869w 841m 768m 742m 691vs 663s 616w 583m 513s 505s 440m; UV-Vis (CH_2Cl_2) (λ_{max}, nm; ε, mol^{-1}cm^{-1}) 335(7483), 494(31791); ^{1}H NMR δ_H (400 MHz; $CDCl_3$) 1.80 [2 H, m, $CH_2CH_2CH_2$], 2.34 [2 H, m, PCH_2], 2.45 [2 H, m, PCH_2], 6.42 – 7.86 [30 H, m, Ph]; ^{31}P NMR δ_P (121 MHz; $CDCl_3$) -13.04 [d, ^{2}J(PP) 37.5 Hz, ^{1}J(Pt-P_A) 2775.8 Hz, PtP_2], 1.35 [d, ^{2}J(PP) 36.6 Hz, ^{1}J(Pt-P_B) 2826.2 Hz, PtP_2].

[Pd(Hdptc)dppf]Ph_4B [5.12]

[Bis(diphenylphosphino)ferrocene](1,5-diphenylthiocarbazonato)palladium(II) tetraphenylborate

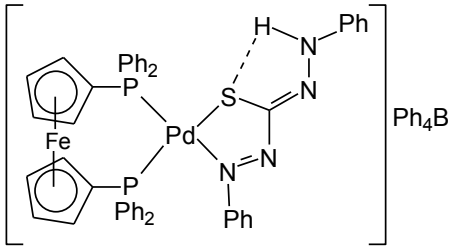

(0.11 g, 68%); m.p. 176°C (dec); (Found: C, 68.66; H, 4.64; N, 4.12; S, 5.44 %; $C_{71}H_{59}BN_4P_2SFePd$ requires C, 68.97; H, 4.78; N, 4.53; S, 5.59 %); FTIR (KBr)/cm^{-1} 3134m (NH) 1579m 1531w 1479s 1436s 1387m 1337m 1229m 1168s 1100s 1031s 1065m 998m 838m 742s 699vs 654m 613s 489m; UV-Vis (CH_2Cl_2) (λ_{max}, nm; ε, mol^{-1} cm^{-1}) 505 (39641), 632 (2536); ^{1}H NMR δ_H (300 MHz; $CDCl_3$) 3.76 [2 H, br s, C_5H_4], 4.29 [2 H, br s, C_5H_4], 4.42 [2 H, br s, C_5H_4], 4.62 [2 H, br s, C_5H_4], 6.68 – 7.92 [20 H,

m; Ph] 9.17 [1 H, s, NH]; ^{31}P NMR δ_P (121 MHz; $CDCl_3$) 28.31 [d, ^2J(PP) 10.9 Hz, PdP_2], 32.26 [d, ^2J(PP) 10.8 Hz, PdP_2].

[Pd(dptc)dppf] [5.13]

[Bis(diphenylphosphino)ferrocene](1,5-diphenylthiocarbazone) palladium(II)

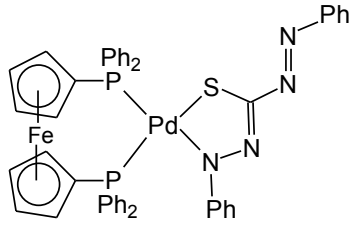

(0.12 g, 71%); m.p. >250°C; (Found: C, 61.71; H, 4.12; N, 5.88; S, 3.22 %; $C_{47}H_{38}N_4P_2SFePd$ requires C, 61.69; H, 4.15; N, 6.12; S, 3.50 %); UV-Vis (CH_2Cl_2) (λ_{max}, nm; ε, $mol^{-1}cm^{-1}$) 500 (24738), 635 (4789); ^{1}H NMR δ_H (300 MHz; $CDCl_3$) 3.69 [2 H, br s, C_5H_4], 4.19 [2 H, br s, C_5H_4], 4.40 [2 H, br s, C_5H_4], 4.69 [2 H, br s, C_5H_4], 6.4-8.0 [20 H, m; Ph]; ^{31}P NMR δ_P (121 MHz; $CDCl_3$) 23.1 [d, ^2J(PP) 26.5 Hz, PdP_2], 23.9 [d, ^2J(PP) 26.5 Hz, PdP_2].

[Pt(Hdptc)dppf]Ph_4B [5.14]

[Bis(diphenylphosphino)ferrocene](1,5-diphenylthiocarbazonato)platinum(II) tetraphenylborate

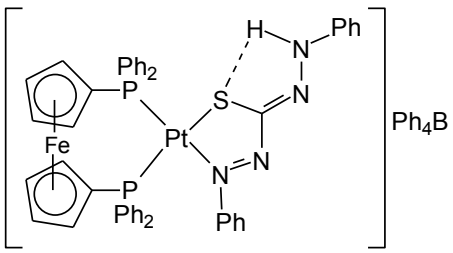

(0.99 g, 67%); m.p. 158°C (dec); (Found: C, 64.12; H, 4.22; N, 4.10; S, 2.12 %; $C_{71}H_{59}BN_4P_2SFePt$ requires C, 64.35; H, 4.47; N, 4.23; S, 2.42%); FTIR (KBr)/cm^{-1} 3215w 1595m 1579m 1529s 1480s 1435s 1387w 1330s 1230vs 1094s 1030m 999m 929m 841m 731s 688vs 703vs 635m 611s 555s 493s; UV-Vis (CH_2Cl_2) (λ_{max}, nm; ε, $mol^{-1}cm^{-1}$) 436(10513), 537(27055), 721(2454); ^{1}H NMR δ_H (300 MHz; $CDCl_3$); ^{1}H NMR δ_H (300 MHz; $CDCl_3$) 3.62 [2 H, s, C_5H_4], 4.21 [2 H, s, C_5H_4], 4.43 [2 H, s, C_5H_4], 4.63 [2 H, s, C_5H_4], 6.68-7.92 [20 H, m; Ph] 9.21 [1 H, s, NH]; ^{31}P NMR δ_P (121 MHz; $CDCl_3$) -0.81 [d, ^2J(PP) 18.2 Hz, ^1J(Pt-P_B) 3287.6 Hz, PtP_2], 23.46 [d, ^2J(PP) 18.4 Hz, ^1J(Pt-P_A) 3316.6 Hz, PtP_2].

[Pt(dptc)dppf] [5.15]

[Bis(diphenylphosphino)ferrocene](1,5-diphenylthiocarbazone)platinum(II)

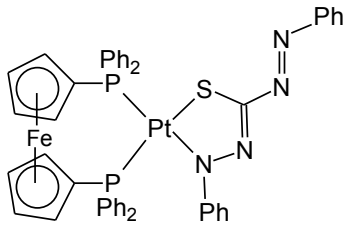

(0.10 g, 69%); m.p. >250°C; (Found: C, 56.11; H, 3.69; N, 5.25; S, 3.09 %; $C_{47}H_{38}N_4P_2SFePt$ requires C, 56.23; H, 3.79; N, 5.58; S, 3.19 %); UV-Vis (CH_2Cl_2) (λ_{max}, nm; ε, $mol^{-1}cm^{-1}$) 518(13246), 724(4214); ^{1}H NMR δ_H (300 MHz; $CDCl_3$) 3.63 [2 H, d, ^3J(HH) 1.8 Hz, C_5H_4], 4.12 [2 H, s, C_5H_4], 4.39 [2 H, s, C_5H_4], 4.69 [2 H, d, ^3J(HH) 2.1 Hz, C_5H_4], 6.4-8.0 [20 H, m; Ph]; ^{31}P NMR δ_P (121 MHz; $CDCl_3$) 2.96 [d, ^2J(PP) 26.5 Hz, ^1J(Pt-P_B) 3100.0 Hz, PtP_2], 21.42 [d, ^2J(PP) 26.5 Hz, ^1J(Pt-P_A) 3167.2 Hz, PtP_2].

[Pt(dptc)(PPh_3)$_2$] [5.16]

Bis(triphenylphosphine)(1,5-diphenylthiocarbazone)-platinum(II)

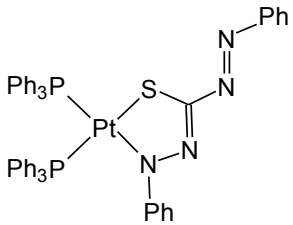

Triphenylphosphine (0.10 g, 0.38 mmol) was added to a suspension of (COD)Pt(dptc) (0.11 g, 0.19 mmol) in ethanol (20 cm^3). The resultant mixture was stirred for 3 hrs, after which the precipitate was filtered and washed with ethanol (2 x 5 cm^3) and dried.

(0.14g, 80%); m.p. 211°C (dec); (Found: C, 60.48; H, 4.09; N, 5.68; S, 3.01%; $C_{49}H_{40}N_4P_2SPt$ requires C, 60.43; H, 4.11; N, 5.78; S, 3.29%); UV-Vis (CH_2Cl_2) (λ_{max}, nm; ε, $mol^{-1}cm^{-1}$) 323(8371), 506(26986); ^{1}H NMR δ_H (400 MHz; $CDCl_3$) 6.40-7.80 [40 H, m, Ph]; ^{31}P NMR δ_P (121 MHz; $CDCl_3$) 6.30 [d, ^2J(PP) 25.5 Hz, ^1J(Pt-P_A) 3073.2 Hz, PdP_2], 19.29 [d, ^2J(PP) 25.5 Hz, ^1J(Pt-P_B) 3097.5 Hz, PdP_2].

[Pt(dptc)(PPhMe$_2$)$_2$] [5.17]

Bis(dimethylphenylphosphine)(1,5-diphenylthiocarbazone)-platinum(II)

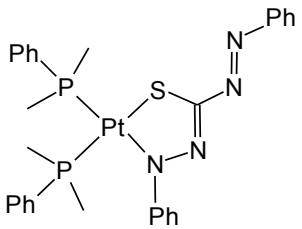

(0.17 g, 85%); m.p. 144°C (dec); (Found: C, 47.99; H, 4.39; N, 7.82; S, 4.17%; $C_{29}H_{32}N_4P_2SPt$ requires C, 47.95; H, 4.41; N, 7.72; S, 4.41%); FTIR (KBr)/cm^{-1} 1587s 1476s 1454s 1417m 1331vs 1284s 1217m 1181m 1124vs 1069s 940s 906s 767s 720s 690s 588m 520s 486m 434m; UV-Vis (CH_2Cl_2) (λ_{max}, nm; ε, mol^{-1}cm^{-1}) 325(11463), 503(36759); ^{1}H NMR δ_H (300 MHz; $CDCl_3$) 1.05 [3 H, d, ^1J(P-H) 9.90 Hz , ^2J(Pt-H) 78 Hz, P_ACH_3], 1.79 [3 H, d, J(P-H) 10.20 Hz, ^2J(Pt-H) 79 Hz, P_BCH_3], 6.95 – 7.91 [40 H, m, Ph]; ^{31}P NMR δ_P (121 MHz; $CDCl_3$) -23.45 [d, ^2J(PP) 27.3 Hz, ^1J(Pt-P_B) 2888.8 Hz, PtP_2], -14.09 [d, ^2J(PP) 27.5 Hz, ^1J(Pt-P_A) 2957.8 Hz, PtP_2].

[Pt(Hdptc)(PEt$_3$)$_2$] [5.18]

Bis(triethylphosphine)(1,5-diphenylthio-carbazone)platinum(II)

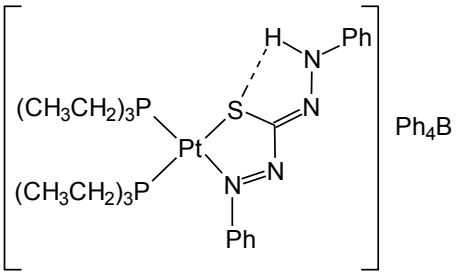

(0.22 g, 71%); m.p. 122-124°C; (Found: C, 58.39; H, 6.01; N, 5.28; S, 32.96 %; $C_{49}H_{61}BN_4P_2SPt$ requires C, 58.45; H, 6.06; N, 5.57; S, 5.18%); FTIR (KBr)/cm^{-1} 3213m (NH) 1595m 1579m (Ph_4B) 1527s 1479m 1454s 1425m 1379w 1321s 1212vs 1072m 1031vs 931m 842w 731vs 703vs 610s 530w 499w 423w; UV-Vis (CH_2Cl_2) (λ_{max}, nm; ε, mol^{-1}cm^{-1}) 445(13406), 544(22100) ;^{1}H NMR δ_H (300 MHz; $CDCl_3$), 1.0 [9 H, t, ^2J(PH) 10.2 Hz, $P_ACH_2CH_3$], 1.19 [9 H, t, ^2J(PH) 9.9 Hz, $P_BCH_2CH_3$], 1.59 [6 H, m, ^2J(PH) 9.9 Hz, $P_ACH_2CH_3$], 2.11 [6 H, , ^2J(PH) Hz, $P_BCH_2CH_3$] 7.02-7.82 [10 H, m, Ph]; ^{31}P NMR δ_P (121 MHz; $CDCl_3$) -0.03 [d, ^2J(PP) 25.4 Hz, ^1J(Pt-P_A) 2966.6 Hz, PtP_2], 5.57 [d, ^2J(PP) 25.8 Hz, ^1J(Pt-P_B) 2943.2 Hz, PtP_2].

8.7 Preparations pertaining to Chapter 6

Hg(Hdptc)Cl [6.1]

Chloromercury dithizonate[22]

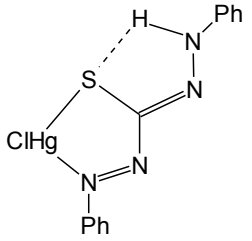

Dithizone (1.0 g, 3.8 mmol) was slowly added to a solution of mercury(II)chloride (4.0 g, 15.2 mmol) in ether (80 cm^3). The reaction mixture was stirred for 4 hrs at room temperature. The resultant orange-red precipitate was filtered and washed with water (2 x 10 cm^3) and ethanol (2 x 10 cm^3).

(0.39 g, 42 %), m.p. >250 °C (dec); (Found: C, 31.68; H, 2.19; N, 11.12; S, 6.22%; $C_{13}H_{11}ClN_4SHg$ requires C, 31.74; H, 2.24; N, 11.39; S, 6.51 %); FTIR (KBr)/cm^{-1} 3232vs (NH) 1594s (Ph) 1530vs (δNH) 1494s 1477s (CS) 1457s 1351vs 1310s (Ph) 1276s 1193s 1174s 1163vs (NCS) 747vs 679vs 570s 527s 481s 431m; UV-Vis (CH_2Cl_2) (λ_{max}, nm) 481.

Bu_4N[Hg(mnt)(Hdptc)] [6.2]

Tetrabutylammonium (1,5-diphenylthiocarbazonato-S,N)
(1,2-maleonitrile-1,2- dithiolato)mercury(II)

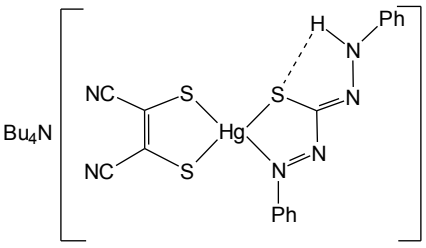

Chloromercurydithizonate (0.10 g, 0.20 mmol) was added to a solution containing maleonitriledithiolate (0.039 g, 0.21 mmol) in ethanol (30 cm^3). The resulting mixture was stirred at 40°C for 8 hrs. The reaction mixture was filtered while hot to remove any unreacted material. Tetrabutylammonium bromide (0.08 g, 0.21 mmol) was added to the resultant filtrate to precipitate the desired product. The red material was filtered and washed with water (10 cm^3), followed by cold ethanol (5 cm^3). Recrystallisation from dichloromethane/methanol gave dark red crystals. (0.14 g, 84%), m.p. 191°C; (Found: C, 47.18; H, 5.55; N, 11.44; S, 11.23%; $C_{33}H_{47}N_7S_3Hg$ requires C, 47.27; H, 5.60; N, 11.69; S, 11.47 %) FTIR (KBr)/cm^{-1} 3245

m (NH) 2190vs (CN) 1595s (Ph) 1523vs 1516 vs 1486vs 1456s 1429vs 1380s 1351vs 1309s 1271s 1196s 1164s 1145vs 1113vs 1071m 915m 877m 861s 802m 763s 748s 683s 602m 512s 476s; UV-Vis (CH_2Cl_2) (λ_{max}, nm; ε, $mol^{-1}cm^{-1}$) 482; 23442; ^1H NMR δ_H (300 MHz; $CDCl_3$) 0.97 [12 H, t, CH_3], 1.39 [8 H, m, CH_3CH_2-], 1.59 [8 H, m, $CH_3CH_2CH_2$-]

3.10 [8 H, m, -CH_2-N], , 7.19-7.85 [10 H, m, Ph], 9.41 [1 H, s, -NH].

Ph_4As[(mnt)Hg(Hdptc)] [6.3]

Tetraphenylarsonium (1,5-diphenylthiocarbazonato-S,N) (1,2-maleonitrile-1,2 dithiolato)mercury(II)

This was prepared in a similar manner to **[5.2]**, with the exception that Ph_4AsCl was used to precipitate the desired product from ethanol.

(0.15 g, 77%); m.p. 186-188°C; (Found: C, 50.15; H, 3.11; N, 8.38; S, 9.64%; $C_{41}H_{31}AsN_6S_3Hg$ requires C, 50.23; H, 3.17; N, 8.58; S, 9.80 %); FTIR (KBr)/cm^{-1} 3199s (NH) 2196s (CN) 1596s (Ph) 1516 vs (δ-NH)1495s 1479s (C=S) 1455s 1434vs 1361vs 1305vs (NPh) 1258s 1182s 1119vs 1081vs 997s 857s 737vs 687vs 604m 592m 511s 477s 463s; UV-Vis (CH_2Cl_2) (λ_{max}, nm; ε, $mol^{-1}cm^{-1}$) 482; 23391; ^1H NMR δ_H (300 MHz; $CDCl_3$) 7.02-7.84 [36 H, m, Ph], 9.39 [1 H, s, NH].

Ph_4As[Hg(dmit)(Hdptc)] [6.4]

Tetraphenylarsonium (1,5-diphenylthiocarbazonato-S,N)(1,3-dithiole-2-thione-4,5-dithiolato)mercury(II)

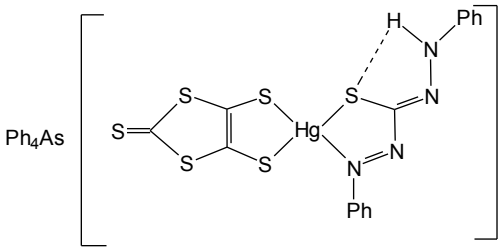

Chloromercurydithizonate, ClHg(Hdtpc), (0.1 g, 0.2 mmol) was added to a solution containing the dithiolate (0.44 g, 0.21 mmol), which was prepared from a solution of dmit and sodium methoxide (0.023 g, 0.45 mmol) in ethanol (10 cm^3). The resultant mixture was stirred for 12 hrs at room temperature. The reaction mixture was filtered to

remove any unreacted material. Tetraphenylarsonium chloride (0.084 g, 0.2 mmol) was used to precipitate the desired product from the filtrate.

(0.13 g, 62%); m.p. 209°C (dec); (Found: C, 46.27; H, 2.91; N, 5.22; S, 18.31%; $C_{40}H_{31}AsN_4S_6Hg$ requires C, 46.35; H, 2.99; N, 5.41; S, 18.54 %); FTIR (KBr)/cm^{-1} 3215m (NH) 1679m (C=S) 1594s (Ph) 1519s 1495s 1480s 1435s 1417s 1368s 1307m 1255m 1184s 1120s 1080s 1051vs 1033vs 995s 878m 734vs 685vs 514m 475m 460vs; UV-Vis (CH_2Cl_2) (λ_{max}, nm; ε, $mol^{-1}cm^{-1}$) 487; 32359; ^1H NMR δ_H (300 MHz; $CDCl_3$) 6.99-7.82 [36 H, m, Ph], 9.41 [1 H, s, NH].

$Ph_4As[Hg(dmid)(Hdptc)]$ [6.5]

Tetraphenylarsonium (1,5-diphenylthiocarbazonato-S,N)(1,3-dithiole-2-one-4,5-dithiolato)mercury(II)

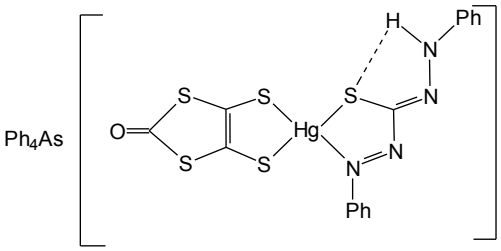

(0.15 g, 65%); m.p. 211°C (dec); (Found: C, 46.99; H, 3.01; N, 5.31; S, 15.42%; $C_{40}H_{31}AsN_4OS_5Hg$ requires C, 47.08; H, 3.04; N, 5.49; S, 15.69%); FTIR (KBr)/cm^{-1} 3219m (NH) 1725s 1661vs (C=O) 1594vs (Ph) 1519s 1496m 1481s 1437vs 1359s 1308s 1259s 1184s 1132vs 1080s 996s 892s 871s 737vs 685vs 475s 461vs; UV-Vis (CH_2Cl_2) (λ_{max}, nm; ε, $mol^{-1}cm^{-1}$) 488; 33133; ^1H NMR δ_H (300 MHz; $CDCl_3$) 7.10-7.85 [36 H, m, Ph], 9.37 [1 H, s, NH].

[(mnt)Pt(COD)] [6.6][23]

(1,5-cyclooctadiene)(1,2-maleonitrile-1,2-dithiolato)platinum(II)

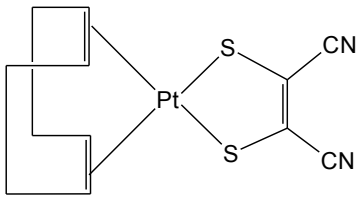

The maleonitrile precursor was prepared according to literature methods from (1,5-cyclooctadiene)platinum(II) chloride and sodium maleonitrile in ethanol.

$Bu_4N[Pt(mnt)(Hdptc)]$ [6.7]

Tetrabutylammonium (1,5-diphenylthiocarbazonato-S,N)(1,2-maleonitrile-2,3-dithiolato)platinum(II)

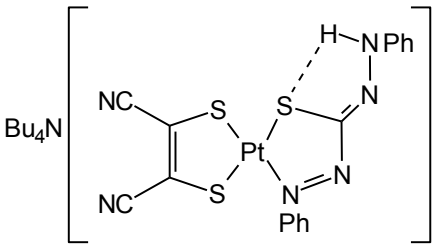

Tetrabutylammoniumdithizonate (0.10 g, 0.20 mmol) was added to a yellow suspension of (mnt)$PtCl_2$ (0.081 g, 0.20 mmol) in ethanol (15 cm^3). The resultant deep red mixture was gently refluxed for 5 hrs. During this time, the solution turned green with the formation of a green precipitate. The solution was allowed to cool and the precipitate filtered and washed with small portions (2 x 5 cm^3) of water and cold ethanol (2 x 5 cm^3).

(0.13 g, 76%); m.p. 177-179°C; (Found: C, 47.48; H, 5.59; N, 11.31; S, 11.35%; $C_{33}H_{47}N_7S_3Pt$ requires C, 47.54; H, 5.64; N, 11.76; S, 11.52%); FTIR (KBr)/cm^{-1} 3201m (NH) 2199vs (CN) 1595s (Ph) 1520vs 1482vs 1379m 1318s 1302s 1267s 1187br 1166vs 1151vs 879m 781m 756s 731s 712m 689s 608w 578w 545m 507s 424w; UV-Vis (CH_2Cl_2) (λ_{max}, nm; ε, $mol^{-1}cm^{-1}$) 456; 22164; 699; 12800; ^{1}H NMR δ_H (300 MHz; $CDCl_3$), 0.97 [12 H, t, -CH_2CH_3], 1.39 [8 H, m, -$CH_2CH_2CH_3$], 1.48 [8 H, m, $NCH_2CH_2CH_2$], 3.03 [8 H, t, $NCH_2CH_2CH_2$], 7.08-7.51 [10 H, m, Ph], 8.89 [1 H, s, N*H*]; ^{13}C NMR δ_C (75 MHz; $CDCl_3$), 13.75 (-CH_2CH_3) 19.83 (-$CH_2CH_2CH_3$) 24.04 ($NCH_2CH_2CH_2$-) 59.20 ($NCH_2CH_2CH_2$-) 115.44 (C=C) 123.54 (Ph) 127.97 (Ph) 129.41 (Ph) 163.01 (CN).

REFERENCES

1 Z. Otwinowski and W. Minor, *Methods in Enzymology, Macromolecular Crystallograpohy,* ed. C. W. Carter Jr. and R. M. Sweet, Part A, 1997, **276**, 307-326, Academic Press.

2 G. M. Sheldrick, *SHELX97, Programme for solving Crystal Structures*, University of Göttengen, Germany, 1997.

3 G. M. Sheldrick, *SHELX97, Programme for the Refinement of Crystal Structures*, University of Göttengen, Germany, 1997.

4 L. J. Barbour, *J. Supramol. Chem.*, 2001, **1**, 189.

5 G. T. Velde, F. M. Bickelhaupt, E. J. Baerends, C. F. Guerra, S. J. A. van Gisbergen, J. G. Snijders and T. J. Ziegler, *J. Comput. Chem*., 2001, **22**, 931.

6 C. Lee, W. Yang and R. G. Parr, *Phys. Rev*. 1988, **B37**, 785.

7 A. D. Becke, *J. Chem. Phys*., 1993, **98**, 5648.

8 M. J. Frisch, G. W. Trucks, H. B. Schlegel, G. E. Scuseria, M. A. Robb, J. R. Cheeseman, G. Scalmani, V. Barone, B. Mennucci, G. A. Petersson, H. Nakatsuji, M. Caricato, X. Li, H. P. Hratchian, A. F. Izmaylov, J. Bloino, G. Zheng, J. L. Sonnenberg, M. Hada, M. Ehara, K. Toyota, R. Fukuda, J. Hasegawa, M. Ishida, T. Nakajima, Y. Honda, O. Kitao, H. Nakai, T. Vreven, J. A. Montgomery, Jr., J. E. Peralta, F. Ogliaro, M. Bearpark, J. J. Heyd, E. Brothers, K. N. Kudin, V. N. Staroverov, R. Kobayashi, J. Normand, K. Raghavachari, A. Rendell, J. C. Burant, S. S. Iyengar, J. Tomasi, M. Cossi, N. Rega, J. M. Millam, M. Klene, J. E. Knox, J. B. Cross, V. Bakken, C. Adamo, J. Jaramillo, R. Gomperts, R. E. Stratmann, O. Yazyev, A. J. Austin, R. Cammi, C. Pomelli, J. W. Ochterski, R. L. Martin, K. Morokuma, V. G. Zakrzewski, G. A. Voth, P. Salvador, J. J. Dannenberg, S. Dapprich, A. D. Daniels, O. Farkas, J. B. Foresman, J. V. Ortiz, J. Cioslowski, and D. J. Fox, *Gaussian, Inc*., Wallingford CT, 2009.

9 K. Wolinski, K. J. F. Hilton and P. Pulay, *J. Am. Chem. Soc*., 1990, **12**, 8251.

10 H. F. Hameka, *Mol. Phys*., 1958, **1**, 203.

11 J. Barluenga, A. M. Bayon, J. Perez-Prieto and G. Asensio, *Tetrahedron*, 1984, **40**, 5053.

12 K. Hui and B. L. Shaw, *J. Organomet. Chem.*, 1977, **124**, 262.

13 E. J. Fernandez, M. Concepcion Gimeno, P. G. Jones, A. Laguna, M. Laguna and E. Olmos, Inorg. Chim. Acta, 1995, **238**, 173.

14 C. E. Johnson, R. Eisenberg, T. R. Evans and M. S. Burberry, *J. Am. Chem. Soc*., 1983, **105**, 1795.

15 G. Bahr and G. Schleitzer, *Ber*., 1957, **90**, 438.

16 M. P. Brown, R. J. Puddephatt and M. Rashidi, *J. Chem. Soc., Dalton Trans*., 1977, 951.

17 N. Svenstrup and J. Becher, *Synthesis*, 1995, 215.

18 J. M. Jenkins and J. G. Verkade, *Inorg. Synth*., 1968, **11**, 108.

19 G. S. Ashby, M. L. Bruce, I. B. Tomkins and R. C. Wallis, *Aus. J. Chem*., 1979, **32**, 1003.

20 K. G. von Eschwege and J. C. Swarts, *Polyhedron*, 2010, **29**, 1727.

21 H. C. Clark and L. E. Manzer, *J. Organometal. Chem.*, 1973, **59**, 411.

22 J. L. A. Webb, I. Singh Bhatia, A. H. Corwin and A. G. Sharp, *J. Am. Chem. Soc*., 1950, **72**, 91.

23 C. E. Keefer, S. T. Purrington, R. D. Bereman, B. W. Knight, D. R. Bedgood, Jr. and P. Boyle, *Inorg. Chim. Acta*.,1998, **282**, 200.